University of Kentucky
UKnowledge

Theses and Dissertations--Chemical and Materials Engineering

Chemical and Materials Engineering

2018

SYNTHESIS OF BIOLOGICALLY-INSPIRED NANOFILTRATION MEMBRANES USING PROTECTED, MUTATED, AND SIMULATED AQUAPORINS

Priyesh Ashokrao Wagh
University of Kentucky, priyesh.wagh@uky.edu
Author ORCID Identifier:
https://orcid.org/0000-0003-0125-6852
Digital Object Identifier: https://doi.org/10.13023/etd.2018.470

Right click to open a feedback form in a new tab to let us know how this document benefits you.

Recommended Citation

Wagh, Priyesh Ashokrao, "SYNTHESIS OF BIOLOGICALLY-INSPIRED NANOFILTRATION MEMBRANES USING PROTECTED, MUTATED, AND SIMULATED AQUAPORINS" (2018). *Theses and Dissertations--Chemical and Materials Engineering*. 92.
https://uknowledge.uky.edu/cme_etds/92

This Doctoral Dissertation is brought to you for free and open access by the Chemical and Materials Engineering at UKnowledge. It has been accepted for inclusion in Theses and Dissertations--Chemical and Materials Engineering by an authorized administrator of UKnowledge. For more information, please contact UKnowledge@lsv.uky.edu.

STUDENT AGREEMENT:

I represent that my thesis or dissertation and abstract are my original work. Proper attribution has been given to all outside sources. I understand that I am solely responsible for obtaining any needed copyright permissions. I have obtained needed written permission statement(s) from the owner(s) of each third-party copyrighted matter to be included in my work, allowing electronic distribution (if such use is not permitted by the fair use doctrine) which will be submitted to UKnowledge as Additional File.

I hereby grant to The University of Kentucky and its agents the irrevocable, non-exclusive, and royalty-free license to archive and make accessible my work in whole or in part in all forms of media, now or hereafter known. I agree that the document mentioned above may be made available immediately for worldwide access unless an embargo applies.

I retain all other ownership rights to the copyright of my work. I also retain the right to use in future works (such as articles or books) all or part of my work. I understand that I am free to register the copyright to my work.

REVIEW, APPROVAL AND ACCEPTANCE

The document mentioned above has been reviewed and accepted by the student's advisor, on behalf of the advisory committee, and by the Director of Graduate Studies (DGS), on behalf of the program; we verify that this is the final, approved version of the student's thesis including all changes required by the advisory committee. The undersigned agree to abide by the statements above.

Priyesh Ashokrao Wagh, Student

Dr. Isabel C. Escobar, Major Professor

Dr. Stephen Rankin, Director of Graduate Studies

SYNTHESIS OF BIOLOGICALLY-INSPIRED NANOFILTRATION MEMBRANES USING PROTECTED, MUTATED, AND SIMULATED AQUAPORINS

DISSERTATION

A dissertation submitted in partial fulfillment of the
requirements for the degree of Doctor of Philosophy in the
College of Engineering
at the University of Kentucky

By
Priyesh Ashokrao Wagh
Lexington, Kentucky
Director: Dr.Isabel C. Escobar, Professor of Chemical and Materials Engineering
Lexington, Kentucky
2018

Copyright © Priyesh Ashokrao Wagh 2018
https://orcid.org/0000-0003-0125-6852

ABSTRACT OF DISSERTATION

SYNTHESIS OF BIOLOGICALLY-INSPIRED NANOFILTRATION MEMBRANES USING PROTECTED, MUTATED, AND SIMULATED AQUAPORINS

Gram-negative bacterial cells are surrounded by a cell membrane which protects the cell and controls the transport of nutrients and waste products in and out of the cells at a fast rate. This rapid transport of nutrients and wastes through the cell membrane is made possible by channel proteins called porins. Various types of porins present in the cell membrane have specific functions depending on their selectivity towards different nutrients, and channel proteins selective towards water are called aquaporins. These proteins restrict the passage of all entities except water molecules and they provide a fast transport rate of water molecules at 10^9 molecules/second per channel.

The high selectivity of porins has led to their incorporation into synthetic systems, and one example is the addition of porins to separations membranes in order to enhance their performance in terms of selectivity and permeability, in a field called biomimetics. The concept of incorporating aquaporins into synthetic membranes has been studied for the last 10 years in order to enhance the water permeability and selectivity of membranes for water purification; however, there are still limitations such as high costs, difficulties in fabrication of aquaporins, their alignment into synthetic membrane assembly, low stability, and limitations on number of aquaporin molecules that can be introduced into synthetic membranes limit their applicability.

In recent years, concurrent with the work on aquaporin-based biomimetic membranes, there has been an increase in the study of synthesizing molecules with similar structure-function relationships of aquaporins. These artificial channels attempt to mimic the high-water permeability and selectivity of aquaporins, while being synthesized using simple chemistry, being solvent compatible, and requiring less space on the membrane surface which helps to incorporate more channels into the membrane assembly.

The objectives of this study were to first incorporate aquaporins into synthetic nanofiltration membranes without chemical alteration them to prevent flattening or denaturing of aquaporins; then, the second objective was to install functional groups on aquaporins and align them in the direction of water flow; lastly, the third objective was to synthesize artificial channels in order to overcome the issues with aquaporin stability, alignment, and efficient packing of water channels onto the membrane surface.

For the first objective, aquaporins were treated with a polysaccharide, gum Arabic, and incorporated into an amphiphilic polymer, polyvinyl alcohol with alkyl side chains (PVA-alkyl), in order to simulate the natural housing of lipid bilayer for aquaporins and to protect them from denaturing. Long alkyl chains provided the hydrophobic component, while PVA provided the hydrophilic component of the amphiphilic polymer. Membranes modified with aquaporins displayed lower flux declines and higher flux recoveries after reverse flow filtration, along with improved rejection values for both protein and salt solutions as compared to PBI and PBI-PVA-alkyl membranes. However, there was leakage of ions between channels.

Therefore, in order to improve the rejection of protons, ions and other impurities, the channels were aligned with the direction of water flow. Functional groups were installed on Aquaporins using site-directed mutagenesis for covalent attachment to the polymer matrix so that the proteins could be immobilized to the membranes and aligned in the direction of the flow. Aquaporin constructs were modified to bear affinity tags or unique amino acids at the N-terminus of the aquaporin molecule, which was used to facilitate directional immobilization. Each aquaporin monomer was modified with a unique amino acid Cys group at the N-terminus right after the first Met, and due to the aquaporin tetrameric nature, these Cys groups became four anchors for attachment. The presence of these four Cys anchors per aquaporin tetramer was used to attach on the membrane surface in alignment with the feed water flow direction. Membranes modified with mutated aquaporins showed consistently higher salt rejection values of ~70% irrespective of feed concentration, along with higher flux recoveries and lower flux declines. Commercial NF-270 membranes provide a monovalent salt (NaCl) rejection of ~50% and divalent salt ($MgCl_2$) rejection of 97%. Also, approximate coverage of membrane surface with attached aquaporins was calculated using simulation studies. Simulation studies showed that immobilized aquaporins with PVA-alkyl provided a diffusion rate equivalent to 64% coverage on the membrane surface. This showed that aquaporins didn't cover the entire surface area of the membrane. However, immobilized aquaporins were responsible for the rejection of a portion of ions passing through the membrane.

In order to overcome the limitations of aquaporin incorporation into polymer membranes, artificial organic frameworks were added as surface modification on PBI

membranes. Organic frameworks were synthesized as derivatives of hybrid bisamides. The series of bisamides 1-4 consist of 6-amino-pyridine-2-dicarboxylic acid, 6-hydroxymethyl-pyridine-2-carboxylic acid and ethylenediamine, trimethylenediamine, putrescine, and cadaverine depending on the length of carbon chain. These frameworks are amphiphilic in nature and have strong chemical attachment due to the presence of amines and carboxylic acids into each building block. These molecules were introduced into the membrane matrix using carbodiimide chemistry. FTIR results showed the attachment of these bisamide molecules onto the surface of a modified PBI membrane. Also, modified membranes showed a reduced molecular weight cut off (MWCO) for neutral organic molecules.

Overall, membranes modified with aquaporins have shown a potential to provide consistently high salt rejections with increasing feed solutions. Also, preliminary results have shown that bisamide molecules can be attached onto the membrane surface as organic frameworks and have a potential to be an alternative for aquaporins based biomimetic membranes.

KEYWORDS: Aquaporins, Biomimetic Membranes, Bioinspired Membranes, Nanofiltration, Water Treatment.

Priyesh Ashokrao Wagh

(Name of Student)

10/23/2018

Date

SYNTHESIS OF BIOLOGICALLY-INSPIRED NANOFILTRATION MEMBRANES USING PROTECTED, MUTATED, AND SIMULATED AQUAPORINS

By
Priyesh Ashokrao Wagh

Isabel C. Escobar
Director of Dissertation

Stephen Rankin
Director of Graduate Studies

10/23/2018
Date

DEDICATION

To *my parents and my elder brother Jayesh.*

ACKNOWLEDGMENTS

First of all, my sincere gratitude is to my advisor, Dr. Isabel Escobar, who has taught me so much in last 6 years. She has always supported me, motivated me, and taken care of me as her own child. I feel privileged to have an advisor like her who gave me freedom to pursue my ideas and guided me in the right direction during my PhD study. I really admire her wisdom, knowledge, meticulousness, and helpful nature. She always believed in me and gave me a huge emotional support through tough times. She is and will always be my mentor in PhD and in life.

I would like to thank Dr. Dibakar Bhattacharyya for many helpful discussions, and continuous guidance, Dr. Maria Coleman for her useful insights regarding polymer chemistry, Dr. Barbara Knutson for suggesting new ideas and insightful comments throughout my research, Dr. Yinan Wei for providing protein solutions, and helping with characterizations, and Dr. Peter Kekenes-Huskey for helping with simulation studies. I would also like to thank Dr. Viola's group at the University of Toledo for providing protein solutions.

This research and dissertation would not have been possible without the monetary support provided by the KY NSF EPSCoR program, NSF EAGER program, and OH Water Dev Authority. PBI Performance Products, inc provided with the commercial dope solutions throughout this project.

Completing PhD and moving to another university halfway through it would not have been possible without my friends; my family away from home. Particularly, I would like to thank Sneha, Abhinav, Deepesh, Ashish, Saket, Michael, Anup, Abhishek, Ishan, Raghava, Sai, Suraj, Vinod, Prachi, Shreya, Sunitha, Udaka, Godwin, and Yaser for their

continuous support, help, and making this journey memorable. My colleagues at the Center of Membrane Sciences made my life in the lab a lot of fun. Joyner, Max, Conor, Andrew, Derek, Saiful, Sebastián, Rupam, Anthony, Michael, John, and Nathan have played a crucial part in helping me complete my PhD study. Undergraduate and high school students I have worked over the last 6 years have also helped me immensely in research.

Most importantly, all of this would not have been possible without my parents Vandana and Ashok, and my elder brother Jayesh. Their love and support, their sacrifice, and their belief in me have always encouraged me at every step of my life. Words cannot describe my gratitude and my love for them. I owe everything to them.

TABLE OF CONTENTS

Acknowledgements ..... **iii**

List of Tables ..... **ix**

List Of Figures ..... **x**

CHAPTER 1.Introduction **1**

CHAPTER 2. Literature Review **9**

2.1.1 Non-specific channels: 10
2.1.2 Specific channels: 14
2.1.3 TonB dependent receptors or gated channels: 17

2.2 Water transport across cell membrane: 19

2.3 Mechanisms of water transport through aquaporins 22
2.3.1 Electrostatic barrier for proton transport 22
2.3.2 Hydrodynamics of water flow through water channels 24

2.4 Incorporation of aquaporins in synthetic systems 28

2.5 Bioinspired membranes 32

2.6 Applications of aquaporin-based biomimetic membranes: 37

2.7 Nanofiltration membranes and their applications: 40

CHAPTER 3. Research Objectives **44**

3.1 Hypotheses 44

3.2 Objectives 45

CHAPTER 4. Materials and Experimental **49**

4.1 Methodology 49
4.1.1 Glassware and Labware: 49
4.1.2 PBI membranes casting: 49
4.1.3 Surface activation of membranes: 50
4.1.4 Preparation of PVA–alkyl: 52
4.1.4.1 Preparation of carboxy-methyl PVA (PVA-COOH): 52
4.1.4.2 Preparation of PVA-alkyl: 54
4.1.5 AquaporinZ expression and purification: 55
4.1.6 AquaporinZ modification with single cysteine at the N-terminus: 56
4.1.7 Treatment of AqpZ with gum arabic: 57
4.1.8 Surface modification of PBI membrane using Aqp-PVA-alkyl: 58

4.1.9 Chemical attachment of –Cys modified Aqp to PBI backbone: 59
4.2 Membrane characterization: 61
4.2.1 Fourier Transform Infrared Spectroscopy (FTIR): 61
4.2.2 Contact angle measurements: 61
4.2.3 Zeta potential and surface charge analysis 61
4.2.4 Flux analysis: 62
4.2.5 Morphological characterization: 63
4.2.6 Dynamic light scattering: 64
4.2.7 Molecular weight cut off: 65
4.2.8 Depth profiling using XPS: 66
4.2.9 Elemental analysis using TEM: 66
4.2.10 Diffusion studies: 67
4.2.11 Estimation of Aquaporin packing in membrane assembly: 68

CHAPTER 5. A new technique to fabricate high-performance biologically inspired membranes for water treatment 72

5.1 Introduction: 72
5.2 Research Objective: 75
5.3 Methodology: 76
5.3.1 PBI membranes casting: 76
5.3.2 Surface activation of membranes: 78
5.3.3 Preparation of PVA–alkyl: 80
5.3.3.1 Preparation of carboxy-methyl PVA (PVA-COOH): 80
5.3.3.2 Preparation of PVA-alkyl: 82
5.3.4 AqpZ expression and purification: 83
5.3.5 Treatment of AqpZ with gum arabic: 85
5.3.6 Surface modification of PBI membrane using Aqp-PVA-alkyl: 86
5.3.7 Membrane characterization: 87
5.3.7.1 Fourier Transform Infrared Spectroscopy (FTIR): 87
5.3.7.2 Contact angle measurements: 88
5.3.7.3 Flux analysis: 88
5.3.7.4 Morphological characterization: 89
5.4 Results and Discussion: 90
5.4.1 Chemical analysis: 90
5.4.2 Hydrophobicity: 92
5.4.3 Flux analysis: 93
5.4.3.1 Flux profile: 93
5.4.4 Morphological analysis: 104
5.5 Discussion: 106
5.6 Conclusions: 108

5.7 Acknowledgements: 108

CHAPTER 6. Alignment and Immobilization of Aquaporins on Polybenzimidazole Nanofiltration Membranes 110

6.1 Introduction: 110

6.2 Experimental: 112
6.2.1 Materials: 112
6.2.1.1 Polybenzimidazole (PBI): 112
6.2.1.2 PVA-alkyl: 113
6.2.1.3 AquaporinZ modification with single cysteine at the N-terminus: 113
6.2.1.4 AquaporinZ expression and purification: 114
6.2.2 Methodology: 116
6.2.2.1 PBI membranes casting: 116
6.2.2.2 Surface activation of membranes: 116
6.2.2.3 Preparation of PVA–alkyl: 116
6.2.2.4 Chemical attachment of –Cys modified Aqp to PBI backbone: 117
6.2.2.5 Surface modification of PBI membrane using PVA-alkyl: 118
6.2.3 Membrane characterization: 118
6.2.3.1 Dynamic light scattering: 118
6.2.3.2 Molecular weight cut off: 119
6.2.3.3 Contact angle measurements: 120
6.2.3.4 Zeta potential and surface charge analysis: 120
6.2.3.5 Elemental analysis: 121
6.2.3.6 Membrane morphology: 121
6.2.3.7 Flux analysis: 122
6.2.3.8 Diffusion studies: 123
6.2.3.9 Estimation of Aquaporin packing in membrane assembly: 124

6.3 Results: 127
6.3.1 Dynamic light scattering: 127
6.3.2 Molecular weight cut off analysis: 128
6.3.3 Aquaporin attachment verification through elemental analysis: 130
6.3.4 Hydrophobicity: 132
6.3.5 Zeta potential and surface charge analysis: 133
6.3.6 Membrane morphology: 134
6.3.7 Flux analysis: 135
6.3.8 Estimations of aquaporin packing in membrane assembly: 144

6.4 Concluding remarks 148

6.5 Acknowledgements 149

CHAPTER 7. Bisamide-based organic framework for synthesis of membranes with specific molecular weight cutoff 150

7.1 Introduction 150
7.2 Experimental 153
7.2.1 Polybenzimidazole (PBI) membrane preparation 153
7.2.2 Surface functionalization of PBI membranes: 154
7.2.3 PVA-alkyl synthesis: 155
7.2.4 Synthesis of Bisamide molecules 155
7.2.5 Attachment of bisamide channels on PBI membranes surface 158
7.2.6 Fourier transform Infrared Spectroscopy (FTIR) 159
7.2.7 Molecular weight cut off: 159
7.2.8 Contact angle analysis: 160
7.2.9 Flux and selectivity experiments 160
7.3 Results 161
7.3.1 Chemical analysis using FTIR 161
7.3.2 Molecular weight cut off analysis: 164
7.3.3 Contact angle analysis: 166
7.3.4 Flux analysis 167
7.4 Concluding remarks 169
7.5 Acknowledgements 170
CHAPTER 8. Conclusions And Recommendations 171
8.1 Conclusions 171
8.2 Recommendations 174
Appendices 176
Appendix A. Flux Data for membranes: 176
Appendix B. Elemental analysis: 194
Appendix C. Diffusion Data 200
Appendix D. Simulation input files and generated Data 201
References 212
VITA 229

LIST OF TABLES

Table 2-1 Outer membrane non-specific channel proteins in wild type and K-12 mutants of *E. Coli* 12
Table 2-2 Specific channel proteins in cell membrane 15
Table 2-3 Iron chelate receptors and gated channels in the outer membrane 18
Table 2-4 Recent approaches followed for synthesis of aquaporin based biomimetic membranes 30
Table 2-5 Applications of Aqp-based biomimetic membranes, design approach and their performance 37
Table 2-6 Applications of NF membranes and their performance 41
Table 4-1 Neutral solutes used for molecular weight cut off analysis and their Stokes-Einstein radii in nm [25, 229-232] 65
Table 5-1 Functional groups and corresponding wave numbers in IR spectra. 91
Table 5-2 Protein rejection and flux recovery comparisons. 97
Table 5-3 Rejection and flux recoveries for protein filtrations 100
Table 6-1 Neutral solutes used for molecular weight cut off analysis and their Stokes-Einstein radii in nm [25, 229-232] 120
Table 6-2 Rejections obtained for unmodified PBI, PBI-CMBA and Aqp-SH modified PBI membranes 130
Table 6-3 Elemental composition of elements in PBI-COOH membrane 131
Table 6-4 Elemental composition of elements in Aqp-SH modified PBI membrane 131
Table 6-5 Hydrophobicity via contact angle 133
Table 7-1 Neutral solutes used for molecular weight cut off analysis and their Stokes-Einstein radii in nm [25, 229-232] 160
Table 7-2 Functional groups and corresponding wave numbers in IR spectra. 162
Table 7-3 Rejections obtained for unmodified PBI, and Bisamide-modified PBI membranes 166
Table 7-4 Hydrophobicity via contact angle 167

LIST OF FIGURES

Figure1-1 Biological cell membrane separation strategies [20] 2
Figure2-1 Structure of Ompf porin of *Escherichia Coli* (*E. Coli*). (a) top view of Ompf trimer. (b) side view of the monomer (c) top view of Ompf monomer, showing the constricted region of the channel. The constricted region is formed by Glutamic acid117 (E117), Aspartic acid113 (D113), Lysine16 (K16), Arginine42 (R42), Arginine82 (R82), and Arginine132 (R132) [24] 11
Figure2-2 structure of LamB protein (a) side view of LamB monomer (b) top view of the LamB monomeric unit. The greasy slides: Tyrosine41 (Y41), Tyrosine6 (Y6), Tryptophan420 (W420), Tryptophan358 (W358), and Phenylalanine227 (F227) are shown as blue stick diagrams. Tyrosine118 (Y118) constricts the diffusion channel (shown in yellow). (c) side view of the monomer with greasy slide and interaction of greasy slide with maltotriose [24]. 15
Figure2-3 TonB-dependent uptake of iron chelate complex through iron receptor [13].. 18
Figure2-4 Illustration of Grotthuss mechanism and reorientation of water molecules while passing through AQP pore [15]. 21
Figure2-5 Mechanisms of water transport through Aquaporin. Amino acids responsible for this highly selective water transport are Histidine 180 (his 180), Arginine 185 (arg185), Asparagine 192 (asn192), and Asparagine 76 (asn 76) [14]. 22
Figure2-6 All-atom simulation system used to quantify electrostatic barrier in an aquaporin monomer [12] 23
Figure2-7 Macroscopic hydrodynamics following Hagen-Poiseuille equation with no-slip flow on the left and single-file flow in an AQP channel with perfect slip [7] 25
Figure2-8 Unitary water permeability values of various single-file water channels as calculated by finkelstein's model [9] 26
Figure2-9 Plot of unitary water permeability of water channel proteins against the available number of hydrogen bonding sites in the single-file region of pore walls [8-10] 27
Figure2-10 Types of artificial channels and their applications [1-6] 36
Figure4-1 CMBA modification of membrane. 51
Figure4-2 PVA-COOH synthesis. 54
Figure4-3 PVA-alkyl synthesis. 55
Figure4-4 schematic of cysteine attachment at the n-terminus of aquaporins 57
Figure4-5 (a) and (b) carbodiimide membrane activation chemistry 59
Figure4-6 chemical attachment of AQP-SH to –COOH modified PBI membranes 60
Figure4-7 contact angle measurement [227] 61
Figure4-8 Diffusion cell assembly with 1000 ppm NaCl and DI water in two compartments separated by membrane. 68
Figure5-1 Schematic of biomimetic membranes 75
Figure5-2 PBI molecule structure. 76
Figure5-3 CMBA modification of membrane. 79

Figure5-4 PVA-COOH synthesis. 82
Figure5-5 PVA-alkyl synthesis. 83
Figure5-6 SDS-PAGE showing purification of AQPz with the protein band migrating at 22 kda. 85
Figure5-7 (a) and (b) carbodiimide membrane activation chemistry 87
Figure5-8 Contact angle measurement [227]. 88
Figure5-9 FTIR analysis of unmodified, CMBA modified and PVA-alkyl modified membranes. 91
Figure5-10 AQPz-PVA-alkyl modified PBI molecule. 92
Figure5-11 Hydrophobicity via contact angle 93
Figure5-12 Flux analysis of unmodified PBI membrane. 95
Figure5-13 Flux analysis of PVA-alkyl modified PBI membrane. 96
Figure5-14 Flux analysis of AQPz-PVA-alkyl modified PBI membranes. 96
Figure5-15 Flux analysis of unmodified PBI membranes. 98
Figure5-16 Flux analysis of AQPz modified PBI membranes. 99
Figure5-17 Sodium Chloride and Calcium Chloride filtration rejection. 102
Figure5-18 (a), (b) and (c) SEM images of cross sectional areas of unmodified PBI, PVA-alkyl and PVA-alkyl-AQPz modified PBI membranes. 104
Figure5-19 (a) and (b) SEM image of surface area of unmodified PBI membrane and PVA-alkyl-AQPz modified PBI membrane respectively 105
Figure5-20 (a) and (b) SEM image of surface area of unmodified PBI membrane and PVA-alkyl-AQPz modified PBI membrane respectively after filtration 106
Figure6-1 Cys modified aquaporin molecule 111
Figure6-2 Attachment of AQP-SH to –COOH modified PBI membrane 112
Figure6-3 Schematic of cysteine attachment at the n-terminus of aquaporins 114
Figure6-4 Chemical attachment of AQP-SH to –COOH modified PBI membranes 118
Figure6-5 Diffusion cell assembly with 1000 ppm nacl salt solution on one side and di water on other side. Both compartments are separated by a membrane. 124
Figure6-6 Size measurement of AQP-SH by dynamic light scattering 128
Figure6-7 Molecular weight cut off analysis of unmodified PBI, -COOH modified PBI, and PVA-alkyl modified PBI membranes 129
Figure6-8 Zeta potential values of unmodified PBI, PBI-CMBA, and AQP-SH modified PBI membranes over a ph range of 2-10 134
Figure6-9 Cross sectional cut out of the modified membrane using fib 135
Figure6-10 (a), (b), (c), and (d). Flux analyses of (a) unmodified PBI, (b) PVA-alkyl modified PBI, (c) inactive AQP-SH modified PBI membranes and (d) AQP-SH modified PBI membranes at constant pressure of 70 psi (4.83 bar) 139
Figure6-11 Flux linearity and permeability consistency for unmodified PBI and AQP-SH modified PBI membranes 141
Figure6-12 Sodium chloride and calcium chloride filtration rejection 143
Figure6-13 Predictions and experimentally measured effective diffusion coefficients, based on the geometry in Figure6-14. Black lines correspond to experimental data found in table c.1 in appendix c. Blue lines represent aggregate (solid) and

monomeric (dots) AQP models, respectively. The red vertical line marks the packing fraction at which both AQP configurations agree with experimental data (~64% packing fraction). 147
Figure6-14 Representative simulation geometry of membrane occluded by aquaporin (AQP) aggregate. In this picture, the left reservoir contained 1000 ppm nacl solution while right reservoir was di water (0 m). Aggregate was simulated by cylinders of increasing diameter overlayed onto membrane surface. The effective ion diffusion rate was obtained by integrating the concentration gradient along the membrane surface. 147
Figure7-1 Schematic representation of Bisamide molecules synthesized by Bera et al.[11] 152
Figure7-2 (a) and (b) Schematic of incorporation of artificial Bisamide molecules onto the membrane surface via carbodiimide chemistry and hydrogen bonding between Bisamide molecules 153
Figure7-3 Structure of Bisamide monomer with 5 carbon atom chain..... 156
Figure7-4 (a) and (b) Synthesis reactions for the formation of Bisamide channel with 2 carbon atoms chain length 157
Figure7-5 Covalent attachment of Bisamide channels on –COOH modified PBI membrane..... 158
Figure7-6 FTIR analysis of unmodified, CMBA modified and PVA-alkyl modified membranes. 162
Figure7-7 Bisamide modified PBI molecule 163
Figure7-8 Molecular weight cut off analysis of unmodified PBI, PVA-alkyl modified PBI, and Bisamide-modified PBI membranes. 165
Figure7-9 Flux analyses of unmodified PBI, PVA-alkyl modified PBI, and Bisamide-modified PBI membranes at constant pressure of 70 psi (4.83 bar) 168

CHAPTER 1. INTRODUCTION

A typical cell consists of cell membrane, mitochondria, golgi complex, lysosomes, endoplasmic reticulum, ribosomes, plastids, peroxisomes, cilia, flagella, nucleus, and the cytosol. The cell membrane is composed of the plasma membrane and an inner membrane, which act as the protection system of the cell components against macromolecules such as proteases[16], larger oligopeptides, neutral sugars with molecular weights more than 600 Da, and hydrophobic dyes and antibiotics [17]. However, this protection system allows certain small biomolecules and entities, such as mono- and disaccharides and nucleosides, into the cytoplasm for proper functioning of the cells (Figure 1-1). This system acts as a molecular sieve with various proteins, called porins, that allow rapid diffusion of small molecules across the membranes acting as the sieves [18]. Porins can provide a size exclusion ranging from 600 Da to 5000 Da, and they form a major integral component of the cell membrane making it a molecular sieve [19].

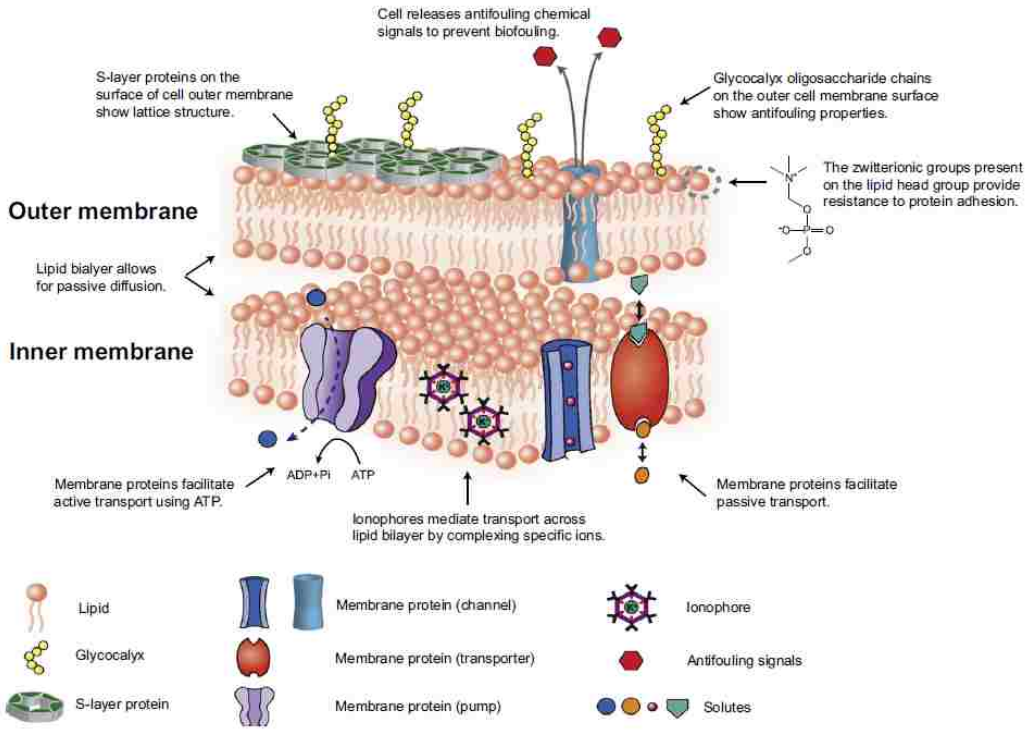

Figure 1-1 Biological cell membrane separation strategies [20]

Porins can be divided into three main categories: (1) non-specific or general porins, (2) specific channels, and (3) high-affinity, energy-dependent transport systems. Non-specific or general porins allow nonspecific and spontaneous diffusion of small molecules through cell membrane. Specific channels have ligand-binding sites and have facilitative transport of specific ligands. High-affinity, energy-dependent transport systems carry out energy-intensive translocation of large nutrients present in very small amount outside cell membrane [21, 22].

The first class of porins is known as non-specific or classical porins. These porins allow the influx of small, hydrophilic nutrients at very high permeability, while rejecting larger lipophilic molecules [22]. An example of classical porins is outer membrane protein F (OmpF). The monomeric unit of OmpF acts as a size-selective membrane with

a molecular weight cut off of 600 Da. The three-dimensional structures of these porins determine their function and properties, and transport of various entities through these porins is highly affected by physical properties, and charge [23]. These porins have preference for neutral and positively charged molecules over negatively charged ones [22, 24]. Incorporating these porins into synthetic polymeric membrane can potentially improve membrane selectivity while attaining greater water permeability as compared to conventional ultrafiltration membranes [25].

However, some of nutrients are too large to go through non-specific porins or too slow to get transported through them; thus, in order to allow these nutrients to be transported into the cell, a second class of porins exists, which comprises of specific porins present in cell membranes. These specific porins have stereospecific ligand-binding sites that facilitate the transport of a particular entity through these channels [23, 24]. An example of the specific porins is maltose outer membrane protein, Phage Lambda (LamB) that facilitates the influx of maltose and higher oligosaccharides of the maltose series into the cell [24, 26]. LamB is not very discriminating among monosaccharides, but becomes more selective for larger saccharides [23]. The permeability for maltose and higher oligosaccharides through LamB is much higher than through non-specific porins. Also, the diffusion rate of these oligosaccharides through LamB is not affected even in low concentrations [24].

The third class of porins is comprised of high affinity transporters where the ligands are bound strongly with high energy intensity, and catalyze active transport across the cell membrane. These transporters carry out uphill transport through energy coupling via TonB protein [27]. An example of such transporters is ferrichrome receptor

FhuA. FhuA binds to the ferrichrome ligands and transports those ligands through an interaction with TonB. [28]. The ß-barrel in these monomeric receptors is composed of 22 strands, the N-terminal portion of the protein consists of 150 to 200 residues that are inserted into the barrel. These residues form a “plug” for ligands to bind [24]. Binding of these ligands induces conformational changes in the receptor and in turn promote TonB to contact the receptor physically. TonB transduces energy, enabling further changes in the receptor such that the affinity for ligand is decreased, and ligand enters the periplasm. TonB dissociates from the receptor after this detachment [13].

Along with nutrients, minerals, and sugars, water is also an integral part of all living systems [29], and it is the major component of cells and of surrounding extracellular spaces. The organization of water and its flow across the cells within biological compartments is fundamental to life. Water must be able to flow not only into and out of the cell, but also into and out of all sub-cellular compartments [30]. In order to provide water to all cells and their sub-cellular components, cell membranes contain lipid bilayers through which water can be transported via diffusion; however, diffusive permeability is fairly low, so lipid bilayers are not solely responsible for the actual water flow across cells. This higher flow of water through cells is provided by membrane proteins present in the cell membrane. These transmembrane proteins have a specific three-dimensional structure with pores that provide a pathway for water permeation across cell membranes [30]. In 1992, Peter Agre and coworkers discovered a 28kDa “water channel” protein responsible for this high transport of water across the cells, and named it aquaporin [31-33]. Since 1992, hundreds of water channels proteins have been discovered in organisms from all kingdoms of life [30].

Aquaporins possess a high capacity of water permeation based on an osmotic gradient driving force, while being completely selective for water and preventing the passage of ions and other solutes including protons [29, 34, 35]. A unique hourglass shaped structure, conserved hydrogen bonding groups from asparagine-proline-alanine (NPA) signature motifs, and a pore diameter of 3 A^o that is large enough to transport single chain of water molecules (size exclusion) allow aquaporins to selectively transport water through cell membranes with a high permeability and selectivity [36-39]. Since the discovery of aquaporins, these proteins have been of great interest in the field of synthetic membrane separations. Membrane separation processes are widely used for various applications owing to their ability to produce desired water quality, high stability, efficiency, smaller footprint compared with conventional water treatment technologies. However, membranes suffer from selectivity-permeability trade-off, inherent materials limitations, performance decline and cleaning requirements [40, 41]. Learning from nature and adapting those concepts into synthetic systems has become a popular philosophy in scientific communities through biomimetics and bioinspiration [42].

The term biomimetics was introduced in the 1960s, and it refers to the study of the structures and functions of biological systems as models for synthetic systems in order to enhance the performance of synthetic systems with respect to various parameters [42]. Biomimetics is essentially limited to copying or imitating the solutions nature has adapted over the course of billion years. In this context, aquaporins represent a new material, which can provide high selectivity and permeability as compared to traditional synthetic systems. Thus, in theory, one would be able to completely reject all the solutes, including ions and protons except water if functional aquaporins were successfully

incorporated with proper orientation into synthetic membrane systems. Inspired by this concept, Kumar et al. incorporated aquaporins into polymersomes with water permeability through these polymersomes up to two orders of magnitude higher than commercial membranes and at an almost perfect selectivity [43].

Since the introduction of biomimetics using aquaporins into the field of membrane separations, a number of approaches have been developed to incorporate aquaporins in synthetic membranes in order to improve the selectivity of membranes towards water [20, 40, 43-58]. Biomimetic membranes have three main components: aquaporins, amphiphilic molecules where aquaporins are reconstituted, and a polymer support. The amphiphilic molecules can either be a lipid bilayer or an amphiphilic polymer. Amphiphilic polymers are shown to have more stability and flexibility and hence are more widely used to synthesize biomimetic membranes [59, 60]. The goal has been to fabricate biomimetic membranes that are as stable, robust, scalable and cost-effective as already established technologies [61]. At the commercial level, the Aquaporin Inside^{TM} flat sheet is the first thin film commercial forward osmosis membrane fabricated with aquaporins incorporated in its polyamide selective layer [62]. These commercial membranes have been synthesized using conventional interfacial polymerization, where aquaporin-based proteoliposomes were dispersed in the aqueous solution. These membranes incorporated with proteoliposomes have shown water permeability values greater than 4 LMH/bar and salt rejection values of more than 96% [47].

However, there are certain challenges that are associated with incorporating aquaporins into synthetic assembly with respect to synthesis, stability and functioning of

the membranes. One of the challenges is high costs involved in the expression and purification of aquaporins on a large scale. Another challenge is scalability of current approaches to synthesize biomimetic membranes on a large scale [61]. Along with the work going on in the field of biomimetic membranes based on aquaporins, there has been an increase in the research associated with bioinspired materials [4]. A number of artificial structures with similar structure-function relationships of aquaporins have been introduced in the recent years. These structures have the potential to overcome the aforementioned challenges in the commercialization of biomimetic membranes [4].

Biomimetic and bioinspired membranes is one of the most promising scientific and technological challenges in coming years. Extensive research has been carried out in order to incorporate a number of biological molecules into synthetic systems to enhance their performance. However, the structure-functional relationships of biological systems need to be explored fully in order to strengthen the technological development in the field of biomimetic membranes. Also, the cost involved in large-scale expression of biological molecules and synthesis of biomimetic and bioinspired membranes should be reduced significantly. In summary, the future of aquaporin-based biomimetic and bioinspired membranes will be based on what can be understood in terms of structure-functional relationships of aquaporins, how can uniform and narrowly distributed pores with higher level of imitation be recreated, and how can biomimetic and bioinspired membranes be fabricated on a commercial scale [61].

This study is focused on synthesis of biomimetic nanofiltration membranes with protected and immobilized aquaporins, as well as on synthesis of bio-inspired membranes with artificial water channels imitating the structure-function relationships of aquaporins.

The objectives of this study were to first incorporate aquaporins into synthetic nanofiltration membranes without chemically altering them to prevent flattening or denaturing of aquaporins during operation. Then, the second objective was to install functional groups on aquaporins and align them in the direction of water flow. Lastly, the third objective was to synthesize artificial channels in order to overcome the issues with aquaporin stability, alignment, and efficient packing of water channels onto the membrane surface. Membranes synthesized here had as a primary goal to match or exceed the permeability of ~11 LMH/bar and a divalent salt rejection of 97% of commercially-available NF-270 membranes [62, 63].

CHAPTER 2. LITERATURE REVIEW

2.1 Diffusion channels in bacterial cell membrane

Bacterial cells consist of a cell wall, cytoplasm, nucleus, endoplasmic reticulum (ER), ribosomes, golgi body apparatus, lysosomes, mitochondria, vacuoles, and cilia and flagella [64]. The cell wall of gram positive bacteria has several layers of peptidoglycan with teichoic acid molecules perpendicular to the layers of peptidoglycan. Gram negative bacteria have a cell wall with a single layer of peptidoglycan surrounded by outer membrane [65], which allows selective passage of nutrients from the outside in and waste products from the inside of cell out. The cell membrane is composed of three layers; the outer membrane, the peptidoglycan cell wall, and the inner membrane [66]. The outer membrane is made of lipid bilayers, which show little permeability for hydrophilic solutes, including most nutrients. Therefore, these lipid bilayers are embedded with protein channels to provide influx of nutrients and removal of waste products.

The proteins present in the outer membrane are categorized into two classes, lipoproteins and ß barrel proteins. Lipoproteins contain lipid moieties attached to an amino terminal cysteine residue[67]. These proteins are embedded in the inner leaflet of the outer membrane and hence are not considered as transmembrane proteins. There are three main categories of transmembrane proteins: (1) non-specific or general porins, (2) specific channels, and (3) high-affinity, energy-dependent transport systems. Non-specific or general porins allow nonspecific and spontaneous diffusion of small molecules through cell membrane. Specific channels allow facilitative transport of

specific ligands via ligand-binding sites. High-affinity, energy-dependent transport systems carry out energy-intensive translocation of large nutrients present in very small amount outside cell membrane [21, 22].

2.1.1 Non-specific channels:

Nearly all of the transmembrane proteins of the outer membrane are ß barrel proteins. These proteins are essentially ß sheets with a cylindrical conformation. Some of these outer membrane proteins (OMPs), such as classical or non-specific porins, regulate the uptake of nutrients and disposal of waste products via passive diffusion. Porins have monomer molecular weights in the range of 28000 to 48000 Da. They exist as trimers where each monomer acts as an individual channel (Figure 2-1). These proteins are present in abundance in the outer membrane; there are approximately 250,000 copies of OMP per cell [68]. The expression of these porins depends on growth conditions. For example, OmpF and OmpC are regulated by osmotic pressure and temperature. OmpF, OmpC, and PhoE porins are highly homologous with 63% sequence identity [68]. OmpF and OmpC are weakly cation selective whereas PhoE is weakly anion selective porin [69]. The interior of the porins contains charged amino acids lining the inner pore walls (Figure 2-1), while the number and position of these charged entities with respect to the most constricted portion of the porin channel determines ion selectivity of the channel [70]. These ion selectivities are the strongest determinants of the sieving properties of the porins for antibiotics of different charges. These porins have distinct channel conductances and voltage gating behaviors when they are incorporated into lipid bilayers. OmpF, OmpC, and PhoE show conductance of 0.8, 0.5, and 0.6 nS in 1M salt,

respectively. Also, the threshold potentials observed are 90, 160 and 100 mV, respectively, above which the channels close [71, 72].

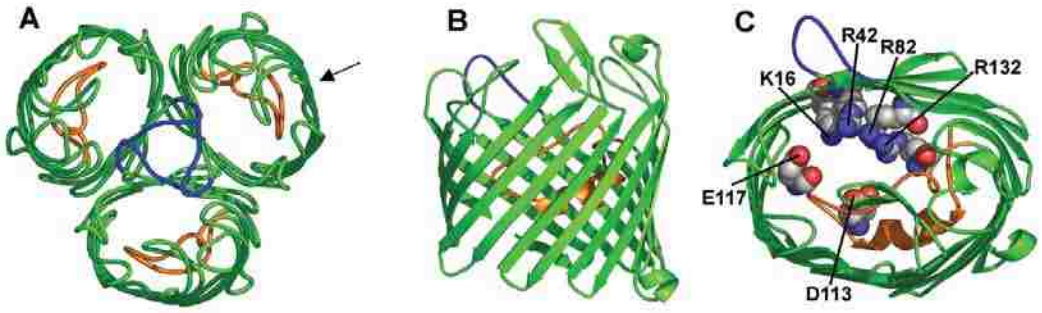

Figure 2-1 Structure of OmpF porin of *Escherichia Coli* (*E. coli*). (A) Top view of OmpF trimer. (B) Side view of the monomer (C) Top view of OmpF monomer, showing the constricted region of the channel. The constricted region is formed by Glutamic acid117 (E117), Aspartic acid113 (D113), Lysine16 (K16), Arginine42 (R42), Arginine82 (R82), and Arginine132 (R132) [24]

Diffusion of solute molecules passing through porin channels is strongly affected by their lipophilicity. Cationic and anionic amino acid residues located in the opposite sides in the most constricted region of the channels are responsible for the retarded diffusion of lipophilic solutes. Due to this structure of the constricted region, water molecules are oriented in a highly directional manner, making the disruption of this ordered structure by hydrophobic solutes unfavorable in terms of energy [73-75].

Molecular dynamics simulation studies of OmpF porin have shown that the channel is remarkably efficient in the transport of cations even in micromolar solutions. The constriction of the channel is very stable and water molecules are highly ordered in the constriction region. Cations bind to the anionic side chain of the constriction region

and this binding plays a significant role in the permeation of cations over anions. Therefore, the transport of cations through these non-specific porins is also through a binding mechanism similar to specific porins. This shows that the difference between non-specific and specific porins is quantitative rather than qualitative [76, 77]. Some other outer membrane proteins present in *E. Coli* are listed in Table 2-1.

Table 2-1 Outer membrane non-specific channel proteins in wild type and K-12 mutants of *E. Coli*

Porin	**Bacteria**	**Function**	**Reference**
OmpF	*E. Coli*	Diffusion of small cations, pore diameter 1.2 nm	[24, 25]
OmpC	*E. Coli*	Transport of small cations, pore diameter 1.0 nm	[24]
PhoE	*E. Coli*	Transport of small anions, pore diameter 1.1 nm	[24]
NmpC	*E. Coli K-12 mutant*	Similar to OmpF and OmpC, pore diameter 1.0 nm	[78, 79]

OmpN	*E. Coli K-12 mutant*	Similar to OmpF and OmpC	[79]
OmpG	*E. Coli K-12 mutant*	Unusually large channel with monomeric form (uptake of large oligosaccharides)	[24, 80]
OmpW	*E. Coli*	Used as a receptor by a colicin, relatively small in size	[24, 81]
OmpX	*E. Coli*	Promotes bacterial adhesion to mammalian cells	[82]
OmpT	*E. Coli*	Secretion of colicins	[83, 84]
OmpLA	*E. Coli*	Cleavage of ferric enterobactin receptor protein	[85]

2.1.2 Specific channels:

The second class of transmembrane proteins are specific porins that catalyze the spontaneous diffusion of specific classes of nutrients. An example of this class of porins is phage lambda receptor (LamB) protein of *E. coli*. LamB facilitates the influx of maltose and higher oligosaccharides of the maltose series. The permeability for maltose and large oligosaccharides observed through LamB is much higher than other porin channels [86]. Also, the diffusion rates through non-specific porin channels are proportional to the difference in concentration across cell membrane. As a result, the rates become very low as concentration drops below millimolar level. However, the diffusion rate is not affected in LamB even at low concentrations [24].

Each subunit within the LamB trimer has a ß barrel containing 18 transmembrane ß-strands as compared to 16 ß-strands in classical porins. The pore of LamB is more constricted than those porin channels owing to the infolding of 2 additional loops [87, 88]. However, in order to facilitate the transport of maltose and derivatives, the entire length of inner wall consists of six aromatic residues, which is called greasy slide (Figure 2-2). Sugar residues in maltose and other oligosaccharides interact with this greasy slide via van der Waals forces [89, 90]. Also, there are many charged residues at the constriction region that form hydrogen bonding with the hydroxyl groups in sugars [91]. Thus, LamB channel is a specific channel that facilitates wide variety of carbohydrates when they are present in low concentrations. Table 2-2 shows examples of other specific channels.

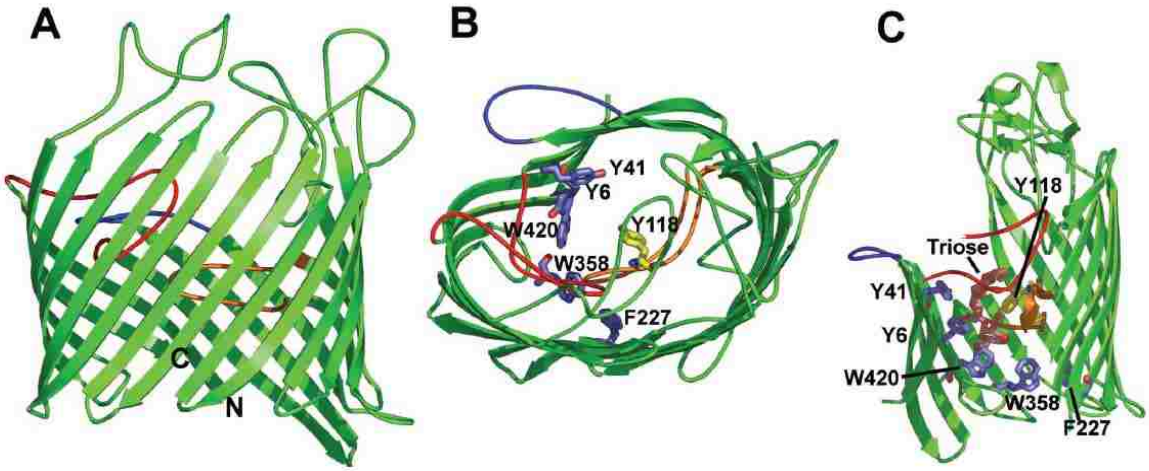

Figure 2-2 Structure of LamB protein (A) Side view of LamB monomer (B) Top view of the LamB monomeric unit. The greasy slides: Tyrosine41 (Y41), Tyrosine6 (Y6), Tryptophan420 (W420), Tryptophan358 (W358), and Phenylalanine227 (F227) are shown as blue stick diagrams. Tyrosine118 (Y118) constricts the diffusion channel (shown in yellow). (C) Side view of the monomer with greasy slide and interaction of greasy slide with maltotriose [24].

Table 2-2 Specific channel proteins in cell membrane

Protein	**Bacteria**	**Function**	**Reference**
Sucrose channel (ScrY)	*E. Coli, Salmonella*	Utilize sucrose as a carbon source, allows rapid diffusion of large variety of sugars	[92-95]

Aryl-ß-D-glucoside channel (BglH)	*E. Coli*	Degradation of aryl-ß-glucoside	[96]
Receptor protein of phage T6 (Tsx)	*E. Coli*	Nucleoside transport, uptake of antibiotic albicidin	[97, 98]
Cytochrome protein (CymA)	*Klebsiella oxytoca*	Exists as monomers, binds cyclodextrins at high affinity	[99, 100]
Long chain fatty acid outer membrane protein (FadL)	*E. Coli*	Efficient utilization of long-chain fatty acids as carbon source	[101, 102]
TbuX channel	*Ralstonia picketii*	Diffusion of Toluene	[103]
XylN channel	*P. putida*	Diffusion of m-xylene	[104]
SalD channel	*Acinetobacter*	Diffusion of salicylate ester	[105]
CymD channel	*P. putida*	Diffusion of p-cymene	[106]
KdgM channel	*Erwinia*	Diffusion of	[107]

	chrysanthemi	oligogalacturonate	

2.1.3 TonB dependent receptors or gated channels:

Iron is particularly important for living cells due to its importance in cellular metabolism. It is a constituent of enzymes that play a vital role in oxygen metabolism, electron transfer, RNA synthesis, and dissolution of reactive oxygen intermediates [13, 108]. Iron complexes originated from microbes and vitamin B_{12} are larger than the pore diameter of non-specific channels. For a bacterial cell membrane, having a specific channel large enough for these complexes to go through poses a challenge of compromising the resistance of bacterial system to environmental toxic compounds. In order to transport these complexes through cell membranes, there are receptors in the outer membrane of a bacterial cell [24]. Some examples of these receptors include BtuB for vitamin B_{12}, and receptors for Fe^{+3} chelator complexes (FhuA for ferrichrome, FepA for Fe^{+3} enterobactin, FecA for Fe^{+3} citrate, FhuE for Fe^{+3} coprogen, and Cir for Fe^{+3} catecholates, IroN for Fe^{+3} salmochelin and Fiu for Fe^{+3} dihydroxybenzoylserine) [109, 110].

These receptors bind to the ligand with high affinity. The transport of complexes through the cell membrane, however, requires the protein TonB, which spans the thickness of periplasm (Figure 2-3) [13]. The TonB-dependent receptors transport chelated iron with maximum efficiency at very low concentrations of ligand. This characteristic distinguishes them from non-specific porins. From the periplasm, they carry out this transport into the cytoplasm using an ATP-dependent mechanism which

distinguishes them from specific channels. These TonB-dependent uptake systems enable bacterial growth in a wide range of iron-limited environments [28]. These

systems are also considered as targets for novel antibiotics because of their contribution to the specific permeability of the cell envelope [111]. Some examples of receptors and gated channels are listed in Table 2-3.

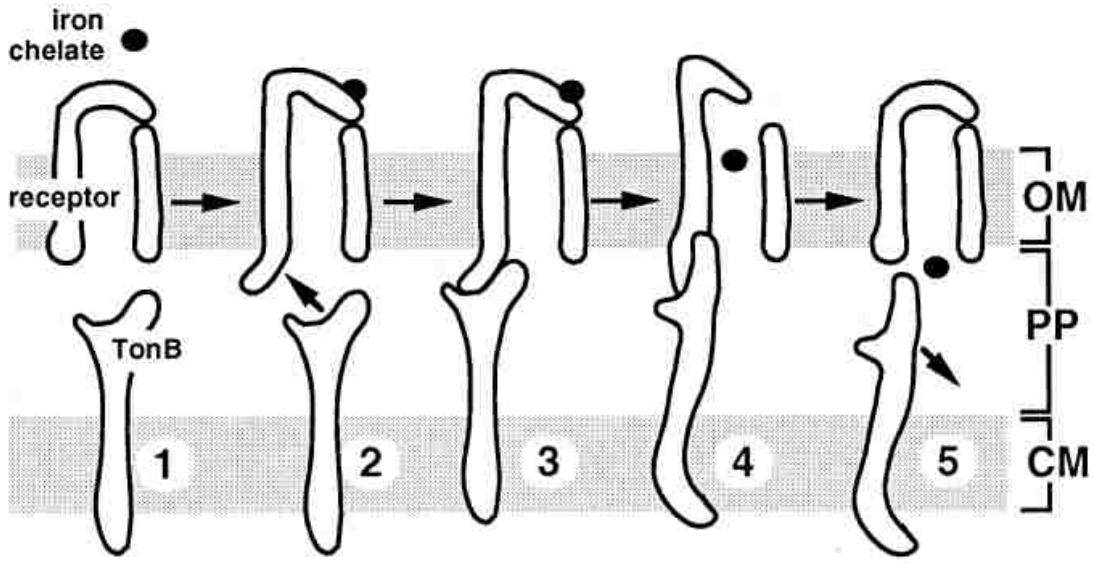

Figure 2-3 TonB-dependent uptake of iron chelate complex through iron receptor [13]

Table 2-3 Iron chelate receptors and gated channels in the outer membrane

Receptor	**Bacteria**	**Uptake**	**Reference**
BtuB	*E. Coli*	B_{12}	[24, 27]
FhuA	*E. Coli*	Ferrichrome	[109]

FepA	*E. Coli*	Fe^{+3} enterobactin	[109, 112]
FecA	*E. Coli*	Fe^{+3} citrate	[13]
FhuE	*E. Coli*	Fe^{+3} coprogen	[28, 108]
Cir	*E. Coli*	Fe^{+3} catecholates	[28]
IroN	*E. Coli*	Fe^{+3} salmochelin	[110]
Fiu	*E. Coli*	Fe^{+3} Dihydroxybenzoylserine	[28]

2.2 Water transport across cell membrane:

In addition to nutrients, hydrophilic molecules, and complexes, water gets transported through cell membranes at a very high permeability via water channel proteins, known as aquaporins (Aqp). Aquaporins are not porins similar to the ones previously described here; rather, they are helix bound proteins. The structure and functions of aquaporins have been studied extensively in the last two decades [9, 30, 35-37, 113-124]. More than 450 homologs of aquaporins are found in bacterial and mammalian cells [125]. Aqp1 is the first recognized and characterized homolog, and it is found in abundance and actively in mammalian red cells, renal proximal tubules, and other epithelia [126]. Aqp2 and Aqp3 are found in the renal collecting duct, and they are regulated by vasopressin and are permeable to glycerol [127-131] . Other aquaporins are found in brain (Aqp4) [132, 133], salivary and lacrimal glands, cornea, and lung (Aqp5)

[134], and a weak water transporter is in eye lens (Aqp0) [135]. The homolog of aquaporins found in *E. Coli* is aquaporinZ (aqpZ) and is responsible for water transport through cell membrane [113].

Aquaporins are present in cell membrane in the form of tetramers with each monomer acting as an individual channels. They selectively transports water in and out of the cell at a rate of 10^9 water molecules/second per monomer, while rejecting solutes and ions present in it [136]. This ability of aqps to transport water with extremely high selectivity and permeability results from their unique hour-glass shape [123]. Aqps have a conserved aromatic/arginine (Ar/R) region in the constriction site of the channel. The pore diameter at this constriction is 3 A^o, which is slightly bigger than the diameter of water molecule (2.8 A^o), so all solutes larger than water molecules are rejected by size exclusions [14].

Water travels through the channels of aquaporins as a single file of molecules. However, in an aqueous solution, there is hydrogen bonding between two adjacent water molecules that allows free movement of protons between molecules. This phenomenon is called as Grotthuss Mechanism [137]. This phenomenon is responsible for the formation of H^3O^+ ions. Thus, a single file of water molecules through aqp is expected to transport a proton with it by acting as a proton wire. However, due to the presence of highly conserved asparagine-alanine-proline (NPA) motifs present on the inner walls of aqp pores, every water molecule passing through the pore has to form a series of hydrogen bonds with the aquaporin residues. This hydrogen bonding leads to reorientation of water molecules causing the breakage of proton wire (Figure 2-4) [136]. In the constricted region of aqp, arginine and histidine, provide fixed positive charges to prevent the

passage of any positively charged solute present in water [39]. Figure 2-5 illustrates all the mechanisms of water transport through Aqp channel.

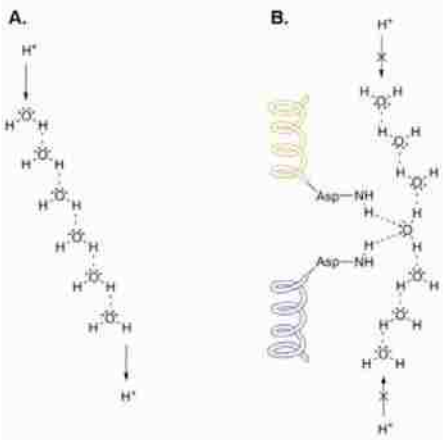

Figure 2-4 Illustration of Grotthuss mechanism and reorientation of water molecules while

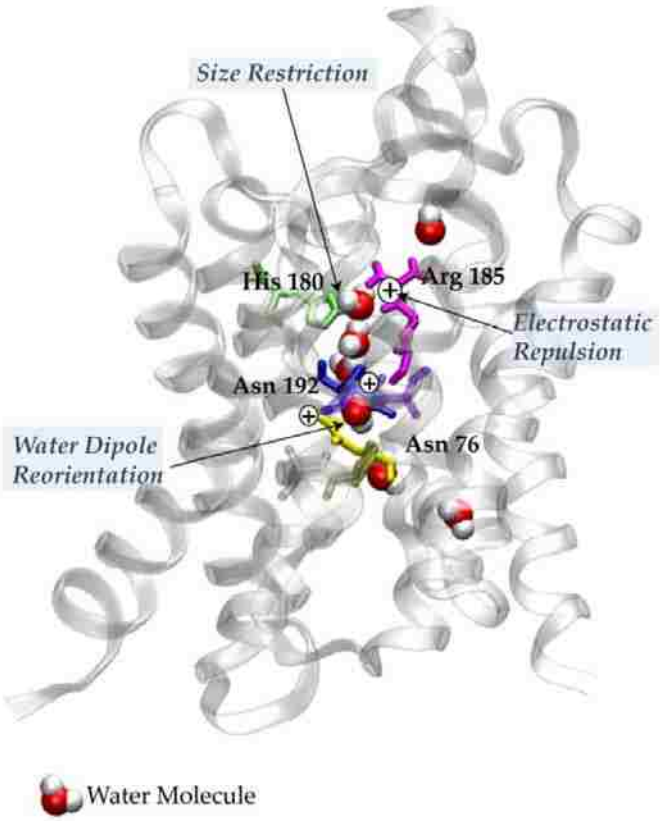

Figure 2-5 Mechanisms of water transport through Aquaporin. Amino acids responsible for this highly selective water transport are Histidine 180 (His 180), Arginine 185 (Arg185), Asparagine 192 (Asn192), and Asparagine 76 (Asn 76) [14].

2.3 Mechanisms of water transport through aquaporins

2.3.1 Electrostatic barrier for proton transport

The pores of aquaporins have a constriction in the middle and become wide at the opening. Protons are prevented from their passage through aquaporins via hydrogen bond disruption between adjacent water molecules and the electrostatic barrier. A number of studies have been done in order to understand the origin of this electrostatic barrier and magnitude [12]. Some studies have shown that NPA motif present in aqp is responsible for this electrostatic barrier [138, 139]. Burykin and Warshel carried out the evaluation of electrostatic free energies using the free-energy perturbation (FEP) method [12]. FEP has been used extensively in free energy calculations for biological systems [12]. It uses the relation of free energy with the change of potential surface from U_1 to U_2 by gradually changing the potential surface as shown in equation (2-1):

$$U_m\lambda_m = U_1 (1-\lambda_m) + U_2\lambda_m \quad (2\text{-}1)$$

Where λ_m is a parameter that changes between ($0 \leq \lambda_m \leq 1$), and U_m is potential surface at point m.

The overall free energy is then calculated by changing λ_m in n equal increments and evaluating the sum of the corresponding δG as given by equation (2-2):

$$\Delta G\ (U_1 \rightarrow U_2) = \sum_{m=0}^{n-1} \delta G\ (\lambda_m \rightarrow \lambda_{m+1}) \tag{2-2}$$

In some cases such as binding of large ligands to proteins, converging of FEP calculations is harder, and an equation (equation 2-3) derived by Lee et al. [140] can be used.

$$\Delta G\ (U_1 \rightarrow U_2) = \frac{1}{2}\ (\langle U_1 - U_2 \rangle_1 + \langle U_2 - U_1 \rangle_2) \tag{2-3}$$

Burykin and Warshel [12] carried out molecular dynamics (MD) simulations using the framework described above. The system chosen for the MD simulations in order to quantify electrostatic barrier for aquaporins is shown in Figure 2-6. An aquaporin monomer was placed in a grid of 30 × 20 × 20 A^o size and 2.5 A^o spacing of carbon-like atoms that representing the low dielectric membrane. Also an H_3O^+ ion (shown in yellow) was placed at the NPA region in the center of the pore.

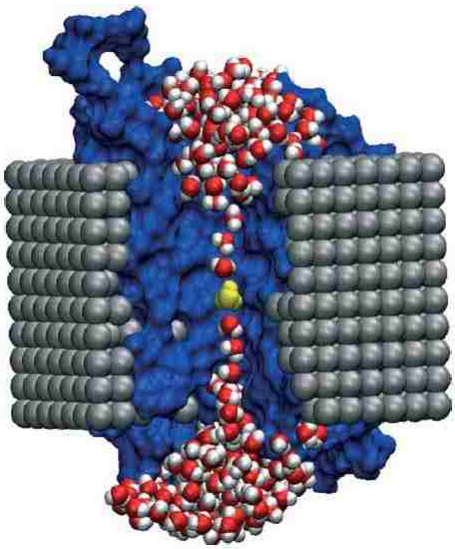

Figure 2-6 All-atom simulation system used to quantify electrostatic barrier in an aquaporin monomer [12]

The results showed that the electrostatic barrier at the center of the channel for the passage of an H_3O^+ ion was 17 kcal/mol. The study also showed that the difference between the energy at the center of the aqp channel and at the entrance was mainly due to solvation of the charge by bulk water and water molecules other than the two water molecules on both sides of the hydronium ion. The ion was influenced greatly at the entrance because of the bulk solvent whereas it was not solvated significantly in the channel by the bulk solvent [12].

2.3.2 Hydrodynamics of water flow through water channels

Water passes through aqp as a single unbroken file of water molecules. Due to a pore size only slightly bigger than a water molecule (3 A^o), macroscopic laws of hydrodynamics, such as Hagen-Poiseuille's, do not apply. Hagen-Poiseuille equation considers a no-slip condition at the wall which is not the case in an aqp pore. The aqp channel is wide enough only to allow one water molecule, so there is no outer layer of water molecules in the flow that adheres to the channel wall since otherwise there would be no flow across the pore [7]. In aquaporins, the slippage during water flow is perfect; that is, the mobility of water molecule is the same as that in the bulk (Figure 2-7) [7-9]. Water molecules lose two of the four neighboring molecules upon entering the aqp channel, and only the hydrogen bonds to the preceding and following water molecules remain. Furthermore, water molecules form new hydrogen bonds with pore lining residues of aqp [10].

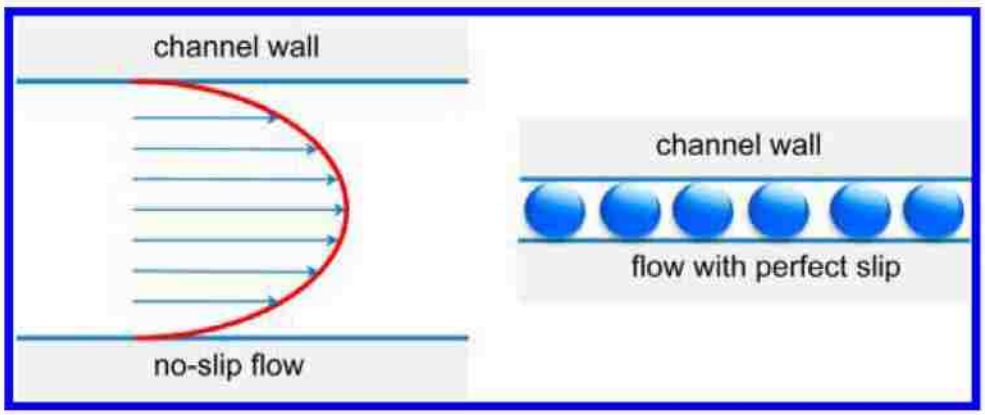

Figure 2-7 Macroscopic hydrodynamics following Hagen-Poiseuille equation with no-slip flow on the left and single-file flow in an aqp channel with perfect slip [7]

Horner et al. [9] showed water permeability values (Figure 2-8) for different channels through which water flow was shown as a single file of molecules based on Finkelstein's model [141]. According to Finkelstein's model, the water permeability P_f through a water channel was given by equation (2-4).

$$P_f = \frac{v_w D_1}{zL} \tag{2-4}$$

Where, P_f is unitary water permeability of water channel, v_w is the volume of one water molecule, D_1 is the diffusion coefficient of a single-water molecule in the pore (typically 10^{-10} m^2/s), Z is the distance between two water molecules (typically 0.31 nm), and L is channel length.

Based on equation 2-4, the model predicted that with a constant D_1, P_f varied no more than two times between different channels because single file water channels are at least 4 molecules long (K^+ channels) and accommodate a maximum 8 water molecules (aquaporins). Considering D_1 is constant in equation 2-4, P_f would depend on length of water channels, and in turn on number of water molecules in the channels (number of

water molecules in the channel = L × z). However, experimental results showed very high variability of water permeability through these water channels as shown in Figure 2-8. Hence, variation in L cannot be related to variability of unitary water permeability [9].

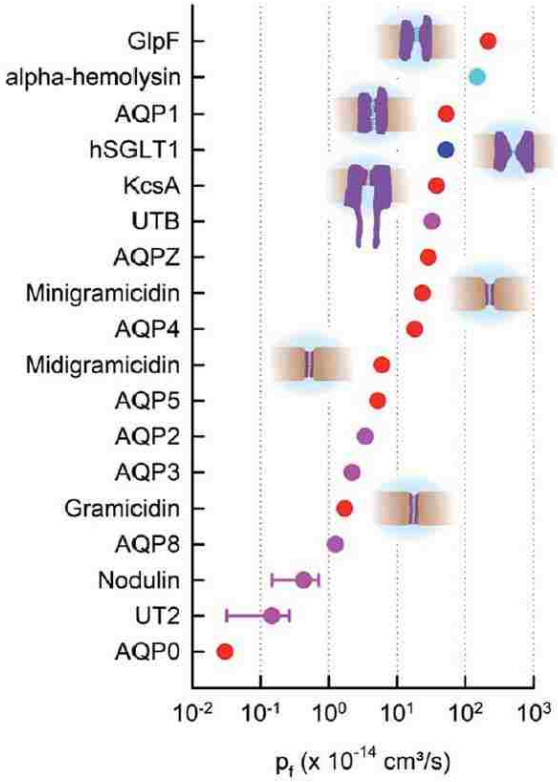

Figure 2-8 Unitary water permeability values of various single-file water channels as calculated by Finkelstein's model [9]

Horner et al suggested that availability of hydrogen bond donating and receiving residues in the channel walls of aquaporins was a major component determining the water mobility through these channels [9]. For example, it was observed that the unitary water permeability through potassium channels (KcsA) was much lower than through aqps even though the potassium channels are shorter than aqps. As KcsA is shorter than aqp, water molecules should complete the passage through KcsA pore faster than an aqp pore. However, long stretches of aqp pores contain only a few residues that form

hydrogen bonding with water molecules passing through these channels; on the other hand, the number of hydrogen bonding sites in KcsA is much higher than aquaporins. Thus, there are so many hydrogen bonding sites in KcsA that the distance between two different hydrogen bonding partners of water molecules is shorter than the diameter of water molecule [8]. Figure 2-9 shows a plot of unitary water permeability against the number of potential hydrogen bond donors and acceptors (N_H) in the single-file region of pore walls. It was observed that the relation between permeability and N_H was of logarithmic nature which meant a faster decrease in permeability with an increase in N_H. GlpF showed highest water permeability amongst biological water channels due to shorter single-file region and smaller value of N_H than aquaporins, which confirmed the results obtained in Figure 2-8. Only carbon nanotubes showed higher permeability than GlpF in Figure 2-8. The reason behind this is the lack of hydrogen bonding partners for water inside pore walls [142, 143].

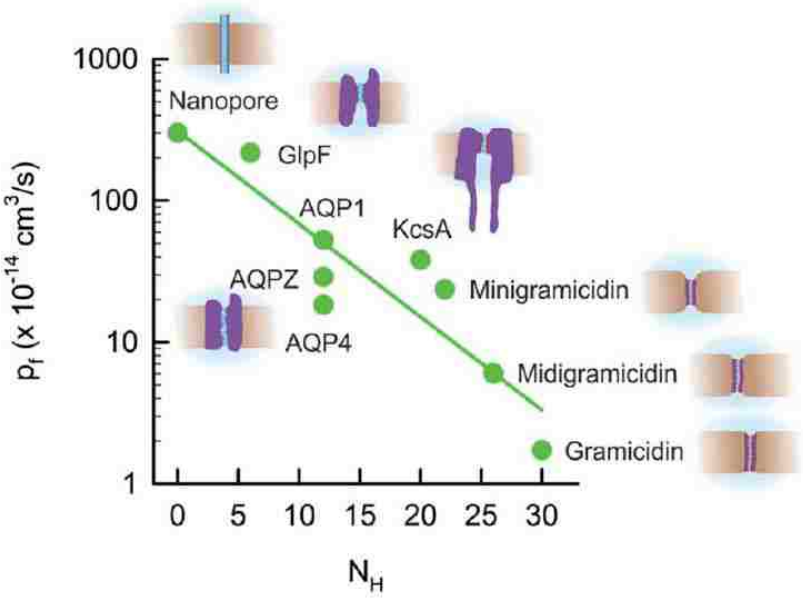

Figure 2-9 Plot of unitary water permeability of water channel proteins against the available number of hydrogen bonding sites in the single-file region of pore walls [8-10]

2.4 Incorporation of aquaporins in synthetic systems

Aquaporins have been studied extensively in the recent years in terms of their structures, unique functions, and potential applications in various separations [15, 144]. The highly selective nature of aquaporins towards water and their ability to allow water molecules pass through them at a very high permeability value have given rise to new research directions in clinical and biotechnological research [145, 146], physiological research [147, 148], membrane materials and synthesis of biomimetic membranes [61, 149].

Biomimetic membranes usually have three main components: aquaporins which is the biological element in the assembly, amphiphilic molecules where aquaporins are reconstituted, and a polymeric support structure. The amphiphilic molecules can either be lipid bilayers or amphiphilic polymers. Amphiphilic polymers are shown to have higher stability and flexibility and hence are more widely used to synthesize biomimetic membranes [59, 60].

The first attempt to synthesize biomimetic membranes using aquaporins was performed by Kumar et al. [43], where aquaporins were incorporated into amphiphilic triblock-polymer vesicles. These vesicles were made of a block copolymer with symmetric poly-(2-methyloxazoline)-poly-(dimethylsiloxane)-poly-(2-methyloxazoline) ($PMOXA_{15}$-$PDMS_{110}$-$PMOXA_{15}$) repeat units. Water permeability for aqp embedded vesicles was found to be ~3000 times greater than the vesicles without aqp. Also of note, Kaufman et al [150] used supported phospholipid bilayer (SPB) for the first time on a

commercial nanofiltration membrane to study the feasibility of synthesizing aquaporin-embedded membranes using lipid vesicles. The lipid bilayer showed consistent permeability; however, there were some issues with the assembly, such as ruptured vesicles and defects. Wang et al. [53] later used a planar lipid bilayer to incorporate aquaporins using a pore-suspending technique for possible applications in forward osmosis. Liposomes were ruptured on a porous alumina support for this purpose. Liposomes incorporated with aqpZ displayed a 3000 fold increase in permeability as compared to pristine liposomes. It was also observed that the performance of aquaporins was highest at an optimal lipid-protein molar ratio of 2000:1. A similar design strategy was applied in preparing proteopolymersomes using a block copolymer; however, under a pressure driven environment, it was observed to be challenging to keep aquaporins functional and stable [52].

Zhong et al. [56] attempted a vesicle rupture method using triblock copolymer and UV polymerization to form a selective layer on a nanofiltration support. Aquaporin-modified membranes using this method displayed water permeability of 34 LMH/bar and NaCl rejection of more than 30%, which showed that the assembly still had some defects in terms of coverage by aquaporins. Since 2012, a number of innovative approaches have been adapted to keep aquaporins stable and functional in biomimetic membrane assemblies. Examples include supported-lipid membranes using spin coating of surface with positively charged lipids [44], incorporation of aqpZ embedded vesicles into interfacial polymerization where the proteoliposomes were incorporated into m-phenylene-diamine aqueous solution [47], reconstitution of aqpZ into a lipid bilayer formed by Langmuir - Blodgett technique [49], functionalization of proteoliposomes

using amine followed by their deposition on polydopamine-coated microporous membranes [50], encapsulation of proteoliposomes with positively charged poly-L-lysine molecules and their adsorption onto a polyanion support film [51], incorporation of aqpZ using surface imprinting [55], and pressure-assisted sorption on gold-coated polycarbonate substrate [151]. Table 2-4 shows some of the recent approaches followed in synthesis of biomimetic membranes.

At the commercial level, the Aquaporin Inside^{TM} flat sheet is the first thin film commercial forward osmosis membrane fabricated with aquaporins incorporated in its polyamide selective layer [62]. These commercial membranes were synthesized using conventional interfacial polymerization, where aquaporin-based proteoliposomes were dispersed in the aqueous solution. These membranes incorporated with proteoliposomes showed water permeability values greater than 4 LMH/bar and salt rejection values of more than 96% [47].

Table 2-4 Recent approaches followed for synthesis of Aquaporin based biomimetic membranes

Biomimetic membrane fabrication strategy	**Remarks**	**Author reference**
Using a propargyl functionalized ß sheet peptide to bind to aqp and using click chemistry to incorporate into synthetic membranes.	Successful covalent attachment onto the membrane and improved salt rejection.	[152]
Commercially available Aquaporin Inside^{TM} for forward osmosis.	Similar performance to other commercially available membranes.	[62]
Aqp-based polymersomes in a TFC membrane using interfacial polymerization.	Good chemical stability; adverse effect on flux after chemical cleaning in long-term use.	[153]

Hollow fiber membranes; Incorporation of aquaporins into lipid vesicles using thin film rehydration method.	Enhanced water permeability of selective layer.	[154]
RO membranes using polymersomes.	Sensitive to temperature and pressure changes.	[155]
Electrostatic layer by layer assembly, with AqpZ-embedded DOPC/DOTAP.	Excellent separation under high pressure environment.	[156]
Hollow fiber composite ABM.	Robust and easily scalable.	[157]
Polymer crosslinking using polyamide as substrate.	Easily scalable, less fouling.	[45]
Thin film composite aquaporin biomimetic membranes by interfacial polymerization.	High permeability, able to withstand pressure till 10 bar.	[42]
Amine functionalized proteoliposomes vesicles deposited on the PDA layer.	Chances of protein deactivity.	[50]
AqpZ-implanted liposomes on a PDA coated microporous membrane (NF).	Controlled properties of membrane but vesicle rupture under pressure.	[51]
Aquaporin-embedded through pressure assisted sorption on gold-coated polycarbonate substrates.	Better performance than other pore spanning membranes.	[54]
AqpZ embedded membrane on cellulose acetate using surface imprinting technology.	High strength; protein flattening causing low salt rejection.	[55]
LBL adsorption ABM.	Easy to scale up.	[51]

As mentioned above, a number of studies have been carried out in order to successfully incorporate functional and stable aquaporins into synthetic membranes. In the initial approaches, alteration and denaturing of aqps, alignment of the channels, and mechanical stability of the whole membrane assembly were some of the key issues observed. Recent studies carried out to tackle these issues have encountered new challenges. One of the challenges is high costs involved in the expression and purification

of aquaporins on a large scale. Another challenge is scalability of current approaches to synthesize biomimetic membranes on a large scale [61]. Along with the work going on in the field of biomimetic membranes based on aquaporins, there has been an increase in the research associated with bioinspired materials [4]. A number of artificial structures with similar structure-function relationships of aquaporins have been introduced and studied in the recent years. These structures have the potential to overcome the aforementioned challenges in the commercialization of biomimetic membranes [4].

2.5 Bioinspired membranes

Bioinspiration connects basic science and applied engineering, and it extracts fundamental concepts and ideas from biological systems to form a bridge between fundamental science and engineering applications [158]. Recent work on synthesis of materials inspired by the functions of aquaporins consists of artificial water channels [159] and carbon nanotube porins [6, 160]. These artificial materials attempt to mimic the ability of aquaporins to provide high water permeability and selectivity. Ideally, artificial channels can be synthesized using simple chemistry and are compatible with various solvents which makes them convenient to synthesize. There has been an increase in recent years in studies discussing the design considerations, challenges encountered, and performance of membranes with artificial water channels [2-4, 11, 159, 161-166]. There are mainly two types of artificial channel types: self-assembling channels and unimolecular channels [159].

Self-assembling channels consist of a number of building blocks that interact with each other via hydrophobic interactions or hydrogen bonding to form a stable structure.

Percec et al. [1, 167] synthesized dendritic dipeptide pores which could self-assemble into helical columnar structures with a pore size of 12.8 ± 1.2A^{o}. The building blocks interacted via hydrogen bonding. These channels were reconstituted into lipid bilayers and they were shown to simulate gramicidin, which is a biological proton channel. The study strongly indicated that these dipeptide pores could mediate water transport across lipid bilayers [137, 168, 169]. However, these channels showed low thermal stability owing to the dynamic equilibrium states of Dendron monomers at approximately 22^{o}C. In order to overcome this low stability, the channels were modified structurally such that the benzyl ether moiety of the monomers was replaced by naphthyl groups at the periphery of helical pores. The purpose of this replacement was to enhance Π-Π stacking interactions between monomers and in turn increase the stability. Although this change in the structure enlarged the pore diameters to 14.5 ± 1.5 A^{o}, the pores showed enhanced stability between 20^{o}C to 40^{o}C [159]. These modified channels showed selective water and proton transport over Li^{+}, Na^{+} and Cl^{-} monovalent ions.

Barboiu and coworkers synthesized I-quartet channels [2, 161], which were inspired by Influenza A M2 proton channels. M2 proton channel is a pH gated channel, and its key functions are proton selectivity and low-pH gating [161]. The rate of proton flux through M2 channels has been reported from 10 to 1000 sec^{-1} depending on the electrical and chemical potential applied [170]. The proton channels facilitate water and proton transport via diffusion through water-filled pores. In order to mimic these proteins, ureido imidazole compounds were synthesized. It was shown that these ureido imidazole compounds crystallized into bulk states and self-assembled into lipid bilayers. These pores provided an inner diameter of 2.6 A^{o} and these channels were stabilized by

continuous and repetitive hydrogen bonding between water molecules and imidazole moieties. A number of factors, such as the number of alkyl chains, and chirality of alkyl chains and lipids in the bilayer, affected the permeabilities obtained through these channels. For the most optimal I-quartet channel, water permeability obtained by a single channel was ~1.5 × 10^6 H_2O molecules per second while single channel proton conduction rate was ~5 H^+ molecules per second, which is almost half of proton transport through M2 protein. These channels have restricted pore structures compatible for transport of water molecules, suggesting that the critical pore diameter is ~3 A^o for desalination applications of artificial channel-based membranes.

Similarly, in order to mimic Gramicidin A protein channel, triazole channels were synthesized. These channels showed an average 5 A^o diameter pores with an hourglass shape. However, they showed increased cation conduction rates due to hydration of their inner surfaces with four continuous water wires [171]. Gong et al. [172] synthesized Hexa (m-phenylyene ethynylene) channels that formed a stable self-assembled structures with a pore diameter of 6.4 A^o and an outer diameter of ~3.7 nm. These channels showed sufficiently high water conductance but their single channel permeability was not clear. The distinctive features of these channels were that they could be modified to reduce proton conductance through the channels, and also the alkyl chains could be altered in order to provide more stability [173]. Zhao et al. [5, 174] designed pyridine-based foldamers of diameter 2.8 A^o with high affinity to capture water molecules and similar stacked pores that mimic aquaporins. Aromatic stacking of pyridine monomers in these structures provided them stability. In addition to the approaches mentioned above,

triarylamine channels have also been studied as basic building blocks to form columnar structures [175-180].

Unimolecular channels are single molecules with tubular pore structures. These channels are more stable that self-assembled channels and provide smaller pores. However, they are challenging to synthesize [159]. Pillararenes were one of the first unimolecular channels synthesized [164, 181-185]. These channels were hollow-pillar shaped and easy to chemically modify in order to restrict pore sizes [182]. Hou et al. [185] developed hydrazide-appended pillar[5]arenes (HAPs) showing complete rejection of proton diffusion, which was similar to aquaporin water channels [36, 116]. These channels can be considered as the first approach that simulated the functions of aquaporins, which is high water conductance while rejecting protons. Peptide-appended pillar[5]arenes (PAP[5]) had hydrophobic tripeptide chains of phenylalanine isomers in pillar[5]arene backbone. These channels had single-channel permeability of 3.5×10^8 H_2O molecules per second, showing continuous and efficient water wire formation in the pores [4, 159].

Carbon nanotubes are regarded as an important material for energy-efficient water purification [186-189]. Experimental and simulation studies have shown enhanced water flux as compared to biological cellular channels through carbon nanotubes (CNT) with less than 1 nm in diameter [187, 190]. McGinnis et al. [191] reported CNTs with a diameter range of 0.67 -127 nm covering a nonporous polysulfone film with permeability 1000 times that calculated by Hagen-Poiseuille flow. CNTs can be tuned according to their applications in terms of variations in their diameters or by adding functional groups within the CNT or at the ends [192]. Recently, carbon nanotube porins (CNTP) were

found to have a water permeability of $2.27\pm0.47\times10^{10}$ water molecules per second per channel, which is higher than that observed in Aqp1 [6]. This was explained by MD simulations of a water molecule confined in a CNTP. It was observed that CNTPs could sterically confine water to a single file. Since a water molecule present in bulk solution has a higher number of hydrogen bonds than a water molecule in a confined channel with a single file of molecules, the energy barrier for the transport of a water molecule in bulk is higher than that in the channel. Furthermore, CNTPs had hydrophobic inner surfaces which enabled them to have a six-fold increase in water permeability relative to Aqp1 [6, 159]. Figure 2-10 shows a schematic of types of bio-inspired membranes based on various channels and their applications.

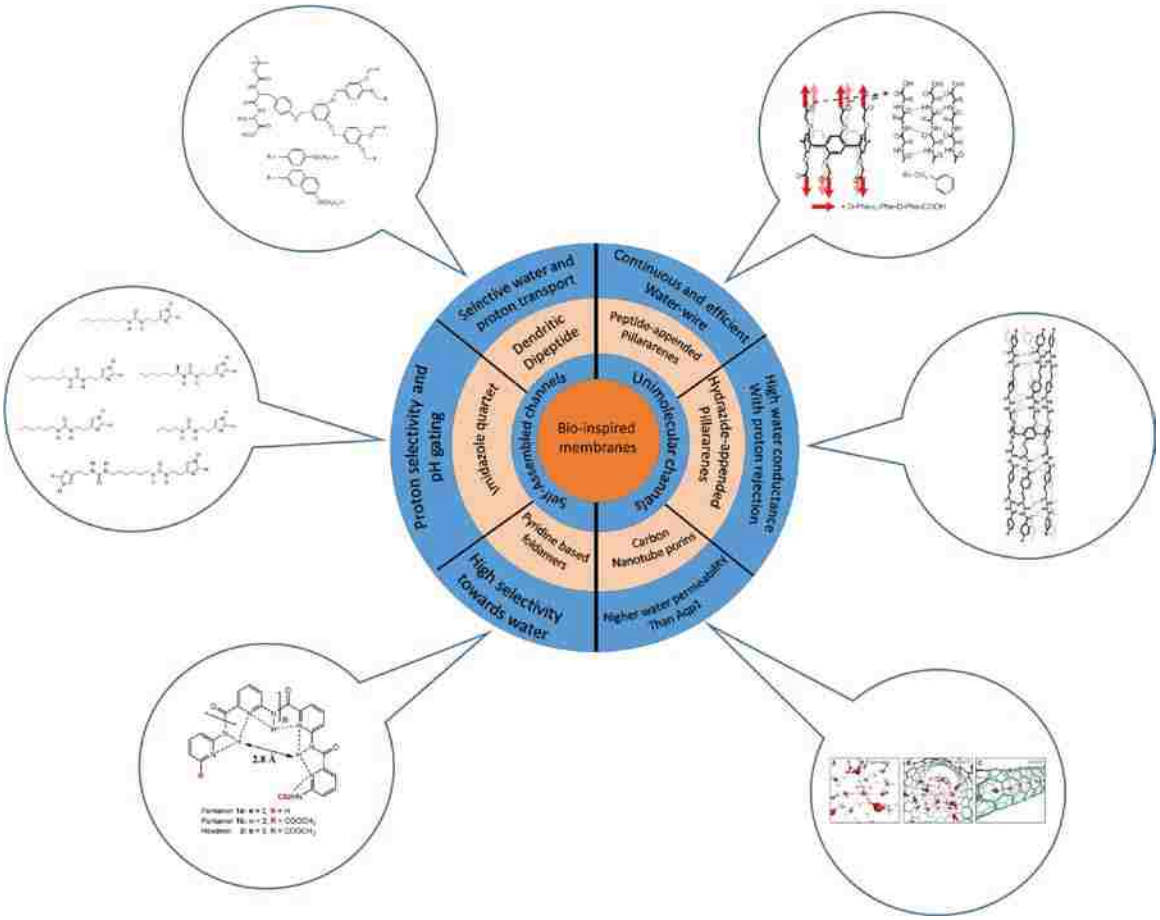

Figure 2-10 Types of artificial channels and their applications [1-6]

2.6 Applications of aquaporin-based biomimetic membranes:

Along with the traditional microfiltration (MF), ultrafiltration (UF), nanofiltration (NF), and reverse osmosis (RO) membranes, there has been additional incentive to integrate next generation membranes incorporated with novel materials and biological molecules in various fields [61]. Because of their controlled selective transport and stability, biomimetic membranes have found their applications in various areas, such as sustainable resources, energy management and environmental applications [61]. The development of aqp-based biomimetic membranes has created a number of possibilities in the field of water and wastewater treatment. Table 2-5 shows some of the applications of aqp-based biomimetic membranes and their performance.

Table 2-5 Applications of aqp-based biomimetic membranes, design approach and their performance

Application	**Membrane and design approach**	**Performance**	**Author reference**
Removal of trace organic contaminants in osmotic membrane bioreactor (OMBR).	Commercial aquaporin FO membrane (Aquaporin Asia, Singapore). Interfacial	Much better transport properties, better smaller reverse salt flux without compromising	[193]

	polymerization with embedded aquaporin vesicles into a polyamide selective layer on polysulfone support.	water permeation resulting in less severe salinity build-up. More than 85% removal of trace organics.	
Treatment of sugarcane molasses distillery wastewater and concentration of distillery wastewater by FO by removing melanoidins.	Aquaporin inside™ membranes by Aquaporin A/S. Thin film composite (TFC) FO membranes	70% water recovery from distillery wastewater over 24h study period.	[194]
Coconut milk concentration	Aquaporin inside™ tubular FO membranes by Aquaporin A/S	2 times concentration of 10 kg coconut milk corresponding to approximately 50% recovery.	[195]
Removal of trace organics such as the herbicide 2, 4-dichlorophenoxyacetic	Aquaporin inside™ hollow fiber FO membrane by Aquaporin A/S	Over 95% rejection of methyl paraben while over 99% rejection of 2, 4-	[195]

acid, plastic component bisphenol A (BPA), and the preservative methyl paraben.		dichlorophenoxyacetic acid, and BPA.	
Algae dewatering in algal harvesting with low energy requirement	Aqp based polyethersulfone membrane for FO	81% algae dewatering was achieved with 29% flux drop.	[196]
Multifiltration bed system in the International Space Station (ISS) Water Processor Assembly (WPA)	Aquaporin inside™ hollow fiber module	Water recovery ratio of 97.6%±0.47% with a ~50% rejection of total organic carbon. No degradation of membrane over at least 8711.8 hours.	[197]

Despite having a number of applications in various fields, there are still some challenges involved in the use of aqp-based biomimetic membranes, such as high costs involved in the expression and purification of aquaporins on a large scale, and scalability of current approaches to synthesize biomimetic membranes on a large scale [61], which limit their applicability comparative to commercial nanofiltration membranes.

2.7 Nanofiltration membranes and their applications:

Nanofiltration has been extensively studied and commercialized over the last two decades and is one of promising technologies for the separation of neutral and charged solutes in aqueous solutions [198]. NF membranes provide an average pore size in the order of 1 nm and a molecular weight cut off (MWCO) of 200-2000 Da, which lies between RO and UF. They typically have a moderate level of surface charge, which plays an important role during various separations. This makes NF highly competitive in terms of selectivity and cost effectiveness as compared to traditional separation processes [199, 200].

NF has found a wide variety of applications in a number of industries, such as water and wastewater treatment, pharmaceutical and biotechnology industry, food processing, among others. In water and wastewater treatment, NF membranes are used to remove small dissolved organic molecules such as micro-pollutants, partial mineral components such as sulfates and nitrates, and multivalent electrolytes [198]. In food industry, NF is required to avoid product contamination in order to meet quality and safety standards. In dairy industry, NF membranes are mainly used for concentration and demineralization of salty whey [201]. NF membranes have also been used to separate different saccharides and sugar from salt solutions [202]. Table 2-6 shows some of the applications of NF membranes and their performance. In summary of Table 2-6, the average permeability expected from nanofiltration membranes is approximately 10 LMH/bar with average divalent salt rejection of approximately 97%.

Table 2-6 Applications of NF membranes and their performance

Applications	**Membrane**	**Performance**	**Author reference**
Removal of Perfluorooctanoic acid (PFOA) and different salts from water.	Negatively charged, with a selective polyamide layer consisting of trimesoyl chloride, and a mixture of bipiperidine and piperazine.	High retention of PFOA (~90%) and a reduced scaling as compared to commercial NF270 membrane at an initial flux of 80 LMH.	[203]
Removal of pharmaceutical and personal care products (PPCP) and mitigation of organic and biological fouling by humic acid and sodium alginate	In-situ radical graft polymerization technique using monomers of 3-sulfopropyl methacrylate potassium salt (SPM) and 2-hydroxyethyl methacrylate (HEMA) on a commercial NF 90 membrane	Considerably improved fouling resistance as compared to virgin NF90 membrane. Effective removal of PPCP (>98.7%)	[204]
Separation of Molybdenum, Germanium, Cobalt,	Commercial NF99HF obtained from Alfa Laval AB (Sweden) and UTC-60	NF99HF: ~100% rejection of Co, Cu, Zn, ~70% rejection of	[205]

Copper, Zinc, Rhenium	obtained from Toray Ind. Inc. (Japan)	Mo, 20-30% rejection of Re, ~20% rejection of Ge. UTC-60: ~100% rejection of Co, Cu, Zn, ~70% rejection of Mo, ~25% rejection of Ge, ~20% rejection of Re,	
Wastewater by-produced during tomato manufacturing and canned products	Commercial spiral-wound module (Desal-5 membrane, model DK2540, Osmonics)	Permeate flux of ~8.2 LMH, purification of of the wastewater up to a water compatible with the municipal sewer system requirements, with a recovery rate of 90%.	[206]
Artichoke wastewater: extract from artichoke solid waste	NF270 (Dow, polyamide)	Total retention of prebiotic sugar with a high flux up to 120	[207]

		LMH	
Removal of $MgSO_4$	DOW FILMTEC™ NF90-400/34i Element	98.7% rejection of $MgSO_4$, at a permeability of 8.88 LMH/bar	[208]
Removal of $MgSO_4$	DOW FILMTEC™ NF270-400/34i Element	97.0% rejection of $MgSO_4$ at a permeability of 11.10 LMH/bar	[209]
Removal of NaCl	CSM NE8040-90 7500 GPD Nano-filtration Membrane 8 x 40	85-97% NaCl rejection with 6.60 LMH/bar permeability	[210]
Removal of NaCl	CSM NE4040-90 1700 GPD NF Membrane, 4″ x 40″	85-97% NaCl rejection with 6.42 LMH/bar permeability	[211]

CHAPTER 3. RESEARCH OBJECTIVES

The overarching goals of this study were to first incorporate aquaporins into synthetic nanofiltration membranes without chemical alteration and to prevent flattening or denaturing of aquaporins; then, the second objective was to install functional groups on aquaporins and align them in the direction of water flow; lastly, the third objective was to synthesize artificial channels in order to overcome the issues with aquaporin stability, alignment, and efficient packing of water channels onto the membrane surface.

3.1 Hypotheses

A) AqpZ can be incorporated in an amphiphilic PVA-alkyl matrix. PVA-alkyl has the hydrophilicity of polyvinyl alcohol (PVA) and hydrophobicity of long alkyl chains. Being amphiphilic in nature, it is proposed that it act as a synthetic alternative for the lipid bilayer in cell membrane, where aquaporins are naturally constituted. PVA-alkyl has good film forming properties and outstanding physical and chemical stability. It has been used for cell surface modifications in order to provide new biological functions. PVA-alkyl was observed to get attached to the cell surface by spontaneous hydrophobic interactions. A capping phenomenon by PVA-alkyl chains onto the cell surface was observed thereby maintaining its viability [212, 213]. Because of the hydrophobic

interactions of long alkyl chains of PVA-alkyl and its tendency to maintain cell viability, it was hypothesized to be able to support aquaporins.

B) Aquaporins modified with cysteine (-SH) groups at the N-terminus can be immobilized on the membrane surface and aligned in the feed direction in order to orient water flow through the aquaporins to reject protons, ions and other impurities. Being located at the end groups, cysteine groups would be accessible to attach to –COOH groups on modified PBI membranes.

C) Bisamide channels can be synthesized and incorporated into synthetic polymeric membranes in an attempt to mimic aquaporin selectivity towards water. It was hypothesized that pyridine-carboxylic acid provided rigidity at the end groups of compounds while diamine remained flexible and adjusted accordingly to get hydrogen bonding partners. These channels were proposed to form via intermolecular hydrogen bonding within themselves and with water molecules forming a passage through them. These artificial channels would have less footprint on the membrane surface as compared to aquaporins, would be more stable than aquaporins, and would have lower cost associated with their synthesis as compared to aquaporin expression.

In order to investigate above hypotheses, the objectives of this study are the following:

3.2 Objectives

Objective 1. Addition of protected aquaporins on the surface of the membranes.

1.1 Synthesis and surface modification of polymeric support structure

Flat sheet polybenzimidazole (PBI) membranes were prepared in dimethylacetamide (DMAc) solvent. The surface of PBI membranes was then modified with 4-chloromethyl benzoic acid (CMBA) in order to add carboxylic acid (-COOH) groups on membrane surface. In order to make subsequent functionalization, a stable ester intermediate was formed using N-hydroxysuccinimide (NHS) and N-(3-Dimethlyaminopropyl)-N'-ethylcarbodiimide hydrochloride (EDCH) via carbodiimide chemistry.

1.2 Synthesis of amphiphilic polymer for aquaporin incorporation

The amphiphilic polymer, PVA-alkyl was prepared in two steps. In first step, carboxyl methyl-polyvinyl alcohol (PVA-COOH) was synthesized using polyvinyl alcohol (PVA) and sodium monochloroacetate ($CH_2ClCOONa$). In the second step of this synthesis, polyvinyl alcohol carrying long alkyl chains (PVA-alkyl) was synthesized using PVA-COOH and Hexadecanal ($CH_2(CH_2)_{14}CHO$).

1.3 Aquaporin expression and incorporation

AquaporinZ (AqpZ) were expressed from *E. Coli* and purified. These aquaporins were treated with a polysaccharide, gum arabic to form Aqp-GA, in order to prevent functionalization of aquaporins in synthetic system. Aqp-GA were then physically embedded into PVA-alkyl to form a homogenous solution. Amphiphilic PVA-alkyl incorporated with Aqp-GA was then covalently attached to the stable ester intermediate of PBI membrane to form biomimetic membranes.

Objective 2. Align genetically engineered Aquaporins to the membrane backbone.

2.1 Stable ester intermediate of surface modified PBI membrane was prepared as explained in (1.1)

2.2 Aquaporin expression, mutation, and incorporation into the membrane

AqpZ were expressed from *E. Coli* and purified. In order to modify aquaporins, cysteine groups were added at the N-terminus of each monomer using Quikchange^{TM} site directed mutagenesis. These cysteine groups served as anchors for aquaporins to get immobilized on the modified surface of PBI membrane. Subsequently, cysteine modified AqpZ were covalently attached to the ester intermediate of –COOH modified PBI membranes.

2.3 PVA-alkyl was synthesized as explained in (1.2) and attached covalently to the membranes simultaneously with cysteine modified AqpZ.

Objective 3 Incorporate artificial water channels into synthetic PBI membranes in order to obtain more selectivity of membrane towards water.

3.1 Stable ester intermediate of –COOH modified PBI membranes was synthesized as explained in (1.1).

3.2 Bisamide channels were synthesized using a three step synthesis process. In first step, 6-aminopyridine-2-carboxylic acid and cadaverine were attached using dicyclohexylcarbodiimide (DCC) under nitrogen (N_2) environment. 6-hydroxymethyl

pyridine-2-carboxylic acid was then added to form a monomer of artificial channel using DCC again.

3.3 PVA-alkyl was synthesized as mentioned in (1.2).

3.4 Bisamide channels attached to –COOH modified PBI membrane using carbodiimide chemistry. PVA-alkyl was incorporated in situ to provide mechanical support for artificial channels.

CHAPTER 4. MATERIALS AND EXPERIMENTAL

4.1 Methodology

4.1.1 Glassware and Labware:

All glassware required for experiments and material synthesis, i.e., beakers, measuring cylinders, vials, bottles, flasks, burettes, stirring rods were cleaned before use by a detergent wash followed by acetone wash, acid wash, and multiple rinses of DI water. Acid wash solution was prepared by adding 4 mL of hydrochloric acid to 250 mL of DI water. After thorough cleaning, glassware were wrapped in aluminum foil and dried in Furnace (Oakton, VA) oven for 5 hours to remove any traces of organic contaminants.

4.1.2 PBI membranes casting:

The dope polymer used to cast the backbone of the membranes was polybenzimidazole (PBI). The solvent used to make the dope solution was N, N-Dimethylacetamide. Commercially-available 26% w/w dope solution, containing 26% PBI polymer, 72% N, N- Dimethylacetamide (DMAc) and 2% Lithium chloride (LiCl), was used and obtained from PBI Performance Products, inc. (Charlotte, NC). LiCl served the function of a pore former, preventing PBI polymer from phasing out of the solution [214, 215] and imparting long shelf life to the solution. The dope solution was diluted to 21% PBI by adding solvent, and the solution was sealed with parafilm to prevent air

bubbles from being trapped inside the solution and affecting its homogeneity. Because of very high viscosity of the solution, the solution was kept in the sonicator and degassed for 2 days in order to ensure homogeneous mixing of the solvent and the solute. After sonication, the solution was allowed to come to room temperature and then the solution was ready for membrane casting using the phase inversion process. The non-solvent phase that was used in this process was water.

A casting knife, or doctor's blade (Paul N Gardner Co, U.S. Pat 4869200, Pompano Beach, FL.) was used to make flat sheet membranes. A clean glass mirror was used as a surface, which provides optimum hydrophobicity to the membranes and helps for detachment of polymer films during phase inversion [216]. The solution was placed in an even line on the surface and the casting knife was used to push the solution across the glass surface to make a thin film. The thickness of the membranes was kept between 150 µm and 200 µm. A water coagulation bath was used to induce phase inversion with subsequent pore formation within the membranes. Once the phase inversion had taken place, the membrane came out of the surface of the water. The membrane was thoroughly washed with water and kept in a 50/50 glycerol-DI water solution. Glycerol was added to DI water to ensure that the membranes would stay wet during storage because when they are dried, they can become brittle and susceptible to breakage [217]. The membranes were kept in the solution at least one day before they were analyzed.

4.1.3 Surface activation of membranes:

The polybenzimidazole membrane surface needs to be activated for further modifications with PVA-alkyl and additions of Aqp-GA to the PVA-alkyl matrix.

Activation was achieved by reaction of a highly reactive chlorine atom, from 4-chloromethyl benzoic acid (CMBA) purchased from Sigma-Aldrich (USA), with the secondary amine group in the imidazole ring of the repeat unit in PBI backbone. It is important to note that there are two secondary amine sites in PBI molecule, so after the reaction, carboxylic groups are added on both sites on the molecule. For simplicity, the reaction at only one site is shown (Figure 4-1).

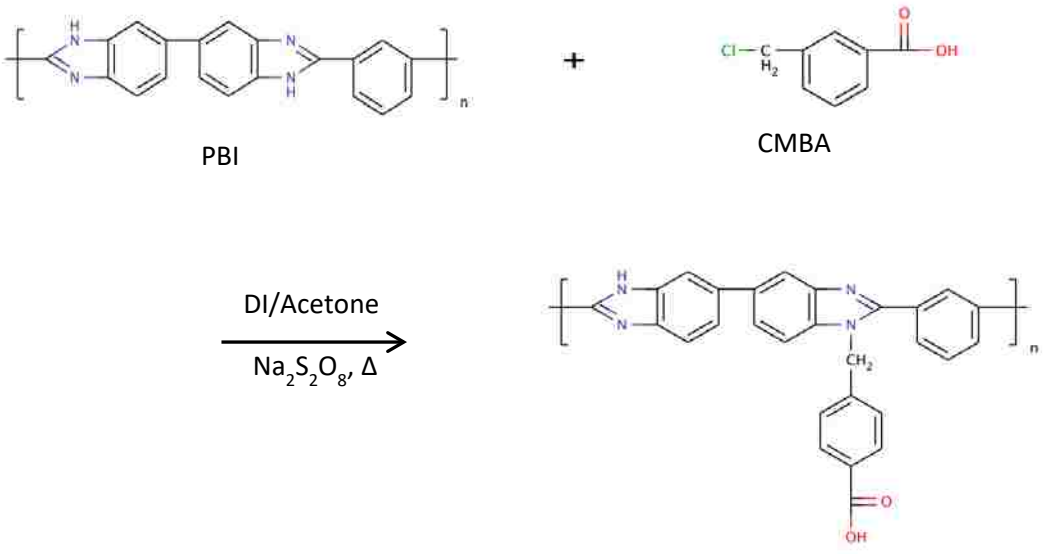

Figure 4-1 CMBA modification of membrane.

Modification was performed according to previous studies [217]. For the reaction, 1 wt% solution of sodium persulphate in water was prepared for use as a free radical initiator for the reaction. 200 ml DI water were taken in a 500mL beaker with a stir bar. 2.02g sodium persulphate was added to the water, and the solution was stirred on hot plate at 40°C. Two membranes were added to the solution, which were kept fully submerged and were not stuck under the stir bar. In a second beaker, 0.5 wt% solution of CMBA in acetone was prepared. 0.788 g CMBA was added to 200 mL acetone and was

stirred until dissolved. Then acetone/CMBA solution was slowly added to the beaker on a hot plate while stirring, and then covered. This was done in order to prevent the precipitation of CMBA as it is insoluble in water. The final solution was a 50/50 mixture. The temperature of the solution was kept at 40^{o}C and it was stirred for 24 hours to keep all the reactants in solution and prevent the evaporation of CMBA. Once the reaction was finished, the membranes were washed with copious amounts of DI water to remove excess sodium persulphate and immediately placed in glycerol/water bath.

4.1.4 Preparation of PVA–alkyl:

PVA-alkyl was prepared in two steps [218, 219], the preparation of (1) carboxy-methyl PVA followed by (2) PVA-alkyl.

4.1.4.1 Preparation of carboxy-methyl PVA (PVA-COOH):

The preparation of carboxy-methyl PVA (PVA-COOH) followed literature methods [220, 221], explained here. Initially, 50 mL water were taken in a 100 mL beaker, 1 g PVA (Acros Organics, USA) was added to it, and the solution was kept at 70^{o}C. The mixture was stirred for 1 hour continuously to prevent PVA from sticking to the bottom of the beaker until it completely dissolved. The solution was transferred to a 500 mL beaker, and 50 g of sodium monochloroacetate (Fisher Scientific, Pittsburgh PA) were added. The solution was then covered with aluminum foil and was incubated at 4 ^{o}C for 24 hours. After that, 42 mL water were taken in a 100 mL beaker, 42 g sodium hydroxide (Fisher Scientific, Pittsburgh PA) were added, and the mixture was stirred until the sodium hydroxide dissolved.

NaOH/water solution was added to the incubated solution of PVA and sodium monochloroacetate in water, and stirred at room temperature for 24 hours. Then, it was neutralized using a 6 M solution of hydrochloric acid (Fisher Scientific, Pittsburgh PA) in water was prepared in a separate beaker with pH being continuously monitored. This neutralized solution was dialyzed against deionized water. The molecular weight cut-off for the dialysis was chosen as high as possible, which was 12-14 kDa in order to maximize dialysis rate. The dialysis tubing (Fisher Scientific, Pittsburgh PA) used was soaked in water for 3 hours in order to open it and fill it with the solution. It was then sealed with dialysis locking membrane clamps. A 2000 mL beaker with a stir bar in it was filled with DI water to be used as a dialysate. It was kept stirring and the water was changed after every 4-5 hours to make sure that the driving force for the dialysis is high. The procedure was continued for 3 days, and the remaining solution in the tube was taken out and stored in another beaker. Then, the stored solution after dialysis was deionized using ion-exchange resins. DOWEX 1X8 (Acros Organics, USA) was used for negatively charged ions and DOWEX 50WX8 (Acros Organics, USA) was used for positively charged ions. The output solution after the ion exchange was lyophilized using freeze dryer. For that, the solution was kept in centrifuge tubes and was allowed to freeze dry for 3 days. PVA-COOH was obtained as a white solid after freeze-drying. The weight of the product was 0.45 g and the yield was 39%. The overall reaction is shown in Figure 4-2.

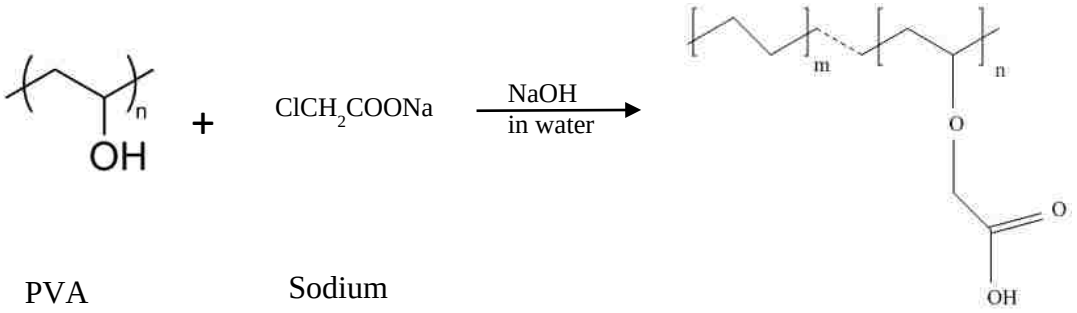

PVA Sodium monochloroacetate PVA-COOH

Figure 4-2 PVA-COOH synthesis.

4.1.4.2 Preparation of PVA-alkyl:

The second step of making PVA-alkyl was synthesis of hexadecanal. Chemicals used for the preparation were celite, pyridinium chlorochromate and 1-hexadecanol. Dichloromethane was used as the solvent. 11.2 mL dichloromethane were taken in a 50 mL beaker while stirring, and 0.95 g celite, 0.95 g pyridinium chlorochromate and 0.5 g 1-hexadecanol were added to the beaker under a fume hood. The solution was sealed with aluminum foil and stirred for 6 days at room temperature. After that, the reaction mixture was diluted by adding 40 mL diethyl ether. Florisil columns were used to remove excess celite, pyridinium chlorochromate and 1-hexadecanol. Then the mixture was evaporated, and hexadecanal was obtained as a white solid.

PVA-COOH obtained after first reaction was dissolved in DMSO. Hexadecanal and 200µL of 12 M hydrochloric acid were added to the solution, which was maintained at 70 ^{o}C and stirred for 25 hours. The reaction mixture was extracted with diethyl ether.

The mixture was then neutralized with 1M sodium hydroxide. The neutralized solution was dialyzed against DI water using dialysis tubing of 12-14kDa following the same procedure as described previously. The solution was then desalted with ion exchange

resins previously mentioned and lyophilized using a freeze dryer for 3 days. PVA-alkyl was obtained as a white solid with yield of 49% at a final weight of the product was 0.22 g. The overall reaction for the second step of the process is shown in Figure 4-3.

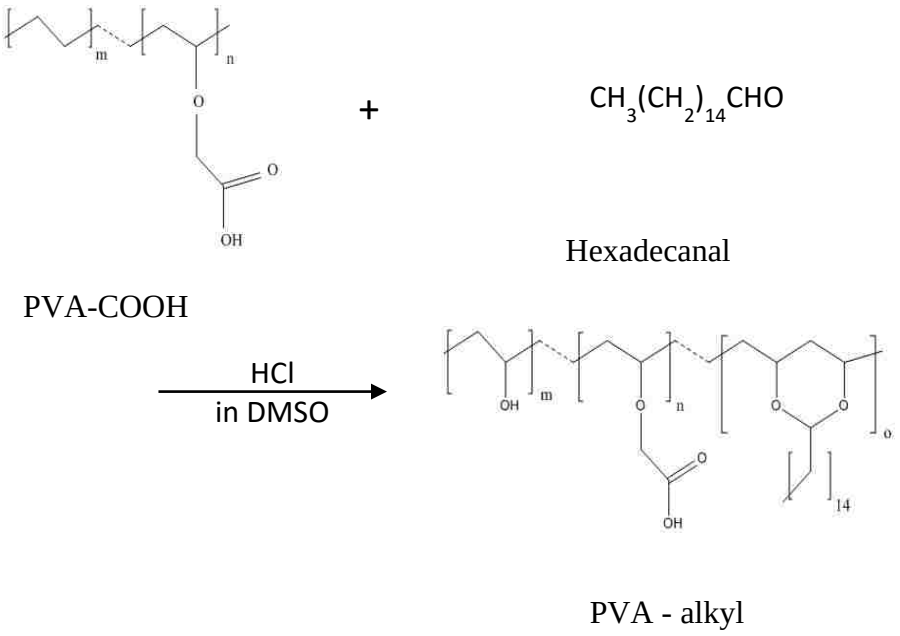

Figure 4-3 PVA-alkyl synthesis.

4.1.5 AquaporinZ expression and purification:

The constructed plasmid was transformed into *E. coli* strain C43 (DE3). Single colony was cultured overnight at 37 ℃ in 5 ml LB medium containing 50 µg/ml kanamycin. The overnight culture was then inoculated into 300 ml fresh LB medium with 50 µg/ml kanamycin and shaking at 250 rpm at 37 ℃. The cells were induced with 1 mM IPTG when the absorbance at 600 nm reached 0.8. After 4 hours incubation, the cells were collected by centrifugation at 8,000×g for 10 min.

To purify the protein, cell pellet was re-suspended with 30 ml PBS buffer (20 mM Na-PO_4, 0.3 M NaCl and pH 7.9) supplied with 0.5 mM protease inhibitor phenylmethylsulfonyl fluoride (PMSF) and sonicated for 20 min on an ice-water bath. The cell lysate was clarified by centrifugation at 10,000 rpm, 4 ℃ for 20 min. Then cell debris was dissolved using 2 % Triton in PBS buffer and incubated with shaking for 2 hours at 4 ℃ to extract membrane protein. The re-suspension was clarified with centrifugation at 10,000 rpm, 4 ℃ for 20 min and the supernatant was collected. Ni-NTA agarose beads (Qiagen) was mixed with the supernatant for 40 min at 4 ℃ with shaking. The resin was then loaded into an empty column, drained, and washed with PBS buffer supplemented with 0.03 % DDM (n-Dodecyl β-D-maltoside) and 40 mM imidazole. Protein was eluted with 500 mM imidazole and 0.03 % DDM in PBS buffer. Imidazole was removed by dialysis against PBS buffer supplemented with 0.03 % DDM overnight.

4.1.6 AquaporinZ modification with single cysteine at the N-terminus:

Cysteine contains a thiol group in its side chain, which can be used for immobilization. To prevent cysteine from being buried in the structure of AqpZ with limited accessibility for binding, a cysteine was added before the his-tag which was used to facilitate protein purification via the conventional metal-affinity chromatograph as shown in figure 4-4. In this study, cysteine was added using QuikChange site-directed mutagenesis following manufacturer's instruction (Agilent). Primers are: 5'-GAGATATACCATGGGTTGCTCTGGTCTGAACGAC-3', and 5'-

GTCGTTCAGACCAGAGCAACCCATGGTATATCTC-3', using pET28a-ApqZ as template [222]. The modification was verified by DNA sequencing.

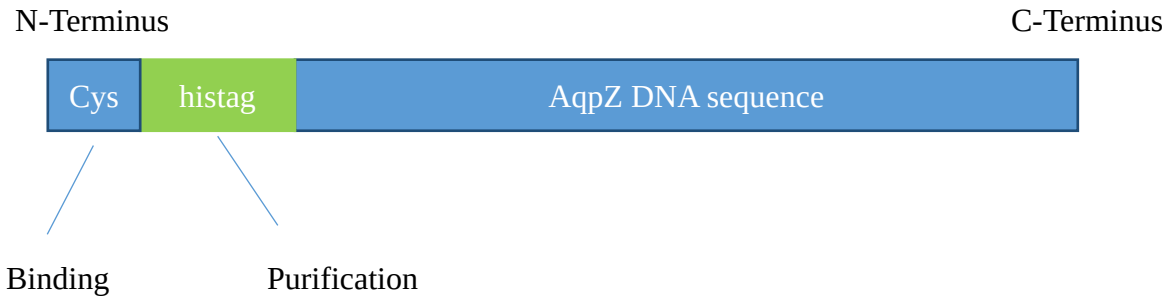

Figure 4-4 Schematic of Cysteine attachment at the N-terminus of aquaporins

4.1.7 Treatment of AqpZ with gum arabic:

A 15wt. % solution of gum arabic (Fisher Scientific, USA) in water was prepared. AqpZ was added to this solution and sonicated under mild conditions for 4 hours in order to disperse it in the gum arabic solution. The concentration of AqpZ was 1ml/3ml of GA. Gum arabic has been used previously to disperse carbon nanotubes to PVA without either shortening the nanotubes or disrupting their structures. After the addition of GA to carbon nanotubes solution, the suspension was found to be stable over few months and was not affected by centrifugation. Hence, it was proposed to protect the structure of aquaporins. The weight ratio of AqpZ to gum arabic was kept at 1:4. The mixture was kept stirring at room temperature for 72 hours and then heated slowly to remove water [223, 224]. Gum arabic-treated AqpZ were then added to de-ionized water and sonicated for 30 minutes. The solution with gum arabic-treated AqpZ was physically dispersed into the PVA-alkyl solution. The ratio of AqpZ-GA to PVA-alkyl solution was 1:1 by volume. Aquaporin is

bidirectional water channel protein; hence the orientation of the protein isn't expected to change the water flux through the protein [225].

4.1.8 Surface modification of PBI membrane using Aqp-PVA-alkyl:

Aqp-PVA-alkyl was attached to the membrane using carbodiimide chemistry [217], for the reaction between a carboxylic group and the hydroxide group present in PVA-alkyl molecule. For the reaction, N-(3-dimethylaminopropyl)-N'-ethylcarbodiimidehydrochloride (EDCH) and N-hydroxysuccinimide (NHS), both purchased from Sigma-Aldrich were used. The reactions were performed in 2-(N-morpholino) ethanesulfonic acid (MES) buffer (Sigma-Aldrich, USA).

400 mL water were taken in a 500 mL beaker and 7.85 g MES buffer was added with stirring, Followed by the addition of 11.75g NaCl with stirring. The solution was titrated to pH 6 using NaOH, 0.23 g NHS and 0.153 g EDCH were added to the solution and stirred well. CMBA modified PBI membranes were added to the solution, stirred for 15 minutes, and then the reaction mixture was titrated to pH 7 using NaOH. PVA-alkyl was added to the solution and stirred for 24 hours, and then the membranes were removed and rinsed well with DI water and stored in a beaker filled with DI water. The membranes were stored for 24 hours before using it for analysis. The overall reaction is shown in Figure 4-5.

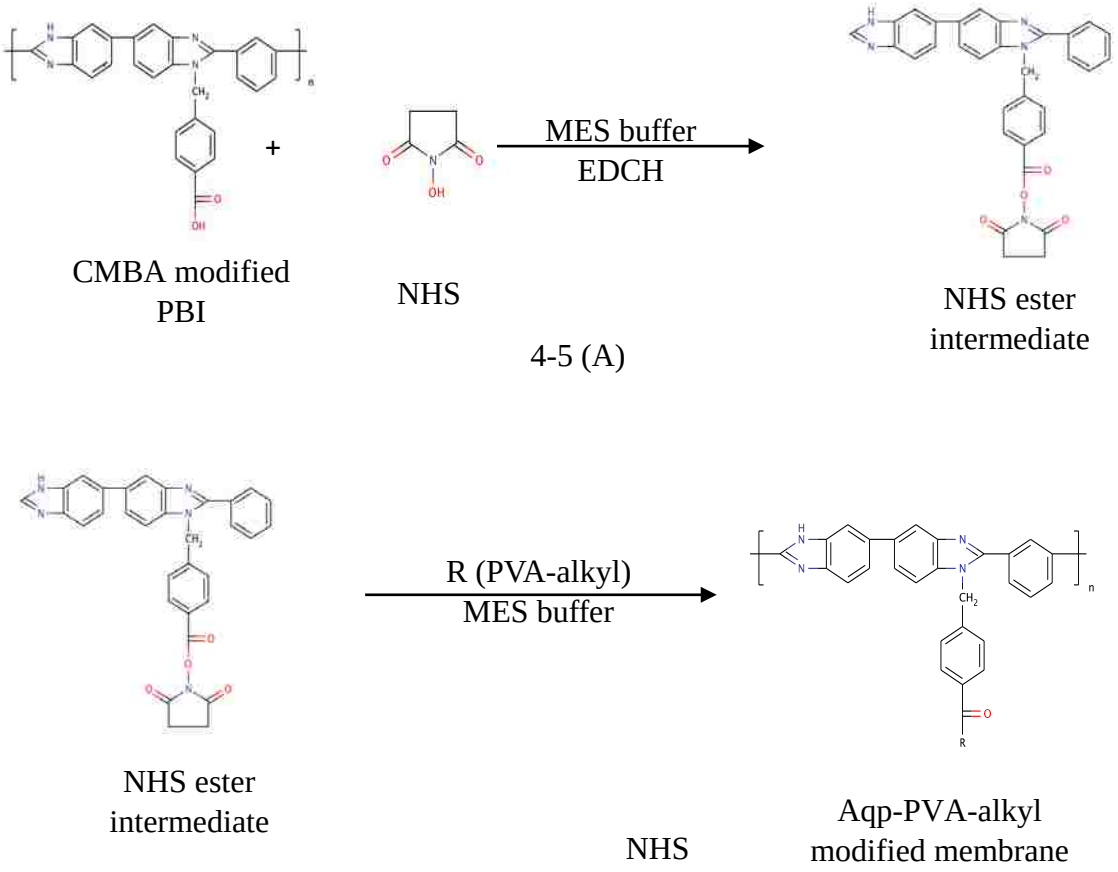

Figure 4-5(b)

Figure 4-5 (a) and (b) Carbodiimide membrane activation chemistry

4.1.9 Chemical attachment of –Cys modified Aqp to PBI backbone:

Immobilization of aquaporins into polymer matrix was done in order to align their channels with the direction of water flux and to optimize their performance. Aquaporins were covalently attached to the modified PBI backbone with carbodiimide chemistry. For this task, flat sheet PBI membranes were prepared and modified with CMBA. In the

next step, Cys modified Aquaporin (Aqp-SH) were covalently attached in a reducing environment to the –COOH modified PBI membrane using EDCH chemistry, as shown in figure 4-6. In this mechanism, Aqp-SH acted as a nucleophile to get covalently attached to the –COOH group present on the surface of PBI membrane. Cys groups present after the N-terminus acted as anchors the Aquaporin molecules to prevent the swaying and to help with the alignment of the aquaporin molecules in the direction of the flow. PVA-alkyl was used in order to bind to the remaining –COOH groups present in the membrane and to seal the gaps in between the attached Aqp-SH molecules following the EDCH chemistry previously used.

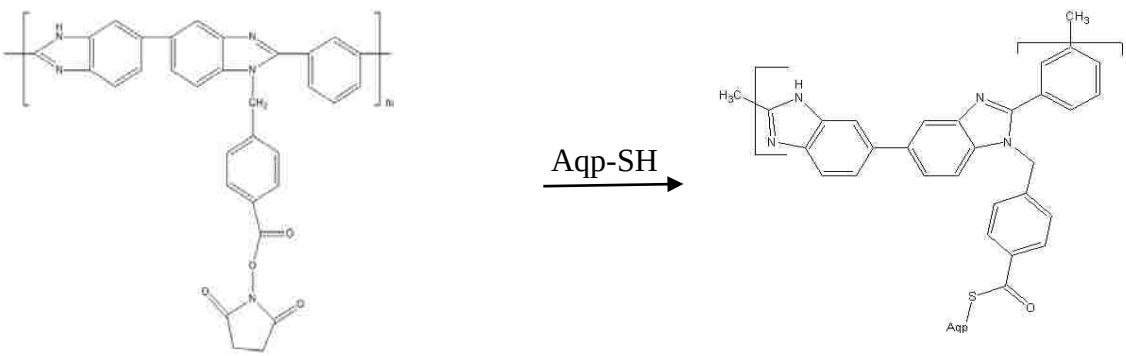

Figure 4-6 Chemical attachment of Aqp-SH to –COOH modified PBI membranes

4.2 Membrane characterization:

4.2.1 Fourier Transform Infrared Spectroscopy (FTIR):

A vibrational spectrum is a characteristic of every molecule and is considered a unique property of that molecule [226]. FTIR was used in ATR mode to determine the chemistry of the proposed reactions and modifications on the membrane surface. Digilab UMA 600 FT-IR microscope was used for all the analysis of membrane samples performed in this study.

4.2.2 Contact angle measurements:

Contact angle was used as a measure to determine the hydrophilicity of the membrane surface. A drop shape analyzer – DSA 100 (KRUSS USA, Matthews, NC) was used for contact angle measurements using sessile drop technique (Figure 4-7).

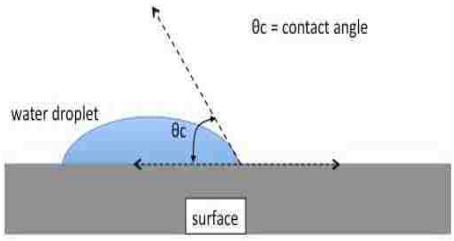

Figure 4-7 Contact angle measurement [227].

4.2.3 Zeta potential and surface charge analysis

Zeta potential is a parameter used to characterize the surface charge property of membranes at different pH environments. This analysis is particularly important to

understand the acid-base properties and to predict the separation efficiency of membranes [228]. Zeta potential measurements indicate the degree of repulsion between adjacent, similarly charged particles. Surface charge was analyzed by measuring the zeta potential using an Anton Paar SurPASS electrokinetic analyzer (Anton Paar, Ashland, VA) in surface analysis mode. Before analysis, membranes were rinsed with copious amounts of DI water to remove any residual solvent or glycerol from the storage solution. The KCl electrolyte solution used in these measurements had an ionic strength of 1.0 mM. The pH values for the various readings were adjusted using 0.5 M HCl and 0.5 M NaOH solutions for acid and base titrations.

4.2.4 Flux analysis:

Dead end filtration was used to monitor the flux decline of both PBI and PVA-alkyl-AqpZ membranes. Filtration experiments were performed using Amicon filtration cell (Amicon Stirred Cell 8010 – 10 ml). Using a constant membrane surface area of 4.1 cm^2, the time to collect a 2-ml permeate sample was measured for each feed and flux was calculated. A constant pressure of 70 psi (4.83 bar) for laboratory purposes and continuous stirring was applied in all tests. Flux values were calculated as L/m^2-hr and plotted against the total time of filtration. Membrane samples were cut into circular pieces of area 4.1 cm^2 and supported by a Whatman^{TM} filter paper (110 mmø). Each membrane was precompacted with DI water for 7-8 hours until a stable flux was reached. Precompaction was followed by filtration of protein solutions of 10 ppm each of bovine serum albumin (BSA) and lipase protein in water. The same filtration cell was used for protein filtration under the same conditions of pressure and stirring. Protein rejections

were calculated using UV-VIS spectrometer (Varian Inc. Cary 50, Agilent Technologies, Santa Clara, CA) according to following equation (4-1):

$$R = \left(1 - \frac{C_p}{C_f}\right) \times 100\% \quad (4\text{-}1)$$

where C_p and C_f are solute concentrations in permeate and feed solutions respectively.

Salt rejection was tested using five solutions of different concentrations of sodium chloride and calcium chloride in DI water: 3.4, 10, 20, 35 and 100 mM solutions. Solutions were run through the 10 ml dead-end cell under the same conditions as used for the pure water flux testing. Continuous stirring was applied inside the cell to prevent salt build-up on the membrane surface. Two mL permeate samples were collected for each feed. Salt rejections were calculated using conductivity meter. The apparent solute rejection R (%) was calculated using equation (4-1).

After each feed water filtration, the membrane was backwashed for 1 hour with DI water and filter paper support was changed. The flux recovery of the membrane was measured after backwash.

4.2.5 Morphological characterization:

Environmental scanning electron microscopy (ESEM) was used to verify the asymmetric morphology of the membranes and monitor the surface of both unmodified and PVA-alkyl-AqpZ modified membranes before and after filtration. An FEI Quanta 3D FEG Dual Beam Electron Microscope (FEI, USA) was used to test the samples. By freezing small samples of the membranes in liquid nitrogen and cracking them, smooth

cross-sectional areas could be observed. In order to get an image of cross-section of the membranes, the frozen and cracked samples were attached vertically to a carbon tape while the samples were attached horizontally to the carbon tape to get an image of membrane surface. The surfaces of the samples were dusted with a thin layer of palladium-gold using a Cressington 108 auto sputtering device and then observed under scanning electron microscope.

To investigate the cross-section of the membrane and measure the thickness of selective layer of modified membrane, ion beam of the FEI Helios Nanolab Dual beam was used to cut out a small piece of the membrane. A small deposit of platinum with a thickness of around 60 nm was deposited over the area in order to protect the underlying surface during the process of cutting of cross-section by ion beam. A small cross section was cut out and lifted away from the rest of the membrane sample by welding a small bead of platinum to the platinum layer. This sample was then thinned out with a low power ion beam until the morphology of the mesoporous layer was visible using STEM mode in the Dual Beam. This sample was transferred into the JEOL 2010F for TEM imaging of the cross-section.

4.2.6 Dynamic light scattering:

Since aquaporins form the functional element of biomimetic membranes, producing high quality proteins is critical. Before immobilizing proteins on membrane surface, it is important to evaluate the proteins for their concentration, purity and aggregation state. For this purpose, analysis of protein solution with dynamic light scattering to determine the presence and extent of aggregation was carried out in Litesizer

500 particle analyzer by Anton Paar (Ashland, VA). An aquaporin solution was taken in a glass cuvette and a plot of particle size vs relative frequency and polydispersity index (PDI) of the solution was obtained. Good quality protein samples would have PDI of 0.08, acceptable quality protein would have PDI of 0.1 to 0.4, while the precipitated protein would have PDI of 0.4 to 0.9 [57].

4.2.7 Molecular weight cut off:

The molecular weight cut off analysis of unmodified PBI, CMBA modified PBI, and PVA-alkyl modified PBI membranes was conducted using 100 ppm solutions of various molecular weights of polyethylene glycol (PEG) and sucrose solutions. The total organic carbon (TOC) of both feed and permeate solutions were measured using Teledyne Tekmar Fusion TOC analyzer (Mason, OH). The various samples that were used in this study along with their Stokes-Einstein radii are shown in Table 4-1. The rejection values of all solutes were used to determine the molecular weight cut off of both unmodified and modified PBI membranes. The molecular weight of solute in feed solution for which the membranes showed more than 90% rejection was considered the molecular weight cut off of the membranes. The apparent solute rejection R (%) was calculated using equation (4-1).

Table 4-1 Neutral solutes used for molecular weight cut off analysis and their Stokes-Einstein radii in nm [25, 229-232]

Solute	**Mol. Wt. (gm/mol)**	**Stokes-Einstein radii (nm)**
PEG 200	200	0.41

Sucrose	342.3	0.47
PEG 400	400	0.57
PEG 600	600	0.68
PEG 1000	1000	0.94

4.2.8 Depth profiling using XPS:

Membranes modified with Aqp-SH were analyzed for changes in the concentration of sulfur since unmodified PBI, -COOH modified PBI, and PVA-alkyl modified PBI membranes do not contain any sulfur present in their structures. Hence, Aqp-SH modified membranes were analyzed for the sulfur concentration in them as a confirmation for attachment of aquaporins to the membranes. K-Alpha x-ray photoelectron spectrometer (XPS) was used in order to analyze the elemental composition along the cross section of both unmodified and Aqp-SH modified membranes. Depth profiling was performed using an ion beam to etch layers of membrane surfaces and elemental composition was measured after each etching cycle. An ion beam of 200eV was used to etch the surface. Three etching cycles were performed for 120 seconds each for elemental analysis along cross sections of membranes.

4.2.9 Elemental analysis using TEM:

Membranes modified with Aqp-SH were analyzed for changes in the concentration of sulfur since unmodified PBI, -COOH modified PBI, and PVA-alkyl

modified PBI membranes do not contain any sulfur present in their structures. Hence, Aqp-SH modified membranes were analyzed for the sulfur concentration in them as a confirmation for attachment of aquaporins to the membranes. For that purpose, electron energy loss spectroscopy (EELS) mode was used in a transmission electron microscope (TEM), which is sensitive towards low atomic weight elements in samples. A JEOL 2010F TEM (Akishima, Tokyo, Japan) was used for this purpose. Samples were prepared using a Helios Nanolab 660 focused ion beam (FIB) instrument (FEI, USA). Sample preparation was carried out in a high vacuum in FIB chamber, thereby keeping oxidation of sample to a minimum. Thin lamella were lifted out from precise locations of the samples and thinned down to 50 nm for subsequent analysis in TEM. Energy dispersive X-ray spectroscopy (EDX) was also performed on the sample. The reduced thickness of the samples decreased scattering of the beam and optimized EDX lateral resolution. Only sulfur, oxygen, carbon and nitrogen were considered to calculate the elemental composition during the analysis. Other observed elements, such as Pt (coating), Ga (beam) and Cu (holder), were ignored to clearly analyze the elemental composition and sulfur concentration in the sample.

4.2.10 Diffusion studies:

In order to compare salt diffusion rates through unmodified PBI and Aqp-SH modified PBI, the membrane was mounted in the middle of a stainless-steel diffusion cell to separate two compartments (salt solution side and DI water side). Each compartment in the cell had a volume of 250 mL, and an effective membrane area available for diffusion of 3.5 cm^2. Continuous stirring was provided during the experiment in order to avoid

deposition at the bottom of the compartments. A solution of 1000 ppm NaCl solution was added into the salt solution side and the same amount of DI water solution was added into the other compartment [233, 234]. In order to measure the change in concentration, a sample of 2 mL was collected from each compartment every day. The experiment was run for 7 days to measure the rate of salt diffusion through the membranes and salt concentrations of collected samples were measured using ICP analysis. Initial conditions of the experimental setup is shown in Fig 4-8.

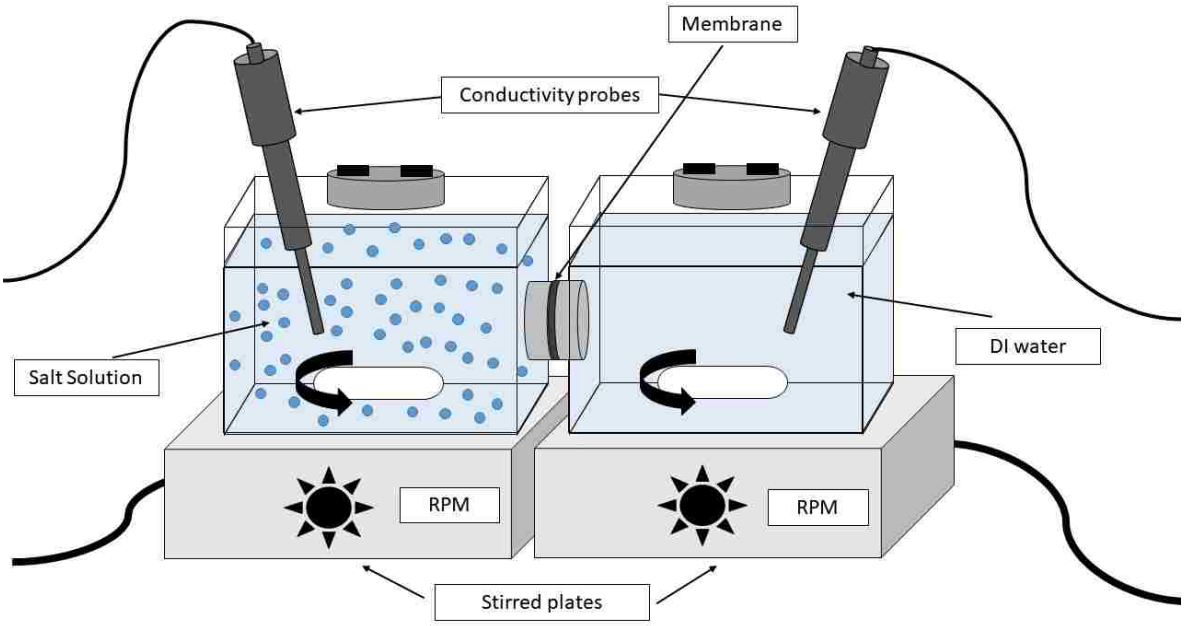

Figure 4-8 Diffusion cell assembly with 1000 ppm NaCl and DI water in two compartments separated by membrane.

4.2.11 Estimation of Aquaporin packing in membrane assembly:

Membrane porosity and double layer properties influence ion fluxes through the membrane. The flux values measured for aqp-SH modified membranes exhibited weak

sensitivity to ionic strength. These fluxes could be estimated via an ion's concentration (c) gradient and its diffusion coefficient (D), as shown in equation (4-2):

$$j = - D\nabla c \tag{4-2}$$

assuming a concentration gradient was imposed perpendicular to a porous film. This concentration gradient was set by the ion concentrations in reservoirs to either side of the membrane as well as their separation (see figure 6-11). By relating the measured flux to the concentration gradient, an effective diffusion coefficient, D_e, could be determined. This allowed the inference of relative packing densities of aqp molecules incorporated in the active layer of membrane. This effective diffusion coefficient would be generally smaller than the ion's intrinsic diffusion rate in bulk media, and moreover, it would be proportional to the ratio of the accessible pores' surface area to the total surface area, assuming the channels were perfectly linear and aligned with the concentration gradient, e.g. $D_e = \frac{SA_{pore}}{SA_{total}} \times D$. According to the SEM imaging data of cross-sections of membranes published previously [149], It was further assumed that the PVA-alkyl and PBI were stacked in layers aligned perpendicular to the concentration gradient.

Based on these assumptions, a numerical partial differential equation was used to estimate how ionic fluxes were modulated by aquaporin surface densities, from which aquaporin packing densities compatible with experimentally-measured flux data could be determined. Namely, finite element simulations of the steady state Fickian diffusion equation (4-3) were performed,

$$\frac{dc}{dt} = -Dd^2 \frac{c(x)}{dx^2} = 0 \tag{4-3}$$

subject to c (L) = 1 mM and c(R) =0 mM, where c is the concentration of the ionic solution and D is the diffusion coefficient and L, R correspond to the left and right reservoir boundaries. From these simulations, an effective diffusion coefficient that reflected the impact of the channel geometry on transport was determined. This proceeded through recognizing the flux was related to the concentration gradient via equation (4-4)

$$< J > = \frac{1}{A} \int D \, \nabla c \, dS \tag{4-4}$$

where A is the surface area of the film and S represents the surface.

Flux could be expressed in terms of concentrations and D_e was given by equation (4-5)

$$<J>*A \sim D_e \, \frac{(c(L) - c(R))}{(x(L) - x(R))} \tag{4-5}$$

where c(i) is the concentration at boundary i (left and right) and x(i) is the position of the boundary. By numerically evaluating <J> at the film boundary, the equation was solved for D_e based on the concentrations imposed at the reservoir boundaries and their separation distance.

These equations were solved on three-dimensional finite element meshes [235, 236], based on potential membrane and aquaporin configurations using the mesh generation tool GMSH [235, 237]. The meshes consisted of two reservoirs separated by a porous domain representing the film. Aqp or aggregates thereof were represented by cylinders of varying radii aligned parallel to the membrane. In principle, atomistic resolution surface geometries could have been used for the aqp molecules [235, 236], but since specific knowledge of the membrane structure at the solvent/membrane interface is

not known, a simple cylindrical representation of the protein was used. These equations were solved, assuming Dirichlet conditions of c=1.0 M and c=0.0 M on the left and right reservoir boundaries [235, 236] via the finite element method using FEniCS [235, 238]. The diffusion coefficient was arbitrarily set to D=1.0 [m^2/s]. Specifically, the weak form of these equations was solved using a piecewise linear Galerkin basis with FEniC's default direct linear solver and parameters. Concentration fluxes were determined by performing an 'assemble' call on an immersed boundary located at the middle and oriented parallel of the porous film. Details of the numerical procedure follow from previously published work [235, 236]. To capture the behavior of monomeric AqpZ, the flux found at the boundary of a pore was normalized [235, 236]. The packing fraction observed in the boundary layer then represented a boundary condition surrounding individual aquaporins. All code written in support of this study is publicly available at https://bitbucket.org/pkhlab/pkh-lab-analyses. Simulation input files and generated data are provided in Appendix D.

CHAPTER 5. A NEW TECHNIQUE TO FABRICATE HIGH-PERFORMANCE BIOLOGICALLY INSPIRED MEMBRANES FOR WATER TREATMENT

5.1 Introduction:

Water is an essential component in all separation processes involved in any application. Water is required in varying degrees of purity depending on the application for which it is used. Membrane separations play an important role in different industrial applications related to water, energy, pharmaceutical and life sciences. These membranes provide an alternative to conventional separation processes to obtain cost effective and high quality water [239-241]. However, there are some drawbacks involved with membrane separation processes; in particular, desalination membranes provide very low water flux values. In addition, limited lifetime of membranes, insufficient pollutant rejection, further treatment of concentrates, and chemical resistance of membranes are some of the problems faced while dealing with membrane separations [242-246] Nanofiltration membranes can be used for brackish water desalination but membrane fouling, pretreatment, membrane cleaning, limited recoveries and feed water loss, and short lifetimes of membranes are some of the problems involved in it [239]. Therefore, even though membrane separations are now established processes for water treatment, there is still need to develop improved membranes that would avoid these limiting issues.

Aquaporin is a bidirectional water channel protein present in cell membranes, and it regulates the flow of water in and out of cells. Aquaporin has, therefore, a potential to improve the water flux through incorporation into synthetic polymeric membranes. Water

passes through porous structures as a single unbroken column of molecules with hydrogen bonds between adjacent water molecules. These water molecules can carry protons as well through these structures in the form of H_3O^+ ions. However, this flow of protons along with water is prevented while passing through aquaporins. Aquaporins have pores which are constricted in the middle and wider at the openings. This constriction leads to a high dielectric barrier for charged entities like protons or other ions, while allowing the passage of small, neutral solutes. The backbone amide and carbonyl groups in the Asparagine-Proline-Alanine motif that lines the pore walls in aquaporin make hydrogen bonds with the water oxygen atoms, causing reorientation of water molecules to become perpendicular to the pore axis. In this orientation the water hydrogen atoms can't make H-bonds with adjacent water molecules. All of the other groups present on the pore-walls are hydrophobic, leaving the water hydrogen atoms without hydrogen bonding partners. This raises the energy by nearly equal 3 kcal/mol [114, 120, 136, 247] thus allowing water passage with a minimal energy barrier. The activation energy for the transport of water through Aqp is about 3 kcal which is close to hydrogen-bonding energy, suggesting breakage of hydrogen bonds in the water flow [248].

For this research project, AqpZ, a water channel protein found in *Escherichia coli* was used, since it is inexpensive and can be expressed in large quantities. AqpZ has been shown to be robust under different reducing conditions and at low temperatures. It can retain 100% activity for up to 6 months of storage at 4^{o}C. [114, 150]. The overarching purpose is to improve water permeability while enhancing ion rejection, by incorporating AqpZ into the membrane. Successful formulation could then lead to the formation of

biomimetic membranes with high selectivity and high water flux. In this study, aquaporins were treated with gum arabic (GA), a polysaccharide used previously to disperse carbon nanotubes to PVA successfully with the key purpose of preventing excessive functionalities that lead to disruption of the original structures.[224]. Gum arabic is a water soluble polysaccharide produced by Acacia Senegal trees. . In modern times, the most important applications of gum arabic have been as an emulsifier in the food and pharmaceutical industries and as an adhesive [249-251]. Gum arabic has been used in the food industry as a stabilizer, thickener, emulsifier, anti-caking agent as well as color preservative [252]. It has also been used to slow down the deterioration of inks [253, 254], and it has been observed to be significantly enhance the stability of iron-gall inks [255]. Gum arabic has been used to increase the durability of the functional textiles and add value to them [256]. Gum arabic conjugated polysaccharides showed an unusually high tolerance to salts, thermal instability and lower stability in alkaline conditions [257]. This ability of GA to prevent functionality of materials is exploited here with the purpose to have it protect the aquaporins from being functionalized in the presence of PVA. GA acted as an intermediate layer to enhance the interfacial interaction between the selective layer and the substrate, thus making the assembly stronger. Aqp-GA was then dispersed in a polyvinyl alcohol matrix carrying alkyl side chains (PVA-alkyl). PVA-alkyl is amphiphilic in nature with high hydrophilicity of PVA and hydrophobicity of the long alkyl side chains. This polymer has good film forming properties and outstanding physical and chemical stability [258], and is proposed to be an excellent material to support aquaporins. Thus, by attaching PVA-alkyl matrix with Aqp-GA dispersed in it to the hydrophilized PBI membranes, the assembly was made

mechanically stronger and was designed to withstand higher hydraulic water pressure gradients.

5.2 Research Objective:

The objective of the project is to make a new class of biomimetic nanofiltration membranes made of aquaporin dispersed in a membrane selective layer and capable of operation under high hydraulic pressure. The PVA-alkyl with embedded aquaporins will be used as the nanofiltration membrane active layer (Figure 5-1). Aquaporins are dispersed into PVA-alkyl layer, but not necessarily aligned into the layer. Aquaporins are bidirectional in nature; hence, even if their orientation is different than aligned, it does not affect the transmembrane water transport.

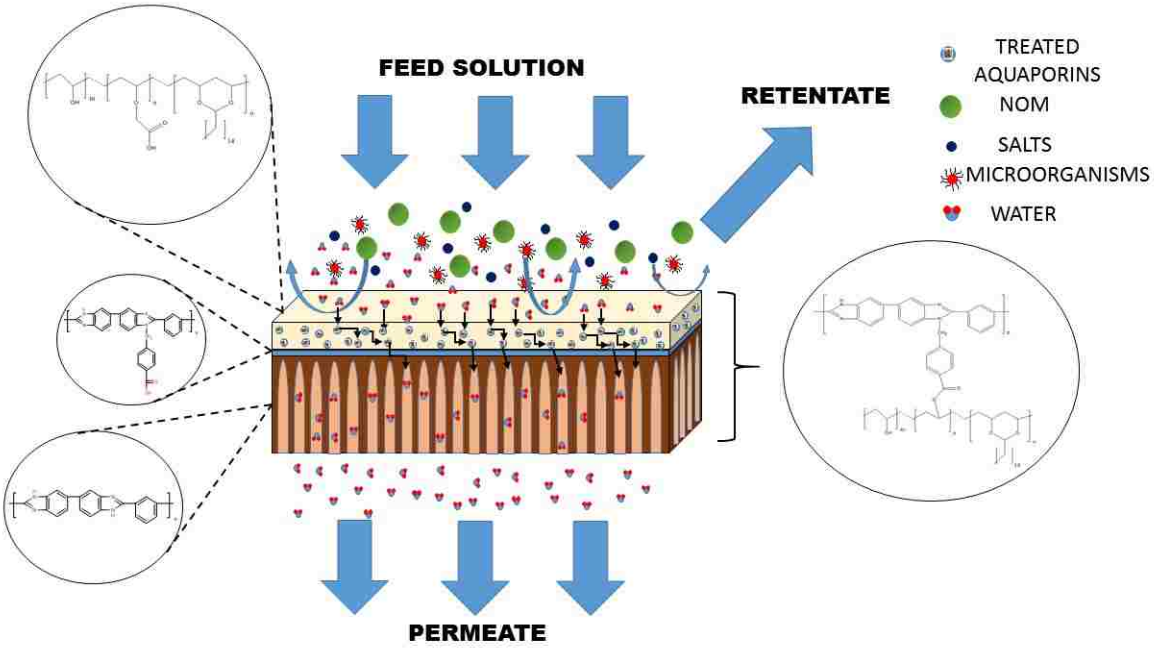

Figure 5-1 Schematic of biomimetic membranes

5.3 Methodology:

5.3.1 PBI membranes casting:

The dope polymer used to cast the backbone of the membranes was polybenzimidazole (PBI). PBI is stable polymer, which has robust mechanical strength with thermal stability for a wide range of high temperature applications and it also provides chemical stability over a wide pH range. PBI membranes are hydrophobic [259, 260], and are strong but brittle [214, 217, 261]. The structure of PBI molecule is shown in Figure 5-2. The imidazole ring of PBI contains two nitrogen atoms, one protonated to serve as a potential hydrogen bond donor and the other nitrogen has a lone pair, which can act as a proton acceptor.

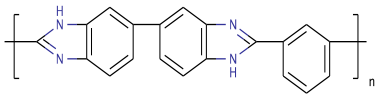

Figure 5-2 PBI molecule structure.

The solvent used to make the dope solution was N, N-Dimethylacetamide. Commercially-available 26% w/w dope solution, containing 26% PBI polymer, 72% N, N- Dimethylacetamide (DMAc) and 2% Lithium chloride (LiCl), was used and obtained from PBI Performance Products, inc. (Charlotte, NC). LiCl served the function of a pore former, preventing PBI polymer from phasing out of the solution [214, 215] and imparting long shelf life to the solution. The dope solution was diluted to 21% PBI by adding solvent, and the solution was sealed with parafilm to prevent air bubbles from

being trapped inside the solution and affecting its homogeneity. Because of very high viscosity of the solution, the solution was kept in the sonicator and degassed for 2 days in order to ensure homogeneous mixing of the solvent and the solute. After sonication, the solution was allowed to come to room temperature and then the solution was ready for membrane casting using the phase inversion process. Phase inversion is the phenomenon whereby the phases of a liquid-liquid dispersions interchange such that the dispersed phase spontaneously inverts to become the continuous phase [216, 261]. The non-solvent phase that was used in this process was water. The PBI chemistry used here was identical to that of previous studies which made nanofiltration membranes with a pore size of 0.61 nm, so the unmodified PBI membranes of this study should also be suitable for nanofiltration [217].

A casting knife, or doctor's blade (Paul N Gardner Co, U.S. Pat 4869200, Pompano Beach, FL.) was used to make flat sheet membranes. A clean glass mirror was used as a surface, which provides optimum hydrophobicity to the membranes and helps for detachment of polymer films during phase inversion [216]. The solution was placed in an even line on the surface and the casting knife was used to push the solution across the glass surface to make a thin film. The thickness of the membranes was kept between 150 µm and 200 µm. A water coagulation bath was used to induce phase inversion with subsequent pore formation within the membranes. Once the phase inversion had taken place, the membrane came out of the surface of the water. The membrane was thoroughly washed with water and kept in a 50/50 glycerol-DI water solution. Glycerol was added to DI water to ensure that the membranes would stay wet during storage because when they

are dried, they can become brittle and susceptible to breakage [217]. The membranes were kept in the solution at least one day before they were analyzed.

5.3.2 Surface activation of membranes:

The polybenzimidazole membrane surface needs to be activated for further modifications with PVA-alkyl and additions of Aqp-GA to the PVA-alkyl matrix. Activation was achieved by reaction of a highly reactive chlorine atom, from 4-chloromethyl benzoic acid (CMBA) purchased from Sigma-Aldrich (USA), with the secondary amine group in the imidazole ring of the repeat unit in PBI backbone (Figure 5-2). CMBA adds a carboxylic group to the surface, which serves two purposes: 1) to impart negative charge on the membrane surface, and 2) to act as a platform for subsequent functionalization of the membrane. It is important to note that there are two secondary amine sites in PBI molecule, so after the reaction, carboxylic groups are added on both sites on the molecule. For simplicity, the reaction at only one site is shown (Figure 5-3).

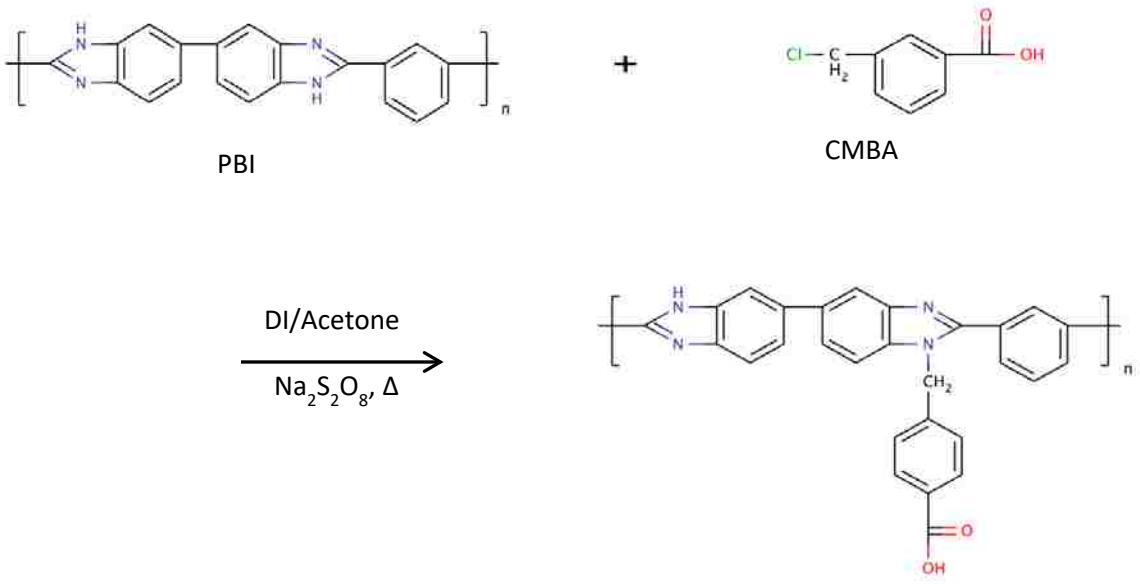

Figure 5-3 CMBA modification of membrane.

Modification was performed according to previous studies [217]. For the reaction, 1 wt% solution of sodium persulphate in water was prepared for use as a free radical initiator for the reaction. 200 ml DI water were taken in a 500mL beaker with a stir bar. 2.02g sodium persulphate was added to the water, and the solution was stirred on hot plate at 40°C. Two membranes were added to the solution, which were kept fully submerged and were not stuck under the stir bar. In a second beaker, 0.5 wt% solution of CMBA in acetone was prepared. 0.788 g CMBA was added to 200 mL acetone and was stirred until dissolved. Then acetone/CMBA solution was slowly added to the beaker on a hot plate while stirring, and then covered. This was done in order to prevent the precipitation of CMBA as it is insoluble in water. The final solution was a 50/50 mixture. The temperature of the solution was kept at 40°C and it was stirred for 24 hours to keep

all the reactants in solution and prevent the evaporation of CMBA. Once the reaction was finished, the membranes were washed with copious amounts of DI water to remove excess sodium persulphate and immediately placed in glycerol/water bath.

5.3.3 Preparation of PVA–alkyl:

PVA-alkyl is polyvinyl alcohol carrying long alkyl side chains. It is amphiphilic as it has both hydrophilic (PVA) and hydrophobic (alkyl chains) elements present. This polymer has good film forming properties and outstanding physical and chemical stability. Using PVA as skin layer provides the resulting membranes with high water permeation rate, good antifouling nature, and excellent integrity in acidic and alkaline and remarkable resistance to abrasion [258, 262]. PVA-alkyl was prepared in two steps [218, 219], the preparation of (1) carboxy-methyl PVA followed by (2) PVA-alkyl.

5.3.3.1 Preparation of carboxy-methyl PVA (PVA-COOH):

The preparation of carboxy-methyl PVA (PVA-COOH) followed literature methods [220, 221], summarized here. Initially, 50 mL water were taken in a 100 mL beaker, 1 g PVA (Acros Organics, USA) was added to it, and the solution was kept at 70^{o}C. The mixture was stirred for 1 hour continuously to prevent PVA from sticking to the bottom of the beaker until it completely dissolved. The solution was transferred to a 500 mL beaker, and 50 g of sodium monochloroacetate (Fisher Scientific, Pittsburgh PA) were added. The solution was then covered with aluminum foil and was incubated at 4 ^{o}C for 24 hours. After that, 42 mL water were taken in a 100 mL beaker, 42 g sodium

hydroxide (Fisher Scientific, Pittsburgh PA) were added, and the mixture was stirred until the sodium hydroxide dissolved.

NaOH/water solution was added to the incubated solution of PVA and sodium monochloroacetate in water, and stirred at room temperature for 24 hours. Then, it was neutralized using a 6 M solution of hydrochloric acid (Fisher Scientific, Pittsburgh PA) in water was prepared in a separate beaker with pH being continuously monitored. This neutralized solution was dialyzed against deionized water. The molecular weight cut-off for the dialysis was chosen as high as possible, which was 12-14 kDa in order to maximize dialysis rate. The dialysis tubing (Fisher Scientific, Pittsburgh PA) used was soaked in water for 3 hours in order to open it and fill it with the solution. It was then sealed with dialysis locking membrane clamps. A 2000 mL beaker with a stir bar in it was filled with DI water to be used as a dialysate. It was kept stirring and the water was changed after every 4-5 hours to make sure that the driving force for the dialysis is high. The procedure was continued for 3 days, and the remaining solution in the tube was taken out and stored in another beaker. Then, the stored solution after dialysis was deionized using ion-exchange resins. DOWEX 1X8 (Acros Organics, USA) was used for negatively charged ions and DOWEX 50WX8 (Acros Organics, USA) was used for positively charged ions. The output solution after the ion exchange was lyophilized using freeze dryer. For that, the solution was kept in centrifuge tubes and was allowed to freeze dry for 3 days. PVA-COOH was obtained as a white solid after freeze-drying. The weight of the product was 0.45 g and the yield was 39%. The overall reaction is shown in Figure 5-4.

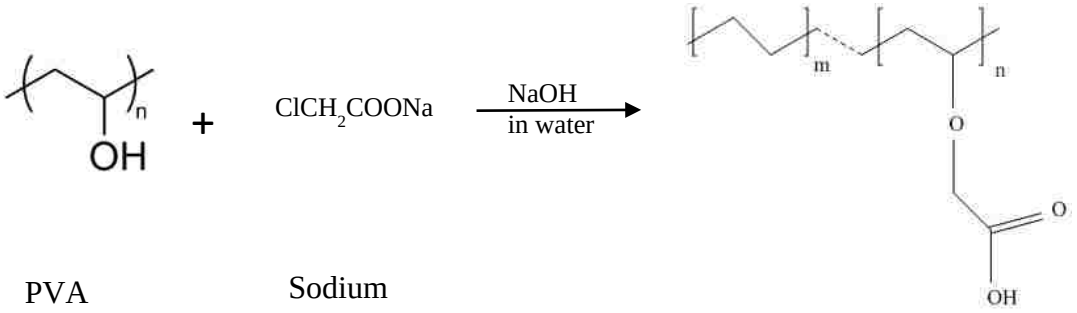

PVA

Sodium monochloroacetate

PVA-COOH

Figure 5-4 PVA-COOH synthesis.

5.3.3.2 Preparation of PVA-alkyl:

The second step of making PVA-alkyl was synthesis of hexadecanal. Chemicals used for the preparation were celite, pyridinium chlorochromate and 1-hexadecanol. Dichloromethane was used as the solvent. 11.2 mL dichloromethane were taken in a 50 mL beaker while stirring, and 0.95 g celite, 0.95 g pyridinium chlorochromate and 0.5 g 1-hexadecanol were added to the beaker under a fume hood. The solution was sealed with aluminum foil and stirred for 6 days at room temperature. After that, the reaction mixture was diluted by adding 40 mL diethyl ether. Florisil columns were used to remove excess celite, pyridinium chlorochromate and 1-hexadecanol. Then the mixture was evaporated, and hexadecanal was obtained as a white solid.

PVA-COOH obtained after first reaction was dissolved in DMSO. Hexadecanal and 200µL of 12 M hydrochloric acid were added to the solution, which was maintained at 70 ^{o}C and stirred for 25 hours. The reaction mixture was extracted with diethyl ether. The mixture was then neutralized with 1M sodium hydroxide. The neutralized solution was dialyzed against DI water using dialysis tubing of 12-14kDa following the same

procedure as described previously. The solution was then desalted with ion exchange resins previously mentioned and lyophilized using a freeze dryer for 3 days. PVA-alkyl was obtained as a white solid with yield of 49% at a final weight of the product was 0.22 g. The overall reaction for the second step of the process is shown in Figure 5-5.

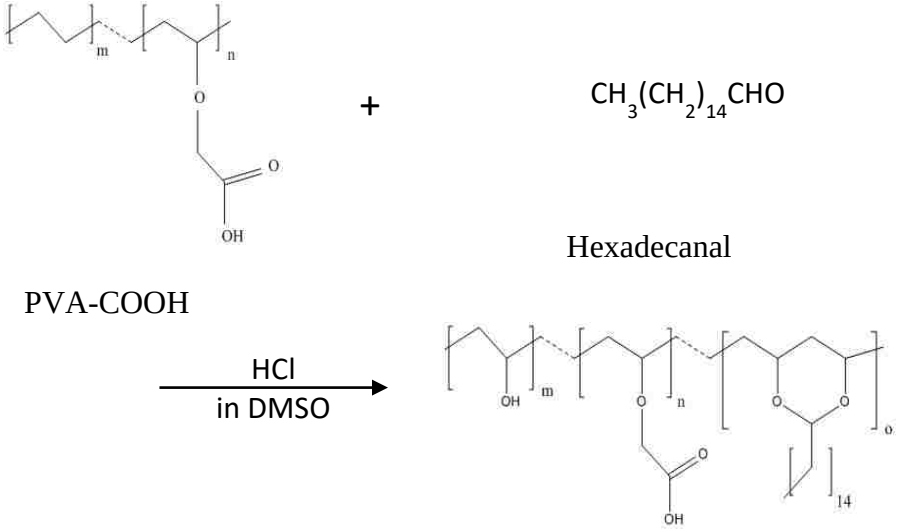

Figure 5-5 PVA-alkyl synthesis.

5.3.4 AqpZ expression and purification:

Aquaporin Z (AqpZ) is a bacterial aquaporin from *Escherichia coli*, which shows high degree of homology to its mammalian counterparts and can be expressed in a bacterial host. Furthermore, it is highly stable and resists denaturing due to heat, detergent, voltage, and pH changes [114, 150]. This makes the protein suitable for commercial use.

The pET-NH6 plasmid (a generous gift from Dr. Michael Weiner, University of Virginia) was transformed into an Escherichia coli C43(DE3) cell line for protein

expression. Single colonies bearing the plasmid were used to inoculate four liters of LB media containing 100 μg/mL ampicillin at 37 °C with shaking at 250 rpm. After reaching an OD600 of 1.0, AqpZ protein expression was induced by addition of 1 mM isopropyl β-D-thiogalactopyranoside (IPTG) with further incubation for 3 hours at 30 °C and shaking at 250 rpm. Cells were harvested and stored at -80 °C until use.

The protein was purified by using a modified version of a previously published protocol [263]. Five grams of cells paste were resuspended in 50 ml cold buffer (20 mM Tris-HCl pH 7.4, 500 mM NaCl and 1 mM Pefabloc). The suspension was lysed by ultrasonication using 30 sec pulse on and 2 min pulse off cycle for a total exposure time of 8 min. The lysate was centrifuged at 12,500 rpm for 30 minutes to pellet cell debris. Membrane fractions were collected by high speed at 40,000 rpm for 1 hr. The total membrane pellet was resuspended in cold buffer (20 mM Tris-HCl pH 7.4, 500 mM NaCl, 1 mM Pefabloc and 10% glycerol) and 270 mM of n-octyl-D-glucopyronoside (OG) was added with incubation at room temperature on a rocking platform.

The solubilized membrane was loaded onto a 5 mL TALON superflow metal affinity (Co2+-IMAC) equilibrated with Buffer A (20 mM Tris–HCl, pH 7.4, 500 mM NaCl, 10% glycerol and 40 mM OG) using an ÄKTA chromatography system. The column was washed with 10% buffer B (20 mM Tris–HCl, pH 7.4, 500 mM NaCl, 10% glycerol, 40 mM OG and 500 mM imidazole) for 10 column volumes. The protein was eluted with a linear gradient from 50 mM to 500 mM imidazole and the peak fractions were analyzed by SDS-PAGE (NuPAGE Novex 4-12% Bis–Tris gels). The calculated monomer mass of hexahistidine-tagged AqpZ is 27 kDa, but on this gel the AqpZ protein run at a lower electrophoretic mass of approximately 22 kDa, as shown in Figure 5-6.

The AqpZ containing fractions were pooled and stored at -80 °C until ready for incorporation into the membranes.

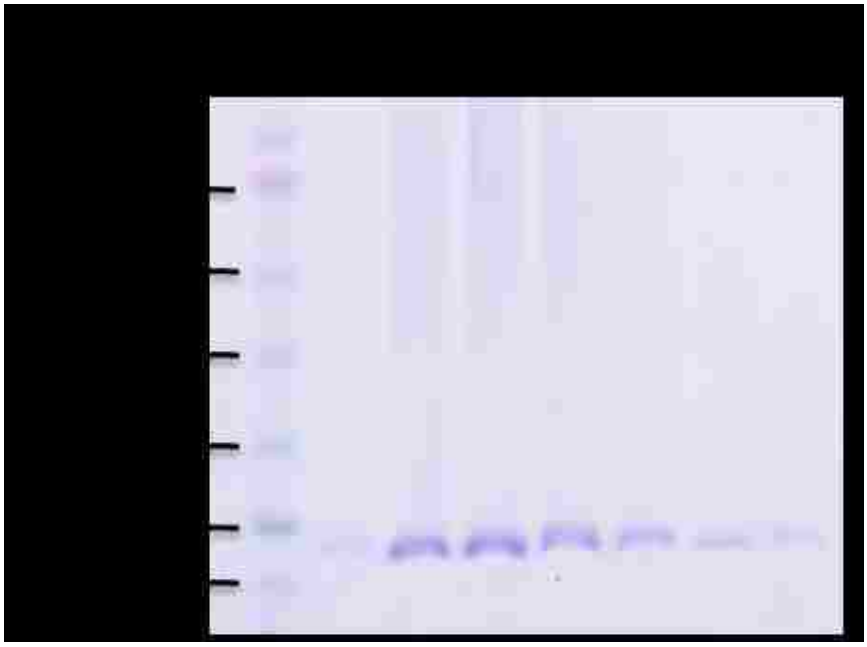

Figure 5-6 SDS- PAGE showing purification of AqpZ with the protein band migrating at 22 kDa.

5.3.5 Treatment of AqpZ with gum arabic:

A 15wt. % solution of gum arabic (Fisher Scientific, USA) in water was prepared. AqpZ was added to this solution and sonicated under mild conditions for 4 hours in order to disperse it in the gum arabic solution. The concentration of AqpZ was 1ml/3ml of GA. Gum arabic has been used previously to disperse carbon nanotubes to PVA without either shortening the nanotubes or disrupting their structures. After the addition of GA to carbon nanotubes solution, the suspension was found to be stable over few months and was not affected by centrifugation. Hence, it was proposed to protect the structure of aquaporins.

The weight ratio of AqpZ to gum arabic was kept at 1:4. The mixture was kept stirring at room temperature for 72 hours and then heated slowly to remove water [223, 224]. Gum arabic-treated AqpZ were then added to de-ionized water and sonicated for 30 minutes. The solution with gum arabic-treated AqpZ was physically dispersed into the PVA-alkyl solution. The ratio of AqpZ-GA to PVA-alkyl solution was 1:1 by volume. Aquaporin is bidirectional water channel protein; hence the orientation of the protein isn't expected to change the water flux through the protein [225].

5.3.6 Surface modification of PBI membrane using Aqp-PVA-alkyl:

Aqp-PVA-alkyl was attached to the membrane using carbodiimide chemistry [217], for the reaction between a carboxylic group and the hydroxide group present in PVA-alkyl molecule. For the reaction, N-(3-dimethylaminopropyl)-N'-ethylcarbodiimidehydrochloride (EDCH) and N-hydroxysuccinimide (NHS), both purchased from Sigma-Aldrich were used. The reactions were performed in 2-(N-morpholino) ethanesulfonic acid (MES) buffer (Sigma-Aldrich, USA).

400 mL water were taken in a 500 mL beaker and 7.85 g MES buffer was added with stirring, Followed by the addition of11.75g NaCl with stirring. The solution was titrated to pH 6 using NaOH, 0.23 g NHS and 0.153 g EDCH were added to the solution and stirred well. CMBA modified PBI membranes were added to the solution, stirred for 15 minutes, and then the reaction mixture was titrated to pH 7 using NaOH. PVA-alkyl was added to the solution and stirred for 24 hours, and then the membranes were removed and rinsed well with DI water and stored in a beaker filled with DI water. The

membranes were stored for 24 hours before using it for analysis. The overall reaction is shown in Figure 5-7.

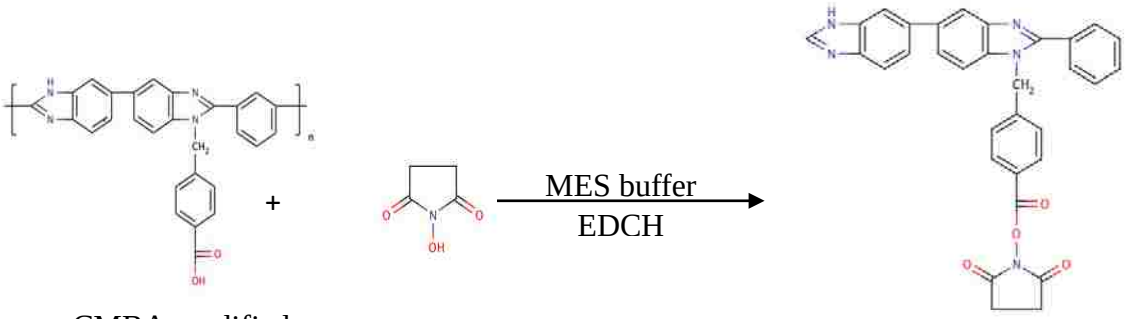

CMBA modified PBI + NHS → NHS ester intermediate

5-7 (A)

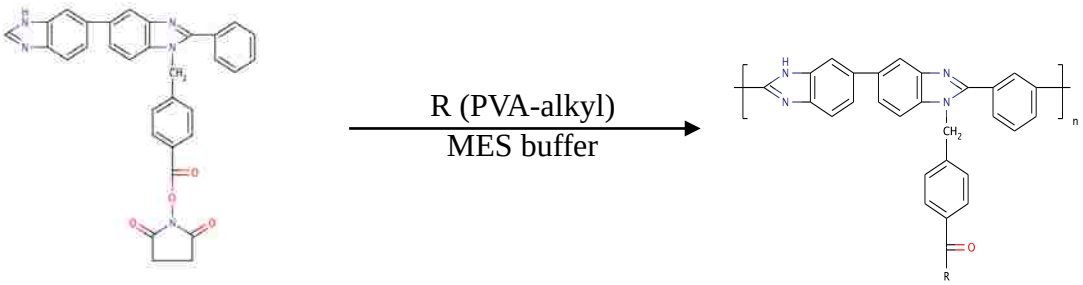

NHS ester intermediate → Aqp-PVA-alkyl modified membrane + NHS

Figure 5-7 (b)

Figure 5-7 (a) and (b) Carbodiimide membrane activation chemistry

5.3.7 Membrane characterization:

5.3.7.1 Fourier Transform Infrared Spectroscopy (FTIR):

A vibrational spectrum is a characteristic of every molecule and is considered a unique property of that molecule [226]. FTIR was used in ATR mode to determine the

chemistry of the proposed reactions and modifications on the membrane surface. Digilab UMA 600 FT-IR microscope was used for all the analysis of membrane samples performed in this study.

5.3.7.2 Contact angle measurements:

Contact angle is defined as the measure of wettability of a surface. Cam-Plus Micro contact angle meter (Tantec Inc., Schaumburg, IL) was used for the contact angle measurement of all the membrane samples. A small drop of water was placed on the membrane surface and resultant angle of the droplet to the surface was measured as shown in Figure 5-8. The higher the hydrophobicity of the membrane, the higher the contact angle.

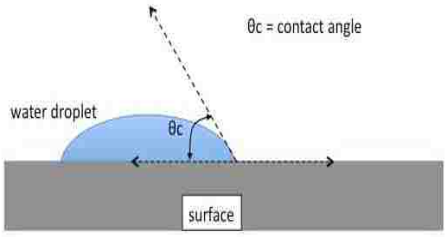

Figure 5-8 Contact angle measurement [227].

5.3.7.3 Flux analysis:

Dead end filtration was used to monitor the flux decline of both PBI and PVA-alkyl-AqpZ membranes. Filtration experiments were performed using Amicon filtration cell (Amicon Stirred Cell 8010 – 10 ml). Using a constant membrane surface area of 4.1 cm^2, the time to collect a 2-ml permeate sample was measured for each feed and flux was calculated. A constant pressure of 70 psi (4.83 bar) for laboratory purposes and

continuous stirring was applied in all tests. Flux values were calculated as L/m^2-hr and plotted against the total time of filtration. Membrane samples were cut into circular pieces of area 4.1 cm^2 and supported by a Whatman^{TM} filter paper (110 mmø). Each membrane was precompacted with DI water for 7-8 hours until a stable flux was reached. Precompaction was followed by filtration of protein solutions of 10 ppm each of bovine serum albumin (BSA) and lipase protein in water. The same filtration cell was used for protein filtration under the same conditions of pressure and stirring. Protein rejections were calculated using UV-VIS spectrometer (Varian Inc. Cary 50, Agilent Technologies, Santa Clara, CA) according to following equation (4-1).

Salt rejection was tested using five solutions of different concentrations of sodium chloride and calcium chloride in DI water: 3.4, 10, 20, 35 and 100 mM solutions. Solutions were run through the 10 ml dead-end cell under the same conditions as used for the pure water flux testing. Continuous stirring was applied inside the cell to prevent salt build-up on the membrane surface. Two mL permeate samples were collected for each feed. Salt rejections were calculated using conductivity meter. The apparent solute rejection R (%) was calculated using equation (4-1).

After each feed water filtration, the membrane was backwashed for 1 hour with DI water and filter paper support was changed. The flux recovery of the membrane was measured after reverse flow filtration with DI water.

5.3.7.4 Morphological characterization:

Environmental scanning electron microscopy (ESEM) was used to verify the asymmetric morphology of the membranes and monitor the surface of both unmodified

and PVA-alkyl-AqpZ modified membranes before and after filtration. An FEI Quanta 3D FEG Dual Beam Electron Microscope (FEI, USA) was used to test the samples. By freezing small samples of the membranes in liquid nitrogen and cracking them, smooth cross-sectional areas could be observed. In order to get an image of cross-section of the membranes, the frozen and cracked samples were attached vertically to a carbon tape while the samples were attached horizontally to the carbon tape to get an image of membrane surface. The surfaces of the samples were dusted with a thin layer of palladium-gold using a Cressington 108 auto sputtering device and then observed under scanning electron microscope.

5.4 Results and Discussion:

5.4.1 Chemical analysis:

Figure 5-9 shows the FTIR analysis of PBI, CMBA and PVA-alkyl-AqpZ membranes, and Table 5-1 identifies all peaks. FTIR showed peaks at ~1050 cm^{-1} for C-O stretch, ~1200 cm^{-1} for alkyl substituted ether, which is observed after PVA-alkyl is attached to CMBA-modified PBI molecule using carbodiimide chemistry (Figure 5-10). A peak at 1660 cm^{-1} corresponds to C=O stretch that is present in the final molecule due to addition of CMBA. FTIR spectrum of PBI molecule also shows a peak at 1650 cm^{-1}, which identifies the presence of secondary amine group present in PBI. Peak 4 corresponds to O-H stretch, which is present in CMBA-modified PBI molecule as well as PVA-alkyl-AqpZ-modified molecule (Figure 5-10). Peak 5 in the analysis is due to long

alkyl chains that are present in the PVA-alkyl-AqpZ-modified molecule [226]. A very broad peak around 3400 cm^{-1} is observed in all the membrane samples, which is associate with N-H stretching [264]. Bonds corresponding to different functional groups are indicated in Figure 5-10.

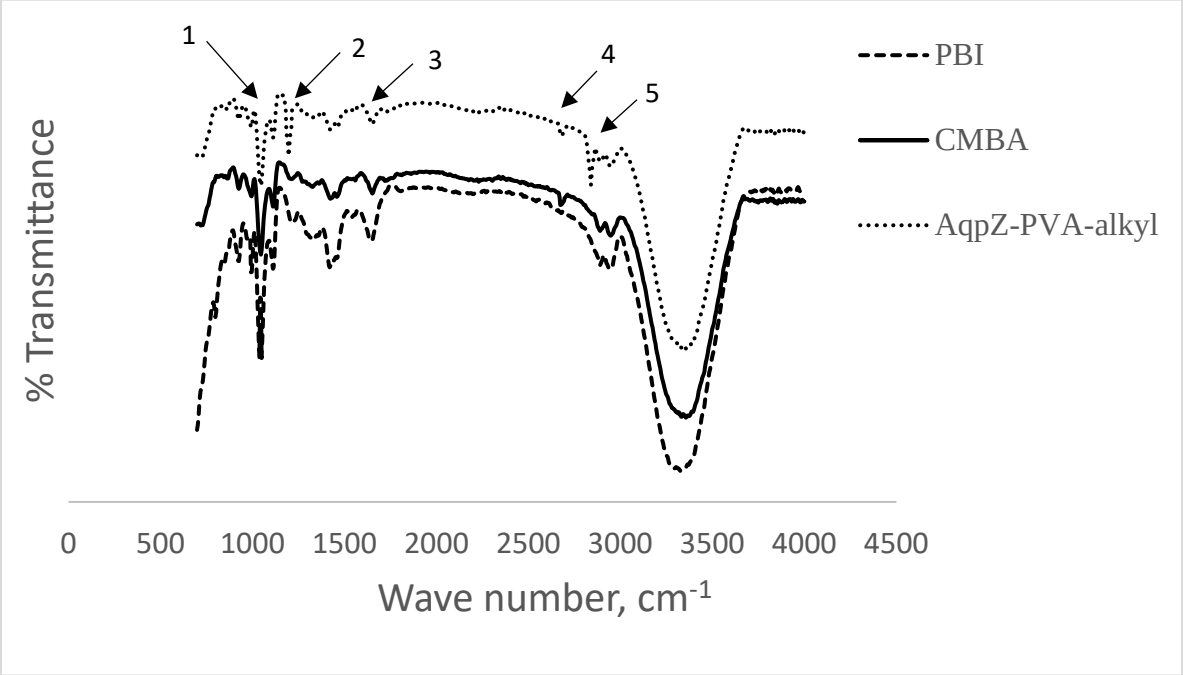

Figure 5-9 FTIR analysis of unmodified, CMBA modified and PVA-alkyl modified membranes.

Table 5-1 Functional groups and corresponding wave numbers in IR spectra.

Band number	Functional group	Wave number (cm^{-1})
1	C-O	1057
2	C-O (ether)	~ 1200
3	C=O	1670-1820

4	OH	~ 2670
5	C-H	~ 2850
6	>N-H	1550-1650

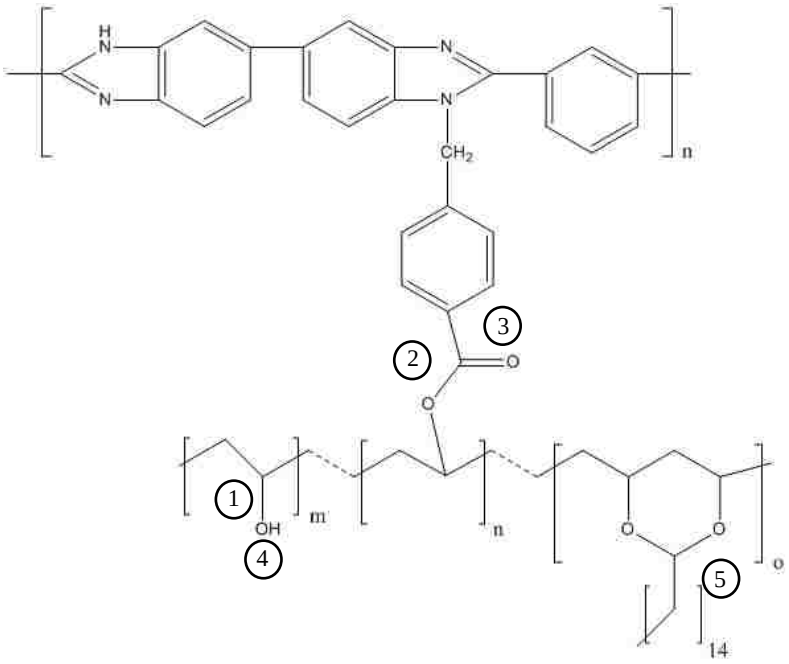

Figure 5-10 AqpZ-PVA-alkyl modified PBI molecule.

5.4.2 Hydrophobicity:

Contact angle was used as a measure of hydrophobicity, and results are shown in Figure 5-11. CMBA modified membranes were found to be more hydrophilic than PBI membranes [217, 261]. This was most likely due to addition of a –COOH group in the modified molecule and its increased ability to form hydrogen bonds because of the

presence of oxygen with a lone pair. However, the change is not statistically significant because of the overlap of standard deviations. After the addition of PVA-alkyl to the membranes, the contact angle decreased further showing a significant increase in the hydrophilicity of the membrane. This was most likely due to high hydrophilicity of PVA [258]. After AqpZ was added to the membrane, there was no significant difference between its contact angle and that of the PVA-alkyl membranes, which is likely because the aquaporins that were added to PVA-alkyl matrix were embedded inside the matrix and not on the surface of the membrane.

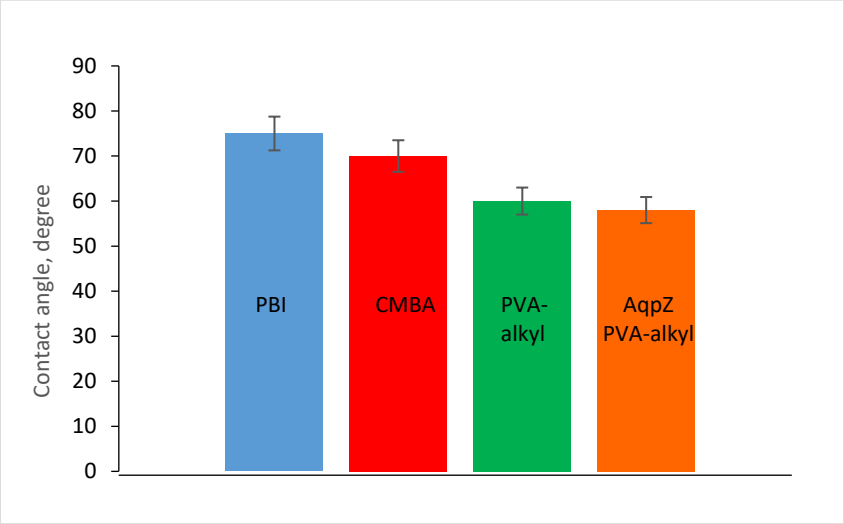

Figure 5-11 Hydrophobicity via contact angle

.

5.4.3 Flux analysis:

5.4.3.1 Flux profile:

Before comparing observations between PBI and PVA-alkyl-AqpZ (or AqpZ-modified) membranes, it is important to separate the effects of the addition of PVA-alkyl only and PVA-alkyl-AqpZ to the membrane in order to separate the effect of the presence of the amphiphilic/polar PVA-alkyl inclusions from that of the presence of AqpZ. Experiments were conducted in parallel comparing PBI, PVA-alkyl and PVA-alkyl-AqpZ membranes using BSA and lipase solution filtration. The flux analyses are shown in Figures 5-12, 5-13 and 5-14. For PBI membranes, the pure water flux was 7.90 L/m^2-h (LMH), the initial flux for BSA filtration was 5.77 LMH, the recovery after BSA filtration (i.e. after DI backwash) was 5.47 LMH (or a 69% flux recovery, as compared to the initial pure water flux), and the final flux after lipase filtration was 3.82 LMH. BSA and lipase rejections were approximately 86% and 84%, respectively. After the addition of PVA-alkyl (no aquaporins), the pure water flux was lower at 6.0 LMH, which is likely due to the extra resistance added by the addition of PVA-alkyl to the surface of the membrane. The initial flux for BSA filtration was 4.36 LMH, the recovery after BSA filtration was 4.80 LMH (or an 81% flux recovery), and the final flux after lipase filtration was 4.13 LMH. BSA and lipase rejections were approximately 90% and 87%, respectively. While flux values for the PVA-alkyl membranes were not as high as for the PBI membranes, it is clear that the flux decline during filtration was improved and the final flux after the 36-hour filtration period was higher. This was associated with the increase in hydrophilicity of PVA-alkyl (Figure 5-11). Lastly, after the addition of PVA-alkyl with embedded aquaporins (PVA-alkyl-AqpZ), the initial pure water flux was lower at 5.32 LMH, which again is likely due to the extra resistance. The initial flux for BSA filtration was 5.0 LMH, the recovery after BSA filtration was 5.0 LMH (or a complete

recovery of the filtration flux, or 96% flux recovery as compared to the initial flux), and the final flux after lipase filtration was 4.43 LMH. BSA and lipase rejections were approximately 91% and 87%, respectively. Protein rejection and flux recovery data is shown in Table 5-2. Therefore, it is concluded that the addition of aquaporins to the membrane led to a more consistent flux value and a nearly complete recovery of flux back to its initial pure water flux after cleaning. Actual data for Figures 5-12, 5-13, and 5-14 is presented in Appendix A, Tables A-1, A-2, and A-3.

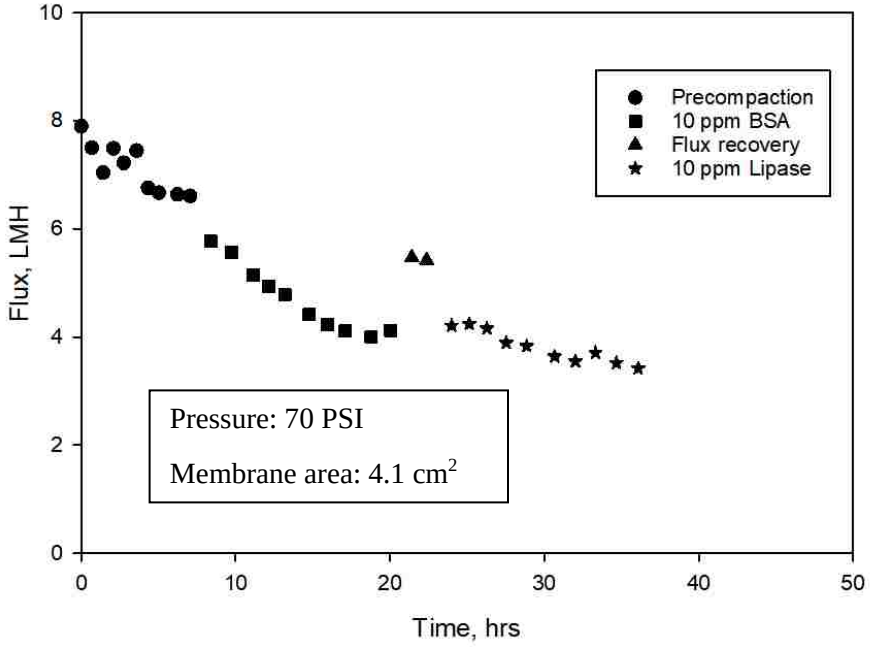

Figure 5-12 Flux analysis of unmodified PBI membrane.

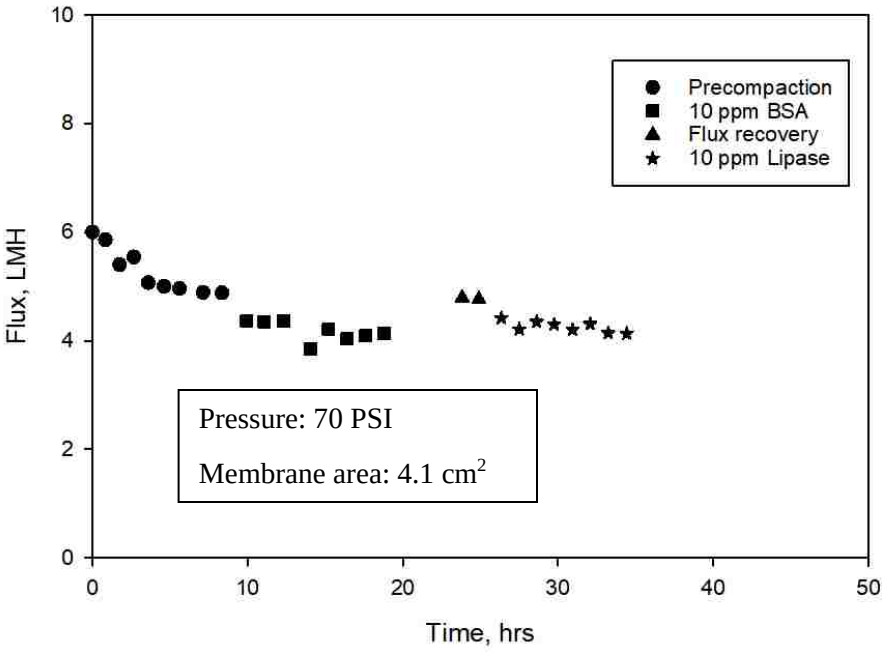

Figure 5-13 Flux analysis of PVA-alkyl modified PBI membrane.

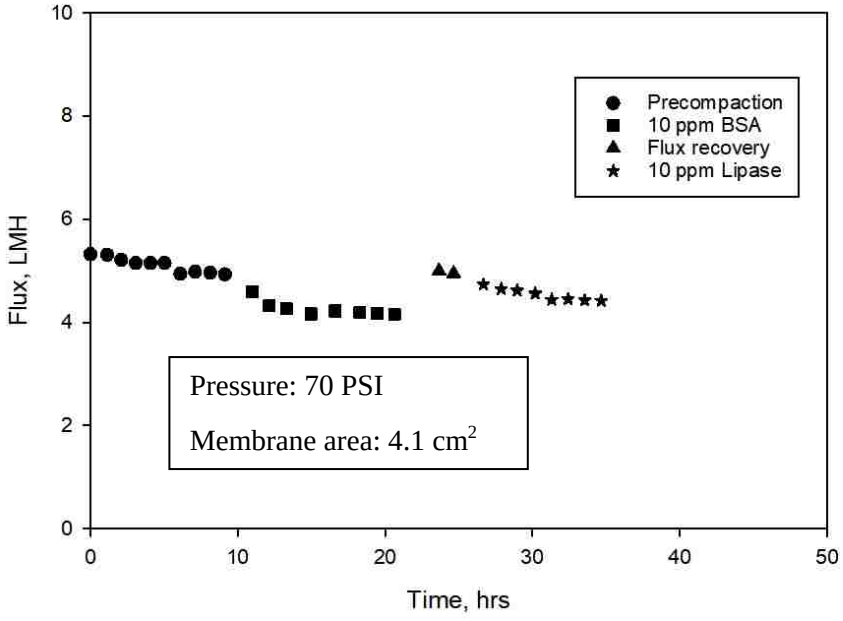

Figure 5-14 Flux analysis of AqpZ-PVA-alkyl modified PBI membranes.

Table 5-2 Protein rejection and flux recovery comparisons.

	Unmodified PBI membranes	PVA-alkyl modified PBI membranes	AqpZ-PVA-alkyl modified PBI membranes
BSA Rejection	86%	90%	91%
Lipase Rejection	84%	87%	87%
Flux Recovery	69%	81%	96%

More in-depth flux comparisons were then conducted between PBI and PVA-alkyl-AqpZ membranes for a period of 140 hours with protein solutions and salt solutions. These flux analyses are shown in Figures 5-15 and 5-16, respectively. For unmodified PBI membranes, initial flux values observed were higher than for the PVA-alkyl-AqpZ membranes due to extra increased thickness, and hence resistance, associated with the addition of PVA-alkyl to the membrane matrix. However, the flux decline observed was greater in unmodified membrane than modified membrane.

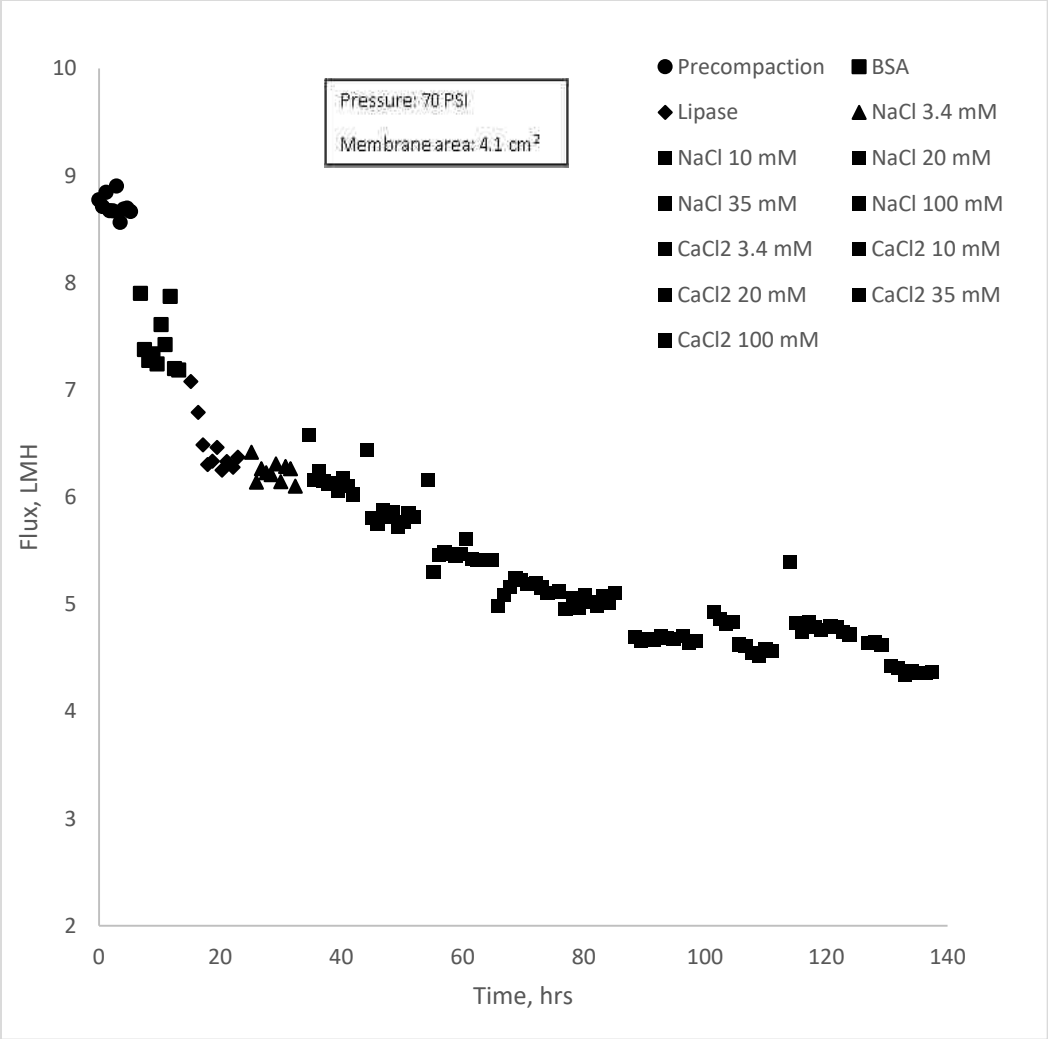

Figure 5-15 Flux analysis of unmodified PBI membranes.

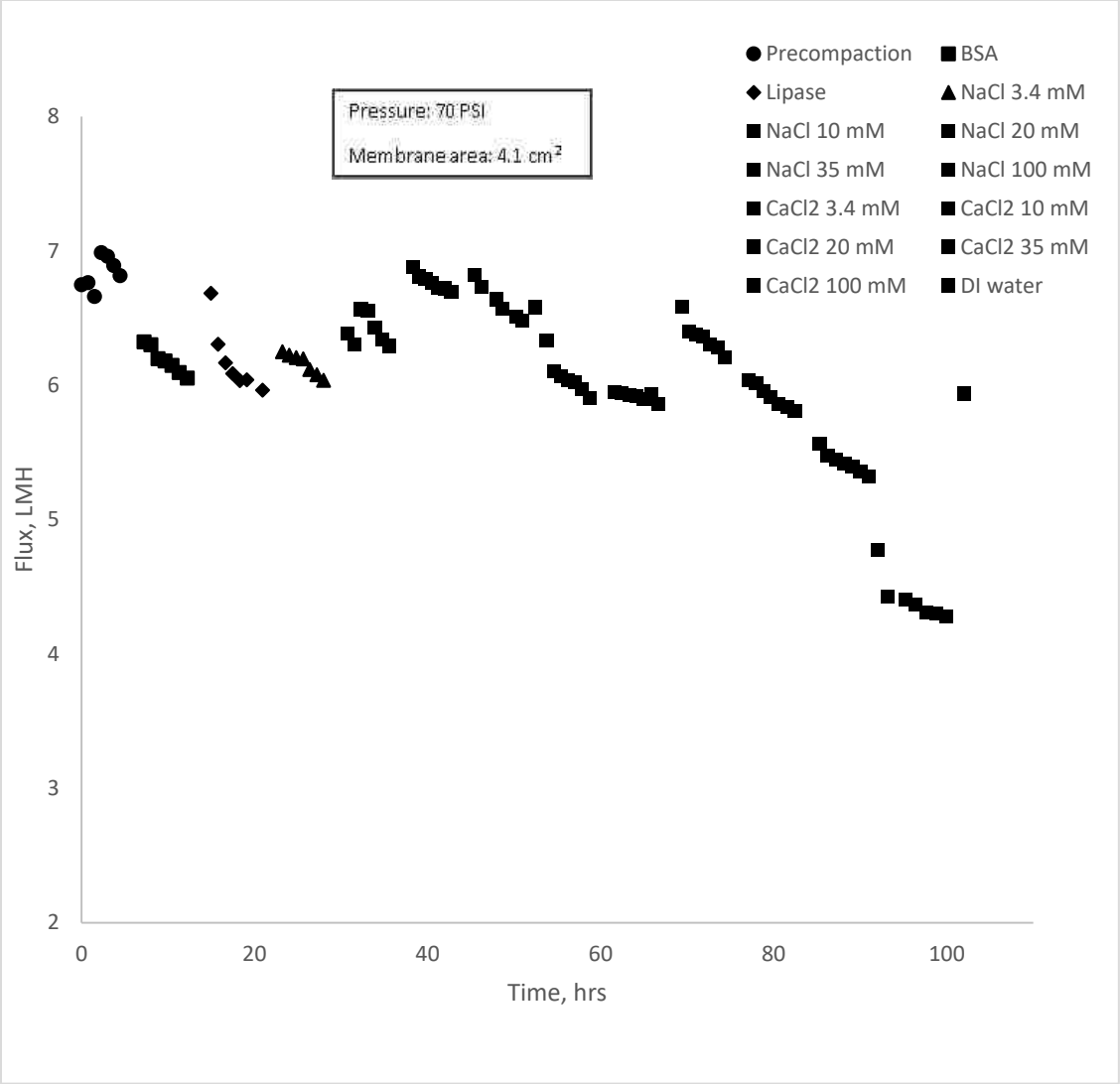

Figure 5-16 Flux analysis of AqpZ modified PBI membranes.

For PBI membranes, initial pure water flux was 8.77 LMH, initial flux for BSA filtration was 7.89 LMH and that for lipase filtration was 6.79 LMH. The flux recovery obtained after BSA filtration was 7.07 LMH (or an 80% flux recovery as compared to the initial pure water flux). Final flux after lipase filtration was 6.37 LMH and flux recovery after DI backwash was 6.41 LMH (a 73% of initial water flux). Rejections for protein filtrations are shown in Table 5-3. BSA and lipase rejections for unmodified PBI

membranes were 84% and 83%, respectively, and these were not significantly different from our initial PBI studies. For PVA-alkyl-AqpZ membranes, initial pure water flux was 6.74 LMH, which again was likely lower due to the additional resistance to flow from the addition of PVA-alkyl to the surface of PBI membranes. Initial flux for BSA solution for these membranes was 6.32 LMH and for lipase solution was 6.30 LMH. The flux recovery after BSA filtration was 6.68 LMH (or a 99% as compared to initial pure water flux). The final flux after lipase filtration was 5.96 LMH, and flux recovery after that was 6.24 LMH (a 92% of initial water flux). Rejection values for both BSA and lipase solutions increased for PVA-alkyl-AqpZ membranes. For BSA solution, an 88% and for lipase, an 86% rejection was observed. This might be due to addition of AqpZ in the PVA-alkyl matrix since aquaporins block the flow of protein molecules through the aquaporin structure. Any protein going through the membrane would be moving through the membrane regular pores.

Table 5-3 Rejection and flux recoveries for protein filtrations

	PBI membranes	AqpZ-PVA-alkyl membranes
BSA rejection	84%	88%
Lipase rejection	83%	86%
Flux recovery	61.11%	87.98%

Filtrations with protein solutions were followed by filtration with solutions of NaCl and $CaCl_2$ in water. Five different concentrations of salt solutions were chosen for filtration studies of both unmodified and modified membranes. For unmodified PBI

membranes, initial flux for 3.4 mM NaCl feed solution was 6.14 LMH and final flux was 6.10 LMH, with a flux recovery of 6.58 LMH (75%). For PVA-alkyl-AqpZ membranes, the initial flux for the same NaCl solution was 6.22 LMH, the final flux was 6.03 LMH and flux recovery was 6.38 LMH (94.6%). A 10 mM NaCl solution was used as feed after DI water backwash. For PBI membranes, the initial flux was 6.16 LMH, the final flux was 6.02 LMH and flux recovery was 6.44 LMH (73.43%), while for PVA-alkyl-AqpZ membranes, the initial flux was 6.30 LMH, the final flux was 6.29 LMH and flux recovery was 6.87 LMH (100%). When the NaCl solution concentration was increased to 20 mM, the unmodified PBI membranes showed an initial flux 5.80 LMH, final flux was 5.81 LMH and flux recovery was 6.15 LMH (70%). For PVA-alkyl-AqpZ membranes, initial flux was 6.80 LMH, final flux was 6.69 LMH and flux recovery obtained was 6.81 LMH (100%). Upon another increase in the NaCl feed solution concentration to 35 mM, the initial flux for the PBI membranes was 5.30 LMH, the final flux was 5.41, and flux recovery was 5.41 LMH (61.7%). Again, for PVA-alkyl-AqpZ membranes, flux values remained not significantly different from previous solutions with an initial flux of 6.73 LMH, final flux of 6.47 LMH and flux recovery of 6.33 LMH (93%). For 100 mM NaCl feed solution, PBI membranes showed an initial flux of 4.98 LMH, a final flux of 5.10 LMH and a flux recovery of 5.60 LMH (63.8% flux). For this this concentration of NaCl, the initial flux of PVA-alkyl-AqpZ membranes decreased slightly 6.10 LMH, a final flux was 5.90 LMH and flux recovery of 5.95 LMH (88.3%).

While flux declines during filtration were lower and flux recoveries higher with the PVA-alkyl-AqpZ membranes, flux values after the final recovery were approximately the same as PBI membranes; however, the greatest advantage of the PVA-akyl-AqpZ

membranes seems to be with respect to sodium chloride rejection, as shown in Figure 5-17. AqpZ-PVA-alkyl membranes showed higher rejections for the solutions as compared to PBI membranes. Unmodified PBI membranes showed 19% rejection during filtration of the 3.4 mM NaCl solution, and as the NaCl concentration went up to 100 mM, the rejection decreased to 5.3%. On the other hand, PVA-alkyl-AqpZ membranes showed a much better rejection of 73.5% for 3.4 mM feed solution of NaCl and 36% for 100 mM NaCl.

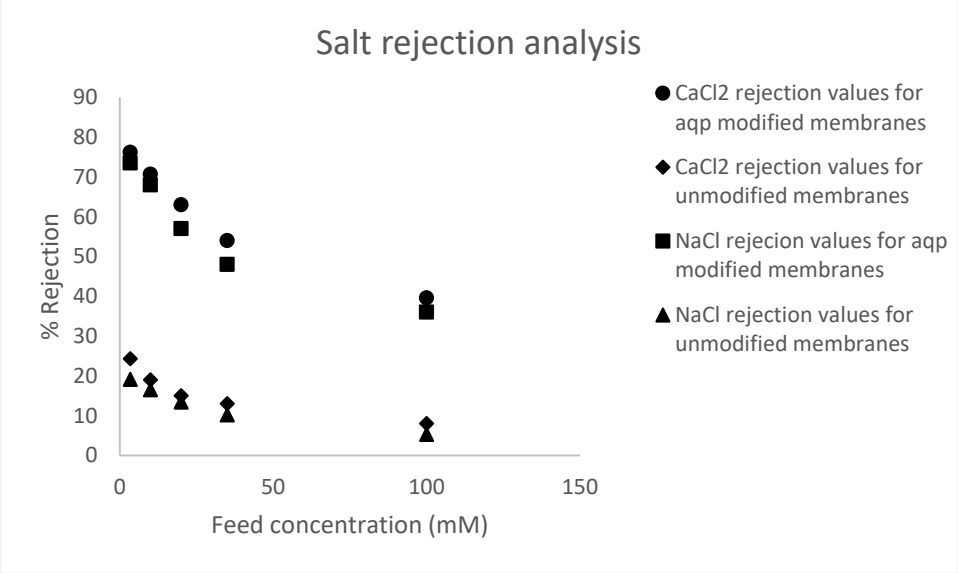

Figure 5-17 Sodium chloride and calcium chloride filtration rejection.

After NaCl filtration and the final flux recovery, $CaCl_2$ solutions of five different concentrations were filtered through the membranes (flux declines and recoveries are shown in Figures 5-12 and 5-13). For a 3.4 mM $CaCl_2$ feed solution, PBI membrane had an initial flux of 4.95 LMH, a final flux of 5.10 LMH and a flux recovery of 6.33 LMH (72.2%). PVA-alkyl-AqpZ membrane displayed an initial flux of 5.94 LMH, a final flux of 5.85 LMH and flux recovery of 6.58 LMH (97.6%) for the same solution. This was

followed by filtration of 10 mM $CaCl_2$ solution. For PBI membranes, the initial flux was 4.69 LMH, final flux of 4.65 LMH and flux recovery of 5.97 LMH (68%), while for PVA-alkyl-AqpZ membranes, these were 6.40 LMH, 6.20 LMH and 6.03 LMH (89.5%), respectively. After that, the concentration of the feed solution was increased again to 20 mM $CaCl_2$. PBI membranes gave initial flux of 4.92 LMH, final flux of 4.56 LMH and flux recovery of 6.02 LMH (68.6%), while PVA-alkyl-AqpZ membranes displayed 6.01, 5.80 LMH and 5.56 LMH (82.5%), respectively. For a feed solution of 35 mM $CaCl_2$ solution, the initial flux for PBI membrane was 5.39 LMH, final flux was 4.71 LMH and flux recovery was 5.76 LMH (65.7%). For the same solution, PVA-alkyl-AqpZ membranes had an initial flux of 5.47 LMH, final flux of 5.31 LMH and flux recovery of 4.77 LMH (70.8%). When feed concentration was increased to 100 mM of $CaCl_2$, the initial flux for PBI membranes was 4.63 LMH, the final flux of 4.36 LMH and flux recovery of 5.36 LMH (61.1%), while PVA-alkyl-AqpZ membranes had an initial flux of 4.42 LMH, final flux of 4.28 LMH and a flux recovery of 5.93 LMH (88%). Figure 5-17 also shows $CaCl_2$ salt rejections. For $CaCl_2$ salt solutions of low concentration (3.4 mM), the maximum salt rejection observed for PBI membranes was 24.3% while for PVA-alkyl-AqpZ membranes was 76.2%. As the concentration of $CaCl_2$ feed solution was increased to 100 mM, the rejection for PBI membranes dropped to 8%, while that for PVA-alkyl-AqpZ membranes was 39.6%. Therefore, as with NaCl filtrations, the final rejection of salts by aquaporin membranes remained significantly higher than for PBI membranes. It is important to note here that salt rejections observed for both the salt solutions for AqpZ-PVA-alkyl modified PBI membranes were not 100%. This might be

because of the feed solution going around aquaporins that are embedded in the PVA-alkyl matrix.

5.4.4 Morphological analysis:

Figures 5-18(a), (b) and (c) show the SEM images of cross sectional areas of clean unmodified PBI, PBI membranes with only PVA-alkyl added and PVA-alkyl-AqpZ modified PBI membranes, respectively, at a magnification of 50 µm before filtration. The cross sectional area of PVA-alkyl modified PBI membrane showed the addition of an extra layer added to the surface of PBI membrane due to the attachment of PVA-alkyl. It is important to note that the layer of PVA-alkyl was added to both sides of the membrane. Unmodified PBI membranes showed more porous structures as compared to modified PBI membranes. Since the modification of the PBI membranes was not controlled to only surfaces, some of the modification might have occurred inside the pores of the PBI membranes resulting in the less porous structure of modified membranes observed. This is in agreement with the lower pure water flux values observed for the PVA-alkyl-AqpZ membranes, shown in Figures 5-15 and 5-16 (during precompaction).

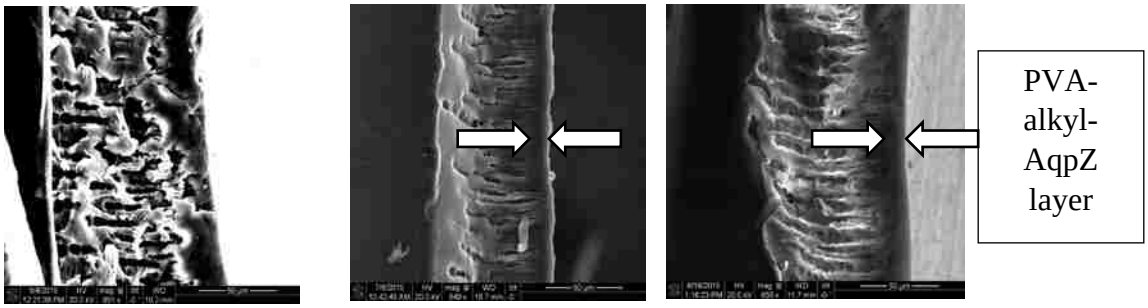

5-18(a) 5-18(b) 5-18(c)

Figure 5-18 (a), (b) and (c) SEM images of cross sectional areas of unmodified PBI, PVA-alkyl and PVA-alkyl-AqpZ modified PBI membranes.

Figures 5-19(a) and (b) show SEM images of the clean surfaces of both unmodified PBI and PVA-alkyl-AqpZ modified PBI membranes, respectively, at a magnification of 10 µm. The surface of unmodified PBI membranes displayed a smoother texture as compared to that of PVA-alkyl-AqpZ modified PBI membranes. This was likely due to the addition of the extra layer of PVA-alkyl containing AqpZ. On the other hand, Figures 5-20(a) and (b) show SEM images of surfaces of both unmodified PBI and PVA-alkyl-AqpZ modified PBI membranes, respectively, at a magnification of 10 µm after filtration. The surface of unmodified PBI membranes showed a rougher texture as compared to PVA-alkyl-AqpZ modified membranes. The reason is hypothesized to be due to the accumulation of foulants on the surface of unmodified PBI membranes. PVA-alkyl-AqpZ modified membranes showed better antifouling characteristics than unmodified PBI membranes. This might be due to addition of aquaporins in PVA-alkyl layer added on the surface of PBI membranes. The addition of aquaporins likely helped during backwash by providing more water channels for water to pass through the membrane resulting in higher removal of foulants. This agrees with flux recoveries shown in Figures 5-15 and 5-16 as well as Table 5-3.

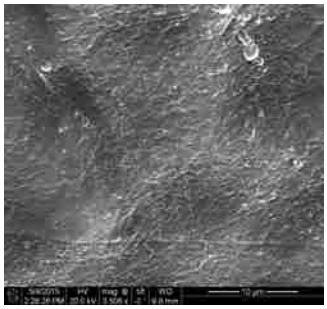

5-19(a)

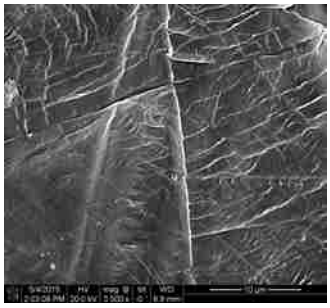

5-19(b)

Figure 5-19 (a) and (b) SEM image of surface area of unmodified PBI membrane and PVA-alkyl-AqpZ modified PBI membrane respectively

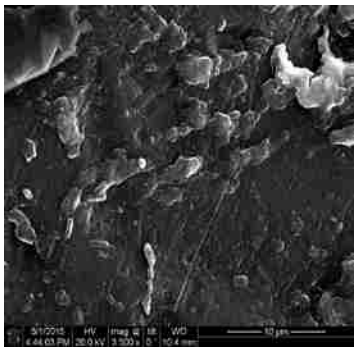

5-20(a)

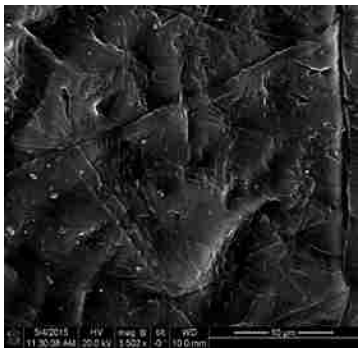

5-20(b)

Figure 5-20 (a) and (b) SEM image of surface area of unmodified PBI membrane and PVA-alkyl-AqpZ modified PBI membrane respectively after filtration

5.5 Discussion:

While the initial water flux values of PVA-alkyl-AqpZ membranes were slightly lower than unmodified PBI membrane, the flux decline was less when using PVA-alkyl-AqpZ membranes, and the final flux after 140 hours of flux experiments was higher for PVA-alkyl-AqpZ membrane as compared to PBI membrane. Therefore, it is believed that the presence of aquaporins helped to increase and maintain the water flux through the membranes, and the addition also led to better flux recoveries. Aquaporins are bidirectional, hence during backwash, aquaporins might have also helped in the increased water flux through the membrane and more removal of reversible fouling resulting in better flux recovery of the membrane. The embedment of AqpZ in the modified membranes is hypothesized to have facilitated water transport through the membrane and brought about an increase in the water flux, which agrees with previous studies [56, 156]. Furthermore, the increase in the hydrophilicity of the membrane after modification (Figure 5-11) could also be associated with the increase in the water being transported

across the membrane [265]. Aquaporins selectively filter water molecules through their porous structures while preventing the passage of ions and other solutes (Figure 5-1). Thus they form channels for water molecules to pass through them and in turn increase the water flux and the flux recovery of the PVA-alkyl-AqpZ membrane.

It is hypothesized that the presence of aquaporins in the PVA-alkyl-AqpZ membranes acted as water channels and prevented the flow of ions and salt solutions that flow along with water molecules. This helped in the increase in water flux and rejection of salt solutions of different concentrations. Previously, Chung et al. [56] prepared Aqp-modified cellulose acetate membranes functionalized with methacrylate end groups. Aqp was introduced into the membranes using vesicle rupture of triblock (ABA) copolymer vesicles and UV polymerization. Maximum salt rejection obtained with NaCl salt solution of concentration 3.4 mM was 32% Fane et al. [47] prepared a thin film composite aquaporin-based biomimetic membrane by interfacial polymerization method. A microporous polysulfone substrate was soaked with an m-phenylene-diamine (MPD) aqueous solution which contained AQP-based proteoliposomes. The substrate was then exposed to trimesoyl chloride (TMC) to form a three-dimensionally crosslinked polyamide layer with the proteoliposomes embedded. Maximum salt rejection obtained for NaCl salt solution of concentration 10 mM was 96.3±1.2% at 5 bar. Also, lipid bilayer was attached to commercial NF-270 membrane under conditions suitable for AqpZ survival and AqpZ was incorporated into the lipid bilayer subsequently [44]. Maximum salt rejection obtained for NaCl salt solution of concentration 1 mM was 20% at 1 bar. In this study, PBI membranes modified with PVA-alkyl-AqpZ showed 73.5% rejection for 3.4 mM NaCl feed solution, whereas for 10 mM NaCl feed solution, the salt

rejection was 68% using nanofiltration membranes. Salt rejections observed in this study were not 100% likely because some of the feed solution might have leaked around the aquaporins embedded in the PVA-alkyl matrix.

5.6 Conclusions:

Aquaporins have received worldwide attention due to their potential to significantly improve water flux across synthetic membranes. Aquaporins provide more water channels while rejecting everything else that is present in the feed including ions and dissolved salts. However, under high pressure, aquaporins can get chemically altered and not function properly, resulting in the failure of the assembly of synthetic membrane and the protein. In this study, aquaporins were protected with gum arabic and dispersed into a PVA-alkyl layer, which was crosslinked to a synthetic PBI membrane backbone using carbodiimide chemistry to minimize the disruptive effects of high pressure. Membranes modified with aquaporins showed higher water fluxes, better flux recoveries and greater ion selectivities as compared to unmodified synthetic membranes. The biomimetic membranes presented here showed promising performance with respect to lower fouling and ion rejection.

5.7 Acknowledgements:

The authors want to acknowledge the sources of funding, NSF 1308095 and USGS 104(b): Ohio Water Development Authority GRT00028988/60040357 for funding this

project. PBI Performance Products Inc. is thanked for supplying the PBI dope for the study.

CHAPTER 6. ALIGNMENT AND IMMOBILIZATION OF AQUAPORINS ON POLYBENZIMIDAZOLE NANOFILTRATION MEMBRANES

6.1 Introduction:

A growing research area in water purification is the incorporation of transmembrane water channel proteins, known as aquaporins in the synthetic membranes owing to the excellent permeability and selectivity of aquaporins (aqp) towards water molecules [29, 38, 52, 56, 121, 266]. These membranes are called biomimetic membranes because of the fact that they mimic the function of aquaporins present in lipid bilayer within cell membranes. In recent years, a number of approaches have been adapted from biological concepts and principles to develop biomimetic membranes [20, 40, 43-58]. However, there are still many challenges associated with aquaporins based membranes. Generally, aquaporin-based biomimetic membranes developed to date consist of three building blocks: aquaporins, amphiphilic molecules in which the aquaporins are embedded in order to simulate the environment of the lipid bilayer in the cell membranes, and a polymer support structure [59]. These amphiphilic molecules in which the aquaporins are incorporated can be either lipids or polymers. Due to the superior mechanical and chemical properties, block copolymers and amphiphilic polymers have been predominantly investigated for the development of aquaporin-based membranes [52, 56, 57, 59, 151, 267-275]. Studies using lipids as the amphiphilic molecules to support aquaporins have shown that these systems were able to maintain membrane integrity [44, 48-50, 55, 150, 156, 276].

The widespread application of aquaporin-based membranes face several challenges with respect to synthesis, stability and function of the membrane assembly. One of the challenges is to design and prepare biomimetic membranes with embedded and aligned aquaporin proteins without losing their integrity and performance, while providing an additional solid support that is sufficiently porous [276]. Toward this goal, aquaporin constructs were modified to bear affinity tags or unique amino acids at the N-terminus of the aquaporin molecule, which was used to facilitate directional immobilization. Each aquaporin monomer was modified with a unique amino acid Cys group at the N-terminus right after the first Met (figure 6-1), and due to the aquaporin tetrameric nature, these Cys groups became four anchors for attachment. There are two intrinsic Cys groups in the sequence of aquaporin. Studies have shown that they are not chemically reactive toward modifications due to their limited accessibility [29]. Therefore, the engineered Cys would be the only site in aquaporin reactive toward the thiol-specific modification. The presence of these four Cys anchors per aquaporin tetramer was used to ensure that all tetramers were attached on the membrane surface in alignment with the feed direction.

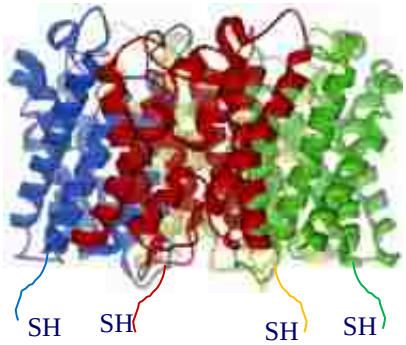

Figure 6-1 Cys modified aquaporin molecule

The objective of this study was to covalently attach Cys modified aquaporins (Aqp-SH) to a polymeric membrane backbone in order to align them in the direction of

flow. PVA-alkyl was used to bind the remaining sites present on the backbone and to seal the gaps in between attached aquaporin molecules. PVA-alkyl has been previously used to enhance the mechanical strength of the membrane assembly and simulate the natural environment for attached aligned aquaporins [149]. Figure 6-2 provides a schematic of the attachment of Cys modified aquaporins to the membrane backbone.

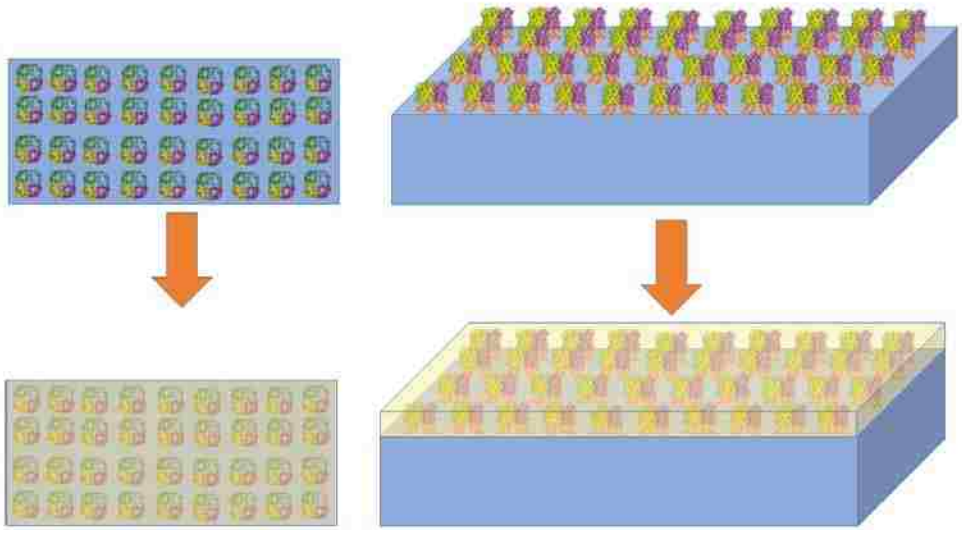

Figure 6-2 Attachment of Aqp-SH to –COOH modified PBI membrane

6.2 Experimental:

6.2.1 Materials:

6.2.1.1 Polybenzimidazole (PBI):

The polymer used to cast the backbone of the membranes was polybenzimidazole (PBI). PBI has found applications in ion-exchange membranes for fuel cells because of

its excellent mechanical, thermal and chemical stability over a wide range of pH [217, 261, 277]. The specific polymer composition used in these membranes is poly [2, 2'-(1, 3-phenylene)-5, 5'-bibenzimidazole]. The absence of aliphatic groups and stability of benzimidazole group in PBI are responsible for its applications in a wide range of pH [278]. Hydrogen bonds can be formed intramolecularly or intermolecularly due to the heterocycle imidazole ring presented in the repeating unit of PBI molecules [279]. The solvent used to make the dope solution was N, N-Dimethylacetamide.

6.2.1.2 PVA-alkyl:

PVA-alkyl is amphiphilic in nature with the high hydrophilicity of PVA and hydrophobicity of the long alkyl side chains. Being amphiphilic in nature, it can be an excellent synthetic alternative for the lipid bilayer in cell membrane where aquaporins are constituted naturally [59]. PVA-alkyl spontaneously attaches to cell surface, anchoring through hydrophobic interactions between the alkyl chains and the lipid bilayer of the cell membrane without reducing cell viability [212]. It carries 28 alkyl side chains per molecule, and interacts strongly with the lipid bilayer in cell membrane because the alkyl chains anchor to the cell surface at multiple points [280]. Because of these hydrophobic interactions and tendency of the polymer to protect the cells, PVA-alkyl is proposed to be an excellent material to support aquaporins.

6.2.1.3 AquaporinZ modification with single cysteine at the N-terminus:

Cysteine contains a thiol group in its side chain, which can be used for immobilization. To prevent cysteine from being buried in the structure of AqpZ with

limited accessibility for binding, a cysteine was added before the his-tag which was used to facilitate protein purification via the conventional metal-affinity chromatograph as shown in figure 6-3. In this study, cysteine was added using QuikChange site-directed mutagenesis following manufacturer's instruction (Agilent). Primers are: 5'-GAGATATACCATGGGTTGCTCTGGTCTGAACGAC-3', and 5'-GTCGTTCAGACCAGAGCAACCCATGGTATATCTC-3', using pET28a-ApqZ as template [222]. The modification was verified by DNA sequencing.

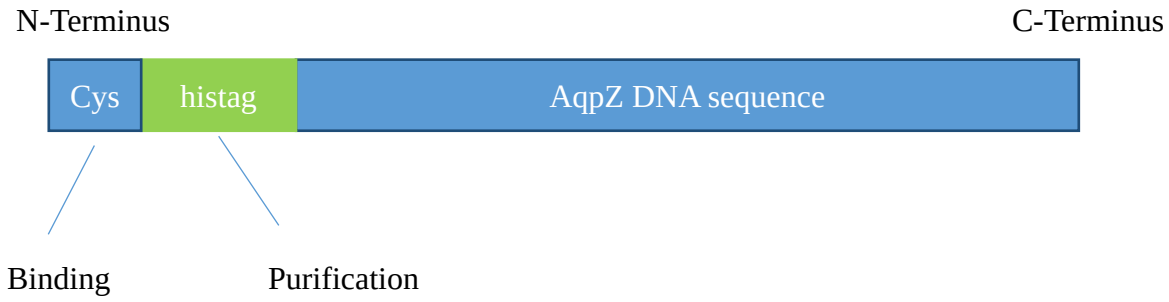

Figure 6-3 Schematic of Cysteine attachment at the N-terminus of aquaporins

6.2.1.4 AquaporinZ expression and purification:

The constructed plasmid was transformed into *E. coli* strain C43 (DE3). Single colony was cultured overnight at 37 ℃ in 5 ml LB medium containing 50 µg/ml kanamycin. The overnight culture was then inoculated into 300 ml fresh LB medium with 50 µg/ml kanamycin and shaking at 250 rpm at 37 ℃. The cells were induced with 1 mM IPTG when the absorbance at 600 nm reached 0.8. After 4 hours incubation, the cells were collected by centrifugation at 8,000×g for 10 min.

To purify the protein, cell pellet was re-suspended with 30 ml PBS buffer (20 mM Na-PO_4, 0.3 M NaCl and pH 7.9) supplied with 0.5 mM protease inhibitor phenylmethylsulfonyl fluoride (PMSF) and sonicated for 20 min on an ice-water bath. The cell lysate was clarified by centrifugation at 10,000 rpm, 4 ℃ for 20 min. Then cell debris was dissolved using 2 % Triton in PBS buffer and incubated with shaking for 2 hours at 4 ℃ to extract membrane protein. The re-suspension was clarified with centrifugation at 10,000 rpm, 4 ℃ for 20 min and the supernatant was collected. Ni-NTA agarose beads (Qiagen) was mixed with the supernatant for 40 min at 4 ℃ with shaking. The resin was then loaded into an empty column, drained, and washed with PBS buffer supplemented with 0.03 % DDM (n-Dodecyl β-D-maltoside) and 40 mM imidazole. Protein was eluted with 500 mM imidazole and 0.03 % DDM in PBS buffer. Imidazole was removed by dialysis against PBS buffer supplemented with 0.03 % DDM overnight.

An inactive mutant Aqp-SH R189A was also expressed, according to previously published protocol [47], to be use as a negative control to the –Cys modified Aqp. In order to express the inactive mutant, the arginine (R) residue at position 189 in AqpZ was replaced with alanine (A) using site-directed mutagenesis. This inactive mutant of aquaporin shows no selectivity towards water [281]. Hence, it was used to prepare a negative control of the functional Aqp-SH modified membrane. The protocol used to incorporate Aqp-SH R189A was the same as that used to incorporate functional Aqp-SH into PBI membranes.

6.2.2 Methodology:

6.2.2.1 PBI membranes casting:

PBI membranes were prepared according to previously published studies [149, 217]. The dope solution was diluted to 21% PBI by adding solvent. The non-solvent phase that was used in this process was water. Flat sheet membranes were prepared using casting knife, or doctor's blade (Paul N Gardner Co, U.S. Pat 4869200, Pompano Beach, FL.) The membranes were stored in a 50/50 glycerol-DI water solution in order to prevent their drying and collapse of pore structure. The membranes were kept in the solution at least one day before they were analyzed.

6.2.2.2 Surface activation of membranes:

In order to attach Aqp-SH and PVA-alkyl to PBI membranes, membrane surfaces were activated following previous techniques [149, 217], in which 4-chloromethyl benzoic acid (CMBA) purchased from Sigma-Aldrich (USA) was used in order for functionalization. CMBA added a carboxylic acid group to the surface of PBI membrane, which could be used as a platform for subsequent functionalization of the membrane [261, 277]. Once the reaction was finished, the membranes were washed with copious amounts of DI water to remove excess reagents and immediately placed in glycerol/water bath.

6.2.2.3 Preparation of PVA–alkyl:

PVA-alkyl was prepared in a two-step process, according to literature protocols [149, 218-220]. Briefly, a reaction between PVA and sodium monochloroacetate yielded carboxy-methyl PVA (PVA-COOH), and PVA-alkyl was prepared by reacting PVA-COOH with hexadecanal [149, 218].

6.2.2.4 Chemical attachment of –Cys modified Aqp to PBI backbone:

Immobilization of aquaporins into polymer matrix was done in order to align their channels with the direction of water flux and to optimize their performance. Aquaporins were covalently attached to the modified PBI backbone with carbodiimide chemistry. For this task, flat sheet PBI membranes were prepared and modified with CMBA. In the next step, Cys modified Aquaporin (Aqp-SH) were covalently attached in a reducing environment to the –COOH modified PBI membrane using EDCH chemistry, as shown in figure 6-4. In this mechanism, Aqp-SH acted as a nucleophile to get covalently attached to the –COOH group present on the surface of PBI membrane. Cys groups present after the N-terminus acted as anchors the Aquaporin molecules to prevent the swaying and to help with the alignment of the aquaporin molecules in the direction of the flow. PVA-alkyl was used in order to bind to the remaining –COOH groups present in the membrane and to seal the gaps in between the attached Aqp-SH molecules following the EDCH chemistry previously used.

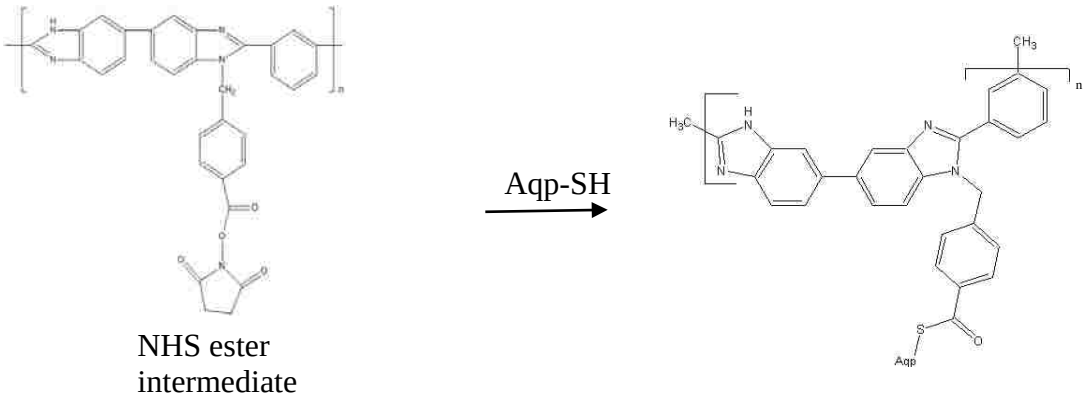

Figure 6-4 Chemical attachment of Aqp-SH to –COOH modified PBI membranes

6.2.2.5 Surface modification of PBI membrane using PVA-alkyl:

PVA-alkyl was attached to the membrane using carbodiimide chemistry. For the reaction, N-(3-dimethylaminopropyl)-N'-ethylcarbodiimidehydrochloride (EDCH) and N-hydroxysuccinimide (NHS), both purchased from Sigma-Aldrich (St. Louis, MO) were used. The reactions were performed in 2-(N-morpholino) ethanesulfonic acid (MES) buffer (Sigma-Aldrich, USA). PVA-alkyl was chemical attached to the CMBA modified PBI membranes using this reaction, as reported in previous studies [149].

6.2.3 Membrane characterization:

6.2.3.1 Dynamic light scattering:

Since aquaporins form the functional element of biomimetic membranes, producing high quality proteins is critical. Before immobilizing proteins on membrane surface, it is important to evaluate the proteins for their concentration, purity and aggregation state. For this purpose, analysis of protein solution with dynamic light

scattering to determine the presence and extent of aggregation was carried out in Litesizer 500 particle analyzer by Anton Paar (Ashland, VA). An aquaporin solution was taken in a glass cuvette and a plot of particle size vs relative frequency and polydispersity index (PDI) of the solution was obtained. Good quality protein samples would have PDI of 0.08, acceptable quality protein would have PDI of 0.1 to 0.4, while the precipitated protein would have PDI of 0.4 to 0.9 [57].

6.2.3.2 Molecular weight cut off:

The molecular weight cut off analysis of unmodified PBI, CMBA modified PBI, and PVA-alkyl modified PBI membranes was conducted using 100 ppm solutions of various molecular weights of polyethylene glycol (PEG) and sucrose solutions. The total organic carbon (TOC) of both feed and permeate solutions were measured using Teledyne Tekmar Fusion TOC analyzer (Mason, OH). The various samples that were used in this study along with their Stokes-Einstein radii are shown in Table 6-1. The rejection values of all solutes were used to determine the molecular weight cut off of both unmodified and modified PBI membranes. The molecular weight of solute in feed solution for which the membranes showed more than 90% rejection was considered the molecular weight cut off of the membranes. The apparent solute rejection R (%) was calculated using equation (6-1).

$$R = \left(1 - \frac{C_p}{C_f}\right) \times 100\% \qquad (6\text{-}1)$$

Table 6-1 Neutral solutes used for molecular weight cut off analysis and their Stokes-Einstein radii in nm [25, 229-232]

Solute	**Mol. Wt. (gm/mol)**	**Stokes-Einstein radii (nm)**
PEG 200	200	0.41
Sucrose	342.3	0.47
PEG 400	400	0.57
PEG 600	600	0.68
PEG 1000	1000	0.94

6.2.3.3 Contact angle measurements:

Contact angle was used as a measure to determine the hydrophilicity of the membrane surface. A drop shape analyzer – DSA 100 (KRUSS USA, Matthews, NC) was used for contact angle measurements using sessile drop technique.

6.2.3.4 Zeta potential and surface charge analysis:

Zeta potential is used to analyze the surface charge of membranes at different pH environments. It is particularly important to analyze the separation efficiency of membranes based on charge and also a confirmation test for surface modification [228]. Surface charge was analyzed by measuring the zeta potential using an Anton Paar

SurPASS electrokinetic analyzer (Anton Paar, Ashland, VA) in surface analysis mode. Before analysis, membranes were rinsed with copious amounts of DI water to remove any residual solvent or glycerol from the storage solution in the case of PBI membranes. The KCl electrolyte solution used in these measurements had an ionic strength of 1.0 mM. The pH values for the various readings were adjusted using 0.5 M HCl and 0.5 M NaOH solutions for acid and base titrations.

6.2.3.5 Elemental analysis:

Membranes modified with Aqp-SH were analyzed for changes in the concentration of sulfur since unmodified PBI, -COOH modified PBI, and PVA-alkyl modified PBI membranes do not contain any sulfur present in their structures. Hence, Aqp-SH modified membranes were analyzed for the sulfur concentration in them as a confirmation for attachment of aquaporins to the membranes. K-Alpha x-ray photoelectron spectrometer (XPS) was used in order to analyze the elemental composition along the cross section of both unmodified and Aqp-SH modified membranes. Depth profiling was performed using an ion beam to etch layers of membrane surfaces and elemental composition was measured after each etching cycle. An ion beam of 200eV was used to etch the surface. Three etching cycles were performed for 120 seconds each for elemental analysis along cross sections of membranes.

6.2.3.6 Membrane morphology:

To investigate the cross-section of the membrane and measure the thickness of selective layer of modified membrane, ion beam of the FEI Helios Nanolab Dual beam

was used to cut out a small piece of the membrane. A small deposit of platinum with a thickness of around 60 nm was deposited over the area in order to protect the underlying surface during the process of cutting of cross-section by ion beam. A small cross section was cut out and lifted away from the rest of the membrane sample by welding a small bead of platinum to the platinum layer. This sample was then thinned out with a low power ion beam until the morphology of the mesoporous layer was visible using STEM mode in the Dual Beam. This sample was transferred into the JEOL 2010F for TEM imaging of the cross-section.

6.2.3.7 Flux analysis:

Dead end filtration was used to monitor the flux decline of PBI, PVA-alkyl modified PBI, inactive Aqp-SH modified PBI, and active Aqp-SH modified PBI membranes (called just Aqp-SH modified membranes). Filtration experiments were performed using Amicon filtration cell (Amicon Stirred Cell 8010 – 10 ml) under a constant pressure of 70 psi (4.83 bar) and continuous stirring. Flux values were calculated as L/m^2-hr and plotted against the total permeate volume. Membrane samples were cut into circular pieces of area 4.1 cm^2 and supported by a Whatman^{TM} filter paper (125 mmø). Each membrane was precompacted with DI water for 1 hour until a stable flux was reached.

Precompaction was followed by feed solutions of monovalent and divalent salt solutions in water under same conditions of pressure and stirring. Salt rejection was evaluated using five solutions of different concentrations of sodium chloride (NaCl) and calcium chloride ($CaCl_2$) in DI water: 3.4, 10, 20, 35 and 100 mM solutions. Salt

concentrations were measured using conductivity meter. Solute rejections were calculated using equation (6-1).

After each feed water filtration, reverse flow filtration using DI water was performed for 1 hour to remove reversibly-attached foulants that were not adsorbed to the membrane and the filter paper support was changed. The flux recovery of the membrane was measured afterwards in order to study the effect of presence of aquaporins on removal of reversible fouling.

In order to analyze linearity of DI water flux through unmodified and Aqp-SH modified PBI membranes, flux values were measured using DI water as feed solution at four different pressure values: 1.38, 2.76, 4.14, and 5.52 bar.

Unmodified and modified membranes were subjected to dead end flow filtration using 0.5M, 1M, and 2M NaCl and $CaCl_2$ solutions in order to compare the rejection trends of membranes under high salt concentration feed solutions. Inductively coupled plasma (ICP) analysis was used to measure the concentrations of permeates obtained from all membranes.

6.2.3.8 Diffusion studies:

In order to compare the salt diffusion rates through unmodified PBI and Aqp-SH modified PBI, the membrane was mounted in the middle of a stainless-steel diffusion cell to separate the two compartments (Salt solution side and DI water side). Each compartment in the cell was of volume 250 mL. The effective membrane area available for diffusion to occur was 3.5 cm^2. Continuous stirring was provided during the

experiment. A solution of 1000 ppm NaCl solution was added into the salt solution side and the same amount of DI water solution was added into the other compartment. A sample of 2 mL was collected from each compartment every day. The experiment was run for 8 days to measure the rate of salt diffusion through the membranes. Salt concentrations of collected samples were measured using inductively coupled plasma (ICP) analysis. Initial conditions of the experimental setup is shown in Fig 6-5. Actual data for diffusion experiment is provided in Table C.1 in Appendix C.

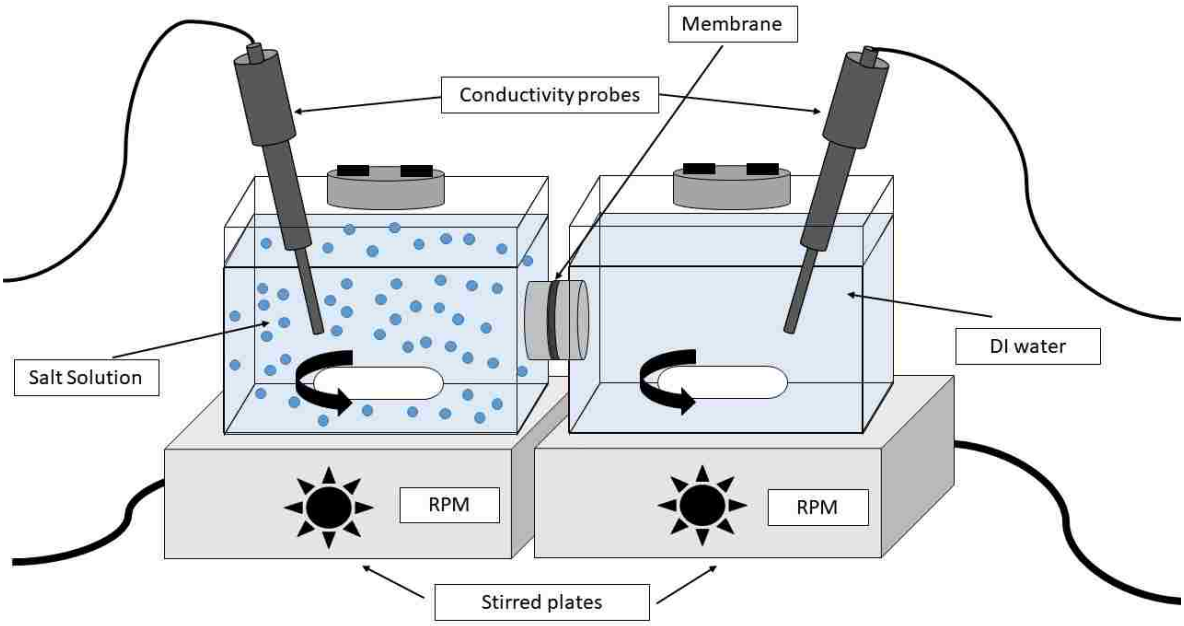

Figure 6-5 Diffusion cell assembly with 1000 ppm NaCl salt solution on one side and DI water on other side. Both compartments are separated by a membrane.

6.2.3.9 Estimation of Aquaporin packing in membrane assembly:

Membrane porosity and double layer properties influence ion fluxes through the membrane. The flux values measured for aqp-SH modified membranes exhibited weak

sensitivity to ionic strength. These fluxes could be estimated via an ion's concentration (c) gradient and its diffusion coefficient (D), as shown in equation (6-2):

$$j = - D\nabla c \tag{6-2}$$

assuming a concentration gradient was imposed perpendicular to a porous film. This concentration gradient was set by the ion concentrations in reservoirs to either side of the membrane as well as their separation (see figure 6-11). By relating the measured flux to the concentration gradient, an effective diffusion coefficient, D_e, could be determined. This allowed the inference of relative packing densities of aqp molecules incorporated in the active layer of membrane. This effective diffusion coefficient would be generally smaller than the ion's intrinsic diffusion rate in bulk media, and moreover, it would be proportional to the ratio of the accessible pores' surface area to the total surface area, assuming the channels were perfectly linear and aligned with the concentration gradient, e.g. $D_e = \frac{SA_{pore}}{SA_{total}} \times D$. According to the SEM imaging data of cross-sections of membranes published previously [149], It was further assumed that the PVA-alkyl and PBI were stacked in layers aligned perpendicular to the concentration gradient.

Based on these assumptions, a numerical partial differential equation was used to estimate how ionic fluxes were modulated by aquaporin surface densities, from which aquaporin packing densities compatible with experimentally-measured flux data could be determined. Namely, finite element simulations of the steady state Fickian diffusion equation (6-3) were performed,

$$\frac{dc}{dt} = -Dd^2\frac{c(x)}{dx^2} = 0 \tag{6-3}$$

subject to c (L) = 1 mM and c(R) =0 mM, where c is the concentration of the ionic solution and D is the diffusion coefficient and L, R correspond to the left and right reservoir boundaries. From these simulations, an effective diffusion coefficient that reflected the impact of the channel geometry on transport was determined. This proceeded through recognizing the flux was related to the concentration gradient via equation (6-4)

$$< J > = \frac{1}{A} \int D \, \nabla c \, dS \tag{6-4}$$

where A is the surface area of the film and S represents the surface.

Flux could be expressed in terms of concentrations and D_e was given by equation (6-5)

$$<J>*A \sim D_e \, \frac{(c(L) - c(R))}{(x(L) - x(R))} \tag{6-5}$$

where c(i) is the concentration at boundary i (left and right) and x(i) is the position of the boundary. By numerically evaluating <J> at the film boundary, the equation was solved for D_e based on the concentrations imposed at the reservoir boundaries and their separation distance.

These equations were solved on three-dimensional finite element meshes [235, 236], based on potential membrane and aquaporin configurations using the mesh generation tool GMSH [235, 237]. The meshes consisted of two reservoirs separated by a porous domain representing the film. Aqp or aggregates thereof were represented by cylinders of varying radii aligned parallel to the membrane. In principle, atomistic resolution surface geometries could have been used for the aqp molecules [235, 236], but since specific knowledge of the membrane structure at the solvent/membrane interface is

not known, a simple cylindrical representation of the protein was used. These equations were solved, assuming Dirichlet conditions of c=1.0 M and c=0.0 M on the left and right reservoir boundaries [235, 236] via the finite element method using FEniCS [235, 238]. The diffusion coefficient was arbitrarily set to D=1.0 [m^2/s]. Specifically, the weak form of these equations was solved using a piecewise linear Galerkin basis with FEniC's default direct linear solver and parameters. Concentration fluxes were determined by performing an 'assemble' call on an immersed boundary located at the middle and oriented parallel of the porous film. Details of the numerical procedure follow from previously published work [235, 236]. To capture the behavior of monomeric AqpZ, the flux found at the boundary of a pore was normalized [235, 236]. The packing fraction observed in the boundary layer then represented a boundary condition surrounding individual aquaporins. All code written in support of this study is publicly available at https://bitbucket.org/pkhlab/pkh-lab-analyses. Simulation input files and generated data are provided in Appendix D.

6.3 Results:

6.3.1 Dynamic light scattering:

As shown in figure 6-6, the particle size analysis of Aqp-SH solution obtained showed a sharp peak around 10 nm, which is the size range of aquaporin molecules and the bound detergent. Also, the PDI obtained from the particle analyzer was 0.19. This

showed that the proteins were not aggregated in the solution and the PDI of aquaporin solution was in the acceptable range [57].

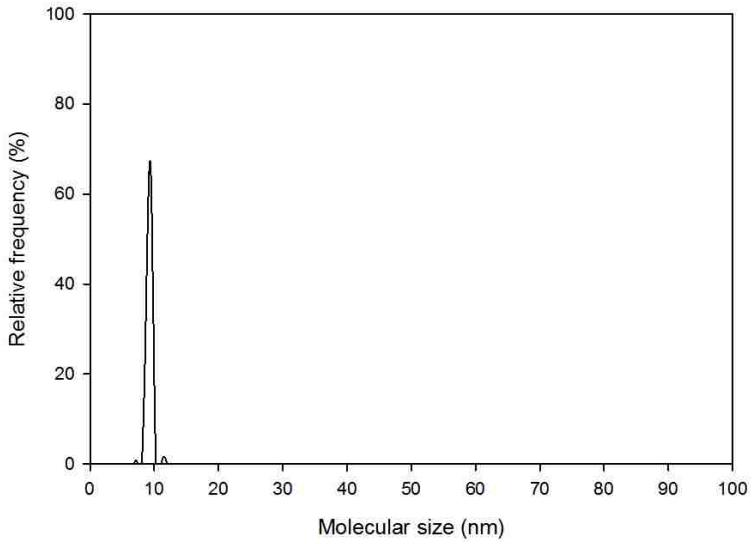

Figure 6-6 Size measurement of Aqp-SH by dynamic light scattering

6.3.2 Molecular weight cut off analysis:

Both unmodified PBI and PBI-CMBA membranes showed 90% rejection for PEG 1000 (figure 6-7 and Table 6-2), which has a Stokes radius of 0.94 nm. This showed that the membranes were in the nanofiltration range. After modification with PVA-alkyl attachment to the membrane, the produced membranes showed a 90% rejection for PEG 600, which has a Stokes radius of 0.68 nm. This showed that PVA-alkyl modified membranes were also nanofiltration membranes but with smaller pores. Aqp-SH modified membranes showed consistent rejections of more than 90% for all solutes used in MWCO studies.

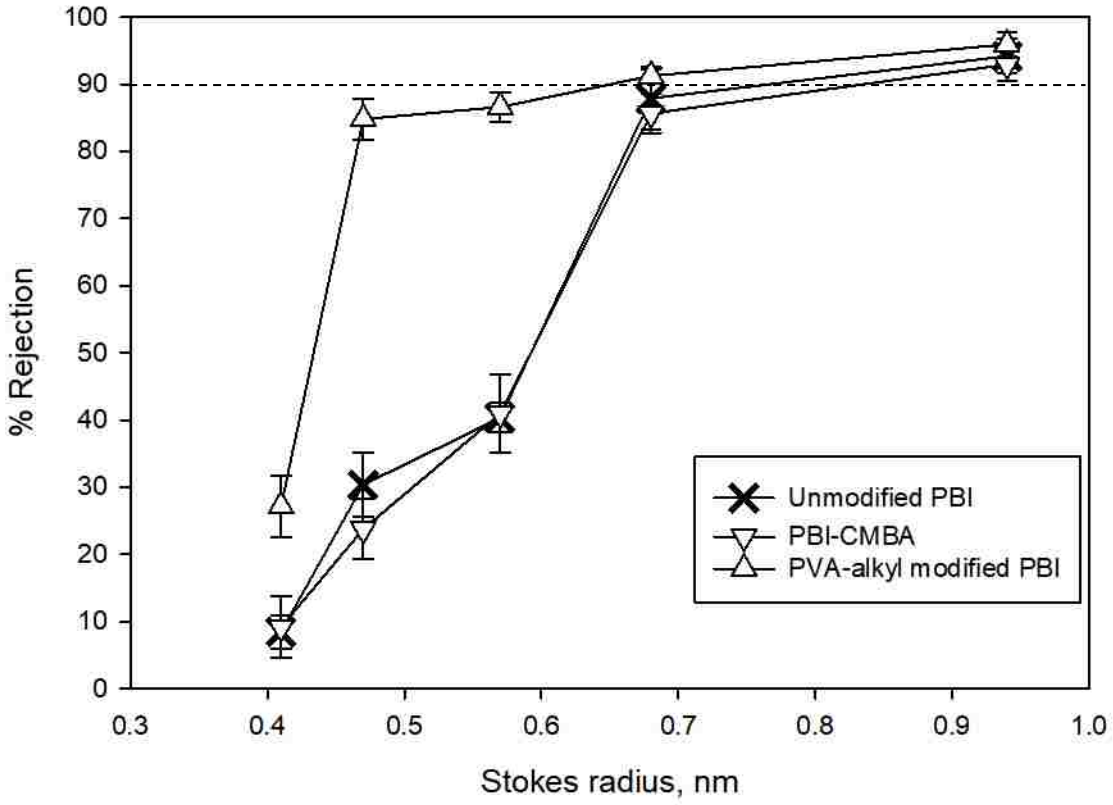

Figure 6-7 Molecular weight cut off analysis of unmodified PBI, -COOH modified PBI, and PVA-alkyl modified PBI membranes

Table 6-2 Rejections obtained for unmodified PBI, PBI-CMBA and Aqp-SH modified PBI membranes

Membrane	**Rejection > 90%**
Unmodified PBI	0.94 nm (94.2%±2.5 %)
PBI-CMBA	0.94 nm (93.0%±2.4 %)
PVA-alkyl modified PBI	0.68 nm (91.3%±1 %)

6.3.3 Aquaporin attachment verification through elemental analysis:

Depth profiling in XPS analysis was performed for both PBI-COOH and Aqp-SH modified PBI membranes in order to prove the change in sulfur concentration in the membranes after modification. Tables 6-3 and 6-4 show weight percentage of atoms of carbon, oxygen, nitrogen and sulfur present in the membrane samples. It can be seen from the Table 6-3 that the amount of sulfur is negligible in PBI-COOH membrane, which was expected since the structure of –COOH modified PBI [149, 217] does not contain any sulfur. Small amount of sulfur shown in unmodified membrane might be due to impurities present on the surface and polymer matrix of the membrane. Table 6-4 shows some amount of sulfur in Aqp-SH modified membrane. Each aquaporin monomer contained 4 cysteine groups including the one attached at the end groups. Considering the tetrameric form of aquaporins, there are 16 sulfur atoms present in one aquaporin molecule. Hence, for a point scan, the amount of sulfur present at a level in Aqp-SH

modified membranes should be between 0.5% and 1%. Therefore, elemental analysis of both unmodified and modified PBI membranes showed the presence of sulfur in the Aqp-SH modified membrane.

Table 6-3 Elemental composition of elements in PBI-COOH membrane

	Carbon	Nitrogen	Oxygen	Sulfur
Surface	85.22	10.7	4	0.07
Level 1	86.28	10.28	3.39	0.05
Level 2	86.2	10.39	3.33	0.09
Level 3	87.3	10.56	2.11	0.03

Table 6-4 Elemental composition of elements in Aqp-SH modified PBI membrane

	Carbon	Nitrogen	Oxygen	Sulfur
Surface	92.13	4.07	3.3	0.5
Level 1	87.18	8.93	3.41	0.48
Level 2	87.58	8.73	2.99	0.7
Level 3	86.82	8.02	3.05	0.62

6.3.4 Hydrophobicity:

Contact angle was used as a measure of hydrophobicity, and results are shown in Table 6-5. CMBA modified membranes were found to be more hydrophilic than PBI membranes [217, 261]. This was most likely due to addition of a –COOH group in the modified molecule and its increased ability to form hydrogen bonds because of the presence of oxygen with a lone pair. After the addition of PVA-alkyl to the membranes, the contact angle decreased further showing a significant increase in the hydrophilicity of the membrane. This was most likely due to high hydrophilicity of PVA. It is hypothesized that hydrophobic part of PVA-alkyl was reoriented so that the alkyl chains were inside the membrane matrix whereas PVA was on the outside, thus making the membranes more hydrophilic [258]. After chemical attachment of Aqp-SH and PVA-alkyl, there was no significant difference in the contact angle showing that most of the surface of Aqp-SH membrane might be covered with PVA-alkyl providing a protection to Aqp-SH. The middle portion of AqpZ is hydrophobic, but the ends are hydrophilic as these parts are exposed to the cytosol/periplasm. In case of aquaporins aligned to the feed direction and exposed to the surface, the hydrophilic ends would be facing up, and this would be responsible for an increase in contact angle if they were exposed on the surface of the membrane [29]

Table 6-5 Hydrophobicity via contact angle

Membrane	Contact angle
Unmodified PBI	$75^{o}\pm0.55$
-COOH modified PBI	$70.56^{o}\pm1.04$
PVA-alkyl modified PBI	$60.5^{o}\pm1.44$
Aqp-SH modified PBI	$57.5^{o}\pm0.93$

6.3.5 Zeta potential and surface charge analysis:

Aquaporins have histidine groups present at the pore opening which are positively charged [15]. In order to confirm that the aquaporins were not exposed on the surface of Aqp-SH modified membranes, zeta potential analysis was carried out of unmodified PBI, PBI-CMBA, and Aqp-SH modified PBI membranes over a pH range of 2-10 (Figure 6-8). It was observed that unmodified PBI membranes showed more positively charged surface as compared to PBI-CMBA and Aqp-SH modified PBI membranes. PBI-CMBA membranes showed the most negatively charged surface among all three membranes owing to the presence of –COOH groups on membrane surface. Aqp-SH modified membranes showed negatively charged surface at a pH of 7. Also, the surface of modified membranes was more negatively charged as compared to unmodified PBI

membranes. This showed the absence of positively charged groups on the surface of Aqp-SH modified membranes.

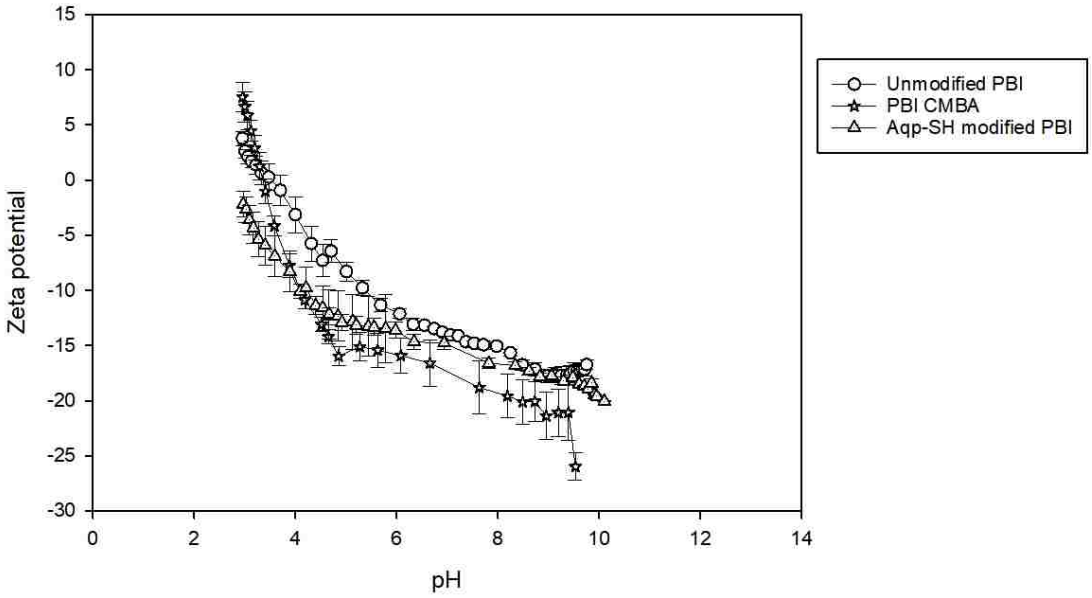

Figure 6-8 Zeta potential values of unmodified PBI, PBI-CMBA, and Aqp-SH modified PBI membranes over a pH range of 2-10

.

6.3.6 Membrane morphology:

Membrane modified with Aqp-SH-PVA-alkyl showed a selective layer of about 50 nm. However, the cross sectional images (Figure 6-9) didn't provide any visual confirmation of Aquaporins present in the selective layer of the membrane. A selective layer as thick as 50 nm might be because of the surface modification of PBI membrane with PVA-alkyl. Lack of any visual confirmation of aquaporins in the selective layer might be because there are no vesicles in the system. Aquaporins are present in the

modification layer as individual molecules surrounded by hydrophobic and hydrophilic groups of PVA-alkyl.

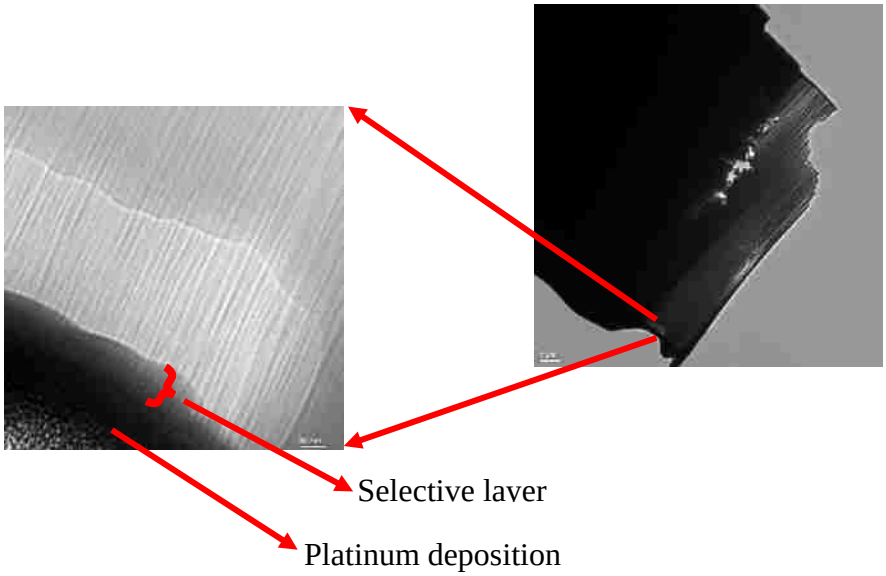

Figure 6-9 Cross sectional cut out of the modified membrane using FIB

6.3.7 Flux analysis:

To investigate the ability of the Aqp-SH membranes to reject ions, filtration studies using different concentration solutions of NaCl and $CaCl_2$ in water were performed under a constant pressure of 4.83 bar. Experiments were conducted in parallel in order to study unmodified and modified membranes, and the flux values were plotted as a function of permeate volume for unmodified, PVA-alkyl modified PBI (to reflect the amphiphilic matrix without aquaporins), inactive Aqp-SH modified PBI (i.e., to be used as a negative control) and Aqp-SH membranes, as shown in figure 6-10 (A), (B) and (C), and (D) respectively. Actual data for Figures 6-10 (A), (B), (C), and (D) is presented in Appendix A, Tables A-2-1, A-2-2, and A-2-3, and A-2-4.

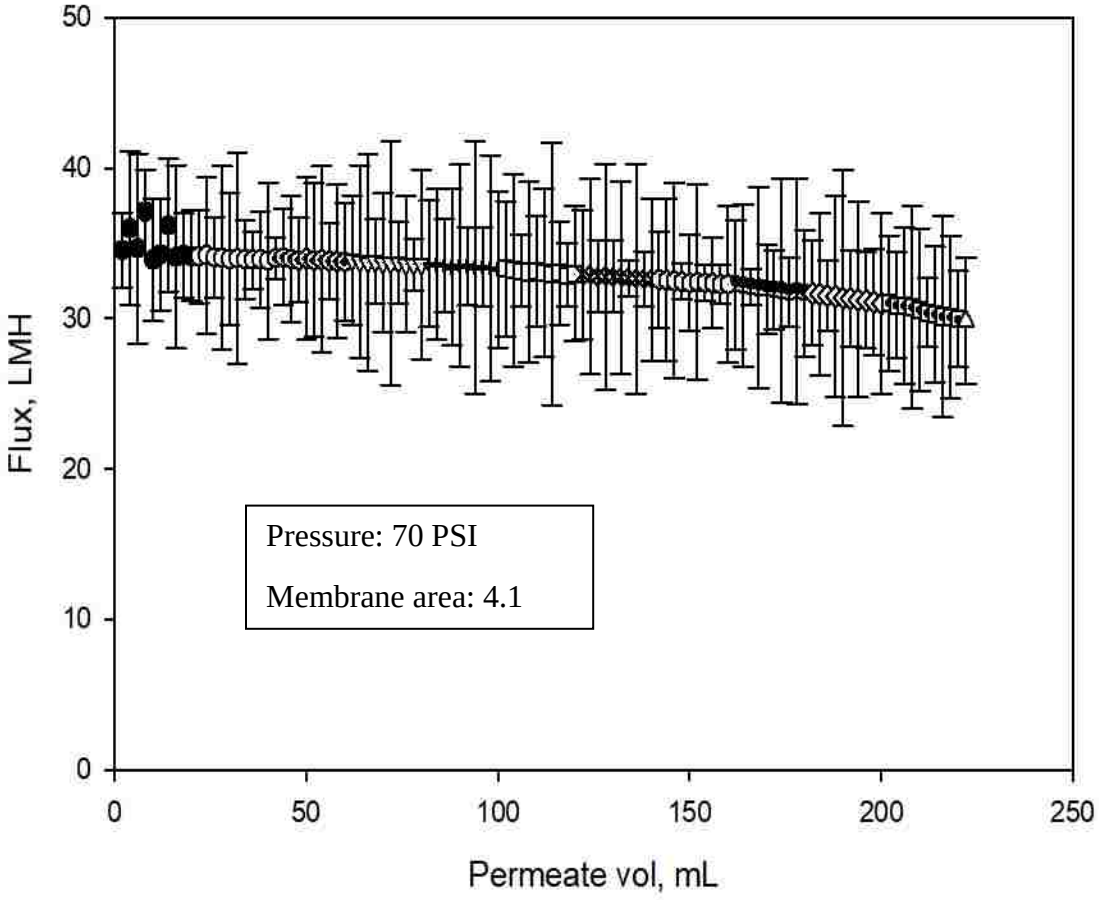
Flux, LMH
Permeate vol, mL
Pressure: 70 PSI
Membrane area: 4.1
0
10
20
30
40
50
0
50
100
150
200
250

6-10 (A)

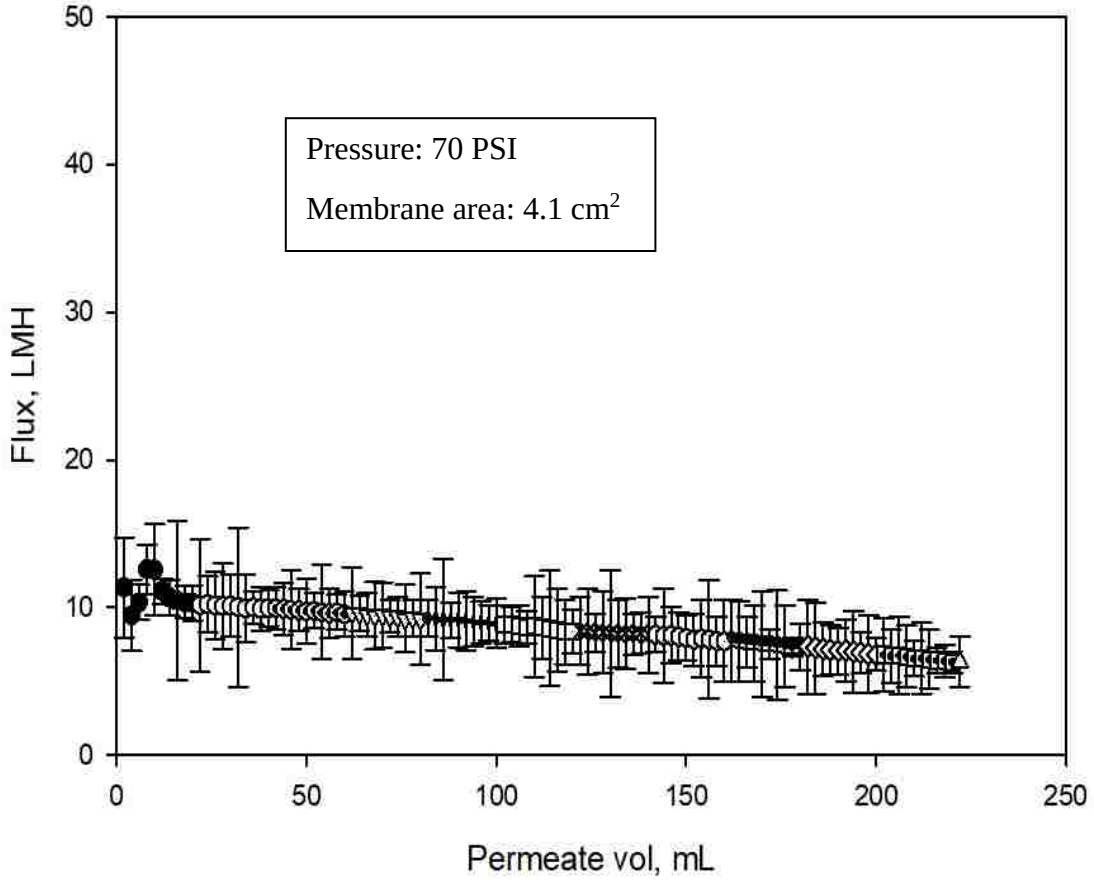
Pressure: 70 PSI
Membrane area: 4.1 cm2
Flux, LMH
Permeate vol, mL
0
10
20
30
40
50
0
50
100
150
200
250

6-10 (B)

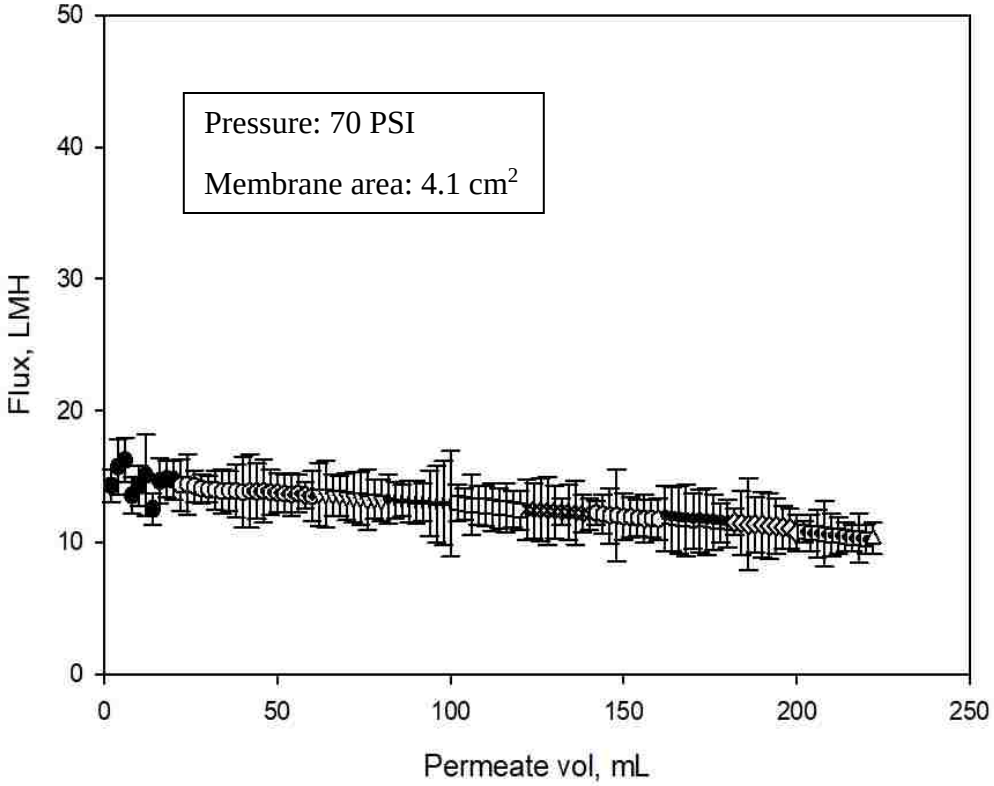
Pressure: 70 PSI
Membrane area: 4.1 cm2
Flux, LMH
Permeate vol, mL
0
10
20
30
40
50
0
50
100
150
200
250

6-10 (C)

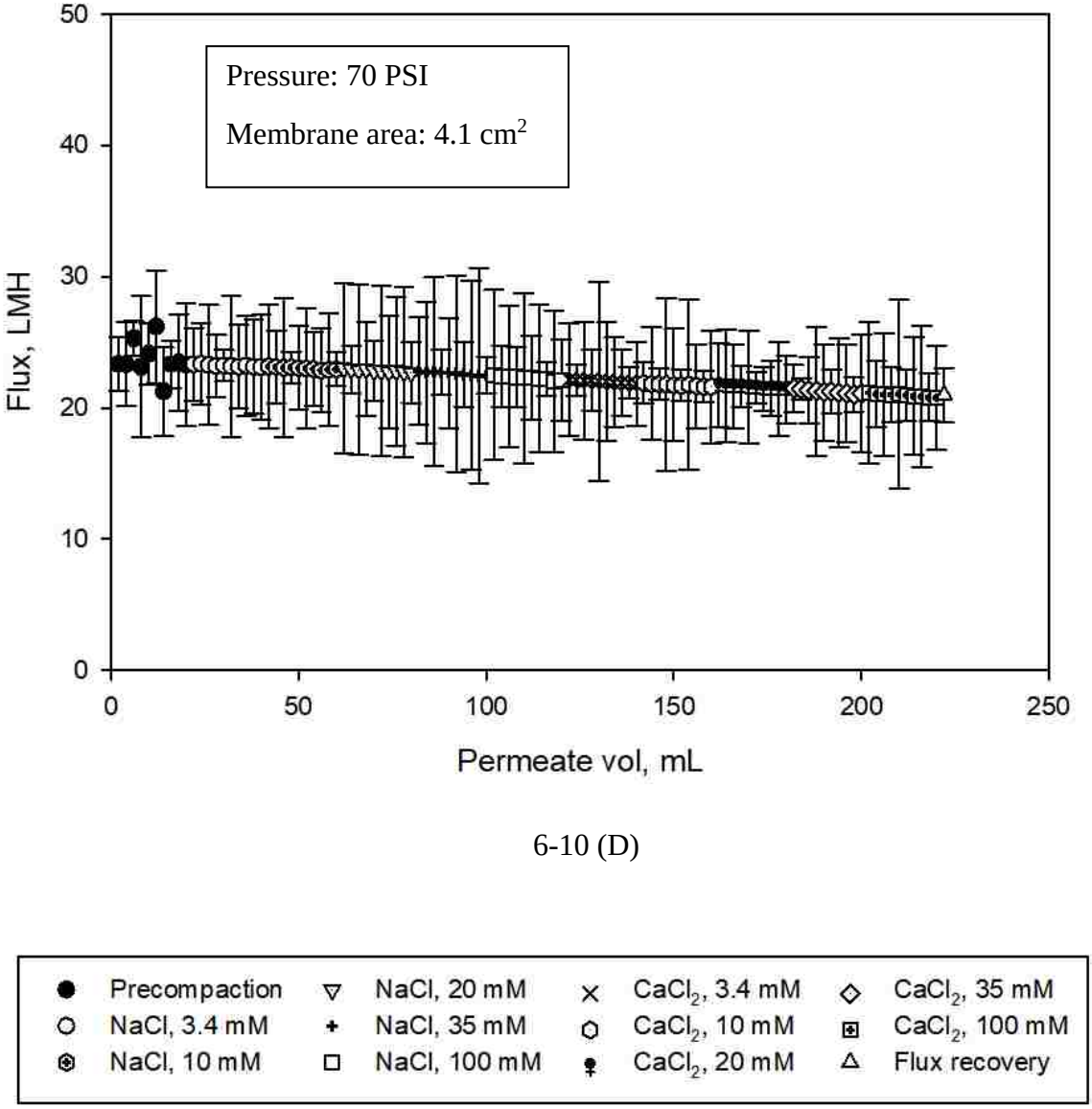

6-10 (D)

Figure 6-10 (A), (B), (C), and (D). Flux analyses of (A) unmodified PBI, (B) PVA-alkyl modified PBI, (C) inactive Aqp-SH modified PBI membranes and (D) Aqp-SH modified PBI membranes at constant pressure of 70 psi (4.83 bar)

PVA-alkyl modified membranes showed the lowest initial flux, filtration flux and recovered flux among all membranes possibly because of added resistance to flow due to

the addition of a dense layer to the surface and because of a decrease in pore size (figure 6-7). Unmodified PBI membranes showed highest initial flux values, which might have been due to the absence of any layer adding resistance on the surface of membranes. The flux profile obtained for the inactive Aqp-SH membranes did not show any significant change when compared to that of PVA-alkyl modified membranes possibly due to the lack of water permeability of inactive mutant of aquaporins (Aqp-SH R189A) [47, 281]. The incorporation of aquaporins on PVA-alkyl modified membranes showed an increase in flux values as compared to PVA-alkyl membranes as well as the membranes modified with inactive mutant; however, the flux values of Aqp-SH membranes were still lower than those of unmodified PBI membranes. The addition of PVA-alkyl alone acted to both block pores and increase resistance to flow, and hence, the decrease in flux. The addition of functional aquaporins to these membranes provided them with flow channels, which increased the flux as compared to PVA-alkyl membranes. However, the flux was not as high as the modified membranes owing likely to the fact that aquaporin coverage was not complete over the surface of the PVA-alkyl, so there were still regions of minimal or no flow.

Additional experiments were conducted in order to analyze the flux linearity of Aqp-SH modified membranes. As shown in figure 6-11, the slope of line represents permeability of unmodified, PVA-alkyl modified, and Aqp-SH modified PBI membranes. Unmodified PBI membranes showed a permeability of 6.27 LMH/bar. PVA-alkyl modified membranes showed the lowest permeability of all the membranes at 1.88 LMH/bar, while Aqp-SH modified PBI membranes showed an increased permeability as compared to PVA-alkyl modified membranes (4.46 LMH/bar). This increased

permeability might have been due to the presence of immobilized aquaporins on modified membranes providing the modified membrane with more flow channels. Figure 6-11 shows that fluxes produced by all the membranes increased linearly with increment in pressure. Also, the incorporation of immobilized aquaporins and dense PVA-alkyl layer on the surface of PBI membrane did not affect the flux linearity of the membranes.

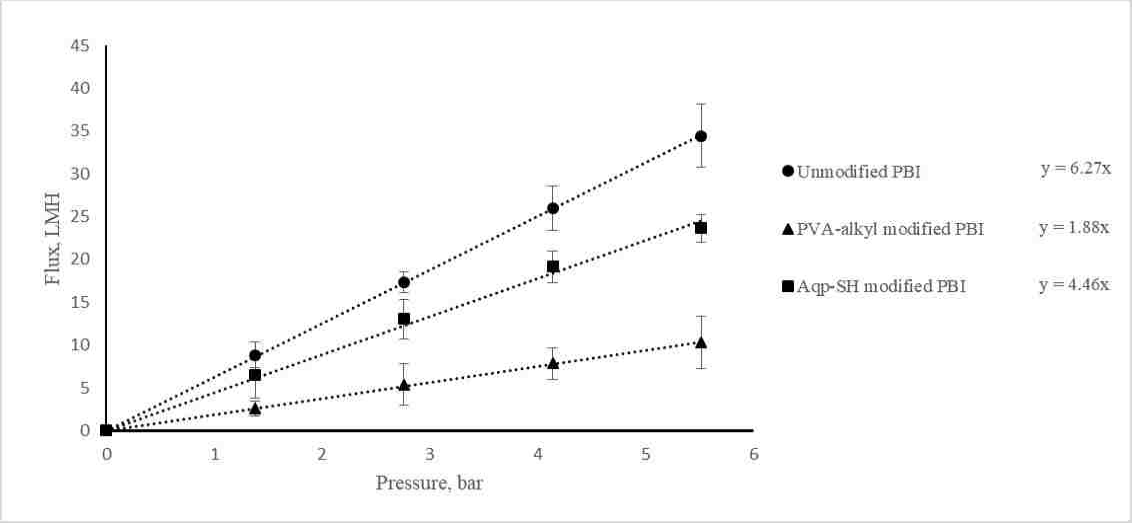

Figure 6-11 Flux linearity and permeability consistency for unmodified PBI and Aqp-SH modified PBI membranes

With respect to salt rejection (figure 6-12), Aqp-SH membranes showed the highest rejections for the solutions as compared to unmodified PBI and PVA-alkyl modified PBI membranes. Unmodified PBI membranes showed 19±2.3% rejection during filtration of the 3.4 mM NaCl solution, and as the NaCl concentration increased to 100 mM, the rejection decreased to 5.3±1.2%. PBI membranes modified with only PVA-alkyl showed a rejection of 37.24±2.5% for a feed solution of 3.4 mM NaCl solution and 19.53±3.7% rejection for 100mM NaCl solution. On the other hand, Aqp-SH membranes

showed a significantly higher rejection of 72.15±4.2% for 3.4 mM feed solution of NaCl and 72.95±1.8% for 100 mM NaCl. Similarly, unmodified PBI membranes showed 24.30±1.5% rejection during filtration of the 3.4 mM $CaCl_2$ solution, and as the $CaCl_2$ concentration increased to 100 mM, the rejection decreased to 8±1.8%. PVA-alkyl modified PBI membranes showed 41.61±4% rejection for 3.4 mM $CaCl_2$ and 25.82±4.5% rejection for 100 mM $CaCl_2$. On the other hand, Aqp-SH membranes showed a rejection of 73.01±3.7% for 3.4 mM feed solution of $CaCl_2$ and 72.0.4±7.4% for 100 mM $CaCl_2$.

All membranes were then subjected to high concentration feed solutions of NaCl and $CaCl_2$ (figure 6-12). Unmodified PBI membranes showed 2.1±0.5% rejection during filtration of the 0.5M NaCl solution, and as the NaCl concentration increased to 2M, the rejection decreased to 0.8±0.4%. PBI membranes modified with only PVA-alkyl showed a rejection of 15.21±5.1% for a feed solution of 0.5M NaCl solution and 2.13±1.7% rejection for 2M NaCl solution. On the other hand, Aqp-SH membranes showed a significantly higher rejection of 62.4±5.4% for 0.5M feed solution of NaCl and 49.3±7.5% for 2M NaCl. Similarly, unmodified PBI membranes showed 3.4±0.8% rejection during filtration of the 0.5 M $CaCl_2$ solution, and as the $CaCl_2$ concentration increased to 2M, the rejection decreased to 1.3±0.2%. PVA-alkyl modified PBI membranes showed 17.52±1.7% rejection for 0.5M $CaCl_2$ and 13.19±5.1% rejection for 2M $CaCl_2$. On the other hand, Aqp-SH membranes showed a rejection of 67.2±3.5% for 0.5M feed solution of $CaCl_2$ and 59.1±5.1% for 2M $CaCl_2$.

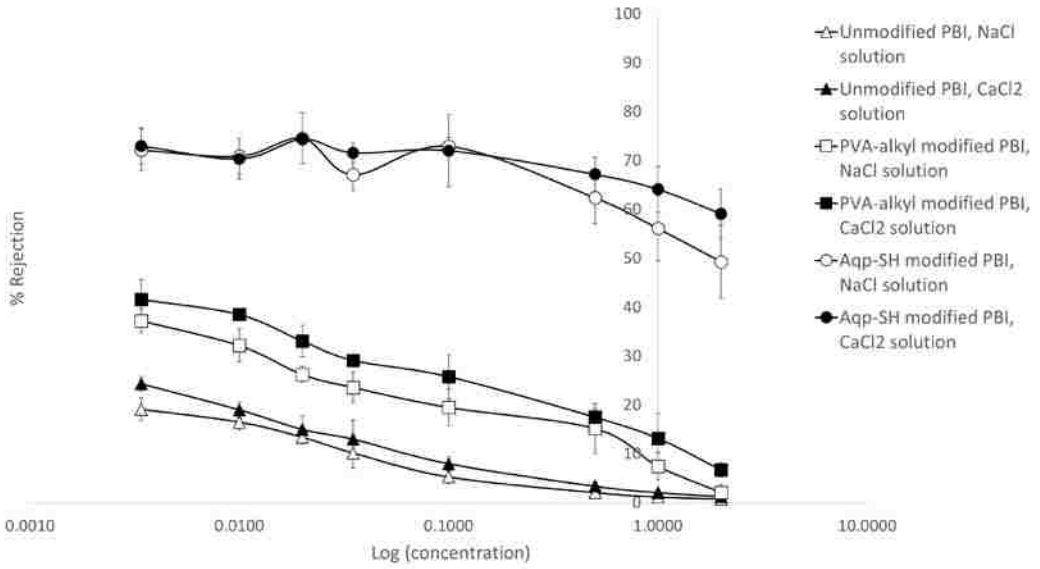

Figure 6-12 Sodium chloride and Calcium chloride filtration rejection

PVA-alkyl modified membranes showed higher salt rejection values as compared to unmodified PBI membranes possibly due to decrease in MWCO, pore size of membranes, and charge interactions with ions. The rejection obtained for Aqp-SH modified PBI membranes for salt solutions were higher as compared to the unmodified PBI membranes. This might be due to the immobilized aquaporins on the membrane surface.

Rejection properties are in part determined by the electric double layer that arises from the electrostatic potential about charged surfaces in aqueous media; the magnitude of this potential and its rate of decay from the surface are determined by the surface charge and ionic strength, respectively [282]. As the ionic strength of feed solution increases, rejection decreases owing to a contraction of the electric double layer that enhances charge shielding [283, 284] and reduces ion transport rates [236]. However, in case of aquaporin modified membranes, membrane rejection remained fairly constant

irrespective of the ionic strength of salt solutions (figure 6-12). In the case of unmodified PBI membranes and membranes modified with PVA-alkyl, a decrease in salt rejection was observed as the ionic strength of feed salt solutions increased, which corresponds to double layer and charge shielding effects. The constant rejection of salt solution obtained with aquaporin modified membranes shows that immobilized aquaporins might be unaffected by charge interactions and provide the same rejection irrespective of the ionic strengths of the feed solutions. The reason might be because of the unique hourglass shaped structure of aquaporin pores and the electrostatic barrier able to reject all the charged entities present in feed other than water molecules [36, 122], which means that any decreases in rejection would be due to leakage around the aquaporins. The free-energy profile for ion penetration through aquaporin modified membrane shows a significant difference between the overall barriers for ion and water penetration. The constant rejection observed with Aqp-SH modified membranes is another evidence of the presence of functionalized aquaporins that opened up more water channels, increased water flux through the membrane, and provided higher and constant rejection of feed salt solutions irrespective of their ionic strength. However, it is likely that aquaporins did not cover entire surface area of the membranes due to the presence of detergent or PVA-alkyl, so some of the feed solution might have gone around the aquaporins on the surface providing a rejection less than the complete rejection that was expected with aquaporins.

6.3.8 Estimations of aquaporin packing in membrane assembly:

Although the polymer layers could be resolved via electron microscopy, the distribution of surface-anchored Aqps were beyond limits of detection. Thus, to

investigate the hypothesis that aquaporin surface deposition was incomplete, a computational model was used to measure ion fluxes across a membrane with aquaporins aggregates of varying sizes. In principle, complete coverage of the film surface with aquaporins should reduce electrolyte flux across the membrane to zero while permitting water flux owing to the high selectivity of aquaporins to water over ions. Although electrostatic interactions with charged surfaces can strongly influence ion conduction [285], the high ion concentrations at which the experiments were conducted strongly attenuated such effects.

To rationalize the flux values reported in Figures 6-10 A-D that demonstrated significant variations in magnitude with respect to polymer membrane configuration, a computational geometry was developed. The 1 nm diameter pores were consistent with MWCO analysis; the pore spacing accounted for 28% surface coverage by nanopores. For this modeling, the PVA-alkyl porosity was assumed to be invariant across the characterized membrane configurations. Since ions do not significantly permeate through the Aqp pore, the proteins were presumed to comprise a monolayer of cylindrical obstructions that resist flow through the PBI layer. It was studied whether the fluxes would be influenced by how the Aqps were distributed: either as single proteins distributed uniformly as aggregates. Toward this end the steady state diffusion equation was solved based on varying Aqp aggregate sizes. Figure 6-13 shows a disk of increasing radius that occluded the underlying pores as a representation of Aqp-aggregates of increasing size. It was observed that as the Aqp packing density approached 0, the faster diffusion observed in the PBI-only case was recovered; as the packing density approached 64%, the diffusion constant estimated for the Aqp-modified membranes was

recovered as shown in Figure 6-10 D. Also figure 6-13 shows the change in D_e with respect to packing density for a single Aqp monomer, by varying the surface area of the film. It was found that the effective diffusion rate scaled comparably to the aggregates, hence these two cases could not be discriminated based on diffusion alone. However, it is important to note that Aqp monomers at a given packing density presented more exposed surface area compared to an aggregate of comparable density. In light of which, packing configurations could be discriminated under conditions for which surface/diffuser interactions were significant. For instance, in the event that these experiments were performed under low ionic strength conditions, it was expected that ions could interact with the Aqp surface and thereby influence diffusion. However, the flux obtained with Aqp-SH modified PBI membranes was lower than that of unmodified PBI membranes. The reason of lower flux might be the aggregation of some portion of aquaporins attached on the surface. These aggregated aquaporins would not increase the water flux through them owing to the loss of functionality. Based on the flux data, it was calculated that 24% of the aquaporins that are attached on the surface contributed to the water transport through the membranes and hence remaining aquaporins might be aggregated on membrane surface.

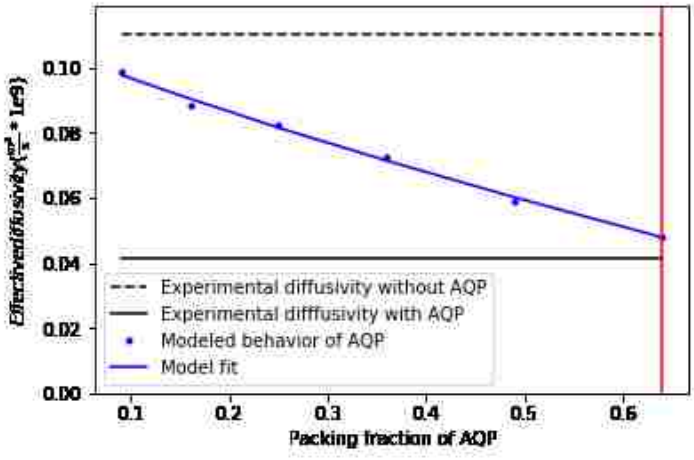

Figure 6-13 Predictions and experimentally measured effective diffusion coefficients, based on the geometry in Figure 6-14. Black lines correspond to experimental data found in Table C.1 in Appendix C. Blue lines represent aggregate (solid) and monomeric (dots) Aqp models, respectively.

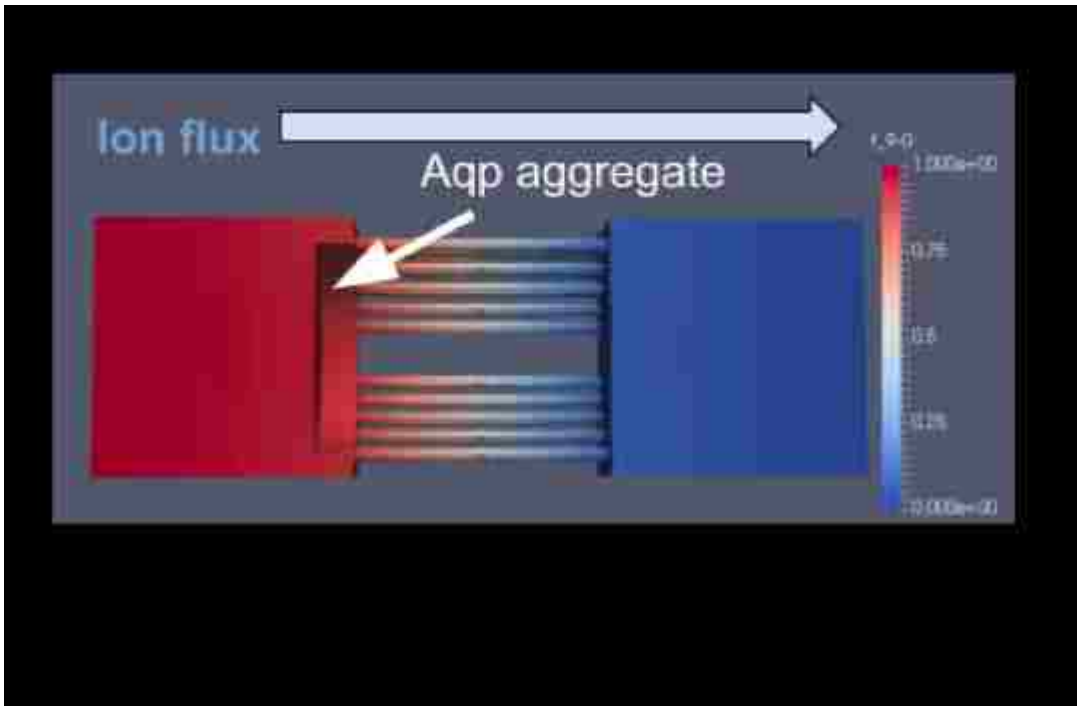

Figure 6-14 Representative simulation geometry of membrane occluded by aquaporin (Aqp) aggregate. In this picture, the left reservoir contained 1000 ppm NaCl solution while right reservoir was DI water (0 M). Aggregate was simulated by cylinders of increasing diameter overlayed onto membrane surface. The effective ion diffusion rate was obtained by integrating the concentration gradient along the membrane surface.

6.4 Concluding remarks

Modification of aquaporins with a cysteine at the N-terminus and immobilization of these modified aquaporins on the membrane surface was successfully accomplished. Elemental analysis showed that aquaporins were immobilized on the membrane surface. It is proposed that four cysteine groups acting as anchors for aquaporin tetramer helped to align aquaporins on the surface of membranes. In agreement with pore size distributions, charge interactions, and added resistance to flow due to modification, PVA-alkyl modified PBI membranes showed lower flux values and slightly higher salt rejection as compared to unmodified PBI membranes. On the other hand, Aqp-SH modified membranes displayed lower flux values as compared to unmodified PBI but higher as compared to PVA-alkyl modified membranes. Membranes modified with an inactive Aqp-SH were used as a negative control to demonstrate the functionality of Aqp-SH incorporated into the membranes. Inactive Aqp-SH modified membranes did not show any improvement in flux values as compared to PVA-alkyl modified PBI membranes. Furthermore, owing to the presence of functional and immobilized aquaporins, Aqp-SH modified membranes displayed the highest salt rejection values among all membranes analyzed in the study. Aqp-SH modified membranes displayed a nearly constant salt rejection irrespective of the salt concentration for low feed concentration, while unmodified PBI and PVA-alkyl modified PBI membranes showed a decrease in rejections as feed salt concentration increased. However, due to the hindrance of detergent or PVA-alkyl in aquaporin solutions, the surface of the membrane was not completely covered with immobilized and aligned aquaporins, which in turn led to rejection values lower than 100%. Simulation studies showed that immobilized

aquaporins with PVA-alkyl provided a diffusion rate equivalent to 24% coverage of active aquaporins. This proved that aquaporins did not cover the entire surface area of the membranes, thereby providing a salt rejection of less than 100%.

6.5 Acknowledgements

This material is based upon work supported by the National Science Foundation under Cooperative Agreement No.1355438, and by the NSF KY EPSCoR Program and in addition the author acknowledges Center of Membrane Sciences at University of Kentucky. In addition, the authors want to acknowledge the sources of funding, NSF 1308095 and USGS 104(b): Ohio Water Development Authority GRT00028988/60040357 for funding this project. PBI Performance Products Inc. is thanked for supplying the PBI dope for the study.

CHAPTER 7. BISAMIDE-BASED ORGANIC FRAMEWORK FOR SYNTHESIS OF MEMBRANES WITH SPECIFIC MOLECULAR WEIGHT CUTOFF

7.1 Introduction

Membranes of specific pore size distribution have found numerous applications for selective separations based on size exclusion [286, 287]. Membranes with tunable pore size and covalent organic frameworks are attractive for separation of larger molecules on the basis of size exclusion by nanofiltration [287-289]. Some of the materials used for these applications are zeolites [290], graphene oxide [291], metal-organic frameworks [292], etc. Organic frameworks are porous materials that consist of light elements (carbon, oxygen, nitrogen, sulfur, hydrogen) that are connected via hydrogen bonding or via covalent bonding. Their inherent porosity, ordered channel structure, large surface area, excellent stability, and functionality make them excellent candidates for mixed matrix membranes [287].

Wang et al. synthesized nanocomposite membranes by embedding the zwitterionic functionalized “cage like” porous organic frameworks into the polyamide layer of membranes. These frameworks provided more and shorter channels for water to go through the membrane. Membranes modified with these organic frameworks displayed higher flux with 90.6% retention of Na_2SO_4. Modified membranes showed higher hydrophilicity and a negatively charged surface as compared to unmodified membranes [293]. Kandambeth et al. fabricated a series of self-standing, porous and crystalline covalent organic frameworks via baking of organic linkers in the presence of p-toluene sulfonic acid and water. Membranes modified with these organic frameworks

provided high flux values towards organic solvents such as acetone and acetonitrile. These membranes showed a 2.5 fold increase in flux with equivalent solute-rejection performances [294].

Despite of a number of approaches being implemented in the field of organic frameworks in membrane matrix or on membrane surface, there are some limitations in the use of these frameworks. Some of the issues observed in incorporation of organic frameworks into membranes are membrane stability [294], difficult synthesis procedures [295], chemical instability [296], and insolubility in solvents [294].

Bera et al. investigated the assembly of encapsulated water molecules with hybrid bisamide hosts [11]. The study reported that a one-dimensional column of water molecules in a single file (or a water wire) promoted a supramolecular framework in solution by bridging two bisamide molecules and thus formed self-assembled channels of internal diameters ranging from 5 A^o to 9 A^o depending on the number of carbon atoms in the chain [11]. These bisamide channels contained monomethyl esters (Figure 1) on each end to prevent intermolecular hydrogen bonding interaction. The addition of water promoted the self-assembly and Π-stacking interactions between these bisamides, and water formed a helical pattern of flow through hydrogen bonding with these artificial channels (Figure 2). The interactions between water and bisamides were studied using FTIR and NMR previously in order to confirm the formation of water channels [11].

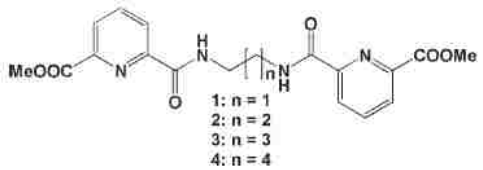

Figure 7-1 Schematic representation of bisamide molecules synthesized by Bera et al.[11]

The objective of this study was to synthesize modified bisamide molecules with amine and carboxylic acid end groups to promote intermolecular hydrogen bonding in order to ultimately form a selective layer on membrane surface. After formed, these bisamide molecules were incorporated into synthetic membranes to act as a layer providing a specific molecular weight cut off. It was hypothesized that single bisamide molecules could be attached onto a membrane surface using carbodiimide chemistry, and they could form a stable selective layer in the form of an organic framework in order to provide a specific molecular weight cut off. The schematic of incorporation of bisamide molecules into synthetic membrane as an organic framework is shown in Figures 3(A) a

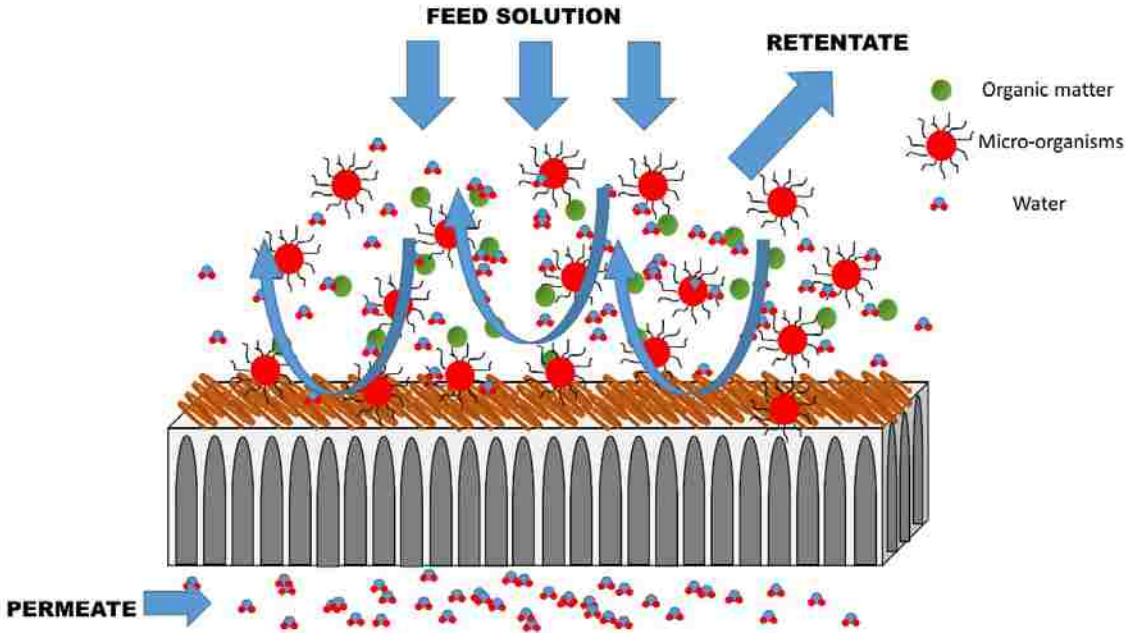

7-2 (a)

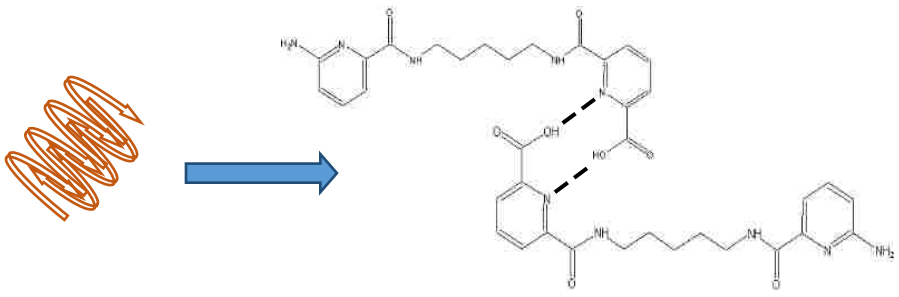

7-2 (b)

Figure 7-2 (a) and (b) Schematic of incorporation of artificial bisamide molecules onto the membrane surface via carbodiimide chemistry and hydrogen bonding between bisamide molecules

7.2 Experimental

7.2.1 Polybenzimidazole (PBI) membrane preparation

Polybenzimidazole was used as the backbone for the assembly of bioinspired membranes. It has been used in the synthesis of biomimetic membranes based on aquaporins in studies published previously [149]. PBI has found its applications in fuel cells [297], hydrogen purification [298], high flux organic solvent nanofiltration [299], anion exchange membranes [300]. It has been shown to have a high alkaline resistant and mechanical stability [300]. Phosphoric acid doped PBI membranes have gained a lot of interest in the last decade because of their stability in high temperature range (120-200^{o}C)

[301]. PBI has a unique functionality because of electron donating groups of imidazoles, and intramolecular and intermolecular hydrogen bonding ability in the presence of Bronsted acids [302]. A number of applications of PBI in areas such as proton conducting membranes, nanofiltration, and other separation membranes have been reported [303, 304].

Flat sheet PBI membranes were synthesized according to the studies published previously [149, 305]. 21% dope solution was prepared in dimethylacetamide (DMAc) solvent. Water was used as the non-solvent in this process. Flat sheet membranes were prepared using casting knife, or doctor's blade (Paul N Gardner Co, U.S. Pat 4869200, Pompano Beach, FL.) The membranes were stored in a 50/50 glycerol-DI water solution in order to prevent their drying and collapse of pore structure. The membranes were kept in the solution at least one day before they were analyzed.

7.2.2 Surface functionalization of PBI membranes:

In order to attach bisamide framework on PBI membrane surface, membrane surfaces were functionalized following previous techniques [149, 217], in which 4-chloromethyl benzoic acid (CMBA), purchased from Sigma-Aldrich (USA), was used to add a carboxylic acid group to the surface of PBI membrane, which could be used as a platform for subsequent functionalization of the membrane [261, 277]. The membranes were washed with copious amounts of DI water to remove excess reagents and immediately placed in glycerol/water bath after the reaction was completed.

7.2.3 PVA-alkyl synthesis:

Polyvinyl alcohol carrying long alkyl chains (PVA-alkyl) is amphiphilic in nature. It has polyvinyl alcohol (PVA) as the hydrophilic component while long alkyl chains are responsible for the hydrophobicity of the molecule [218]. PVA-alkyl has been used to incorporate and immobilize aquaporins into synthetic PBI membranes previously [149]. It has found its applications in cell surface modification without affecting cell viability [212, 213]. It was observed that PVA-alkyl attached to cell surface at multiple points through interactions with 28 alkyl chains of every PVA-alkyl and a capping phenomenon was observed on the surface [306]. Being amphiphilic in nature and flexible because of long alkyl chains, PVA-alkyl can serve as an excellent housing for artificial channels and organic frameworks.

PVA-alkyl was prepared in a two-step process, according to literature protocols [149, 218-220]. Briefly, a two-step reaction procedure was followed. A reaction between PVA and sodium monochloroacetate yielded carboxy-methyl PVA (PVA-COOH) which was then used as a reactant along with hexadecanal to obtain PVA-alkyl as the final product [149, 218].

7.2.4 Synthesis of Bisamide molecules

Hybrid bisamide molecules were first synthesized by Bera et al. [11] to investigate assembly of water molecules encapsulated into confined channels. These bisamide channels formed supramolecular frameworks that were stabilized by the passage of water molecules through them and hydrogen bonding groups between the

monomers in the channels. For this study, a modification of bisamide molecules synthesized by Bera et al. [11] was used. Instead of monomethyl esters as end groups of channels, amines and carboxylic acid groups were added on end groups in order to facilitate intermolecular hydrogen bonding between bisamide molecules. A modified bisamide monomer with 5 carbon atoms chain and a primary amine on one end and carboxylic acid on another end of the molecule is shown below in Figure 7-3.

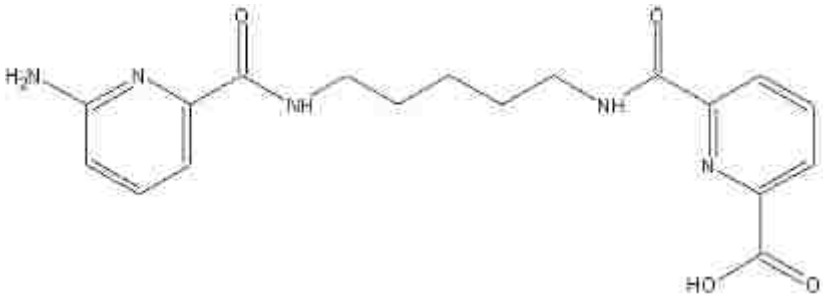

Figure 7-3 Structure of Bisamide monomer with 5 carbon atom chain

6-amino pyridine-2-carboxylic acid, ethanediamine, trimethylenediamine, cadaverine, 6-hydroxymethyl-pyridine-2-carboxylic acid, dicyclohexylcarbodiimide (DCC) were purchased from VWR (Atlanta, GA). A 2-step reaction protocol was followed where addition of diamines, 6-amino-pyridine-2-carboxylic acid, and 6-hydroxymethylpyridine-2-carboxylic acid using DCC as a reagent was performed under nitrogen environment, as shown in Figure 4(a). This was followed by Jones oxidation reaction to form the bisamide monomer with 2 carbon atom chain length. Oxidation reactions are shown in Figure 4(b). Size exclusion chromatography was carried out using Sephadex G-10 (GE healthcare, Chicago, IL) gel filtration resin and methyl red (Alfa

Aesar, Haverhill, MA) as an indicator for separation between product and by-products. Figure 7-4 shows the synthesis reactions for bisamide molecules.

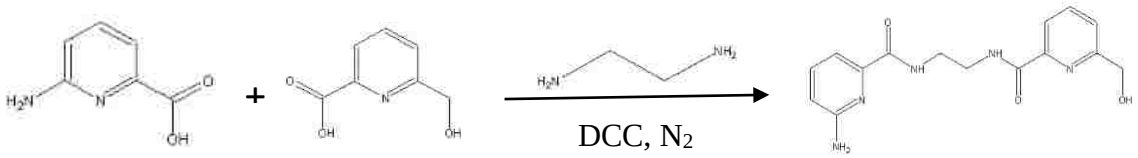

6-amino-pyridine-2-carboxylic acid

6-hydroxymethyl pyridine-2-carboxylic acid

7-4 (a)

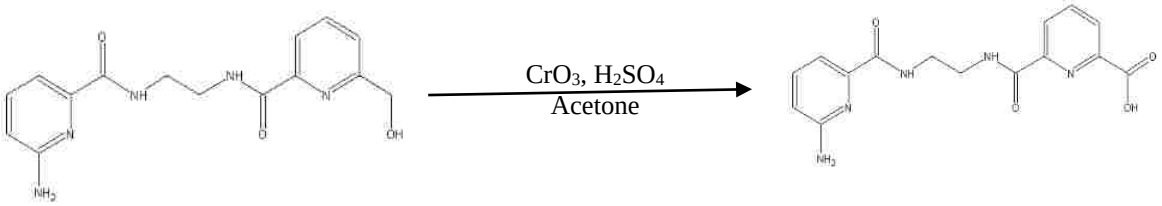

7-4 (b)

Figure 7-4 (a) and (b) Synthesis reactions for the formation of bisamide channel with 2 carbon atoms chain length

7.2.5 Attachment of bisamide channels on PBI membranes surface

Bisamide molecules were covalently attached to CMBA modified PBI membranes using carbodiimide chemistry in the presence of dicyclohexylcarbodiimide (DCC), as shown in Figure 7-5. In this mechanism, the bisamide molecules acted as nucleophiles to get covalently attached to –COOH group present on the surface of PBI membrane. Amines present in the bisamide molecule reacted with –COOH groups in order to form amide groups and helped for the immobilization of bisamide molecules. PVA-alkyl was used in the following step in order to bind to the remaining –COOH groups of PBI membranes.

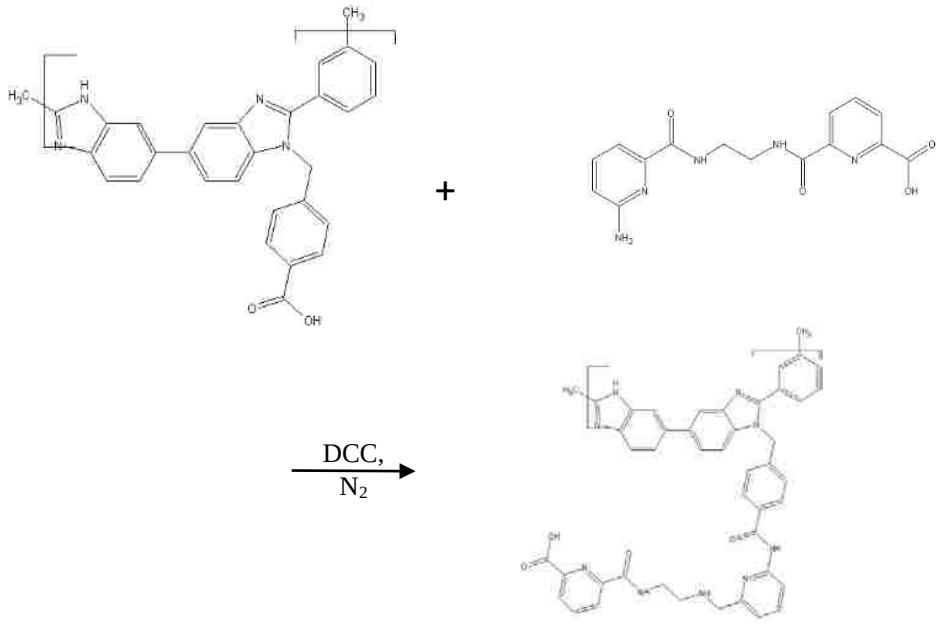

Figure 7-5 Covalent attachment of bisamide channels on –COOH modified PBI membrane

7.2.6 Fourier transform Infrared Spectroscopy (FTIR)

A vibrational spectrum is a characteristic of every molecule and is considered a unique property of that molecule [226]. FTIR was used in ATR mode to confirm the modification with carboxylic acid groups on PBI surface as well attachment of bisamide channels on modified membranes. Digilab UMA 600 FT-IR microscope was used for all the analysis of membrane samples performed in this study.

7.2.7 Molecular weight cut off:

The molecular weight cutoff analysis of unmodified PBI, PVA-alkyl modified PBI, and bisamide-modified PBI membranes was conducted using 100 ppm solutions of sucrose and various molecular weights of polyethylene glycol (PEG) solutions. The total organic carbon (TOC) of both feed and permeate solutions were measured using Teledyne Tekmar Fusion TOC analyzer (Mason, OH). The various samples that were used in this study along with their Stokes-Einstein radii are shown in Table 7-1. The rejection values of all solutes were used to determine the molecular weight cut off of both unmodified and modified PBI membranes. The molecular weight of solute in feed solution for which the membranes showed more than 90% rejection was considered the molecular weight cut off of the membranes. The apparent solute rejection R (%) was calculated using equation (7-1).

$$R = \left(1 - \frac{C_p}{C_f}\right) \times 100\% \qquad (7\text{-}1)$$

Table 7-1 Neutral solutes used for molecular weight cut off analysis and their Stokes-Einstein radii in nm [25, 229-232]

Solute	**Mol. Wt. (Da)**	**Stokes-Einstein radii (nm)**
Sucrose	342.3	0.47
PEG 400	400	0.57
PEG 600	600	0.68
PEG 1000	1000	0.94

7.2.8 Contact angle analysis:

Contact angle was used as a measure to determine the hydrophilicity of the membrane surfaces before and after modification. A drop shape analyzer – DSA 100 (KRUSS USA, Matthews, NC) was used for contact angle measurements using the sessile drop technique.

7.2.9 Flux and selectivity experiments

Dead end filtration was used to monitor the flux decline of unmodified PBI, PVA-alkyl modified PBI, and bisamide-modified PBI membranes. Filtration experiments were

performed using Amicon filtration cell (Amicon Stirred Cell 8010 – 10 ml) under a constant pressure of 70 psi (4.83 bar) and continuous stirring. Flux values were calculated as L/m^2-hr and plotted against the total permeate volume. Membrane samples were cut into circular pieces of area 4.1 cm^2 and supported by a Whatman^{TM} filter paper (125 mmø). Each membrane was precompacted with DI water for 1 hour until a stable flux was reached. Precompaction was followed by feed solution of 100 mM magnesium sulfate ($MgSO_4$) in water under same conditions of pressure and stirring. Salt concentrations were measured using conductivity meter. Solute rejections were calculated using equation (7-1).

7.3 Results

7.3.1 Chemical analysis using FTIR

Figure 7-6 shows the FTIR analysis of unmodified PBI, and bisamide-modified PBI membranes, and Table 2 identifies all peaks. FTIR of bisamide modified PBI membranes showed peaks at ~1050 cm^{-1} for C-O stretch, ~ 1260-1350 cm^{-1} for –OH bend which correspond to terminal carboxylic acid groups present in the molecule. This showed that the terminal alcohol after reaction 1 completion (Figure 7-4(b)) was oxidized to a carboxylic acid group. A peak at 1580-1615 cm^{-1} corresponding to aromatic carbon bond is associated with the pyridine carboxylic acid part of bisamide molecule. This peak showed the covalent attachment of bisamide molecule after reaction 1 (Figure 7-4(a)). The peak at 1630-1680 cm^{-1} corresponds the presence of amide groups in bisamide modified PBI membranes, while the peak in the range of 1310-1360 cm^{-1} corresponds to -

CN stretch of aromatic tertiary amine confirming the presence of pyridine in modified membranes. Lastly, a peak corresponding to aliphatic secondary amine -NH stretch is shown at 3310-3360 cm^{-1} in bisamide modified PBI membranes. Bonds corresponding to different functional groups are indicated in Figure 7-7.

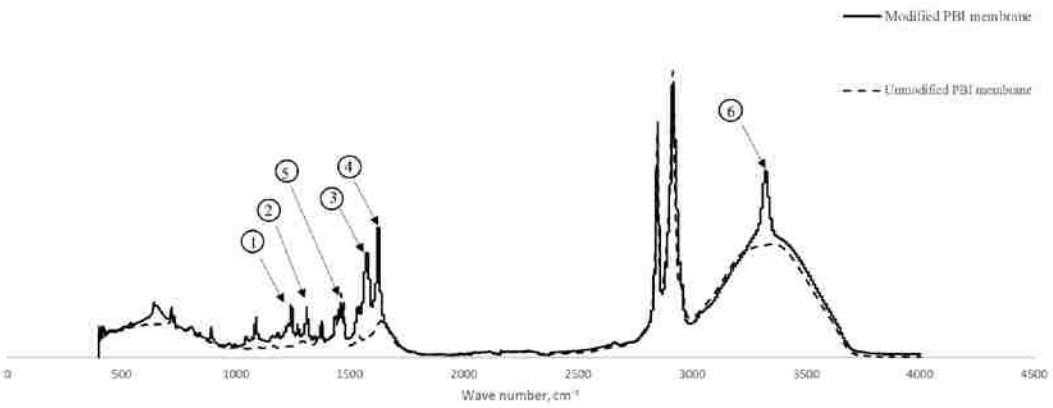

Figure 7-6 FTIR analysis of unmodified, CMBA modified and PVA-alkyl modified membranes.

Table 7-2 Functional groups and corresponding wave numbers in IR spectra.

Band number	Functional group	Wave number (cm^{-1})
1	C-O (stretch)	~ 1050

2	-OH (bend)	~ 1260-1350
3	C=C-C (stretch)	1580-1615
4	N-C=O	~ 1630-1680
5	C-N (Aromatic tertiary amine C-N stretch)	~ 1310-1360
6	>N-H (stretch)	3310-3360

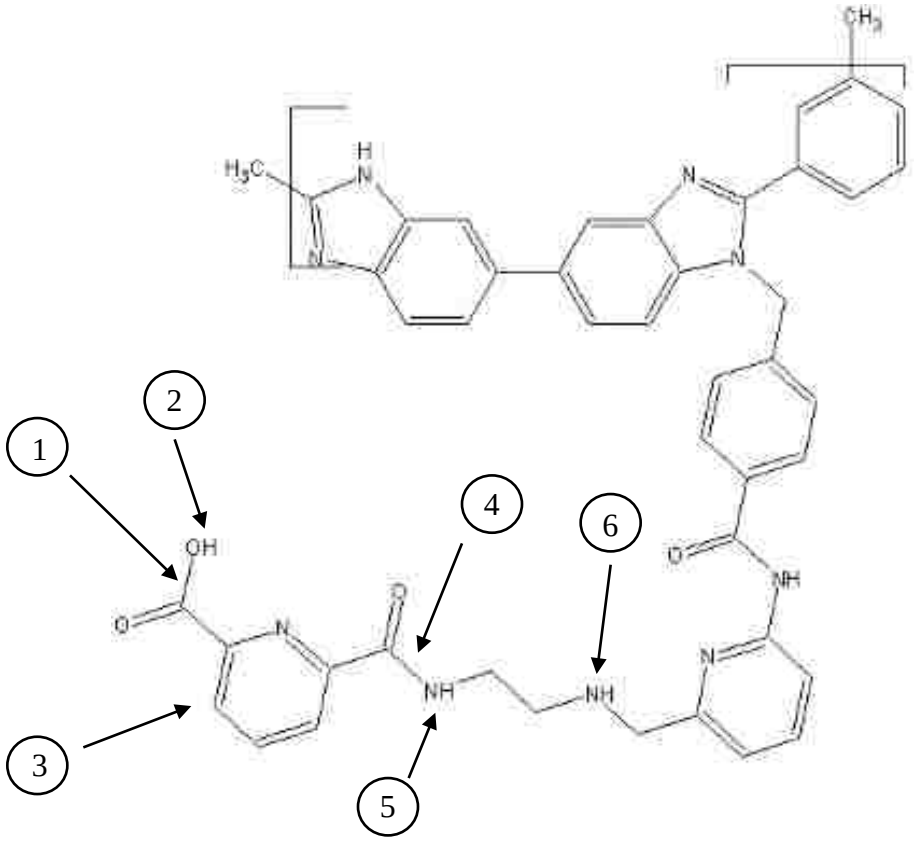

Figure 7-7 Bisamide modified PBI molecule

7.3.2 Molecular weight cut off analysis:

Unmodified PBI membranes showed more than 90% rejection for PEG 1000 (Figure 7-8 and Table 2) which has Stokes radius of 0.94 nm. This showed that the membranes were in nanofiltration range. Membranes modified with only PVA-alkyl showed 90% rejection for PEG 600, which has Stokes radius of 0.68 nm, and molecular weight of 600 Da. After addition of bisamide molecules and PVA-alkyl on membrane surface, modified membranes showed 90% rejection for PEG 400, which has Stokes radius of 0.57 nm and molecular weight 400 Da. Therefore, the decrease in MWCO is not due to the addition of the PVA-alkyl layer. This showed that bisamide-modified membranes were also in nanofiltration range but showed a smaller molecular weight cut off than unmodified membranes. All other larger compounds were rejected at nearly

100%

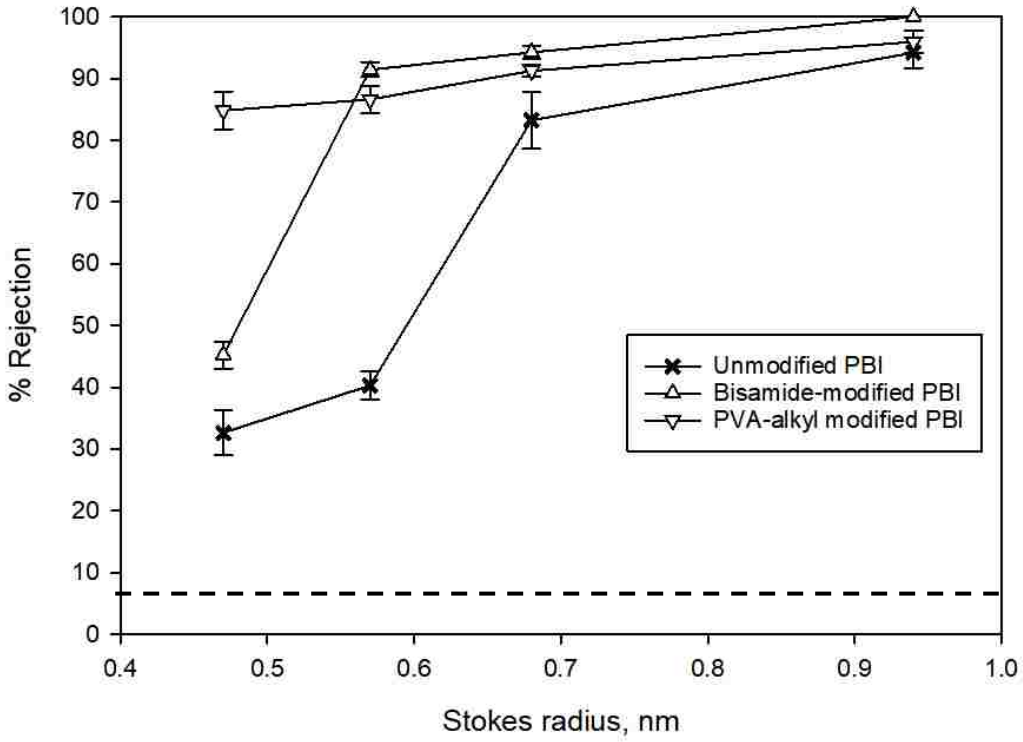

Figure 7-8 Molecular weight cut off analysis of unmodified PBI, PVA-alkyl modified PBI, and bisamide-modified PBI membranes.

Table 7-3 Rejections obtained for unmodified PBI, and bisamide-modified PBI membranes

Membrane	**Rejection > 90%**	**MWCO**
Unmodified PBI	0.94 nm (94.2%±2.5 %)	1000
PVA-alkyl modified PBI	0.68 nm (91.3%±1.0)	600
Bisamide-modified PBI	0.57 nm (91.5%±1.2 %)	400

7.3.3 Contact angle analysis:

Contact angle was used as a measure of hydrophobicity, and results are shown in Table 7-4. Unmodified PBI membranes were more hydrophobic as compared to bisamide-modified PBI membranes. PVA-alkyl modified membranes showed a decrease in contact angle due to the hydrophilicity of PVA groups present on the surface [149]. Bisamide-modified membranes showed a slightly lower contact angle as compared to PVA-akyl. This small decrease might have been due to the presence of more carboxylic acid groups present in bisamide channels.

Table 7-4 Hydrophobicity via contact angle

Membrane	Contact angle
Unmodified PBI	74^{o}
PVA-alkyl modified PBI	63^{o}
Bisamide modified PBI	60^{o}

7.3.4 Flux analysis

To investigate the permeability and selectivity of bisamide-modified PBI membranes, filtration studies using 100 mM $MgSO_4$ were performed under a constant pressure of 4.83 bar. Experiments were conducted in parallel in order to study unmodified PBI, PVA-alkyl modified PBI, and bisamide-modified membranes, and the flux values were plotted as a function of permeate volume as shown in Figure 7-9. For unmodified PBI membranes, the pure water flux was 31.6 L/m^2-h (LMH), the initial flux for $MgSO_4$ filtration was 27.4 LMH, the recovery after $MgSO_4$ filtration (i.e. after reverse flow filtration with DI water) was 26.9 LMH (or a 85% flux recovery, as compared to the initial pure water flux). $MgSO_4$ rejection obtained with unmodified PBI membranes was 32.4%. PVA-alkyl modified PBI membranes provided the lowest flux values among all three membranes. The pure water flux was 19.4 LMH, the initial flux for $MgSO_4$ filtration was 17.5 LMH, the recovery after $MgSO_4$ filtration was 17 LMH (or

a 88% flux recovery, as compared to the initial pure water flux). $MgSO_4$ rejection obtained with PVA-alkyl-modified PBI membranes was 34.7%. On the other hand, for bisamide-modified PBI membranes, the initial pure water flux during precompaction was 26.3 LMH, and the initial flux for $MgSO_4$ filtration was 24.3 LMH. Flux recovery observed after reverse flow filtration with DI water was 24.0 LMH (or 91% as compared to initial pure water flux). Bisamide-modified PBI membranes displayed a rejection of 43.4%. Therefore, bisamide addition increased the flux of water through the addition of water channels and increased the rejection, which supports the addition of one-dimensional water wire channels

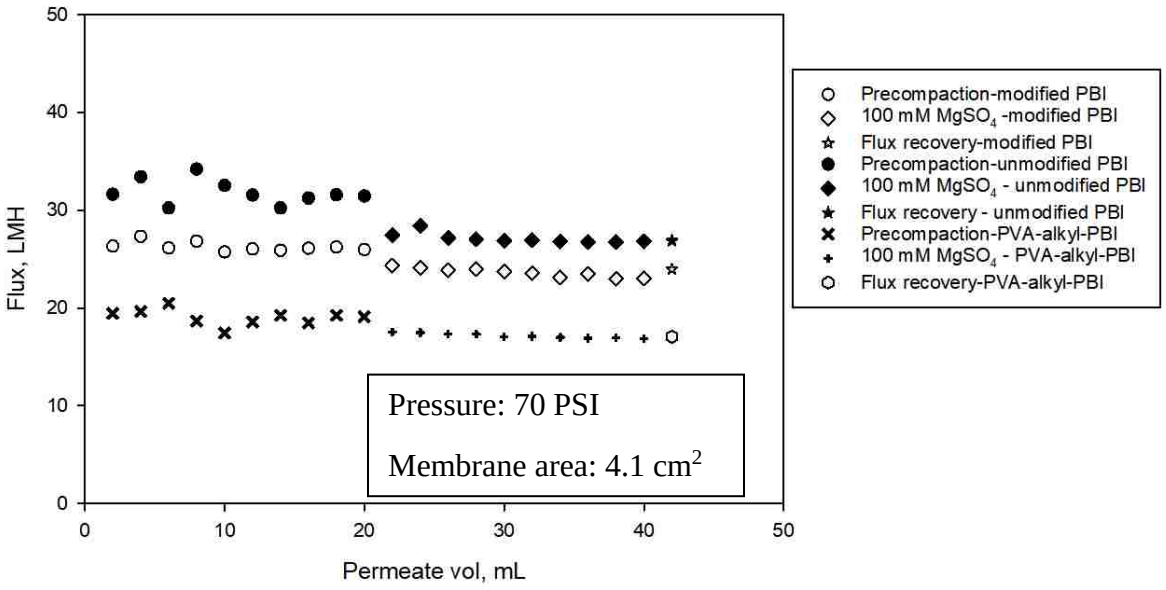

Figure 7-9 Flux analyses of unmodified PBI, PVA-alkyl modified PBI, and bisamide-modified PBI membranes at constant pressure of 70 psi (4.83 bar)

Bisamide-modified PBI membranes showed lower initial flux as compared to unmodified PBI membranes possibly because of added resistance of PVA-alkyl and

decrease in molecular weight cut off. PVA-alkyl modified membranes provided the lowest flux values among all three membranes possibly because of added resistance and the absence of channels facilitating more water flow. The flux recovery obtained after filtration with 100 mM $MgSO_4$ solution in water was slightly higher for bisamide-modified membrane as compared to unmodified PBI membranes. Higher flux recovery obtained with modified membranes might be because of the presence of artificial channels which provided more channels for water to go through and remove reversible impurities better than unmodified membrane. The rejections obtained for both unmodified and modified membranes did not differ much owing to the fact that the pore diameter of bisamide channels was higher than the size of $MgSO_4$ molecules.

7.4 Concluding remarks

Bisamide-based molecules were successfully incorporated into synthetic PBI membranes in order to form an organic framework on the surface of the membrane. Bisamide molecules were incorporated via covalent attachment to the -COOH groups on the membrane surface. FTIR analysis of modified membranes confirmed the presence of functional groups present in bisamide molecules. These hybrid bisamide molecules formed a framework on membrane surface, which translated into a MWCO of approximately 400 Da and average pore size of 0.57 nm. Bisamide modified membranes allowed for a slightly lower passage of divalent salt as compared to unmodified PBI and PVA-alkyl modified PBI membranes. Furthermore, since bisamide was added to PVA-alkyl-modified PBI membranes, when compared, bisamide-modified membranes had higher flux values than PVA-alkyl PBI membranes. This supports the presence of an

organic framework of bisamide molecules on functionalized membranes providing a specific molecular weight cutoff.

7.5 Acknowledgements

This material is based upon work supported by the National Science Foundation under Cooperative Agreement No.1355438, and by the NSF KY EPSCoR Program. In addition, the authors want to acknowledge PBI Performance Products Inc. for supplying the PBI dope for the study.

CHAPTER 8. CONCLUSIONS AND RECOMMENDATIONS

8.1 Conclusions

The overarching goal of this study was to synthesize biomimetic nanofiltration membranes with protected and immobilized aquaporins, as well as to synthesize bio-inspired membranes with artificial water channels imitating the structure-function relationships of biological channels. The objectives of this study were to first incorporate aquaporins into synthetic nanofiltration membranes without chemically altering them to prevent flattening or denaturing of aquaporins during operation. Then, the second objective was to install functional groups on aquaporins and align them in the direction of water flow. Lastly, the third objective was to synthesize artificial channels in order to overcome the issues with aquaporin stability, alignment, and efficient packing of water channels onto the membrane surface. Membranes synthesized here had as a primary goal to match or exceed the permeability of ~11 LMH/bar and a divalent ($MgSO_4$) salt rejection of 97% of commercially-available NF-270 membranes [62, 63].

For the first objective, aquaporins were treated with a polysaccharide, gum Arabic, and incorporated into an amphiphilic polymer, polyvinyl alcohol with alkyl side chains (PVA-alkyl), in order to simulate the natural housing of lipid bilayer for aquaporins and to protect them from denaturing. Long alkyl chains provided the hydrophobic component, while PVA provided the hydrophilic component of the amphiphilic polymer. Membranes modified with aquaporins displayed lower flux declines and higher flux recoveries after reverse flow filtration, along with improved

rejection values for both protein and salt solutions as compared to PBI and PBI-PVA-alkyl membranes. However, there was leakage of ions, as observed by a rejection less than 100% as expected with aquaporins, that occurred likely between channels.

Therefore, it was then hypothesized that in order to improve the rejection of protons, ions and other impurities, the channels were aligned with the direction of water flow. Cysteine functional groups were installed on aquaporins using site-directed mutagenesis in order to covalent attach them to the polymer matrix and to align them in the direction of the flow. Aquaporin constructs were modified to bear affinity tags or unique amino acids at the N-terminus of the aquaporin molecule, which was used to facilitate directional immobilization. Each aquaporin monomer was modified with a unique amino acid Cys group at the N-terminus right after the first Met, and due to the aquaporin tetrameric nature, these Cys groups became four anchors for attachment. The presence of these four Cys anchors per aquaporin tetramer was also used to align the aquaporins with the feed water flow direction. Membranes modified with mutated aquaporins showed consistently higher NaCl and $CaCl_2$ salt rejection values of ~70% irrespective of feed concentration, along with higher flux recoveries and lower flux declines. Unlike unmodified PBI membranes, these membranes showed fairly consistent rejections for salt solutions with increasing feed concentrations. However, these membranes still did not compete against commercial NF-270 membranes, which have a divalent salt ($MgCl_4$) rejection of 97%. In order to investigate the reason for the low rejection, approximate coverage of membrane surface with attached aquaporins was calculated using simulation studies, which showed that immobilized aquaporins with PVA-alkyl provided a diffusion rate equivalent to 64% coverage on the membrane

surface. That is, simulations showed that aquaporins did not cover the entire surface area of the membrane.

The last objective of this project was to assemble artificial water channels and add them as surface modifiers on PBI membranes. Artificial channels were synthesized as derivatives of hybrid bisamides. The series of bisamides 1-4 consist of 6-aminopyridine-2-dicarboxylic acid 6-hydroxymethyl pyridine-2-carboxylic acid, ethylenediamine, trimethylenediamine, putrescine and cadaverine depending on the length of carbon chain. These channels are amphiphilic in nature and have strong chemical attachment due to the presence of amines and carboxylic acids into each building block. These channels were introduced into the membrane matrix using carbodiimide chemistry. The channels acted as an organic framework on membrane surface. FTIR results showed the attachment of these channels onto the surface of a modified PBI membrane. Also, modified membranes showed a reduced molecular weight cut off (MWCO). Membranes modified with bisamide molecules showed higher hydrophilicity than unmodified membranes. These modified membranes showed similar divalent ($MgSO_4$) salt rejections as unmodified membranes.

Overall, results showed that PVA-alkyl could be used as housing for aquaporins in synthetic membranes to prevent their loss of activity due functionalization and flattening under hydraulic pressure. Furthermore, aquaporins could be mutated using specific functional groups and immobilized by covalent attachment on membrane surfaces in order to orient them in feed flow direction. Lastly, artificial framework using modified bisamide molecules could be incorporated into synthetic membranes in order to provide pores with lower MWCO and rejection of larger organic solutes.

8.2 Recommendations

Aquaporin-based biomimetic membranes were fabricated here, and artificial bisamide channel-based bioinspired membranes were synthesized and covalently attached membrane surfaces. Further studies are suggested in order to incorporate aquaporins more effectively into synthetic membranes, and to study more in-depth bioinspired membranes. The following recommendations are suggestions for future studies:

1. PVA-alkyl provided mechanical support for the assembly and prevented the functionalization of aquaporins under synthetic environments. However, there is a possibility of hydrogel formation with PVA-alkyl which might prevent complete coverage of membrane surface with aquaporins. Other amphiphilic polymers, such as poly(maleic anhydride alt-1-tetradecene) and poly(ethylene glycol) methyl ether methacrylate (PEGMA)-b-polysulfone (PSF)-b-P(3-O-methacryloyl)-1,2:5,6-di-O-isopropylidene-D-glucofuranose (MAIpG) (P(PEGMA)-b-PSF-b-PMAIpG), should be investigated. These amphiphilic block copolymers have been used to modify the surface of polysulfone membranes previously and can provide alternatives for PVA-alkyl.

2. Although polybenzimidazole (PBI) provided a strong mechanical support and stability under a wide range of pH and temperature values, the hydrophobicity of PBI membranes can limit the flow rate of water through membrane. Hydrophilic membrane materials should be explored to

incorporate and immobilize aquaporins and their performance could be compared in terms of stability under various operating conditions.

3. In order to increase divalent salt rejection, for a particular aquaporin concentration, various molar ratios of aquaporins and the amphiphilic matrix could be investigated and compared. Simulation studies could be carried out considering various molar ratios of the amphiphilic polymer and aquaporins and different possibilities of aqp-orientations in order to obtain an optimum molar ratio between the two.

4. In order to increase divalent salt rejection by artificial channels, more functionalities could be added to their structure that would provide electrostatic barriers for charged entities and prevent their passage through the channels.

APPENDICES

Appendix A. Flux Data for membranes:

All the filtration experiments were performed at 25°C. Pressure was maintained at 4.83 bar (70 PSI). Effective membrane area for each membrane sample was 0.00041 m^2. Reverse flow filtration was used to remove reversible fouling after filtration with each feed solution.

A.1 Filtration with protein solutions for unmodified PBI, PVA-alkyl modified PBI, and AqpZ-PVA-alkyl modified PBI membranes

Actual data for membranes with BSA and Lipase solutions as appeared in Figures (5-125-13, and 5-14) is presented in Table A.1.1, A.1.2, and A.1.3.

Table A.1.1 Unmodified PBI

Precompaction				
Vol (mL)	Experiment time (hr)	Flux time (min)	Flux time (hr)	Flux (LMH)
2	0	36.08	0.60	7.90
2	0.68	38.03	0.63	7.50
2	1.42	44.56	0.74	7.04
2	2.08	38.03	0.63	7.49
2	2.75	39.45	0.66	7.22
2	3.58	38.25	0.64	7.45
2	4.32	42.20	0.70	6.76
2	5.03	42.76	0.71	6.67
2	6.23	42.90	0.72	6.64

2	7.05	43.12	0.72	6.61
Filtration-10 PPM BSA				
2	8.37	49.4	0.82	5.77
2	9.73	51.13	0.85	5.57
2	11.15	55.33	0.92	5.15
2	12.13	57.72	0.96	4.94
2	13.18	59.60	0.99	4.78
2	14.76	64.52	1.08	4.42
2	15.94	67.53	1.13	4.22
2	17.09	69.38	1.16	4.11
2	18.77	71.26	1.19	4.00
2	20.03	69.16	1.15	4.12
Reverse flow filtration				
2	21.40	52.13	0.87	5.47
2	22.36	52.63	0.88	5.42
Filtration-10 PPM Lipase				
2	23.99	67.65	1.13	4.21
2	25.14	67.16	1.12	4.24
2	26.27	68.53	1.14	4.16
2	27.54	73.23	1.22	3.89
2	28.86	74.45	1.24	3.83
2	30.66	78.33	1.31	3.64
2	32.02	80.4	1.34	3.55
2	33.31	76.8	1.28	3.71
2	34.68	81.00	1.35	3.52
2	36.09	84.4	1.39	3.42

Table A.1.2 PVA-alkyl modified PBI

Precompaction				
Permeate vol (mL)	Experiment time (hr)	Flux time (min)	Flux time (hr)	Flux (LMH)
2	0.00	47.04	0.79	6.00
2	0.83	49.08	0.81	5.86
2	1.75	53.00	0.88	5.40
2	2.66	51.28	0.86	5.54
2	3.59	56.11	0.94	5.07
2	4.61	59.58	1.00	5.00
2	5.61	57.30	0.96	4.96
2	7.13	61.12	1.02	4.89

2	8.35	58.25	0.97	4.88
Filtration 10 PPM BSA				
Permeate vol (mL)	Experiment time (hr)	Flux time (min)	Flux time (hr)	Flux (LMH)
2	9.93	65.29	1.09	4.36
2	11.05	65.49	1.09	4.35
2	12.30	65.09	1.09	4.37
2	14.04	74.05	1.23	3.85
2	15.20	67.40	1.13	4.21
2	16.40	70.48	1.18	4.03
2	17.60	69.38	1.16	4.09
2	18.79	68.52	1.15	4.14
Flux recovery				
Permeate vol (mL)	Experiment time (hr)	Flux time (min)	Flux time (hr)	Flux (LMH)
2	23.81	59.29	0.99	4.79
2	24.88	59.49	1.00	4.76
Filtration 10 PPM Lipase				
Permeate vol (mL)	Experiment time (hr)	Flux time (min)	Flux time (hr)	Flux (LMH)
2	26.34	64.29	1.07	4.42
2	27.51	67.39	1.13	4.21
2	28.62	65.27	1.09	4.35
2	29.76	66.18	1.11	4.30
2	30.94	67.49	1.13	4.20
2	32.07	66.10	1.10	4.31
2	33.24	68.49	1.15	4.14
2	34.44	69.03	1.15	4.13

Table A.1.3 AqpZ-PVA-alkyl modified PBI membrane

Precompaction				
Permeate vol (mL)	Experiment time (hr)	Flux time (min)	Flux time (hr)	Flux (LMH)
2	0.00	54.58	0.92	5.32
2	1.13	55.05	0.92	5.31
2	2.09	56.11	0.94	5.21
2	3.07	56.50	0.95	5.15
2	4.07	56.51	0.95	5.15
2	5.03	56.46	0.95	5.15
2	6.10	62.25	1.04	4.94
2	7.10	58.48	0.98	4.98

2	8.13	59.00	0.98	4.96
2	9.13	59.20	0.99	4.93
Filtration 10 PPM BSA				
Permeate vol (mL)	Experiment time (hr)	Flux time (min)	Flux time (hr)	Flux (LMH)
2	10.97	63.42	1.06	4.59
2	12.12	67.47	1.13	4.32
2	13.29	68.48	1.15	4.26
2	14.96	70.18	1.17	4.16
2	16.61	69.25	1.16	4.22
2	18.28	69.55	1.17	4.19
2	19.45	70.12	1.17	4.17
2	20.62	70.34	1.18	4.15
Flux recovery				
Permeate vol (mL)	Experiment time (hr)	Flux time (min)	Flux time (hr)	Flux (LMH)
2	23.65	58.36	0.98	5.00
2	24.65	59.12	0.99	4.95
Filtration 10 PPM Lipase				
Permeate vol (mL)	Experiment time (hr)	Flux time (min)	Flux time (hr)	Flux (LMH)
2	26.68	61.45	1.03	4.74
2	27.88	62.56	1.05	4.65
2	28.96	63.23	1.06	4.62
2	30.18	64.12	1.07	4.56
2	31.31	65.53	1.10	4.44
2	32.42	65.44	1.10	4.45
2	33.56	66.04	1.10	4.43
2	34.68	66.13	1.10	4.42

A.2 Filtration with salt solutions for unmodified PBI, PVA-alkyl modified PBI, Aqp-SH modified PBI, and Aqp-R189A modified membranes. The tables show total permeate volume, mean flux for 3 filtration runs, and standard deviations. The calculations are same as tables in section A.1.

Actual data for membranes with NaCl and $CaCl_2$ solutions of 3.4 mM, 10 mM, 20 mM, 35 mM, and 100 mM as appeared in Figure 6-10 (A), (B), (C), and (D) is presented in Table A.2.1, A.2.2, A.2.3, and A.2.4.

Table A.2.1 Salt solution filtration for unmodified PBI membrane

Precompaction (DI H_2O)		
Permeate volume (mL)	Mean flux (LMH)	Std. dev.
2	34.56	2.5
4	36.01	5.1
6	34.67	6.3
8	37.12	2.8
10	33.92	4.1
12	34.26	3.7
14	36.2	4.4
16	34.1	6.1
18	34.21	2.8
20	34.16	3
NaCl 3.4 mM		
Permeate volume (mL)	Mean flux (LMH)	Std. dev.
22	34.15	3.1
24	34.2	5.2
26	34.08	2.7
28	34.04	6.1
30	33.97	4.4
32	34.01	7
34	33.94	2.6
36	33.9	1.9
38	33.93	3.2
40	33.87	5.2
NaCl 10 mM		
Permeate volume (mL)	Mean flux (LMH)	Std. dev.
42	34.03	1.4
44	34.09	3.2
46	33.98	4.2

48	33.9	2.8
50	34.02	5.4
52	33.89	5.1
54	33.94	6.2
56	33.84	2.5
58	33.81	5.1
60	33.79	3.9
NaCl 20 mM		
Permeate volume (mL)	Mean flux (LMH)	Std. dev.
62	33.91	4.3
64	33.81	6.4
66	33.75	7.2
68	33.8	2.8
70	33.72	4.6
72	33.69	8.1
74	33.75	2.7
76	33.63	4.5
78	33.6	1.7
80	33.62	6.3
NaCl 35 mM		
Permeate volume (mL)	Mean flux (LMH)	Std. dev.
82	33.64	4.2
84	33.61	5
86	33.52	3.1
88	33.41	5.2
90	33.53	6.7
92	33.48	2.6
94	33.41	8.4
96	33.44	2.6
98	33.35	7.5
100	33.28	5.2
NaCl 100 mM		
Permeate volume (mL)	Mean flux (LMH)	Std. dev.
102	33.31	4.5
104	33.23	6.4
106	33.18	2.4
108	33.1	6
110	33.14	3.7
112	33.04	5.6
114	32.98	8.7

116	33.02	3.4
118	32.91	2.1
120	33.01	4.5
$CaCl_2$ 3.4 mM		
Permeate volume (mL)	Mean flux (LMH)	Std. dev.
122	32.94	4.3
124	32.8	6.5
126	32.85	2.4
128	32.75	7.5
130	32.82	2.4
132	32.73	6.4
134	32.69	1.2
136	32.64	7.6
138	32.66	1.8
140	32.58	5.4
$CaCl_2$ 10 mM		
Permeate volume (mL)	Mean flux (LMH)	Std. dev.
142	32.62	3.2
144	32.56	5.4
146	32.51	6.5
148	32.46	1.2
150	32.38	3.2
152	32.43	6.5
154	32.4	1.2
156	32.36	3
158	32.3	1.3
160	32.31	5.2
$CaCl_2$ 20 mM		
Permeate volume (mL)	Mean flux (LMH)	Std. dev.
162	32.28	4.3
164	32.2	5.4
166	32.1	1.2
168	32.04	6.7
170	31.97	3
172	31.9	2.6
174	31.87	7.4
176	31.73	2.3
178	31.8	7.5
180	31.69	4.2
$CaCl_2$ 35 mM		

Permeate volume (mL)	Mean flux (LMH)	Std. dev.
182	31.71	3.5
184	31.62	5.4
186	31.54	2.3
188	31.47	6.7
190	31.37	8.5
192	31.34	3.2
194	31.27	6.5
196	31.21	3.2
198	31.1	3.5
200	31.01	6
$CaCl_2$ 100 mM		
Permeate volume (mL)	Mean flux (LMH)	Std. dev.
202	31.04	4.5
204	30.91	3.5
206	30.87	5.2
208	30.76	6.7
210	30.61	5.4
212	30.41	2.3
214	30.29	4.5
216	30.15	6.7
218	30.09	5.4
220	29.97	3.2
Flux recovery		
Permeate volume (mL)	Mean flux (LMH)	Std. dev.
222	29.87	4.2

Table A.2.2 Salt solution filtration for PVA-alkyl modified PBI membrane

Precompaction (DI H_2O)		
Permeate volume (mL)	Mean flux (LMH)	Std. dev.
2	11.34	3.4
4	9.45	2.4
6	10.34	1.2
8	12.57	1.7
10	12.54	3.1
12	11.09	0.87

14	10.65	1.2
16	10.45	5.4
18	10.34	1.1
20	10.29	1.2
NaCl 3.4 mM		
Permeate volume (mL)	Mean flux (LMH)	Std. dev.
22	10.14	4.5
24	10.2	1.9
26	10.12	2.3
28	10.06	2.9
30	10.09	2.1
32	10.01	5.4
34	9.91	2.3
36	9.97	1.12
38	9.9	1.5
40	9.92	1.2
NaCl 10 mM		
Permeate volume (mL)	Mean flux (LMH)	Std. dev.
42	9.94	1.43
44	9.89	1.76
46	9.83	2.67
48	9.79	1.43
50	9.74	2.22
52	9.76	1.21
54	9.67	3.21
56	9.6	1.66
58	9.65	1.2
60	9.53	1.55
NaCl 20 mM		
Permeate volume (mL)	Mean flux (LMH)	Std. dev.
62	9.61	3.12
64	9.58	1.22
66	9.5	1.45
68	9.42	2.3
70	9.47	2.22
72	9.38	1.11
74	9.33	1.34
76	9.22	2.3
78	9.27	1.2
80	9.18	3.12

NaCl 35 mM		
Permeate volume (mL)	Mean flux (LMH)	Std. dev.
82	9.27	1.23
84	9.23	2.13
86	9.18	4.12
88	9.11	1.22
90	9.15	1.85
92	9.07	1.98
94	9.03	1.67
96	8.96	1.4
98	8.94	1.2
100	8.89	1.67
NaCl 100 mM		
Permeate volume (mL)	Mean flux (LMH)	Std. dev.
102	8.87	1.3
104	8.8	1.2
106	8.73	1.4
108	8.65	1.1
110	8.69	3.4
112	8.62	2.1
114	8.56	3.9
116	8.45	2.78
118	8.34	2.2
120	8.36	1.5
$CaCl_2$ 3.4 mM		
Permeate volume (mL)	Mean flux (LMH)	Std. dev.
122	8.4	2.32
124	8.34	2.9
126	8.27	1.3
128	8.31	2.8
130	8.22	4.3
132	8.18	2.3
134	8.23	2.4
136	8.14	1.4
138	8.24	1.4
140	8.12	2.6
$CaCl_2$ 10 mM		
Permeate volume (mL)	Mean flux (LMH)	Std. dev.
142	8.15	1.2

144	8.08	3.2
146	8.09	1.9
148	8.01	1.6
150	7.92	1.56
152	7.82	1.78
154	7.88	2.65
156	7.81	3.98
158	7.72	1.68
160	7.7	2.778
$CaCl_2$ 20 mM		
Permeate volume (mL)	Mean flux (LMH)	Std. dev.
162	7.74	2.8
164	7.67	2.7
166	7.62	1.7
168	7.56	2.6
170	7.5	3.6
172	7.48	1
174	7.42	3.7
176	7.34	2.8
178	7.27	0.64
180	7.29	1.54
$CaCl_2$ 35 mM		
Permeate volume (mL)	Mean flux (LMH)	Std. dev.
182	7.34	3.2
184	7.24	3.1
186	7.17	1.8
188	7.11	1.7
190	7.04	1.6
192	7.09	2.1
194	6.97	2.8
196	6.91	1.4
198	6.84	2.6
200	6.8	1.1
$CaCl_2$ 100 mM		
Permeate volume (mL)	Mean flux (LMH)	Std. dev.
202	6.78	2.5
204	6.7	1.8
206	6.74	2.6
208	6.63	2.1
210	6.51	1.2

212	6.54	2.4
214	6.46	2
216	6.4	0.9
218	6.35	1.09
220	6.28	0.73
Flux recovery		
Permeate volume (mL)	Mean flux (LMH)	Std. dev.
222	6.31	1.7

Table A.2.3 Salt solution filtration for Aqp-SH modified PBI membrane

Precompaction (DI water)		
Permeate volume (mL)	Mean flux (LMH)	Std. dev.
2	23.35	2.1
4	23.32	3.2
6	25.31	1.3
8	23.12	5.4
10	24.12	2.3
12	26.21	4.3
14	21.23	3.4
16	23.34	1.8
18	23.45	3.7
20	23.29	4.7
NaCl 3.4 mM		
Permeate volume (mL)	Mean flux (LMH)	Std. dev.
22	23.32	2.8
24	23.35	3.1
26	23.26	4.6
28	23.19	2.38
30	23.22	1.2
32	23.17	5.4
34	23.14	3.2
36	23.22	3.8
38	23.13	3.6
40	23.1	4
NaCl 10 mM		
Permeate volume (mL)	Mean flux (LMH)	Std. dev.
42	9.94	1.43

44	9.89	1.76
46	9.83	2.67
48	9.79	1.43
50	9.74	2.22
52	9.76	1.21
54	9.67	3.21
56	9.6	1.66
58	9.65	1.2
60	9.53	1.55
NaCl 20 mM		
Permeate volume (mL)	Mean flux (LMH)	Std. dev.
62	9.61	3.12
64	9.58	1.22
66	9.5	1.45
68	9.42	2.3
70	9.47	2.22
72	9.38	1.11
74	9.33	1.34
76	9.22	2.3
78	9.27	1.2
80	9.18	3.12
NaCl 35 mM		
Permeate volume (mL)	Mean flux (LMH)	Std. dev.
82	9.27	1.23
84	9.23	2.13
86	9.18	4.12
88	9.11	1.22
90	9.15	1.85
92	9.07	1.98
94	9.03	1.67
96	8.96	1.4
98	8.94	1.2
100	8.89	1.67
NaCl 100 mM		
Permeate volume (mL)	Mean flux (LMH)	Std. dev.
102	8.87	1.3
104	8.8	1.2
106	8.73	1.4
108	8.65	1.1
110	8.69	3.4
112	8.62	2.1
114	8.56	3.9
116	8.45	2.78

118	8.34	2.2
120	8.36	1.5
$CaCl_2$ 3.4 mM		
Permeate volume (mL)	Mean flux (LMH)	Std. dev.
122	8.4	2.32
124	8.34	2.9
126	8.27	1.3
128	8.31	2.8
130	8.22	4.3
132	8.18	2.3
134	8.23	2.4
136	8.14	1.4
138	8.24	1.4
140	8.12	2.6
$CaCl_2$ 10 mM		
Permeate volume (mL)	Mean flux (LMH)	Std. dev.
142	8.15	1.2
144	8.08	3.2
146	8.09	1.9
148	8.01	1.6
150	7.92	1.56
152	7.82	1.78
154	7.88	2.65
156	7.81	3.98
158	7.72	1.68
160	7.7	2.778
$CaCl_2$ 20 mM		
Permeate volume (mL)	Mean flux (LMH)	Std. dev.
162	7.74	2.8
164	7.67	2.7
166	7.62	1.7
168	7.56	2.6
170	7.5	3.6
172	7.48	1
174	7.42	3.7
176	7.34	2.8
178	7.27	0.64
180	7.29	1.54
$CaCl_2$ 35 mM		
Permeate volume (mL)	Mean flux (LMH)	Std. dev.
182	7.34	3.2
184	7.24	3.1
186	7.17	1.8

188	7.11	1.7
190	7.04	1.6
192	7.09	2.1
194	6.97	2.8
196	6.91	1.4
198	6.84	2.6
200	6.8	1.1
$CaCl_2$ 100 mM		
Permeate volume (mL)	Mean flux (LMH)	Std. dev.
202	6.78	2.5
204	6.7	1.8
206	6.74	2.6
208	6.63	2.1
210	6.51	1.2
212	6.54	2.4
214	6.46	2
216	6.4	0.9
218	6.35	1.09
220	6.28	0.73
Flux recovery		
Permeate volume (mL)	Mean flux (LMH)	Std. dev.
222	6.31	1.7

Table A.2.4 Salt solution filtration for Aqp R189A-modified PBI membrane

Precompaction (DI H_2O)		
Permeate volume (mL)	Mean flux (LMH)	Std. dev.
2	14.3	1.2
4	15.73	2.1
6	16.24	1.7
8	13.56	1.4
10	14.28	1.5
12	15.1	3.1
14	12.53	1.2
16	14.67	1.7
18	14.8	1.4
20	14.72	1.5
NaCl 3.4 mM		
Permeate volume (mL)	Mean flux (LMH)	Std. dev.
22	14.34	2

24	14.41	2.3
26	14.27	1.2
28	14.1	1.1
30	14.01	1
32	13.98	1.5
34	13.87	1.7
36	13.91	1.5
38	13.88	2
40	13.82	2.7
NaCl 10 mM		
Permeate volume (mL)	Mean flux (LMH)	Std. dev.
42	13.91	2.8
44	13.87	2.1
46	13.89	2.4
48	13.8	1.7
50	13.77	1.5
52	13.7	1.44
54	13.64	1.6
56	13.72	1.4
58	13.58	1
60	13.51	1.9
NaCl 20 mM		
Permeate volume (mL)	Mean flux (LMH)	Std. dev.
62	13.63	2.4
64	13.67	2.5
66	13.59	1.6
68	13.54	1.5
70	13.48	1.8
72	13.4	1.9
74	13.34	2
76	13.21	2.3
78	13.28	1.5
80	13.2	1.6
NaCl 35 mM		
Permeate volume (mL)	Mean flux (LMH)	Std. dev.
82	13.29	1.9
84	13.21	1.4
86	13.17	1.2
88	13.1	1.6
90	13.04	1.6
92	13.07	1.4
94	12.98	2.5
96	12.9	2.9

98	12.99	3.2
100	12.92	4
NaCl 100 mM		
Permeate volume (mL)	Mean flux (LMH)	Std. dev.
102	12.99	1.4
104	12.9	1.2
106	12.83	2.3
108	12.84	1.5
110	12.77	1.5
112	12.69	1.8
114	12.6	1.5
116	12.62	1.9
118	12.54	1.4
120	12.44	1.5
CaCl2	3.4 mM	
Permeate volume (mL)	Mean flux (LMH)	Std. dev.
122	12.5	2.3
124	12.42	2.1
126	12.47	2.4
128	12.4	2.6
130	12.32	2
132	12.35	1
134	12.29	2.1
136	12.25	2.4
138	12.18	1.4
140	12.11	1.2
CaCl2	10 mM	
Permeate volume (mL)	Mean flux (LMH)	Std. dev.
142	12.23	0.9
144	12.13	1.5
146	12.03	2.1
148	12.05	3.5
150	11.95	1.8
152	11.92	1.5
154	11.86	1.4
156	11.8	1.8
158	11.81	1.4
160	11.75	1.6
CaCl2	20 mM	
Permeate volume (mL)	Mean flux (LMH)	Std. dev.
162	11.83	2.5
164	11.76	2.4
166	11.7	2.6

168	11.67	2.7
170	11.6	2.1
172	11.62	2.4
174	11.57	2.5
176	11.52	2.1
178	11.46	1.5
180	11.41	1.8
CaCl2	35 mM	
Permeate volume (mL)	Mean flux (LMH)	Std. dev.
182	11.53	1
184	11.46	2.4
186	11.37	3.5
188	11.38	2.1
190	11.32	2.5
192	11.26	2.5
194	11.23	2.1
196	11.17	1.6
198	11.04	1.5
200	10.72	1.4
CaCl2	100 mM	
Permeate volume (mL)	Mean flux (LMH)	Std. dev.
202	10.82	0.8
204	10.73	1.4
206	10.69	1.8
208	10.63	2.5
210	10.57	1.6
212	10.51	1.4
214	10.43	1.1
216	10.34	1
218	10.32	1.9
220	10.25	1.1
Flux recovery		
Permeate volume (mL)	Mean flux (LMH)	Std. dev.
222	10.29	1.2

Appendix B. Elemental analysis:

EDS and EELS analysis were performed for both unmodified PBI and Aqp-SH modified PBI membranes in order to prove and quantify the change in sulfur concentration in the membranes after modification. Figure B.1 shows EDS analysis of unmodified PBI membrane. The keV corresponds to energy of X-rays emitted as electrons return from a higher energy shell to a lower energy shell in the element. This energy is a characteristic of the atomic structure of the emitting element. According to the database [307], carbon, nitrogen, oxygen and sulfur have peaks at 0.277 keV, 0.302 keV, 0.525 keV, and 2.307 kev, respectively. Table B.1 shows weight percentage and percentage of atoms of carbon, oxygen, nitrogen and sulfur present in the membrane sample. It can be seen from the Table B.1 and figure 1 that the amount of sulfur is negligible in unmodified PBI membrane which was expected since the structure of PBI, does not contain any sulfur. EELS analysis of unmodified PBI membrane was done in order to support EDS results. Unmodified PBI membranes were analyzed with EELS for carbon, oxygen and nitrogen as EDS revealed that there was no sulfur present in the sample. Figure B.2 shows EELS analysis of a sample of unmodified PBI membrane. Binding energy peaks of elements were corrected after control experiments and based on the values of binding energies of elements in the database [308]. As shown in the diagram, binding energies of carbon, nitrogen, and oxygen were 284 eV, 401 eV, and 532 eV, respectively. Based on the energy loss after incident x-ray on membrane sample, absolute quantification of elements was calculated. Table B.2 shows absolute and relative quantification of elements in the membrane samples.

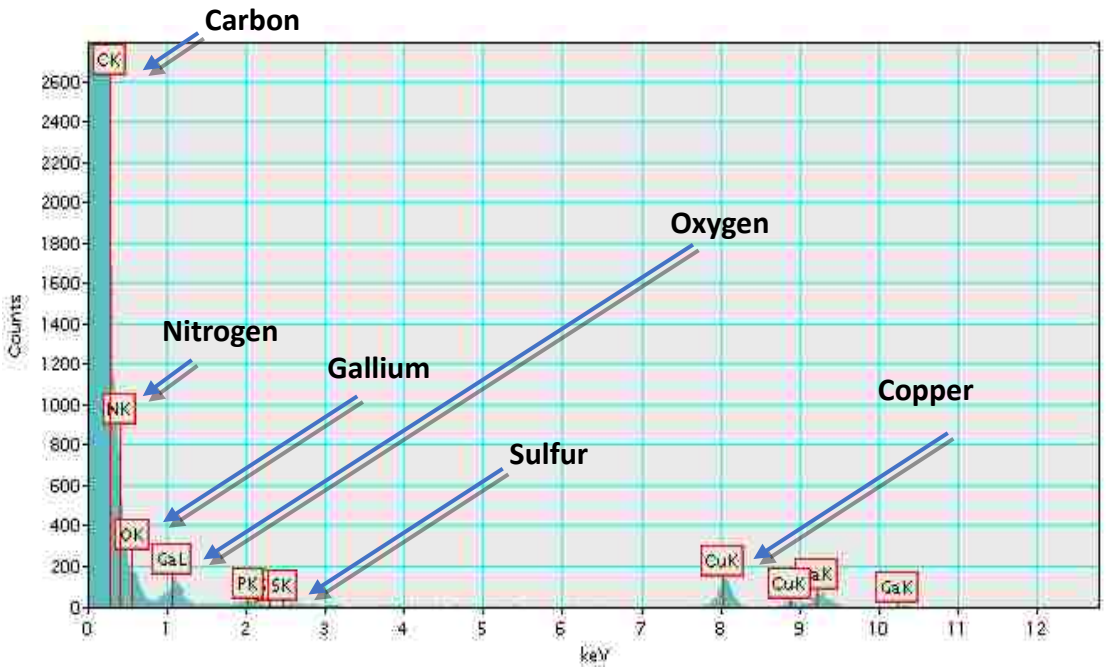

Figure B.1. EDS analysis of unmodified PBI membranes

Table B.1. Elemental and weight composition of elements in unmodified PBI membrane using EDS

Element	Weight%	Atoms%
C	88.92±-0.91	90.54±-0.93
N	8.81±-0.45	7.69±-0.39
O	2.32±-0.23	1.77±-0.18
S	-0.05±0.00	0.00±0.00

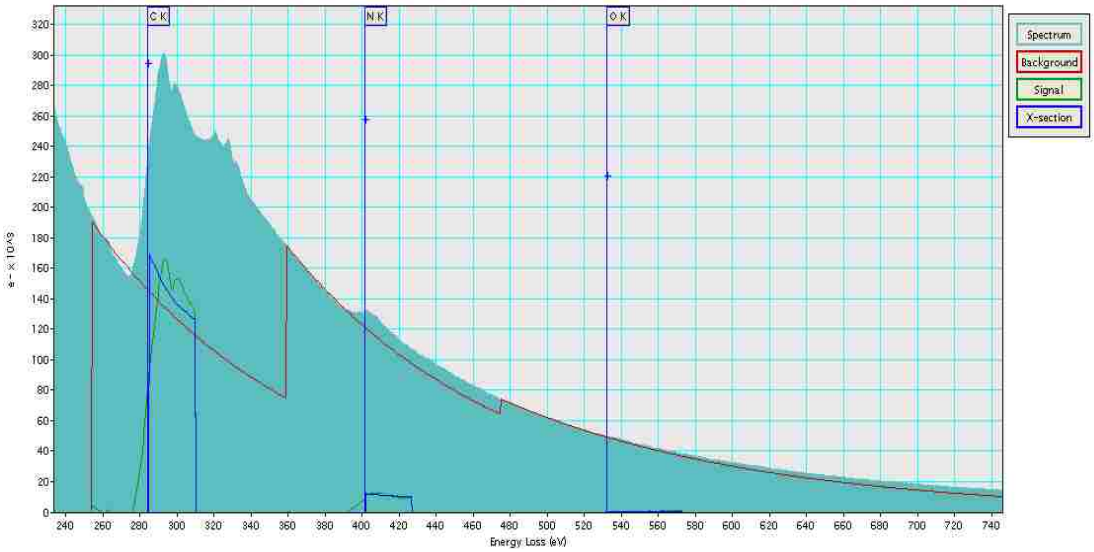

Figure B.2. EELS analysis of unmodified PBI membrane

Table B.2. Absolute quantification of elements in unmodified PBI membrane using EELS analysis

Element	**Areal density (atoms/nm*2)**	**Atomic ratio(/C)**	**Percent content**
C	2.39e+013 ± 2.4e+012	1.00 ± 0.000	83.06
N	3.51e+012 ± 3.5e+011	0.15 ± 0.021	12.24
O	1.35e+012 ± 1.4e+011	0.06 ± 0.008	4.70

Aqp-SH membranes were also analyzed for elemental composition and changes in composition after modification. Figure B.3 shows EDS analysis of Aqp-SH modified PBI membrane and Table B.3 shows weight percentage and percentage of atoms of carbon, oxygen, nitrogen and sulfur present in the membrane sample. It was observed that a significant amount of sulfur was present in the 50 nm membrane sample modified with Aqp-SH molecules. EELS analysis of Aqp-SH modified PBI membrane was performed

in order to support EDS results. Figure B.4 shows EELS analysis of a sample of Aqp-SH modified PBI membrane. Binding energy peaks of elements were corrected after control experiments and based on the values of binding energies of elements in the database [308]. As shown in the diagram, binding energies of carbon, nitrogen, oxygen and sulfur were 284 eV, 401 eV, 532 eV, and 165 eV, respectively. Table B.4 shows absolute quantification of elements and relative quantification of elements present in the membrane sample.

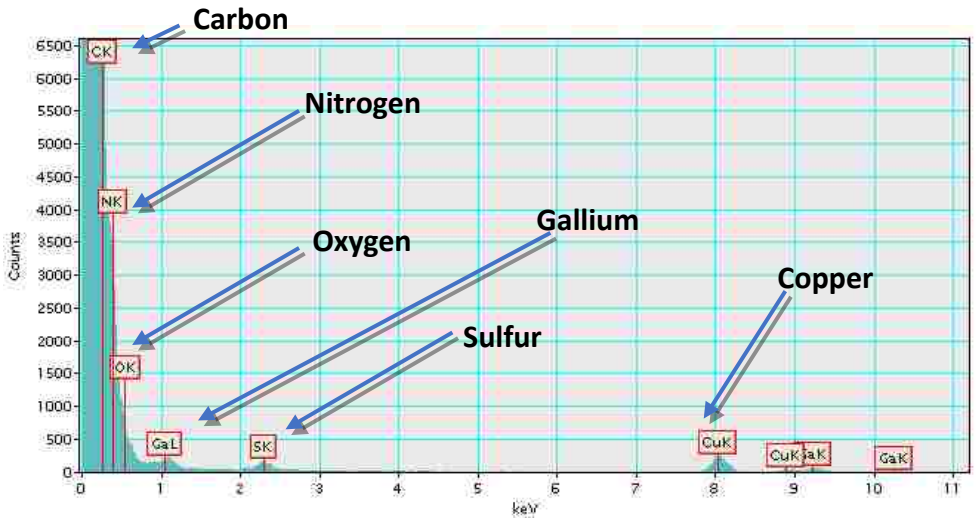

Figure B.3. EDS analysis of Aqp-SH modified PBI membrane

Table B.3. Elemental and weight composition of elements in Aqp-SH modified PBI membrane

Element	**Weight%**	**Atoms%**
C	74.41±-0.98	76.21±-1.00
N	15.83±-0.46	14.91±-0.40
O	5.22±-0.24	4.81±-0.18
S	4.53±0.35	4.07±0.27

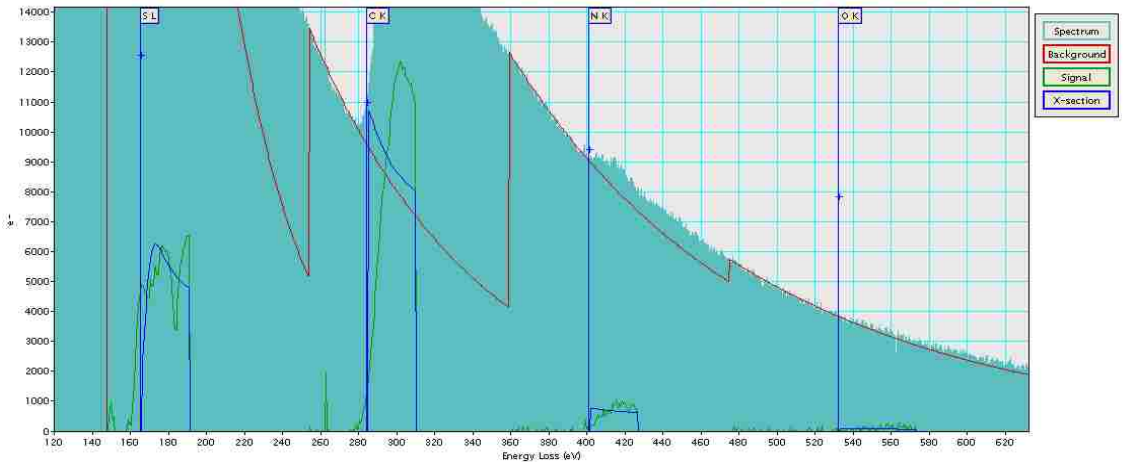

Figure B.4. EELS analysis of Aqp-SH modified PBI membrane

Table B.4. Absolute and relative quantification of elements in Aqp-SH modified PBI membrane

Elements	**Areal density(atoms/Nm^2)**	**Atomic Ratio (/C)**	**Percent content**
S	3.92e+011 ± 3.9e+010	0.007±0.010	5.61
C	5.49e+012 ± 5.5e+011	1.000±0.000	78.61
N	8.69e+011 ± 8.8e+010	0.16±0.023	12.44
O	2.33e+011 ± 2.8e+010	0.04±0.007	3.34

Appendix C. Diffusion Data

Table C.1 NaCl concentrations measured every day for unmodified PBI, PVA-alkyl modified PBI, and Aqp-SH modified membranes in diffusion cell assembly

	Unmodified PBI		PVA-alkyl		Aqp-SH modified PBI	
	NaCl concentration (ppm)	H20 concentration(ppm)	NaCl concentration (ppm)	H20 concentration (ppm)	NaCl concentration (ppm)	H2O concentration(ppm)
Day 1	918.18	80.23	932.15	62.74	969.23	27.12
Day 2	829.35	167.2	851.35	142.75	922.46	72.34
Day 3	788.21	210.45	810.36	183.63	889.35	104.54
Day 4	743.1	253.73	770.12	225.76	872.53	124.65
Day 5	691.53	304.12	744.64	251.73	852.12	144.6
Day 6	676.16	318.63	725.91	270.82	837.81	160.32
Day 7	599.17	398.12	709.51	281.62	826.91	172.64
Day 8	597.81	399.65	705.23	287.13	815.63	179.5

Appendix D. Simulation input files and generated Data

D.1 Mesh generator

In [ ]:
```
from __future__ import division
import numpy as np
import os
from fenics import *
```

In [ ]:
```
### initialize mesh attributes
numPores = 12# number of nanopores per side
radius = 0.5#nm
bR = np.linspace(3,8,6)#nm
boxSize = 10#nm width of reservoir
length = 20#nm pore length
revH = 20#nm height of reservoir
nm = 1e-9
```

In [ ]:
```
### generate HDF5 files
import nanoporousMesher as mesher
import nanoMesherNoAQ as meshNO
name = "AQ_NO"
meshNO.Build(numPores,radius*nm,boxSize*nm,length*nm,revH*nm,name)
for i,num in enumerate(bR):
name = "AQ_{}".format(int(num))
mesher.Build(numPores,radius*nm,num*nm,boxSize*nm,length*nm,revH*nm,name)
```

In [ ]:
```
### construct the command line commands
```

```
myPath = os.path.abspath(__file__)

path = os.path.abspath(os.path.join(myPath,'..'))

path = path+"/"

noAQ = path+"AQ_NO.hdf5"

line = "mpirun -np 20 python noAQP_simulator.py -runner {}".format(noAQ)

print line

os.system(line)

x = np.full((1000,),-7.5e-10)

y = np.full((1000,),-7.5e-10)

zs = np.linspace(-20e-9,30e-9,1000) ### these are the points along the centerline

points = np.stack((x,y,zs))

points=points.transpose()

mesh = Mesh()

facets = MeshFunction("size_t",mesh)

cells = MeshFunction("size_t",mesh)

hdf5=HDF5File(mesh.mpi_comm(),noAQ,'r')

hdf5.read(mesh,'mesh',False)

hdf5.read(facets,'facets')

hdf5.read(cells,'cells')

hdf5.close()

hdf5_solution=HDF5File(mesh.mpi_comm(),path+"AQ_NO_solution.hdf5",'r')

ele = FiniteElement('CG',mesh.ufl_cell(),1)

V = FunctionSpace(mesh,ele)
```

```
F = Function(V) ### This is just the FEM fxn instance
hdf5_solution.read(F,"solution")
hdf5_solution.close()
### to get values along axis:
u = np.zeros_like(zs)
for i, point in enumerate(points):
u[i] = F(point)
import matplotlib as mpl
mpl.use('Agg')
import matplotlib.pyplot as plt
plt.figure()
plt.plot(zs,u)
plt.ylabel("z (m)")
plt.xlabel("concentration (mM)")
plt.savefig("figs/AQ_NO.png")
plt.close()
for i, num in enumerate(bR):
name = path+"AQ_{}.hdf5".format(int(num))
line = "mpirun -np 20 python AQP_realSimulator.py -runner {}
{}".format(name,int(print line
os.system(line)
mesh = Mesh()
facets = MeshFunction("size_t",mesh)
```

```
cells = MeshFunction("size_t",mesh)
hdf5=HDF5File(mesh.mpi_comm(),name,'r')
hdf5.read(mesh,'mesh',False)
hdf5.read(facets,'facets')
hdf5.read(cells,'cells')
hdf5.close()
print "path of HDF5 file: ", path+"AQ_{}_solution.hdf5".format(int(num))
tempPath ="AQ_{}_solution.hdf5".format(int(num))
hdf5_solution=HDF5File(mesh.mpi_comm(),path + tempPath,'r')
mele = FiniteElement('CG',mesh.ufl_cell(),1)
V = FunctionSpace(mesh,mele)
G = Function(V) ### This is just the FEM fxn instance
hdf5_solution.read(G,"solution")
hdf5_solution.close()
plist=[]
ulist=[]
count = 0
for pt in points:
try:
ulist.append(G(pt))
plist.append(zs[count])
count+=1
except RuntimeError:
```

```
ulist.append(0)

plist.append(zs[count])

count+=1

### to get values:

#u = np.zeros_like(np.shape(zs))

#for i, point in enumerate(points):

# u[i] = ck_u(point)

plt.figure()

plt.plot(zs,ulist)

plt.ylabel("concentration (mM)")

plt.xlabel("z (m)")

plt.savefig("figs/AQ_{}.png".format(num))

plt.close()

### run the command line commands

### sort through the resulting .txt files in PostProcessing.ipynb
```

D.2 Post processing

```
In [1]: import numpy as np

import matplotlib.pyplot as plt

%matplotlib inline

In [2]: fileList =[]

import glob, os

for file in glob.glob("*.txt"):
```

```
fileList.append(file)

In [3]: nm=1e-9

noAQs = []

noAQ = {}

AQs = []

AQ = {}

AQ2 = {}

AQ3 = {}

noAQvals = []

noAQvals2 = []

for item in fileList:

if item[0] == 'n':

noAQs.append(item)

f = open(item,'r')

search=f.readlines()

f.close()

val = search[0][5:]

val2 = search[1][5:]

noAQ['{}'.format(item[5])] = float(val)/nm

noAQvals.append(float(val)/nm)

noAQvals2.append(float(val2)/nm)

else:

AQs.append(item)
```

```
AQ['{}'.format(item[3])] ={}

AQ2['{}'.format(item[3])] ={}

AQ3['{}'.format(item[3])] ={}

for item in AQs:


L,R = item.split(".")

num1 = L[3]

f = open(item,"r")

search = f.readlines()

f.close()

val = search[0][5:]

val2 = search[1][5:]

val3 = search[2][8:]

AQ['{}'.format(str(num1))]=float(val)/nm

AQ2['{}'.format(str(num1))]=float(val2)/nm

AQ3['{}'.format(str(num1))]=float(val3)

AQkeys = AQ.keys()
```

In [4]: *### So I want to compare noAQ to AQ with the same # of pores across all charges*

```
print AQ

print AQ.keys()
```

{'3': 0.197738752095, '5': 0.164419473368, '4': 0.176505772214, '7':

0.11684078988299998, '6': ['3', '5', '4', '7', '6', '8']

```
In [5]: noAQvals =
np.stack((noAQvals,noAQvals,noAQvals,noAQvals,noAQvals,noAQvals))
noAQvals2 =
np.stack((noAQvals2,noAQvals2,noAQvals2,noAQvals2,noAQvals2,noAQvals2))
In [6]: ### From notebook "Priyesh_update"
D_experimental_aqp = np.mean([5.84054089e-07, 4.55903537e-07, 3.03720426e-07,
3.17304903e-D_exp_aqp =[]
D_experimental = np.mean([1.34204016e-06, 8.07443611e-07, 9.38828308e-07,
1.33036245e-06])*D_exp =[]
for i in range(6):
D_exp.append(D_experimental)
D_exp_aqp.append(D_experimental_aqp)
In [15]: xs = []
ys=[]
y2=[]
ys2 = []
y3=[]
count =1
monomerics = []
for key in sorted(AQ.iterkeys()):
monomerics.append((100-float(key)**2)/100*D_experimental)
xs.append(float(key)**2/100)
ys.append((AQ['{}'.format(key)])/2)
```

```
y2.append((AQ2['{}'.format(key)]))

y3.append((AQ3['{}'.format(key)]))


In [26]: plt.figure(dpi=500)

fig, ax1 = plt.subplots()

ax1.plot(xs,D_exp,'k--',label="Experimental diffusivity without AQP")

ax1.plot(xs,D_exp_aqp, 'k', label="Experimental difffusivity with AQP")

ax1.plot(xs,ys[:],'b',label="Modeled behavior with aggregated AQP")

ax1.plot(xs,monomerics,'b.',label='Modeled behavor with monomeric AQP')

plt.ylim(0,np.max(ys)+.02)

ax1.set_ylabel(r"$Effective diffusivity ( \frac{m^2}{s} * 1e9)$")

ax1.set_xlabel("Packing fraction of AQP")

plt.axvline(x=0.64,color='r')

#ax2 = ax1.twinx()

#ax2.plot(xs,y3[:],'g',label="Pore occlusion rate")

#ax2.set_ylabel("% of pores occluded")

ax1.legend(loc=3)

#ax2.legend(bbox_to_anchor=(0., 0.05, 1.65, 0),loc=4)

Out[26]: <matplotlib.legend.Legend at 0x7f094dce2690>

<Figure size 3000x2000 with 0 Axes>

In [ ]: plt.figure(dpi=300)


plt.plot(xs,y2[:],label="0mV")
```

```
plt.plot(xs,noAQvals2,label="noAQ")

plt.legend()

plt.ylim(0,np.max(y2)+.01)

plt.xlabel("Diameter of AQP")

plt.ylabel(r"$Deff ( \frac{m^2}{s} * 1e9)$")
```

noAQ = [] AQ = {} AQ[’4’]={} AQ[’5’]={} AQ[’6’]={} for item in fileList: if item[0] == ’n’:

noAQ.append(item) else: if item[3] == ’4’: if ’-10’ in item: f = open(item,"r") search = f.readlines()

f.close() val = search[0][5:] AQ[’4’][’-10’]=float(val) elif ’-5’ in item: f = open(item,"r") search =

f.readlines() f.close() val = search[0][5:] AQ[’4’][’-10’]=float(val elif ’_0’ in item: f = open(item,"r")

search = f.readlines() f.close() val = search[0][5:] AQ[’4’][’-10’]=float(val elif ’_5’ in item: f =

open(item,"r") search = f.readlines() f.close() val = search[0][5:] AQ[’4’][’-10’]=float(val elif ’_10’

in item: AQ[’4’][’10’]=item

elif item[3] ==’5’: if ’-10’ in item: AQ[’5’][’-10’]=item elif ’-5’ in item: AQ[’5’][’-5’]=item elif ’_0’ in

item: AQ[’5’][’0’]=item elif ’_5’ in item: AQ[’5’][’5’]=item elif ’_10’ in item: AQ[’5’][’10’]=item

else: if ’-10’ in item: AQ[’6’][’-10’]=item elif ’-5’ in item: AQ[’6’][’-5’]=item elif ’_0’ in item:

AQ[’6’][’0’]=item elif ’_5’ in item: AQ[’6’][’5’]=item elif ’_10’ in item:

AQ[’6’][’10’]=item

REFERENCES

1. Kaucher, M.S., et al., *Selective transport of water mediated by porous dendritic dipeptides.* Journal of the American Chemical Society, 2007. **129**(38): p. 11698-+.
2. Licsandru, E., et al., *Salt-Excluding Artificial Water Channels Exhibiting Enhanced Dipolar Water and Proton Translocation.* Journal of the American Chemical Society, 2016. **138**(16): p. 5403-5409.
3. Hu, X.B., et al., *Single-Molecular Artificial Transmembrane Water Channels.* Journal of the American Chemical Society, 2012. **134**(20): p. 8384-8387.
4. Shen, Y.X., et al., *Achieving high permeability and enhanced selectivity for Angstrom-scale separations using artificial water channel membranes.* Nature Communications, 2018. **9**: p. 11.
5. Zhao, H., et al., *Proton Gradient-Induced Water Transport Mediated by Water Wires Inside Narrow Aquapores of Aquafoldamer Molecules.* Journal of the American Chemical Society, 2014. **136**(40): p. 14270-14276.
6. Tunuguntla, R.H., et al., *Enhanced water permeability and tunable ion selectivity in subnanometer carbon nanotube porins.* Science, 2017. **357**(6353): p. 792-796.
7. Bellissent-Funel, M.C., et al., *Water Determines the Structure and Dynamics of Proteins.* Chem Rev, 2016. **116**(13): p. 7673-97.
8. Horner, A., et al., *The mobility of single-file water molecules is governed by the number of H-bonds they may form with channel-lining residues.* Science Advances, 2015. **1**(2): p. e1400083.
9. Horner, A. and P. Pohl, *Single-file transport of water through membrane channels.* Faraday Discussions, 2018. **209**(0): p. 9-33.
10. Horner, A., et al., *Positively charged residues at the channel mouth boost single-file water flow.* Faraday Discussions, 2018. **209**(0): p. 55-65.
11. Bera, S., S. Maity, and D. Haldar, *Assembly of encapsulated water in hybrid bisamides: helical and zigzag water chains.* Crystengcomm, 2015. **17**(7): p. 1569-1575.
12. Burykin, A. and A. Warshel, *On the origin of the electrostatic barrier for proton transport in aquaporin.* FEBS Letters, 2004. **570**(1–3): p. 41-46.
13. Moeck, G.S. and J.W. Coulton, *TonB-dependent iron acquisition: mechanisms of siderophore-mediated active transport.* Molecular Microbiology, 1998. **28**(4): p. 675-681.
14. Kumar, M., et al., *Polymer-Based Biomimetic Membranes for Desalination*, in *Biomimetic Membranes for Sensor and Separation Applications*, C. Hélix-Nielsen, Editor. 2012, Springer Netherlands: Dordrecht. p. 43-62.
15. Gonen, T. and T. Walz, *The structure of aquaporins.* Q Rev Biophys, 2006. **39**(4): p. 361-96.
16. Lugtenberg, B. and L. Vanalphen, *MOLECULAR ARCHITECTURE AND FUNCTIONING OF THE OUTER-MEMBRANE OF ESCHERICHIA-COLI AND OTHER GRAM-NEGATIVE BACTERIA.* Biochimica Et Biophysica Acta, 1983. **737**(1): p. 51-115.
17. Decad, G.M. and H. Nikaido, *Outer membrane of gram-negative bacteria. XII. Molecular-sieving function of cell wall.* J Bacteriol, 1976. **128**(1): p. 325-36.

18. Nakae, T., *Identification of the outer membrane protein of E.coli that produces transmembrane channels in reconstituted vesicle membranes.* Biochemical and Biophysical Research Communications, 1976. **71**(3): p. 877-884.
19. Welte, W., et al., *STRUCTURE AND FUNCTION OF THE PORIN CHANNEL.* Kidney International, 1995. **48**(4): p. 930-940.
20. Shen, Y.-x., et al., *Biomimetic membranes: A review.* Journal of Membrane Science, 2014. **454**: p. 359-381.
21. Nikaido, H., *PORINS AND SPECIFIC CHANNELS OF BACTERIAL OUTER MEMBRANES.* Molecular Microbiology, 1992. **6**(4): p. 435-442.
22. Nikaido, H., *PORINS AND SPECIFIC DIFFUSION CHANNELS IN BACTERIAL OUTER MEMBRANES.* Journal of Biological Chemistry, 1994. **269**(6): p. 3905-3908.
23. Nikaido, H. and M. Vaara, *Molecular basis of bacterial outer membrane permeability.* Microbiol Rev, 1985. **49**(1): p. 1-32.
24. Nikaido, H., *Molecular basis of bacterial outer membrane permeability revisited.* Microbiology and Molecular Biology Reviews, 2003. **67**(4): p. 593-+.
25. Hernandez, S., et al., *Layer-by-layer assembled membranes with immobilized porins.* RSC Advances, 2017. **7**(88): p. 56123-56136.
26. Ishii, J.N., Y. Okajima, and T. Nakae, *Characterization of lamB protein from the outer membrane of Escherichia coli that forms diffusion pores selective for maltose-maltodextrins.* FEBS Letters, 1981. **134**(2): p. 217-220.
27. Kadner, R.J., *Vitamin B12 transport in Escherichia coli: energy coupling between membranes.* Mol Microbiol, 1990. **4**(12): p. 2027-33.
28. Guerinot, M.L., *MICROBIAL IRON TRANSPORT.* Annual Review of Microbiology, 1994. **48**: p. 743-772.
29. Agre, P., *Aquaporin Water Channels.* Bioscience Reports, 2005. **24**(3): p. 127-163.
30. Benga, G., *Water Channel Proteins (Later Called Aquaporins) and Relatives: Past, Present, and Future.* Iubmb Life, 2009. **61**(2): p. 112-133.
31. Preston, G.M. and P. Agre, *ISOLATION OF THE CDNA FOR ERYTHROCYTE INTEGRAL MEMBRANE-PROTEIN OF 28-KILODALTONS - MEMBER OF AN ANCIENT CHANNEL FAMILY.* Proceedings of the National Academy of Sciences of the United States of America, 1991. **88**(24): p. 11110-11114.
32. Smith, B.L. and P. Agre, *ERYTHROCYTE MR-28,000 TRANSMEMBRANE PROTEIN EXISTS AS A MULTISUBUNIT OLIGOMER SIMILAR TO CHANNEL PROTEINS.* Journal of Biological Chemistry, 1991. **266**(10): p. 6407-6415.
33. Preston, G.M., et al., *APPEARANCE OF WATER CHANNELS IN XENOPUS OOCYTES EXPRESSING RED-CELL CHIP28 PROTEIN.* Science, 1992. **256**(5055): p. 385-387.
34. Agre, P., *<Aquaporin water channels in kidney.pdf>.*
35. Agre, P., M. Bonhivers, and M.J. Borgnia, *The Aquaporins, Blueprints for Cellular Plumbing Systems.* Journal of Biological Chemistry, 1998. **273**(24): p. 14659-14662.
36. Burykin, A. and A. Warshel, *What Really Prevents Proton Transport through Aquaporin? Charge Self-Energy versus Proton Wire Proposals.* Biophysical Journal, 2003. **85**(6): p. 3696-3706.
37. Calamita, G., *The Escherichia coli aquaporin-Z water channel.* Molecular Microbiology, 2000. **37**(2): p. 254-262.
38. Gena, P., et al., *Aquaporin Membrane Channels: Biophysics, Classification, Functions, and Possible Biotechnological Applications.* Food Biophysics, 2011. **6**(2): p. 241-249.
39. Kozono, D., et al., *Aquaporin water channels: atomic structure and molecular dynamics meet clinical medicine.* Journal of Clinical Investigation, 2002. **109**(11): p. 1395-1399.

40. Tang, C.Y., et al., *Biomimetic aquaporin membranes coming of age.* Desalination, 2015. **368**: p. 89-105.
41. Werber, J.R., C.O. Osuji, and M. Elimelech, *Materials for next-generation desalination and water purification membranes.* 2016. **1**: p. 16018.
42. Zhao, J., et al., *Biomimetic and bioinspired membranes: preparation and application.* Progress in Polymer Science, 2014. **39**(9): p. 1668-1720.
43. Kumar, M., et al., *Highly permeable polymeric membranes based on the incorporation of the functional water channel protein Aquaporin Z.* Proceedings of the National Academy of Sciences of the United States of America, 2007. **104**(52): p. 20719-20724.
44. Li, X., et al., *Preparation of supported lipid membranes for aquaporin Z incorporation.* Colloids Surf B Biointerfaces, 2012. **94**: p. 333-40.
45. Li, X.S., et al., *Preparation of high performance nanofiltration (NF) membranes incorporated with aquaporin Z.* Journal of Membrane Science, 2014. **450**: p. 181-188.
46. TANG, C., et al., *Aquaporin based thin film composite membranes*. 2013, Google Patents.
47. Zhao, Y., et al., *Synthesis of robust and high-performance aquaporin-based biomimetic membranes by interfacial polymerization-membrane preparation and RO performance characterization.* Journal of Membrane Science, 2012. **423-424**: p. 422-428.
48. Zhao, Y., et al., *Effects of proteoliposome composition and draw solution types on separation performance of aquaporin-based proteoliposomes: implications for seawater desalination using aquaporin-based biomimetic membranes.* Environ Sci Technol, 2013. **47**(3): p. 1496-503.
49. Sun, G., et al., *A novel method of AquaporinZ incorporation via binary-lipid Langmuir monolayers.* Colloids Surf B Biointerfaces, 2012. **89**: p. 283-8.
50. Sun, G.F., et al., *Stabilization and immobilization of aquaporin reconstituted lipid vesicles for water purification.* Colloids and Surfaces B-Biointerfaces, 2013. **102**: p. 466-471.
51. Sun, G.F., et al., *A layer-by-layer self-assembly approach to developing an aquaporin-embedded mixed matrix membrane.* Rsc Advances, 2013. **3**(2): p. 473-481.
52. Wang, H., et al., *Highly permeable and selective pore-spanning biomimetic membrane embedded with aquaporin Z.* Small, 2012. **8**(8): p. 1185-90, 1125.
53. Wang, H., et al., *Preparation and characterization of pore-suspending biomimetic membranes embedded with Aquaporin Z on carboxylated polyethylene glycol polymer cushion.* Soft Matter, 2011. **7**(16): p. 7274.
54. Wang, H.L., et al., *Mechanically robust and highly permeable AquaporinZ biomimetic membranes.* Journal of Membrane Science, 2013. **434**: p. 130-136.
55. Xie, W.Y., et al., *An aquaporin-based vesicle-embedded polymeric membrane for low energy water filtration.* Journal of Materials Chemistry A, 2013. **1**(26): p. 7592-7600.
56. Zhong, P.S., et al., *Aquaporin-embedded biomimetic membranes for nanofiltration.* Journal of Membrane Science, 2012. **407-408**: p. 27-33.
57. Grzelakowski, M., et al., *A framework for accurate evaluation of the promise of aquaporin based biomimetic membranes.* Journal of Membrane Science, 2015. **479**: p. 223-231.
58. !!! INVALID CITATION !!! .
59. Habel, J., et al., *Aquaporin-Based Biomimetic Polymeric Membranes: Approaches and Challenges.* Membranes, 2015. **5**(3): p. 307-351.
60. Kita-Tokarczyk, K. and W. Meier, *Biomimetic Block Copolymer Membranes.* Chimia, 2008. **62**(10): p. 820-825.

61. Abdelrasoul, A., et al., *Aquaporin-Based Biomimetic and Bioinspired Membranes for New Frontiers in Sustainable Water Treatment Technology: Approaches and Challenges.* Polymer Science Series A, 2018. **60**(4): p. 429-450.
62. Xia, L.L., et al., *Novel Commercial Aquaporin Flat-Sheet Membrane for Forward Osmosis.* Industrial & Engineering Chemistry Research, 2017. **56**(41): p. 11919-11925.
63. Epsztein, R., et al., *Role of Ionic Charge Density in Donnan Exclusion of Monovalent Anions by Nanofiltration.* Environmental Science & Technology, 2018. **52**(7): p. 4108-4116.
64. Helm, D. and D. Naumann, *Identification of some bacterial cell components by FT-IR spectroscopy *.* FEMS Microbiology Letters, 1995. **126**(1): p. 75-79.
65. Salton, M.R.J., *Studies of the bacterial cell wall: IV. The composition of the cell walls of some gram-positive and gram-negative bacteria.* Biochimica et Biophysica Acta, 1953. **10**: p. 512-523.
66. Silhavy, T.J., D. Kahne, and S. Walker, *The Bacterial Cell Envelope.* Cold Spring Harbor Perspectives in Biology, 2010. **2**(5): p. a000414.
67. Sankaran, K. and H.C. Wu, *LIPID MODIFICATION OF BACTERIAL PROLIPOPROTEIN - TRANSFER OF DIACYLGLYCERYL MOIETY FROM PHOSPHATIDYLGLYCEROL.* Journal of Biological Chemistry, 1994. **269**(31): p. 19701-19706.
68. Cowan, S.W., et al., *Crystal structures explain functional properties of two E. coli porins.* Nature, 1992. **358**: p. 727.
69. Benz, R., A. Schmid, and R.E. Hancock, *Ion selectivity of gram-negative bacterial porins.* J Bacteriol, 1985. **162**(2): p. 722-7.
70. Hancock, R.E.W., *ROLE OF PORINS IN OUTER-MEMBRANE PERMEABILITY.* Journal of Bacteriology, 1987. **169**(3): p. 929-933.
71. Dargent, B., et al., *The selectivity filter of voltage-dependent channels formed by phosphoporin (PhoE protein) from E. coli.* The EMBO Journal, 1986. **5**(4): p. 773-778.
72. Buehler, L.K., et al., *PLASTICITY OF ESCHERICHIA-COLI PORIN CHANNELS - DEPENDENCE OF THEIR CONDUCTANCE ON STRAIN AND LIPID ENVIRONMENT.* Journal of Biological Chemistry, 1991. **266**(36): p. 24446-24450.
73. Nikaido, H. and E.Y. Rosenberg, *Porin channels in Escherichia coli: studies with liposomes reconstituted from purified proteins.* Journal of Bacteriology, 1983. **153**(1): p. 241-252.
74. Nikaido, H., E.Y. Rosenberg, and J. Foulds, *Porin channels in Escherichia coli: studies with beta-lactams in intact cells.* Journal of Bacteriology, 1983. **153**(1): p. 232-240.
75. Schulz, G.E., *Bacterial porins: structure and function.* Current Opinion in Cell Biology, 1993. **5**(4): p. 701-707.
76. Im, W. and B. Roux, *Ions and counterions in a biological channel: A molecular dynamics simulation of OmpF porin from Escherichia coli in an explicit membrane with 1 M KCl aqueous salt solution.* Journal of Molecular Biology, 2002. **319**(5): p. 1177-1197.
77. Im, W. and B. Roux, *Ion permeation and selectivity of OmpF porin: A theoretical study based on molecular dynamics, brownian dynamics, and continuum electrodiffusion theory.* Journal of Molecular Biology, 2002. **322**(4): p. 851-869.
78. Hindahl, M.S., G.W.K. Crockford, and R.E.W. Hancock, *OUTER-MEMBRANE PROTEIN NMPC OF ESCHERICHIA-COLI - PORE-FORMING PROPERTIES IN BLACK LIPID BILAYERS.* Journal of Bacteriology, 1984. **159**(3): p. 1053-1055.
79. Prilipov, A., et al., *Identification and characterization of two quiescent porin genes, nmpC and ompN, in Escherichia coli BE.* J Bacteriol, 1998. **180**(13): p. 3388-92.

80. Misra, R. and S.A. Benson, *A NOVEL MUTATION, COG, WHICH RESULTS IN PRODUCTION OF A NEW PORIN PROTEIN (OMPG) OF ESCHERICHIA-COLI K-12.* Journal of Bacteriology, 1989. **171**(8): p. 4105-4111.
81. Pilsl, H., D. Smajs, and V. Braun, *Characterization of colicin S4 and its receptor, OmpW, a minor protein of the Escherichia coli outer membrane.* Journal of Bacteriology, 1999. **181**(11): p. 3578-3581.
82. Vogt, J. and G.E. Schulz, *The structure of the outer membrane protein OmpX from Escherichia coli reveals possible mechanisms of virulence.* Structure with Folding & Design, 1999. **7**(10): p. 1301-1309.
83. Sugimura, K. and T. Nishihara, *Purification, characterization, and primary structure of Escherichia coli protease VII with specificity for paired basic residues: identity of protease VII and OmpT.* Journal of Bacteriology, 1988. **170**(12): p. 5625-5632.
84. Vandeputte-Rutten, L., et al., *Crystal structure of the outer membrane protease OmpT from Escherichia coli suggests a novel catalytic site.* Embo Journal, 2001. **20**(18): p. 5033-5039.
85. Snijder, H.J., et al., *Structural evidence for dimerization-regulated activation of an integral membrane phospholipase.* Nature, 1999. **401**(6754): p. 717-721.
86. Death, A., L. Notley, and T. Ferenci, *DEREPRESSION OF LAMB PROTEIN FACILITATES OUTER-MEMBRANE PERMEATION OF CARBOHYDRATES INTO ESCHERICHIA-COLI UNDER CONDITIONS OF NUTRIENT STRESS.* Journal of Bacteriology, 1993. **175**(5): p. 1475-1483.
87. Wang, Y.F., et al., *Channel specificity: Structural basis for sugar discrimination and differential flux rates in maltoporin.* Journal of Molecular Biology, 1997. **272**(1): p. 56-63.
88. Schirmer, T., et al., *STRUCTURAL BASIS FOR SUGAR TRANSLOCATION THROUGH MALTOPORIN CHANNELS AT 3.1-ANGSTROM RESOLUTION.* Science, 1995. **267**(5197): p. 512-514.
89. Dutzler, R., et al., *Crystal structures of various maltooligosaccharides bound to maltoporin reveal a specific sugar translocation pathway.* Structure, 1996. **4**(2): p. 127-134.
90. Van Gelder, P., et al., *Sugar Transport through Maltoporin of Escherichia coli: Role of the Greasy Slide.* Journal of Bacteriology, 2002. **184**(11): p. 2994-2999.
91. Luckey, M. and H. Nikaido, *SPECIFICITY OF DIFFUSION CHANNELS PRODUCED BY LAMBDA-PHAGE RECEPTOR PROTEIN OF ESCHERICHIA-COLI.* Proceedings of the National Academy of Sciences of the United States of America-Biological Sciences, 1980. **77**(1): p. 167-171.
92. Andersen, C., et al., *Study of sugar binding to the sucrose-specific ScrY channel of enteric bacteria using current noise analysis.* Journal of Membrane Biology, 1998. **164**(3): p. 263-274.
93. Hardesty, C., C. Ferran, and J.M. Dirienzo, *PLASMID-MEDIATED SUCROSE METABOLISM IN ESCHERICHIA-COLI - CHARACTERIZATION OF SCRY, THE STRUCTURAL GENE FOR A PHOSPHOENOLPYRUVATE-DEPENDENT SUCROSE PHOSPHOTRANSFERASE SYSTEM OUTER-MEMBRANE PORIN.* Journal of Bacteriology, 1991. **173**(2): p. 449-456.
94. Schmid, K., et al., *A SUGAR-SPECIFIC PORIN, SCRY, IS INVOLVED IN SUCROSE UPTAKE IN ENTERIC BACTERIA.* Molecular Microbiology, 1991. **5**(4): p. 941-950.
95. Schulein, K., K. Schmid, and R. Benzl, *THE SUGAR-SPECIFIC OUTER-MEMBRANE CHANNEL SCRY CONTAINS FUNCTIONAL-CHARACTERISTICS OF GENERAL DIFFUSION PORES AND SUBSTRATE-SPECIFIC PORINS.* Molecular Microbiology, 1991. **5**(9): p. 2233-2241.

96. Andersen, C., B. Rak, and R. Benz, *The gene bglH present in the bgl operon of Escherichia coli, responsible for uptake and fermentation of beta-glucosides encodes for a carbohydrate-specific outer membrane porin.* Mol Microbiol, 1999. **31**(2): p. 499-510.
97. Birch, R.G., J.M. Pemberton, and W.V. Basnayake, *STABLE ALBICIDIN RESISTANCE IN ESCHERICHIA-COLI INVOLVES AN ALTERED OUTER-MEMBRANE NUCLEOSIDE UPTAKE SYSTEM.* Journal of General Microbiology, 1990. **136**: p. 51-58.
98. Hantke, K., *PHAGE-T6 - COLICIN-K RECEPTOR AND NUCLEOSIDE TRANSPORT IN ESCHERICHIA-COLI.* Febs Letters, 1976. **70**(1): p. 109-112.
99. Fiedler, G., M. Pajatsch, and A. Bock, *Genetics of a novel starch utilisation pathway present in Klebsiella oxytoca.* Journal of Molecular Biology, 1996. **256**(2): p. 279-291.
100. Pajatsch, M., et al., *Properties of a cyclodextrin-specific, unusual porin from Klebsiella oxytoca.* Journal of Biological Chemistry, 1999. **274**(35): p. 25159-25166.
101. Black, P.N., *PRIMARY SEQUENCE OF THE ESCHERICHIA-COLI FADL GENE ENCODING AN OUTER-MEMBRANE PROTEIN REQUIRED FOR LONG-CHAIN FATTY-ACID TRANSPORT.* Journal of Bacteriology, 1991. **173**(2): p. 435-442.
102. Black, P.N., et al., *PURIFICATION AND CHARACTERIZATION OF AN OUTER MEMBRANE-BOUND PROTEIN INVOLVED IN LONG-CHAIN FATTY-ACID TRANSPORT IN ESCHERICHIA-COLI.* Journal of Biological Chemistry, 1987. **262**(3): p. 1412-1419.
103. Kahng, H.Y., et al., *Characterization and role of tbuX in utilization of toluene by Ralstonia pickettii PKO1.* Journal of Bacteriology, 2000. **182**(5): p. 1232-1242.
104. Kasai, Y., J. Inoue, and S. Harayama, *The TOL plasmid pWWO xylN gene product from Pseudomonas putida is involved in m-xylene uptake.* Journal of Bacteriology, 2001. **183**(22): p. 6662-6666.
105. Jones, R.M., V. Pagmantidis, and P.A. Williams, *sal genes determining the catabolism of salicylate esters are part of a supraoperonic cluster of catabolic genes in Acinetobacter sp strain ADP1.* Journal of Bacteriology, 2000. **182**(7): p. 2018-2025.
106. Eaton, R.W., *p-Cymene catabolic pathway in Pseudomonas putida F1: Cloning and characterization of DNA encoding conversion of p-cymene to p-cumate.* Journal of Bacteriology, 1997. **179**(10): p. 3171-3180.
107. Blot, N., et al., *The oligogalacturonate-specific porin KdgM of Erwinia chrysanthemi belongs to a new porin family.* Journal of Biological Chemistry, 2002. **277**(10): p. 7936-7944.
108. Braun, V., *Avoidance of iron toxicity through regulation of bacterial iron transport.* Biological Chemistry, 1997. **378**(8): p. 779-786.
109. Braun, V., K. Hantke, and W. Koster, *Bacterial iron transport: Mechanisms, genetics, and regulation.* Metal Ions in Biological Systems, Vol 35, 1998. **35**: p. 67-145.
110. Hantke, K., et al., *Salmochelins, siderophores of Salmonella enterica and uropathogenic Escherichia coli strains, are recognized by the outer membrane receptor IroN.* Proceedings of the National Academy of Sciences of the United States of America, 2003. **100**(7): p. 3677-3682.
111. Ghosh, A., et al., *Iron transport-mediated drug delivery using mixed-ligand siderophore-beta-lactam conjugates.* Chem Biol, 1996. **3**(12): p. 1011-9.
112. Larsen, R.A., et al., *Regions of Escherichia coli TonB and FepA proteins essential for in vivo physical interactions.* Journal of Bacteriology, 1997. **179**(10): p. 3213-3221.
113. Calamita, G., et al., *MOLECULAR-CLONING AND CHARACTERIZATION OF AQPZ, A WATER CHANNEL FROM ESCHERICHIA-COLI.* Journal of Biological Chemistry, 1995. **270**(49): p. 29063-29066.

114. Borgnia, M.J., et al., *Functional reconstitution and characterization of AqpZ, the E-coli water channel protein.* Journal of Molecular Biology, 1999. **291**(5): p. 1169-1179.
115. Borgnia, M., et al., *Cellular and molecular biology of the aquaporin water channels.* Annual Review of Biochemistry, 1999. **68**: p. 425-458.
116. Tajkhorshid, E., et al., *Control of the Selectivity of the Aquaporin Water Channel Family by Global Orientational Tuning.* Science, 2002. **296**(5567): p. 525-530.
117. Chakrabarti, N., et al., *Molecular Basis of Proton Blockage in Aquaporins.* Structure, 2004. **12**(1): p. 65-74.
118. Chakrabarti, N., B. Roux, and R. Pomès, *Structural Determinants of Proton Blockage in Aquaporins.* Journal of Molecular Biology, 2004. **343**(2): p. 493-510.
119. Hashido, M., A. Kidera, and M. Ikeguchi, *Water Transport in Aquaporins: Osmotic Permeability Matrix Analysis of Molecular Dynamics Simulations.* Biophysical Journal, 2007. **93**(2): p. 373-385.
120. Heo, J., F. Meng, and S.Z. Hua, *Contribution of aquaporins to cellular water transport observed by a microfluidic cell volume sensor.* Analytical Chemistry, 2008. **80**(18): p. 6974-6980.
121. Zhao, C.X., H.B. Shao, and L.Y. Chu, *Aquaporin structure-function relationships: Water flow through plant living cells.* Colloids and Surfaces B-Biointerfaces, 2008. **62**(2): p. 163-172.
122. Hu, G., L.Y. Chen, and J. Wang, *Insights into the mechanisms of the selectivity filter of Escherichia coli aquaporin Z.* J Mol Model, 2012. **18**(8): p. 3731-41.
123. Gravelle, S., et al., *Optimizing water permeability through the hourglass shape of aquaporins.* Proc Natl Acad Sci U S A, 2013. **110**(41): p. 16367-72.
124. Chowdhury, R., et al., *PoreDesigner for tuning solute selectivity in a robust and highly permeable outer membrane pore.* Nature Communications, 2018. **9**(1): p. 3661.
125. Sasaki, S., *Introduction for Special issue for Aquaporin.* Pflügers Archiv - European Journal of Physiology, 2008. **456**(4): p. 647-649.
126. Agre, P., et al., *Aquaporin CHIP: the archetypal molecular water channel.* Am J Physiol, 1993. **265**(4 Pt 2): p. F463-76.
127. Fushimi, K., et al., *Cloning and expression of apical membrane water channel of rat kidney collecting tubule.* Nature, 1993. **361**(6412): p. 549-52.
128. Nielsen, S., et al., *Cellular and subcellular immunolocalization of vasopressin-regulated water channel in rat kidney.* Proceedings of the National Academy of Sciences of the United States of America, 1993. **90**(24): p. 11663-11667.
129. Deen, P.M., et al., *Requirement of human renal water channel aquaporin-2 for vasopressin-dependent concentration of urine.* Science, 1994. **264**(5155): p. 92-5.
130. Echevarria, M., et al., *Cloning and expression of AQP3, a water channel from the medullary collecting duct of rat kidney.* Proceedings of the National Academy of Sciences of the United States of America, 1994. **91**(23): p. 10997-11001.
131. Ecelbarger, C.A., et al., *Aquaporin-3 water channel localization and regulation in rat kidney.* Am J Physiol, 1995. **269**(5 Pt 2): p. F663-72.
132. Hasegawa, H., et al., *MOLECULAR-CLONING OF A MERCURIAL-INSENSITIVE WATER CHANNEL EXPRESSED IN SELECTED WATER-TRANSPORTING TISSUES.* Journal of Biological Chemistry, 1994. **269**(8): p. 5497-5500.
133. Jung, J.S., et al., *Molecular characterization of an aquaporin cDNA from brain: candidate osmoreceptor and regulator of water balance.* Proceedings of the National Academy of Sciences of the United States of America, 1994. **91**(26): p. 13052-13056.

134. Raina, S., et al., *MOLECULAR-CLONING AND CHARACTERIZATION OF AN AQUAPORIN CDNA FROM SALIVARY, LACRIMAL, AND RESPIRATORY TISSUES.* Journal of Biological Chemistry, 1995. **270**(4): p. 1908-1912.
135. Mulders, S.M., et al., *WATER CHANNEL PROPERTIES OF MAJOR INTRINSIC PROTEIN OF LENS.* Journal of Biological Chemistry, 1995. **270**(15): p. 9010-9016.
136. Murata, K., et al., *Structural determinants of water permeation through aquaporin-1.* Nature, 2000. **407**(6804): p. 599-605.
137. Agmon, N., *The Grotthuss mechanism.* Chemical Physics Letters, 1995. **244**(5): p. 456-462.
138. de Groot, B.L., et al., *The Mechanism of Proton Exclusion in the Aquaporin-1 Water Channel.* Journal of Molecular Biology, 2003. **333**(2): p. 279-293.
139. Ilan, B., et al., *The mechanism of proton exclusion in aquaporin channels.* Proteins: Structure, Function, and Bioinformatics, 2004. **55**(2): p. 223-228.
140. Lee, F.S., et al., *Calculations of antibody-antigen interactions: microscopic and semi-microscopic evaluation of the free energies of binding of phosphorylcholine analogs to McPC603.* Protein Eng, 1992. **5**(3): p. 215-28.
141. Baylis, P.H., *Water movement through lipid bilayers, pores and plasma membranes: Theory and reality. (Distinquished Lecture Series of the Society of General Physiologists, Volume 4). Alan Finkelstein, John Wiley and Sons Ltd: New York. 228 pages, £38.45 (1987).* Cell Biochemistry and Function, 1988. **6**(3): p. 223-223.
142. Hummer, G., J.C. Rasaiah, and J.P. Noworyta, *Water conduction through the hydrophobic channel of a carbon nanotube.* Nature, 2001. **414**(6860): p. 188-90.
143. Berezhkovskii, A. and G. Hummer, *Single-File Transport of Water Molecules through a Carbon Nanotube.* Physical Review Letters, 2002. **89**(6): p. 064503.
144. Fu, D. and M. Lu, *The structural basis of water permeation and proton exclusion in aquaporins.* Mol Membr Biol, 2007. **24**(5-6): p. 366-74.
145. Rajkumar, P., et al., *Aquaporins: Novel Targets for Age-Related Ocular Disorders.* Journal of Ocular Pharmacology and Therapeutics, 2018. **34**(1-2): p. 177-187.
146. Cabrera, M.Á. and J.M. Blamey, *Biotechnological applications of archaeal enzymes from extreme environments.* Biological Research, 2018. **51**(1): p. 37.
147. Tesse, A., et al., *Aquaporins as Targets of Dietary Bioactive Phytocompounds.* Frontiers in Molecular Biosciences, 2018. **5**: p. 30.
148. Tamma, G., et al., *Aquaporin Membrane Channels in Oxidative Stress, Cell Signaling, and Aging: Recent Advances and Research Trends.* Oxidative Medicine and Cellular Longevity, 2018. **2018**: p. 14.
149. Wagh, P., et al., *A new technique to fabricate high-performance biologically inspired membranes for water treatment.* Separation and Purification Technology, 2015. **156**: p. 754-765.
150. Kaufman, Y., A. Berman, and V. Freger, *Supported Lipid Bilayer Membranes for Water Purification by Reverse Osmosis.* Langmuir, 2010. **26**(10): p. 7388-7395.
151. Wang, H., T.-S. Chung, and Y.W. Tong, *Study on water transport through a mechanically robust Aquaporin Z biomimetic membrane.* Journal of Membrane Science, 2013. **445**: p. 47-52.
152. He, Y., et al., *Functionalized polymeric membrane with aquaporin using click chemistry for water purification application.* Journal of Applied Polymer Science, 2018. **135**(35): p. 6.
153. Li, Z.Y., et al., *Aquaporin based biomimetic membrane in forward osmosis: Chemical cleaning resistance and practical operation.* Desalination, 2017. **420**: p. 208-215.

154. Li, X.S., et al., *Fabrication of a robust high-performance FO membrane by optimizing substrate structure and incorporating aquaporin into selective layer.* Journal of Membrane Science, 2017. **525**: p. 257-268.
155. Qi, S.R., et al., *Aquaporin-based biomimetic reverse osmosis membranes: Stability and long term performance.* Journal of Membrane Science, 2016. **508**: p. 94-103.
156. Wang, M.Q., et al., *Layer-by-Layer Assembly of Aquaporin Z-Incorporated Biomimetic Membranes for Water Purification.* Environmental Science & Technology, 2015. **49**(6): p. 3761-3768.
157. Li, X.S., et al., *Nature gives the best solution for desalination: Aquaporin-based hollow fiber composite membrane with superior performance.* Journal of Membrane Science, 2015. **494**: p. 68-77.
158. Vullev, V.I., *From Biomimesis to Bioinspiration: What's the Benefit for Solar Energy Conversion Applications?* The Journal of Physical Chemistry Letters, 2011. **2**(5): p. 503-508.
159. Song, W., et al., *Design Considerations for Artificial Water Channel-Based Membranes*, in *Annual Review of Materials Research, Vol 48*, D.R. Clarke, Editor. 2018. p. 57-82.
160. Geng, J., et al., *Stochastic transport through carbon nanotubes in lipid bilayers and live cell membranes.* Nature, 2014. **514**(7524): p. 612-+.
161. Le Duc, Y., et al., *Imidazole-Quartet Water and Proton Dipolar Channels.* Angewandte Chemie-International Edition, 2011. **50**(48): p. 11366-11372.
162. Kocsis, I., et al., *Oriented chiral water wires in artificial transmembrane channels.* Science Advances, 2018. **4**(3).
163. Hou, X., H.C. Zhang, and L. Jiang, *Building Bio-Inspired Artificial Functional Nanochannels: From Symmetric to Asymmetric Modification.* Angewandte Chemie-International Edition, 2012. **51**(22): p. 5296-5307.
164. Si, W., et al., *Selective Artificial Transmembrane Channels for Protons by Formation of Water Wires.* Angewandte Chemie-International Edition, 2011. **50**(52): p. 12564-12568.
165. vanNostrum, C.F., *Self-assembled wires and channels.* Advanced Materials, 1996. **8**(12): p. 1027-1030.
166. Huo, Y.P. and H.Q. Zeng, *"Sticky"-Ends-Guided Creation of Functional Hollow Nanopores for Guest Encapsulation and Water Transport.* Accounts of Chemical Research, 2016. **49**(5): p. 922-930.
167. Percec, V., et al., *Self-assembly of amphiphilic dendritic dipeptides into helical pores.* Nature, 2004. **430**(7001): p. 764-768.
168. Roux, B., *Computational studies of the gramicidin channel.* Accounts of Chemical Research, 2002. **35**(6): p. 366-375.
169. Allen, T.W., O.S. Andersen, and B. Roux, *Energetics of ion conduction through the gramicidin channel.* Proceedings of the National Academy of Sciences, 2004. **101**(1): p. 117-122.
170. Leiding, T., et al., *Proton and cation transport activity of the M2 proton channel from influenza A virus.* Proceedings of the National Academy of Sciences of the United States of America, 2010. **107**(35): p. 15409-15414.
171. Barboiu, M., et al., *An artificial primitive mimic of the Gramicidin-A channel.* Nature Communications, 2014. **5**: p. 4142.
172. Gong, B., *Hollow crescents, helices, and macrocycles from enforced folding and folding-assisted macrocyclization.* Acc Chem Res, 2008. **41**(10): p. 1376-86.
173. Zhou, X., et al., *Self-assembling subnanometer pores with unusual mass-transport properties.* Nature Communications, 2012. **3**: p. 949.

174. Zhao, H., et al., *Synthesis, structural investigation and computational modelling of water-binding aquafoldamers.* Organic & Biomolecular Chemistry, 2012. **10**(6): p. 1172-1180.
175. Schneider, S., et al., *Columnar Self-Assemblies of Triarylamines as Scaffolds for Artificial Biomimetic Channels for Ion and for Water Transport.* Journal of the American Chemical Society, 2017. **139**(10): p. 3721-3727.
176. Moulin, E., et al., *The Hierarchical Self-Assembly of Charge Nanocarriers: A Highly Cooperative Process Promoted by Visible Light.* Angewandte Chemie International Edition, 2010. **49**(39): p. 6974-6978.
177. Nyrkova, I., et al., *Supramolecular Self-Assembly and Radical Kinetics in Conducting Self-Replicating Nanowires.* ACS Nano, 2014. **8**(10): p. 10111-10124.
178. Armao, J.J., et al., *Healable Supramolecular Polymers as Organic Metals.* Journal of the American Chemical Society, 2014. **136**(32): p. 11382-11388.
179. Wolf, A., et al., *pH and light-controlled self-assembly of bistable [c2] daisy chain rotaxanes.* Chemical Communications, 2015. **51**(20): p. 4212-4215.
180. Armao, J.J., et al., *Long-Range Energy Transport via Plasmonic Propagation in a Supramolecular Organic Waveguide.* Nano Letters, 2016. **16**(4): p. 2800-2805.
181. Shen, Y.-x., et al., *Highly permeable artificial water channels that can self-assemble into two-dimensional arrays.* Proceedings of the National Academy of Sciences, 2015. **112**(32): p. 9810-9815.
182. Si, W., et al., *Tubular Unimolecular Transmembrane Channels: Construction Strategy and Transport Activities.* Accounts of Chemical Research, 2015. **48**(6): p. 1612-1619.
183. Xue, M., et al., *Pillararenes, A New Class of Macrocycles for Supramolecular Chemistry.* Accounts of Chemical Research, 2012. **45**(8): p. 1294-1308.
184. Si, W., Z.-T. Li, and J.-L. Hou, *Voltage-Driven Reversible Insertion into and Leaving from a Lipid Bilayer: Tuning Transmembrane Transport of Artificial Channels.* Angewandte Chemie International Edition, 2014. **53**(18): p. 4578-4581.
185. Chen, L., et al., *Chiral Selective Transmembrane Transport of Amino Acids through Artificial Channels.* Journal of the American Chemical Society, 2013. **135**(6): p. 2152-2155.
186. Holt, J.K., et al., *Fast Mass Transport Through Sub-2-Nanometer Carbon Nanotubes.* Science, 2006. **312**(5776): p. 1034-1037.
187. Majumder, M., et al., *Enhanced flow in carbon nanotubes.* Nature, 2005. **438**: p. 44.
188. Secchi, E., et al., *Massive radius-dependent flow slippage in carbon nanotubes.* Nature, 2016. **537**: p. 210.
189. Fornasiero, F., et al., *Ion exclusion by sub-2-nm carbon nanotube pores.* Proceedings of the National Academy of Sciences, 2008. **105**(45): p. 17250-17255.
190. Corry, B., *Designing Carbon Nanotube Membranes for Efficient Water Desalination.* The Journal of Physical Chemistry B, 2008. **112**(5): p. 1427-1434.
191. McGinnis, R.L., et al., *Large-scale polymeric carbon nanotube membranes with sub–1.27-nm pores.* Science Advances, 2018. **4**(3).
192. Vögele, M., J. Köfinger, and G. Hummer, *Molecular dynamics simulations of carbon nanotube porins in lipid bilayers.* Faraday Discussions, 2018. **209**(0): p. 341-358.
193. Luo, W., et al., *Biomimetic aquaporin membranes for osmotic membrane bioreactors: Membrane performance and contaminant removal.* Bioresource Technology, 2018. **249**: p. 62-68.
194. Singh, N., et al., *Concentrating molasses distillery wastewater using biomimetic forward osmosis (FO) membranes.* Water Research, 2018. **130**: p. 271-280.

195. Pedersen, P.A., et al., *From channel proteins to industrial biomimetic membrane technology.* Faraday Discussions, 2018. **209**(0): p. 287-301.
196. Munshi, F.M., et al., *Dewatering algae using an aquaporin-based polyethersulfone forward osmosis membrane.* Separation and Purification Technology, 2018. **204**: p. 154-161.
197. Shaw, H.L., Howard, Kevin, Flynn, Michael T., Beerler, David, Kawashima, Brian, Andersen, Thomas A. E., Kleinschmidt, Kim, Vogel, Jorg, Parodi, Jurek., *Multilfiltration Bed Replacement (MFBR) System for the International Space Station using Aquaporin Membranes and Humidity Condensate Ersatz Wastewater.* 2017.
198. Wang, X.-L., et al., *Characterization and applications of nanofiltration membranes: State of the art.* Desalination, 2009. **236**(1): p. 316-326.
199. Hilal, N., et al., *A comprehensive review of nanofiltration membranes: Treatment, pretreatment, modelling, and atomic force microscopy.* Desalination, 2004. **170**(3): p. 281-308.
200. Bowen, W.R., A.W. Mohammad, and N. Hilal, *Characterisation of nanofiltration membranes for predictive purposes - Use of salts, uncharged solutes and atomic force microscopy.* Journal of Membrane Science, 1997. **126**(1): p. 91-105.
201. Nath, K., H.K. Dave, and T.M. Patel, *Revisiting the recent applications of nanofiltration in food processing industries: Progress and prognosis.* Trends in Food Science & Technology, 2018. **73**: p. 12-24.
202. Wang, X.-L., C. Zhang, and P. Ouyang, *The possibility of separating saccharides from a NaCl solution by using nanofiltration in diafiltration mode.* Journal of Membrane Science, 2002. **204**(1): p. 271-281.
203. Boo, C., et al., *High Performance Nanofiltration Membrane for Effective Removal of Perfluoroalkyl Substances at High Water Recovery.* Environmental Science & Technology, 2018. **52**(13): p. 7279-7288.
204. Lin, Y.-L., C.-C. Tsai, and N.-Y. Zheng, *Improving the organic and biological fouling resistance and removal of pharmaceutical and personal care products through nanofiltration by using in situ radical graft polymerization.* Science of The Total Environment, 2018. **635**: p. 543-550.
205. Meschke, K., et al., *Characterization and performance evaluation of polymeric nanofiltration membranes for the separation of strategic elements from aqueous solutions.* Journal of Membrane Science, 2018. **546**: p. 246-257.
206. Iaquinta, M., M. Stoller, and C. Merli, *Optimization of a nanofiltration membrane process for tomato industry wastewater effluent treatment.* Desalination, 2009. **245**(1): p. 314-320.
207. Machado, M.T.C., et al., *Clarification and concentration of oligosaccharides from artichoke extract by a sequential process with microfiltration and nanofiltration membranes.* Journal of Food Engineering, 2016. **180**: p. 120-128.
208. Dow, *DOW FILMTEC™ NF90-400/34i Element data sheet.*
209. Dow, *DOW FILMTEC™ NF270-400/34i Element data sheet.*
210. Membranes, T., *CSM NE8040-90 7500 GPD Nano-filtration Membrane 8 x 40 data sheet.*
211. membranes, T., *CSM NE4040-90 1700 GPD NF Membrane, 4" x 40" data sheet.*
212. Inui, O., Y. Teramura, and H. Iwata, *Retention dynamics of amphiphilic polymers PEG-lipids and PVA-Alkyl on the cell surface.* ACS Appl Mater Interfaces, 2010. **2**(5): p. 1514-20.
213. Teramura, Y., et al., *Behavior of synthetic polymers immobilized on a cell membrane.* Biomaterials, 2008. **29**(10): p. 1345-1355.

214. Wang, K.Y. and T.-S. Chung, *Polybenzimidazole nanofiltration hollow fiber for cephalexin separation.* AIChE Journal, 2006. **52**(4): p. 1363-1377.
215. Ma, Y.L., et al., *Conductivity of PBI membranes for high-temperature polymer electrolyte fuel cells.* Journal of the Electrochemical Society, 2004. **151**(1): p. A8-A16.
216. Aerts, P., et al., *The role of the nature of the casting substrate on the properties of membranes prepared via immersion precipitation.* Journal of Membrane Science, 2006. **283**(1-2): p. 320-327.
217. Flanagan, M.F. and I.C. Escobar, *Novel charged and hydrophilized polybenzimidazole (PBI) membranes for forward osmosis.* Journal of Membrane Science, 2013. **434**: p. 85-92.
218. Totani, T., Y. Teramura, and H. Iwata, *Immobilization of urokinase on the islet surface by amphiphilic poly(vinyl alcohol) that carries alkyl side chains.* Biomaterials, 2008. **29**(19): p. 2878-83.
219. Gung, B.W., et al., *A short synthesis of an acetylenic alcohol from the sponge Cribrochalina vasculum.* Synthetic Communications, 2002. **32**(17): p. 2733-2740.
220. Hosono, M.S.S.K.R.M.-H.Y., *polyelectrolyte complex prepared from carboxymethylated and aminoacetalized derivatives of Poly(vinyl) alcohol.* Journal of Applied Polymer Science, 1977. **21**: p. 2125-2134.
221. Dickson, H., et al., *A short synthesis of an acetylenic alcohol from the sponge cribrochalina vasculum.* Abstracts of Papers American Chemical Society, 2002. **223**(1-2): p. 356.
222. Wang, Z., et al., *Cysteine residue is not essential for CPM protein thermal-stability assay.* Analytical and Bioanalytical Chemistry, 2015. **407**(13): p. 3683-3691.
223. Bandyopadhyaya, R., et al., *Stabilization of individual carbon nanotubes in aqueous solutions.* Nano Letters, 2002. **2**(1): p. 25-28.
224. Ni, W.J., et al., *Fabrication and properties of carbon nanotube and poly(vinyl alcohol) composites.* Journal of Macromolecular Science Part B-Physics, 2006. **45**(4): p. 659-664.
225. Hite, R.K., Z. Li, and T. Walz, *Principles of membrane protein interactions with annular lipids deduced from aquaporin-0 2D crystals.* EMBO J, 2010. **29**(10): p. 1652-8.
226. J, C., *Interpretation of Infrared Spectra, A Practical Approach*, in *Encyclopedia of Analytical chemistry, R. A. Meyers, Editor 2000*. 2006, John Wiley and Sons Ltd.: Chichester. p. 10815-10837.
227. Xu, B.L., et al., *A measurement method for contact angle based on Hough Transformation.* Measurement, 2013. **46**(3): p. 1109-1114.
228. Lau, W.J., et al., *Characterization Methods of Thin Film Composite Nanofiltration Membranes.* Separation and Purification Reviews, 2015. **44**(2): p. 135-156.
229. Ling, K., H. Jiang, and Q. Zhang, *A colorimetric method for the molecular weight determination of polyethylene glycol using gold nanoparticles.* Nanoscale Research Letters, 2013. **8**(1): p. 538.
230. Dohmen, M.P.J., et al., *Hydrodynamic Radii of Polyethylene Glycols in Different Solvents Determined from Viscosity Measurements.* Journal of Chemical & Engineering Data, 2008. **53**(1): p. 63-65.
231. Lebrun, L. and G.A. Junter, *Diffusion of sucrose and dextran through agar gel membranes.* Enzyme and Microbial Technology, 1993. **15**(12): p. 1057-1062.
232. Schultz, S.G. and A.K. Solomon, *Determination of the Effective Hydrodynamic Radii of Small Molecules by Viscometry.* The Journal of General Physiology, 1961. **44**(6): p. 1189-1199.

233. Hu, K. and J.M. Dickson, *Nanofiltration membrane performance on fluoride removal from water.* Journal of Membrane Science, 2006. **279**(1): p. 529-538.
234. Xu, J. and D. Bhattacharyya, *Fe/Pd Nanoparticle Immobilization in Microfiltration Membrane Pores: Synthesis, Characterization, and Application in the Dechlorination of Polychlorinated Biphenyls.* Industrial & Engineering Chemistry Research, 2007. **46**(8): p. 2348-2359.
235. Kekenes-Huskey, P.M., et al., *Finite Element Estimation of Protein-Ligand Association Rates with Post-Encounter Effects: Applications to Calcium binding in Troponin C and SERCA.* Computational science & discovery, 2012. **5**: p. 014015.
236. Kekenes-Huskey, P.M., A.K. Gillette, and J.A. McCammon, *Predicting the influence of long-range molecular interactions on macroscopic-scale diffusion by homogenization of the Smoluchowski equation.* The Journal of Chemical Physics, 2014. **140**(17): p. 174106.
237. Geuzaine, C. and J.-F. Remacle, *Gmsh: A 3-D finite element mesh generator with built-in pre- and post-processing facilities.* International Journal for Numerical Methods in Engineering, 2009. **79**(11): p. 1309-1331.
238. Logg, A., G.N. Wells, and J. Hake, *DOLFIN: a C++/Python finite element library*, in *Automated Solution of Differential Equations by the Finite Element Method: The FEniCS Book*, A. Logg, K.-A. Mardal, and G. Wells, Editors. 2012, Springer Berlin Heidelberg: Berlin, Heidelberg. p. 173-225.
239. Van der Bruggen, B., M. Mänttäri, and M. Nyström, *Drawbacks of applying nanofiltration and how to avoid them: A review.* Separation and Purification Technology, 2008. **63**(2): p. 251-263.
240. Brandhuber, P. and G. Amy, *Alternative methods for membrane filtration of arsenic from drinking water.* Desalination, 1998. **117**(1–3): p. 1-10.
241. Waypa, J.J., M. Elimelech, and J.G. Hering, *Arsenic removal by RO and NF membranes.* Journal American Water Works Association, 1997. **89**(10): p. 102-114.
242. Lee, K.P., T.C. Arnot, and D. Mattia, *A review of reverse osmosis membrane materials for desalination—Development to date and future potential.* Journal of Membrane Science, 2011. **370**(1–2): p. 1-22.
243. Hassan, A.M., et al., *A new approach to membrane and thermal seawater desalination processes using nanofiltration membranes (Part 1).* Desalination, 1998. **118**(1–3): p. 35-51.
244. Redondo, J.A., *Brackish-, sea- and wastewater desalination.* Desalination, 2001. **138**(1–3): p. 29-40.
245. Van der Bruggen, B. and C. Vandecasteele, *Distillation vs. membrane filtration: overview of process evolutions in seawater desalination.* Desalination, 2002. **143**(3): p. 207-218.
246. Matsuura, T., *Progress in membrane science and technology for seawater desalination — a review.* Desalination, 2001. **134**(1–3): p. 47-54.
247. Borgnia, M., et al., *Cellular and molecular biology of the aquaporin water channels*, in *Annual Review of Biochemistry*, C.C. Richardson, Editor. 1999, Annual Reviews Inc. {a}, P.O. Box 10139, 4139 El Camino Way, Palo Alto, California 94306, USA. p. 425-458.
248. Zeidel, M.L., et al., *Reconstitution of functional water channels in liposomes containing purified red cell CHIP28 protein.* Biochemistry, 1992. **31**(33): p. 7436-7440.
249. Yadav, M.P., et al., *Chemical investigation of the structural basis of the emulsifying activity of gum arabic.* Food Hydrocolloids, 2007. **21**(2): p. 297-308.
250. Garti, N., *Hydrocolloids as emulsifying agents for oil-in-water emulsions.* Journal of Dispersion Science and Technology, 1999. **20**(1-2): p. 327-355.

251. Randall, R.C., G.O. Phillips, and P.A. Williams, *The role of the proteinaceous component on the emulsifying properties of gum arabic.* Food Hydrocolloids, 1988. **2**(2): p. 131-140.
252. Idris, Y.M.A., Y.A. Ibrahim, and A.A. Mariod, *Color of Dehydrated Tomato: Effects of Gum Arabic.* International Journal of Food Properties, 2013. **16**(4): p. 838-851.
253. De Feber, M., J. Havermans, and P. Defize, *Iron-gall ink corrosion: A compound-effect study.* Restaurator-International Journal for the Preservation of Library and Archival Material, 2000. **21**(4): p. 204-212.
254. Sistach, M.C., J.M. Gibert, and R. Areal, *Ageing of laboratory irongall inks studied by reflectance spectrometry.* Restaurator-International Journal for the Preservation of Library and Archival Material, 1999. **20**(3-4): p. 151-166.
255. Jancovicova, V., et al., *Interactions in iron gall inks.* Chemical Papers, 2007. **61**(5): p. 391-397.
256. Specos, M.M.M., et al., *Aroma Finishing of Cotton Fabrics by Means of Microencapsulation Techniques.* Journal of Industrial Textiles, 2010. **40**(1): p. 13-32.
257. Jadhav, S.B. and R.S. Singhal, *Polysaccharide conjugated laccase for the dye decolorization and reusability of effluent in textile industry.* International Biodeterioration & Biodegradation, 2013. **85**: p. 271-277.
258. Shang, Y. and Y. Peng, *UF membrane of PVA modified with TDI.* Desalination, 2008. **221**(1-3): p. 324-330.
259. Vogel, H. and C.S. Marvel, *Polybenzimidazoles, new thermally stable polymers (Reprinted from Journal of Polymer Science, vol 50, pg 511-539, 1961).* Journal of Polymer Science Part a-Polymer Chemistry, 1996. **34**(7): p. 1125-1153.
260. Chung, T.S., *A critical review of polybenzimidazoles: Historical development and future R&D.* Journal of Macromolecular Science-Reviews in Macromolecular Chemistry and Physics, 1997. **C37**(2): p. 277-301.
261. Hausman, R., et al., *Functionalization of polybenzimidizole membranes to impart negative charge and hydrophilicity.* Journal of Membrane Science, 2010. **363**(1-2): p. 195-203.
262. Li, N., Z.Z. Liu, and S.G. Xu, *Dynamically formed poly (vinyl alcohol) ultrafiltration membranes with good anti-fouling characteristics.* Journal of Membrane Science, 2000. **169**(1): p. 17-28.
263. Mohanty, A.K. and M.C. Wiener, *Membrane protein expression and production: effects of polyhistidine tag length and position.* Protein Expression and Purification, 2004. **33**(2): p. 311-325.
264. Musto, P., F.E. Karasz, and W.J. Macknight, *FOURIER-TRANSFORM INFRARED-SPECTROSCOPY ON THE THERMOOXIDATIVE DEGRADATION OF POLYBENZIMIDAZOLE AND OF A POLYBENZIMIDAZOLE POLYETHERIMIDE BLEND.* Polymer, 1993. **34**(14): p. 2934-2945.
265. Gullinkala, T. and I. Escobar, *Study of the hydrophilic-enhanced ultrafiltration membrane.* Environmental Progress, 2008. **27**(2): p. 210-217.
266. Taubert, A., *Controlling water transport through artificial polymer/protein hybrid membranes.* Proceedings of the National Academy of Sciences of the United States of America, 2007. **104**(52): p. 20643-20644.
267. Zhang, X., et al., *Mimicking the cell membrane with block copolymer membranes.* Journal of Polymer Science Part A: Polymer Chemistry, 2012. **50**(12): p. 2293-2318.
268. Tanner, P., et al., *Polymeric Vesicles: From Drug Carriers to Nanoreactors and Artificial Organelles.* Accounts of Chemical Research, 2011. **44**(10): p. 1039-1049.

269. Choi, H.-J. and C.D. Montemagno, *Artificial Organelle: ATP Synthesis from Cellular Mimetic Polymersomes.* Nano Letters, 2005. **5**(12): p. 2538-2542.
270. Vriezema, D.M., et al., *Positional Assembly of Enzymes in Polymersome Nanoreactors for Cascade Reactions.* Angewandte Chemie, 2007. **119**(39): p. 7522-7526.
271. Stoenescu, R., A. Graff, and W. Meier, *Asymmetric ABC-Triblock Copolymer Membranes Induce a Directed Insertion of Membrane Proteins.* Macromolecular Bioscience, 2004. **4**(10): p. 930-935.
272. Graff, A., et al., *Amphiphilic Copolymer Membranes Promote NADH:Ubiquinone Oxidoreductase Activity: Towards an Electron-Transfer Nanodevice.* Macromolecular Chemistry and Physics, 2010. **211**(2): p. 229-238.
273. Kumar, M., et al., *High-Density Reconstitution of Functional Water Channels into Vesicular and Planar Block Copolymer Membranes.* Journal of the American Chemical Society, 2012. **134**(45): p. 18631-18637.
274. Winterhalter, M., et al., *Controlling membrane permeability with bacterial porins: application to encapsulated enzymes.* Talanta, 2001. **55**(5): p. 965-971.
275. Kumar, M., *Biomimetic membranes as new materials for applications in environmental engineering and biology.* 2010.
276. Nielsen, C.H., *Biomimetic membranes for sensor and separation applications.* Analytical and Bioanalytical Chemistry, 2009. **395**(3): p. 697-718.
277. Digman, B., et al., *Surface functionalization of polybenzimidizole membranes to increase hydrophilicity and charge.* Abstracts of Papers of the American Chemical Society, 2010. **240**: p. 1.
278. Sawyer, L.C. and R.S. Jones, *Observations on the structure of first generation polybenzimidazole reverse osmosis membranes.* Journal of Membrane Science, 1984. **20**(2): p. 147-166.
279. Zhu, W.-P., et al., *Dual-layer polybenzimidazole/polyethersulfone (PBI/PES) nanofiltration (NF) hollow fiber membranes for heavy metals removal from wastewater.* Journal of Membrane Science, 2014. **456**: p. 117-127.
280. Teramura, Y., et al., *Behavior of synthetic polymers immobilized on a cell membrane.* Biomaterials, 2008. **29**(10): p. 1345-55.
281. Xin, L., et al., *Population Shift between the Open and Closed States Changes the Water Permeability of an Aquaporin Z Mutant.* Biophysical Journal, 2012. **103**(2): p. 212-218.
282. Israelachvili, J.N., *Intermolecular and Surface Forces*. III ed. 2011. 710.
283. Braghetta, A., F.A. DiGiano, and W.P. Ball, *Nanofiltration of Natural Organic Matter: pH and Ionic Strength Effects.* Journal of Environmental Engineering, 1997. **123**(7): p. 628-641.
284. Xu, Y. and R.E. Lebrun, *Investigation of the solute separation by charged nanofiltration membrane: effect of pH, ionic strength and solute type.* Journal of Membrane Science, 1999. **158**(1): p. 93-104.
285. Kekenes-Huskey, P.M., C.E. Scott, and S. Atalay, *Quantifying the Influence of the Crowded Cytoplasm on Small Molecule Diffusion.* The Journal of Physical Chemistry B, 2016. **120**(33): p. 8696-8706.
286. Meyer, J. and M. Ulbricht, *Poly(ethylene oxide)-block-poly(methyl methacrylate) diblock copolymers as functional additive for poly(vinylidene fluoride) ultrafiltration membranes with tailored separation performance.* Journal of Membrane Science, 2018. **545**: p. 301-311.

287. Fan, H., et al., *High-Flux Membranes Based on the Covalent Organic Framework COF-LZU1 for Selective Dye Separation by Nanofiltration.* Angewandte Chemie International Edition, 2018. **57**(15): p. 4083-4087.
288. Lively, R.P. and D.S. Sholl, *From water to organics in membrane separations.* Nature Materials, 2017. **16**: p. 276.
289. Fane, A.G., R. Wang, and M.X. Hu, *Synthetische Membranen für die Wasseraufbereitung: aktueller Stand und Perspektiven.* Angewandte Chemie, 2015. **127**(11): p. 3427-3447.
290. Rezakazemi, M., et al., *State-of-the-art membrane based CO2 separation using mixed matrix membranes (MMMs): An overview on current status and future directions.* Progress in Polymer Science, 2014. **39**(5): p. 817-861.
291. Sun, P., K. Wang, and H. Zhu, *Recent Developments in Graphene-Based Membranes: Structure, Mass-Transport Mechanism and Potential Applications.* Advanced Materials, 2016. **28**(12): p. 2287-2310.
292. Denny, M.S. and S.M. Cohen, *In Situ Modification of Metal–Organic Frameworks in Mixed-Matrix Membranes.* Angewandte Chemie, 2015. **127**(31): p. 9157-9160.
293. Wang, C., et al., *Zwitterionic functionalized "cage-like" porous organic frameworks for nanofiltration membrane with high efficiency water transport channels and anti-fouling property.* Journal of Membrane Science, 2018. **548**: p. 194-202.
294. Kandambeth, S., et al., *Selective Molecular Sieving in Self-Standing Porous Covalent-Organic-Framework Membranes.* Advanced Materials, 2017. **29**(2): p. 1603945.
295. Waller, P.J., F. Gándara, and O.M. Yaghi, *Chemistry of Covalent Organic Frameworks.* Accounts of Chemical Research, 2015. **48**(12): p. 3053-3063.
296. Lanni, L.M., et al., *Enhanced hydrolytic stability of self-assembling alkylated two-dimensional covalent organic frameworks.* J Am Chem Soc, 2011. **133**(35): p. 13975-83.
297. Asensio, J.A., E.M. Sanchez, and P. Gomez-Romero, *Proton-conducting membranes based on benzimidazole polymers for high-temperature PEM fuel cells. A chemical quest.* Chemical Society Reviews, 2010. **39**(8): p. 3210-3239.
298. Villalobos, L.F., et al., *Fabrication of Polybenzimidazole/Palladium Nanoparticles Hollow Fiber Membranes for Hydrogen Purification.* Advanced Energy Materials, 2018. **8**(3): p. 1701567.
299. Fei, F., et al., *Robust Covalently Cross-linked Polybenzimidazole/Graphene Oxide Membranes for High-Flux Organic Solvent Nanofiltration.* ACS Applied Materials & Interfaces, 2018. **10**(18): p. 16140-16147.
300. Hao, J., et al., *Functionalization of polybenzimidazole-crosslinked poly(vinylbenzyl chloride) with two cyclic quaternary ammonium cations for anion exchange membranes.* Journal of Membrane Science, 2018. **548**: p. 1-10.
301. Fuentes, I., et al., *Structural and dielectric properties of cobaltacarborane composite polybenzimidazole membranes as solid polymer electrolytes at high temperature.* Physical Chemistry Chemical Physics, 2018. **20**(15): p. 10173-10184.
302. Kumar, V., et al., *Soluble polybenzimidazoles with intrinsic porosity: Synthesis, structure, properties and processability.* Journal of Polymer Science Part A: Polymer Chemistry, 2018. **56**(10): p. 1046-1057.
303. Subianto, S., *Recent advances in polybenzimidazole/phosphoric acid membranes for high-temperature fuel cells.* Polymer International, 2014. **63**(7): p. 1134-1144.
304. Xiao, L., et al., *High-Temperature Polybenzimidazole Fuel Cell Membranes via a Sol–Gel Process.* Chemistry of Materials, 2005. **17**(21): p. 5328-5333.

305. Eke, J., P. Wagh, and I.C. Escobar, *Ozonation, biofiltration and the role of membrane surface charge and hydrophobicity in removal and destruction of algal toxins at basic pH values.* Separation and Purification Technology, 2018. **194**(Supplement C): p. 56-63.
306. Teramura, Y. and H. Iwata, *Cell surface modification with polymers for biomedical studies.* Soft Matter, 2010. **6**(6): p. 1081-1091.
307. *Energy table for EDS analysis*. Available from: https://www.unamur.be/services/microscopie/sme-documents/Energy-20table-20for-20EDS-20analysis-1.pdf.
308. *EELS atlas*. Available from: http://www.eels.info/atlas.

VITA

Priyesh Ashokrao Wagh

Education:

Doctor of Philosophy, Chemical Engineering — August 2012 – November 2018

University of Kentucky, Kentucky, USA

Bachelor of Chemical Engineering — July 2008 – May 2012

Institute of Chemical Technology (Formerly UDCT), Mumbai, India

Work Experience:

Research and Development Intern — May 2018 – September 2018

Pure Blue Tech Inc, Seattle, Washington

Lead Process Engineer — September 2017 – Aug 2018

The Sustainable Products Company (Product registration phase), Paducah, Kentucky

Graduate Research Assistant — August 2015 – November 2018

University of Kentucky, Kentucky, USA.

Graduate Teaching Assistant — August 2012 – August 2015

The University of Toledo, Ohio, USA.

Chemical Engineering Intern — May 2011 – July 2011

Aarti Industries Ltd, Vapi, Gujarat, India.

Scholastic and Professional Honors:

- Winner - Von Allmen Center Entrepreneurship Bootcamp 2017, University of Kentucky
- Student Poster competition award - Advanced Membrane Technology II, 2016
- Elias Klein Award - North American Membrane Society Annual Conference 2014

Professional Publications:

- P. Wagh, G. Parungao, R. Viola, I. Escobar, 'A new technique to fabricate high-performance biologically inspired membranes for water treatment.' Separation and Purification Technology, 2015, 156, 754 – 765.

- J. Eke, P. Wagh, I. Escobar, 'Ozonation, Biofiltration and the Role of Membrane Surface Charge and Hydrophobicity in Removal and Destruction of Algal Toxins at Basic pH Values.' Equal first authorship – Separation and Purification Technology, 2017, 194, 56 -63. `

- P. Wagh, and I. Escobar, 'Biomimetic and bioinspired membranes for water purification: a critical review and future directions.' (Submitted for publication, under peer review).

- P. Wagh, X. Zhang, R. Blood, P. Kekenes-Huskey, P. Rajapaksha, Y. Wei, and I. Escobar, 'Alignment and Immobilization of Aquaporins on Polybenzimidazole Nanofiltration Membranes.' (In preparation).